Towards a Rational Analysis and Design of Partially-Grouted Concrete Block Masonry Walls Under In-Plane Shear

by

Clayton Edward James Pettit

A thesis submitted in partial fulfillment of the requirements for the degree of

Doctor of Philosophy

in

Structural Engineering

Department of Civil and Environmental Engineering
University of Alberta

ABSTRACT

Masonry wall systems are an essential structural component of a building, providing resistance against lateral and gravity loads. Due to its economy and efficiency, most masonry walls in low- to moderate-seismic markets are partially-grouted, in which only the reinforced cells are filled with grout. Designing a partially-grouted masonry wall to resist in-plane forces is complex due to the heterogeneous nature of masonry, the distinct nonlinear behaviour of each component in the assemblage (masonry unit, mortar, grout, reinforcement, etc.), and the relatively unknown interaction existing between solid and void spaces in the wall. As a result, current North American design provisions for masonry structures (CSA S304-14 and TMS 402/602-22) are limited in their ability to predict the diagonal tension shear capacity of partially-grouted walls with consistent accuracy. Particularly concerning is the increasing number of research studies reporting that North American design provisions tend to significantly over-estimate the shear strength of partially-grouted walls and predict behaviour inconsistent with experimental studies involving partially-grouted walls. This poor performance ultimately stems from North American design provisions attempting to quantify the in-plane shear capacity of partially-grouted walls with simplified semi-empirical equations based on a pool of outdated experimental programs that focused on fully-grouted wall specimens. This research aims to (1) develop a rational methodology to estimate the in-plane shear capacity of partially-grouted masonry walls under typical roof-type loading through the creation of a mechanics-based strut-and-tie model (STM) specific to partially-grouted walls and formulated on the basis of the STM methodology currently employed for the design of reinforced concrete structures and (2) identify and quantify the influence of key

design parameters on the in-plane shear strength of partially-grouted walls. To achieve these goals, the research was divided into three steps. The first step consisted of developing a detailed masonry wall micro-model within the finite element framework that considers each component of the masonry assemblage independently and accounts for the cohesive interactions existing between them through the development of innovative shear interfaces. Verified with available experimental data, insights concerning the behaviour of partially-grouted masonry walls under in-plane loads (load paths, strut geometry and magnitudes, and location of nodal zones, etc.) will be extracted from the model to facilitate the development of the STM analysis model. The derivation scheme of the masonry STM will follow a similar path as the STM development for reinforced concrete, with the additional modifications required for masonry made as needed. A parametric study was also be conducted utilizing the micro-model to determine the influence of key design parameters (grout core spacing, vertical reinforcement, horizontal reinforcement, applied axial stress, wall openings, etc.) on the in-plane shear capacity of partially-grouted masonry walls. Finally, the findings from both the experimental validation of the micro-model and the parametric study were used to develop a STM methodology specific to partially-grouted masonry walls under typical roof-type loading. The results from this study are summarized in a transparent guide to allow for a seamless transition into existing design provisions. It is the hope of the author that this study allows for a more complete understanding of the shear strength of partially-grouted masonry walls, ultimately resulting in safer, more economical masonry solutions.

Let it be.

- Paul McCartney

DEDICATION

To my beautiful wife, Wanyan and my loving parents, Ron and Marie:

I would not be here if not for your love and support.

And to my supervisor and friend Dr. Lobo:

Thank you for taking a chance on a kid who couldn't solve a bending moment diagram.

ACKNOWLEDGEMENTS

First and foremost, I would like to thank my supervisor, Dr. Carlos 'Lobo' Cruz-Noguez, for his friendship and guidance over the last eight years, which have proved invaluable throughout this research project.

I wish to thank my wife, Wanyan Pettit, who supported me continuously during this research. Thank you for all that you have done for me and for our son Bowen. I would also like to thank my parents, Ron and Marie Pettit, whose love and support encouraged me to complete this research.

A special thanks to my supervisory committee members, Dr. Samer Adeeb and Dr. Yong Li, who consistently challenged me through this research, ultimately allowing me to grow both as an engineering and an individual.

I would also like to thank fellow wolfpack members Amr Ba Rahim, Odin Guzman-Sanchez, Alan Alonso-Rivers, and Mahmoud Elsayed, who would take the time to listen, understand, and comment on this research.

Finally, I would like to thank the many organizations that have supported me over the years and have made this research possible. This includes the Masonry Contractors Association of Alberta (MCAA), the Alberta Masonry Council (AMC), the Canadian Masonry Design Centre (CMDC), and the National Concrete Masonry Association (NCMA).

TABLE OF CONTENTS

LIST OF TABLES

LIST OF FIGURES

LIST OF SYMBOLS AND ABBREVIATIONS

A	Net Cross-Sectional Area of the Wall
A_h	Area of the Horizontal Reinforcement
CMU	Concrete Masonry Unit
d	Effective Width of the Wall
d'	Distance from the Extreme Vertical Reinforcement to the Edge of the Wall
E_c	Compressive Elastic Modulus
E_t	Tensile Elastic Modulus
FE	Finite Element
FG	Fully-Grouted
f'_m	Peak Compressive Strength of the Masonry Assemblage
f_s	Strut Compressive Capacity
f_{yh}	Yield Stress of the Horizontal Reinforcement
f_{yv}	Yield Stress of the Vertical Reinforcement
h	Wall Height
k_u	Reduction Factor due to the Effects of Flexure on the Tensile Reinforcement
k_p	Grouting Factor
l	Wall Width
PG	Partially-Grouted
RC	Reinforced Concrete
s	Spacing of the Horizontal Reinforcement

STM	Strut-and-Tie Model
t	Wall Out-of-Plane Thickness
β_A	Strut Inclination Factor
β_S	Strut Efficiency Factor
δ	Loading Factor
ε_{cr}	Crushing Strain of the Material
ε_p	Strain Corresponding to the Peak Compressive Strength
ε_t	Uniaxial Strain in Tension
f_c	Peak Compressive Strength
f_r	Rupture Stress
γ	Grout Confinement Factor
δ	Loading Factor
ρ_h	Horizontal Reinforcement Ratio
ρ_v	Vertical Reinforcement Ratio
σ_0	Applied Axial Stress
σ_c	Uniaxial Stress in Compression
σ_t	Uniaxial Stress in Tension

1.0 INTRODUCTION

1.1 Background

From the Egyptian pyramids to the Great Wall of China, masonry has sheltered and aided in the development of civilizations the world over and will forever be renowned for its unparallel beauty and tested durability. Whilst the legend and grandeur associated with famous masonry monoliths are immortalized, the perception of masonry as a modern building material has dwindled in recent decades. What was once the primary building material for all structures, the role of masonry in modern construction is currently limited to wall-type structural systems used to provide resistance against a combination of gravity and lateral loading. Examples of such wall systems include school gymnasiums, low- to mid-rise residential buildings, and industrial warehouses constructed in the mid to late 20th century.

Modern masonry wall systems are comprised of hollow concrete masonry units stacked upon layers of mortar (Fig. 1.1). Tensile capacity and ductility are added to the system by placing steel reinforcing bars within the hollow cells which are then consequently filled with a high slump concrete termed grout to prevent the buckling of the reinforcing bars and provide additional stiffness to the wall. The extent of the grouting distinguishes reinforced masonry walls into two categories: namely, fully-grouted walls in which all cells are grouted and partially-grouted walls where only cells containing reinforcing bars are grouted. Research over the past decade has indicated that the additional grouting featured in FG walls results in an overall structural behaviour similar to reinforced concrete systems (Banting et al., 2012; Banting, 2013; El-Dakhakhni et al., 2013; El-Hashimy et al., 2019) while the response of partially-grouted walls under loading has been reported to be more reminiscent to masonry in-filled frames (Minaie, 2009; Bolhassani et al., 2016). While fully-grouted walls are specified in areas of high seismic activity as large quantities of reinforcement are required, partially-grouted wall systems are becoming popular in low- to mid-seismic regions due to their economic advantages, ease of constructability, and lower seismic mass.

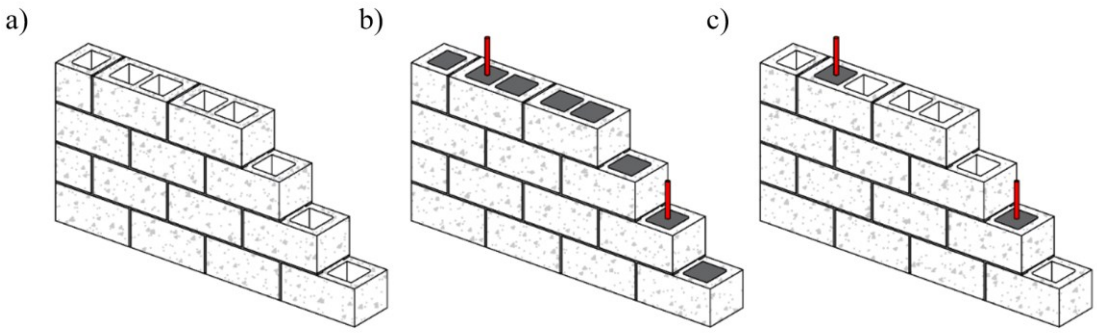

Figure 1.1 – Types of Masonry Walls (a) Unreinforced/Plain (b) Fully-Grouted (c) Partially-Grouted

Research has shown that partially-grouted masonry assemblages also hold an advantage over competing materials in terms of thermal efficiency (El-Adaway et al., 2011) and fire resistance (Furtaw and Hamid, 2004), traits commonly sought after in modern design. However, this advantage is being overshadowed by the rising concerns regarding the ability of partially-grouted masonry walls to safely resist in-plane lateral loads. The design of partially-grouted masonry walls against in-plane loading is challenging due to the complexity of the shear mechanism and the variety of failure mechanisms that may occur among the different material components of the masonry.

The first failure mechanism is flexure which is characterized by the overturning of the wall, with failure occurring once the vertical steel reinforcement at the tension heel yields in tension, followed by the crushing of the masonry at the compression toe. Compared to shear mechanisms described below, flexural mechanisms are highly desirable from a design perspective as the mode of failure is rather ductile due to the excessive yielding of the steel reinforcement and the formation of a plastic hinge near the base of the wall resulting in significant energy dissipation (Dillon, 2015; Rizaee 2015). Flexural behaviour is also well understood from a mechanics standpoint as the 'plane sections remain plane' assumption of Bernoulli beam theory has been deemed valid by several experimental studies (Mayes et al., 1976a; Shing et al., 1989; Pettit, 2020). This allows for the bending moment capacity to be determined from a conventional cross-sectional analysis which can further be translated into simple and transparent design expressions. Unfortunately, it is rather rare to encounter a partially-grouted wall system under in-plane loading governed

by flexure alone, as the relatively low effective height-to-width (aspect) ratio of the walls found in modern construction more commonly results in a shear-governed mechanism.

Shear mechanisms are a critical component at the ultimate limit state as they may prevent the wall from achieving its flexural strength and deformation capacity. Inadequate design against shear can result in brittle failure modes, which can lead to extensive loss of life or property. Within the basis of shear, there exist many categories of shear failure, which also may occur simultaneously with flexural failure. The most common mode is diagonal tension shear which is characterized by the diagonal cracking of the wall either along the mortar joints (step cracks) or directly through the masonry units. Depending on the level of applied axial stress and the distribution of the vertical reinforcement, diagonal tension shear may further be subcategorized into a brittle or ductile failure (Ghanem et al., 1992; Nolph, 2010; Dillon, 2015; Hung, 2018). Brittle failure involves the formation of a single, large diagonal crack that continuously widens until the crushing of the compression toe occurs (Fig. 1.3a). In ductile failure, the widening of the initial crack is prevented by closely distributed horizontal reinforcement, allowing for the preservation of the shear resistance (through ensuring continued aggregate interlock) and additional cracking to occur prior to failure. If large quantities of horizontal reinforcement are specified to prevent diagonal tension failure, a second failure mode associated with the crushing of the masonry along the diagonal compressive strut (termed compressive strut shear) may occur (Fig. 1.3b). A third failure mode involving the sliding of the wall along the mortar bed joints (termed sliding shear failure) has also been observed (Sveinsson et al., 1985) in walls containing little to no vertical reinforcement under light axial stresses (Fig. 1.3c). Henceforth, attention will be focused on diagonal tension shear failure (which will be referred to as 'shear failure') as (a) sliding shear is often prevented in partially-grouted walls due to the combination of the axial load placed on the wall and the dowel action provided by the vertical reinforcing bars and (b) compressive strut shear mainly occurs in fully-grouted walls as partially-grouted walls typically lack the large quantities of horizontal reinforcement required to prolong diagonal tension failure to the point where crushing of the compressive strut occurs.

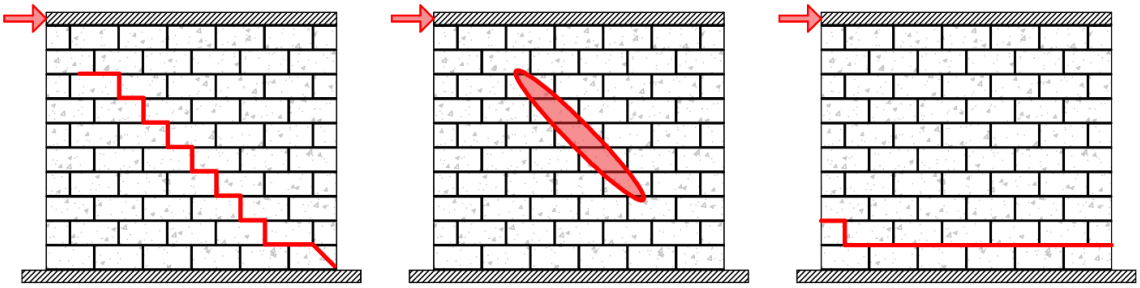

Figure 1.2 – Shear Failure (a) Diagonal Tension (b) Compressive Strut (c) Sliding

The task of providing reliable design provisions to accurately predict the shear capacity of partially-grouted masonry walls has proven challenging. This can be attributed to many factors, including the complexities of the shear mechanism (Park and Paulay, 1975), analytical challenges associated with the heterogeneous, anisotropic, and nonlinear nature of the masonry assemblage, and the limited pool of available experimental and numerical studies in the literature. In consequence, both the Canadian and American masonry design provisions (CSA S304-14 and TMS 402-22, respectively) specify semi-empirical equations to predict the diagonal tension shear capacity of reinforced masonry walls. An additional upper limit is placed on the calculated shear capacity in both standards to ensure that compressive strut shear failure does not occur. While these expressions provide designers with a straightforward methodology to predict the shear capacity of reinforced masonry walls, experimental and analytical research has suggested the performance of the supplied expressions is poor when applied to partially-grouted walls (Voon and Ingham, 2006; Minaie, 2009; Nolph, 2010; Elmapruk, 2010; Dillon, 2015; Hung, 2018; Izquierdo Duque, 2021). This poor performance can mainly be attributed to the expressions being formulated on outdated experimental programs primarily comprised of fully-grouted specimens (Chen et al. 1978; Hidalgo et al. 1978; Hidalgo et al. 1979; Sveinsson et al. 1985; Okamoto et al. 1987; Matsumura 1987; Shing et al. 1990b). While originally derived for fully-grouted walls, the shear capacity design expressions were later adapted to account for partially-grouted walls through the addition of a single reduction factor. Even with this factor, these expressions still fail to include common design parameters such as wall openings and vertical reinforcement distribution, which have been experimentally and analytically shown to influence the shear capacity of the wall (Matsumura, 1988; Voon and Ingham, 2008; Nolph, 2010; Elmapruk, 2010; Dillon, 2015; Hung, 2018; Izquierdo Duque, 2021).

Limitations are expected, however, as the numerous failure modes and complexities of the shear-resisting mechanism of partially-grouted walls restrict the notion that the shear capacity of partially-grouted walls can be accurately defined by a single semi-empirical equation. Therefore, it is necessary to develop a new design methodology to predict the diagonal tension shear capacity of partially-grouted wall systems.

To address the issue of the inconsistent and potentially unsafe in-plane shear capacity design provisions listed in the Canadian and American masonry design standards, this study presents the development of strut-and-tie modelling (STM)-based design provisions capable of accurately predicting the in-plane shear capacity partially-grouted concrete block masonry walls. The foundation of the provisions is based on adapting the strut-and-tie modelling methodology currently specified for reinforced concrete structures to partially-grouted masonry construction. A detailed analysis model for partially-grouted walls subjected to in-plane loads was developed using state-of-the-art finite element (FE) detailed micro-modelling techniques and calibrated specifically for North American masonry wall systems. After validation by several experimental studies from the literature, the finite element model was employed to conduct an extensive parametric study to (a) obtain the required insights into the behaviour of shear-critical partially-grouted walls required to develop partially-grouted-specific STM provisions and (b) quantify the influence of key design parameters on the in-plane shear capacity of partially-grouted masonry walls. Examples of required STM parameters include stress trajectories, geometry and capacity of compressive struts, and the location of nodal zones, while common design parameters include the vertical and horizontal reinforcement spacing and quantities, aspect ratio, applied axial stress, and reinforcement type (e.g., bond-beam vs bed-joint horizontal reinforcement).

The ability of the partially-grouted-specific STM provisions to predict the in-plane strength of shear-critical partially-grouted walls is then compared against experimental results and code equations from Canadian and American masonry standards. It is expected that the partially-grouted STM methodology obtained in this study can be readily codified to provide designers and researchers with a transparent, mechanics-based design tool that improves the safety and economy of partially-grouted masonry wall construction.

1.2 Problem Statement

The in-plane shear capacity expressions in both Canadian and American masonry design provisions (CSA S304-14 and TMS 402-22, respectively) have been found to be inconsistent and potentially unconservative when predicting the diagonal tension shear capacity of partially-grouted masonry walls (Voon and Ingham, 2006; Elmapruk, 2010; Minaie et al., 2010; Nolph, 2010; Dillon, 2015; Hung, 2018; Izquierdo Duque, 2021; Ba Rahim, 2022). The poor performance of the diagonal tension shear expressions present in both design standards can be traced to three major factors: (1) the parameters contributing to the shear mechanism of partially-grouted walls are not well defined due to the lack of analytical and experimental studies found in the literature, (2) the current design expressions for predicting the diagonal tension shear capacity were derived based on research programs focusing primarily on fully-grouted concrete block and clay brick walls (Chen et al. 1978; Hidalgo et al. 1978; Hidalgo et al. 1979; Sveinsson et al. 1985; Okamoto et al. 1987; Matsumura 1987; Shing et al. 1990b), and (3) it is unlikely that the shear response of a partially-grouted wall under in-plane loading can be captured with a single semi-empirical expression, given the large number of parameters that appear to influence the response of the walls tested in previous studies.

As the current Canadian and American in-plane shear strength design provisions are potentially unsafe, there exists a need to develop a new diagonal tension shear capacity design methodology. The developed methodology should be as transparent as possible and mechanics-based, facilitating the incorporation of the methodology into existing design standards with relative ease. The methodology should also realistically capture and quantify the role of common design parameters in resisting diagonal tension shear. Examples of design parameters known to influence the diagonal tension shear capacity of partially-grouted walls include the aspect ratio, quantity of horizontal and vertical reinforcement, distribution of vertical reinforcement, different types of horizontal reinforcement, applied axial stress, and the extent of grouting. Finally, the methodology should incorporate and be consistent with the behavioural findings of all documented experimental programs involving partially-grouted masonry walls failing in diagonal tension shear.

1.3 Objectives, Methods, and Scope

The primary outcome of this study is to develop mechanics-based and transparent strut-and-tie design provisions to accurately predict the in-plane shear capacity of partially-grouted masonry wall systems. To achieve the primary outcome of the study, the following specific objectives and tasks required to achieve each specific objective are identified:

1. *Develop a detailed finite element micro-model to accurately predict the in-plane shear capacity and assess the behaviour of partially-grouted concrete block masonry walls.*
   - Determine the viability of commercially available finite element software to conduct detailed simulations of masonry structures by attempting to replicate South American experimental programs in which all micro-modelling parameters are known.
   - Conduct experimental component testing to determine the parameters required to define the masonry block–mortar interface of North American masonry materials.
   - Develop a detailed finite-element micro-modelling methodology suitable for North American partially-grouted walls with the capabilities of assessing the global and local behaviour of the wall system.
   - Validate the model with several experimental programs available in the literature to assess the performance of the model to predict the shear capacity of walls with varied material strengths, aspect ratios, applied axial stresses, vertical and horizontal reinforcement distributions and quantities, and boundary conditions.
2. *Perform an extensive parametric study using the detailed micro-model developed in Objective 1 to quantify the role of different design parameters on the in-plane shear capacity of partially-grouted wall systems and determine the stress trajectories required to facilitate the development of a partially-grouted STM model.*
   - Define the fixed, independent, and dependent parameters of the parametric study.
   - Conduct the parameter analysis to quantify the roles of the aspect ratio, applied axial stress, quantities and spacing of both vertical and horizontal reinforcement, and horizontal reinforcement type on the in-plane shear capacity.
3. *Develop a strut-and-tie design methodology with the ability to accurately predict the in-plane shear capacity of partially-grouted concrete-block masonry walls.*

- Develop the masonry-specific strut-and-tie model to predict the in-plane shear capacity of partially-grouted masonry walls using a combination of insights obtained from the validation of the micro-model in Objective 1 and the results of the parametric study conducted in Objective 2.
- Validate the ability of the proposed strut-and-tie model to predict the shear capacity of partially-grouted walls with experimental studies available in the literature.
- Summarize the developed strut-and-tie methodology in a series of logical and transparent steps to facilitate the adaptation into existing design provisions.

The outcomes specified in this study are limited to North American partially-grouted concrete block masonry walls without openings under typical roof-type in-plane loading. Wall systems classified as fully-grouted or unreinforced/plain, in addition to wall systems consisting of solid or perforated clay brick units, were not considered. In addition, the strength prediction of the finite element micro-model and STM-based analysis model will be limited to walls failing in diagonal tension shear, meaning that walls that have a ductile (or flexural) mode of failure will not be considered. Other forms of failure, including in-plane or out-of-plane flexural, sliding shear, or instability, were also not considered.

Due to the complexity of capturing the true cyclic response of the masonry unit–mortar and masonry unit–grout interfaces, a simplified interface developed using off-the-shelf constitutive models was implemented. This limits the accuracy of the detailed finite element micro-modelling to monotonic loading. No attempt was made to develop advanced interfaces that incorporate the cyclic degradation of the interfaces, as the shear capacity of a specimen (the main parameter of interest in this study) can be captured reasonably well with monotonic analysis.

1.4 Organization of Thesis

This thesis is organized into six chapters. In Chapter 1, an introduction to the study and problem statement are presented, followed by a discussion of the study objectives, selected methodology, and scope.

In Chapter 2, the literature review is presented. The literature review begins with a detailed summary of how the current Canadian and American in-plane shear capacity design provisions for masonry walls were formulated, followed by the presentation of several experimental and analytical campaigns suggesting the limited capabilities of the design provisions to accurately predict the in-plane shear capacity of partially-grouted masonry wall systems. Methodologies used to predict the in-plane shear capacity of reinforced concrete structures are then presented, followed by a discussion on the adaptability of each methodology to masonry structures. The literature review concludes with a discussion on the development of detailed finite element micro-models and how several research groups have employed such models to determine the behavioural insights required to advance the understanding of masonry wall behaviour.

In Chapter 3, the development of the detailed finite element micro-model is presented. The finalized micro-model is then validated with several experimental studies from the literature that involve varied material strengths, aspect ratios, boundary conditions, applied axial loading, quantities and spacings of vertical and horizontal reinforcement, and different reinforcement types.

In Chapter 4, the details and results of an extensive parametric study conducted to identify and quantify the influence of key design parameters on the in-plane shear capacity of partially-grouted masonry walls are presented.

In Chapter 5, the development of the strut-and-tie methodology specific to partially-grouted wall systems is presented and discussed. Validation of the methodology in terms of predicting the in-plane shear capacity and the ability of the model to resemble experimental observations with select experimental studies available in the literature is also presented.

In Chapter 6, the results and conclusions of the study are presented, in addition to providing recommendations for future research.

2.0 LITERATURE REVIEW

2.1 Introduction

This chapter presents the historical development of the in-plane shear capacity expressions present in the Canadian (CSA S304-14) and American (TMS 402-22) masonry standards. Several experimental and analytical studies focused on the performance of the supplied design provisions are then presented, followed by a discussion on the methodologies employed by reinforced concrete researchers to predict the in-plane shear capacity of wall-type systems. Finally, recent advances in the detailed finite element modelling of masonry wall systems and how such techniques can be implemented to better understand the behaviour of masonry systems under in-plane shear are presented and discussed.

2.2 Formulation of North American In-Plane Shear Strength Design Equations

The foundation of the in-plane shear capacity expressions found in the Canadian and American masonry design provisions can be traced to the experimental observations and data of several studies conducted at the University of California Berkeley, Kanagawa University, and the University of Colorado between the mid-1970s and early-1990s. This collection of over 200 tests was conducted in part of a larger effort by the Technical Coordinating Committee on Masonry Research (TCCMAR) to develop limit state design philosophies for masonry structures (TCCMAR, 1986). Details and findings of the conducted tests in chronological order are summarized below.

2.2.1 University of California, Berkeley Experimental Research Program

Founded in 1969, the U.S. – Japan Cooperative Program in Natural Resources (UJNR) Panel on Wind and Seismic Effects developed a series of joint research programs devoted to developing, implementing, and exchanging wind and seismic technologies between the U.S. and Japan. Following successful programs focused on steel and reinforced concrete structures, the panel shifted their attention to masonry structures. Prior to this, only a handful of investigative programs involving masonry walls had been conducted

(Schneider, 1959; Scrivener, 1966; Scrivener, 1969; Meli, 1972). At the time, masonry walls were constructed in a monolithic fashion with exterior walls spanning several stories high and containing multiple openings (Fig. 2.1). These perforated walls consist of two key components: piers (red shaded area in Fig. 2.1) which span vertically between window openings and spandrel beams (blue shaded area in Fig. 2.1), which span horizontally above and below window openings. In two detailed reports, Mayes and Clough (Mayes and Clough, 1975a; Mayes and Clough, 1975b) identified the masonry piers as the critical lateral load resisting mechanism of the wall system under in-plane loading as many piers were observed to exhibit a shear-type failure under seismic excitation.

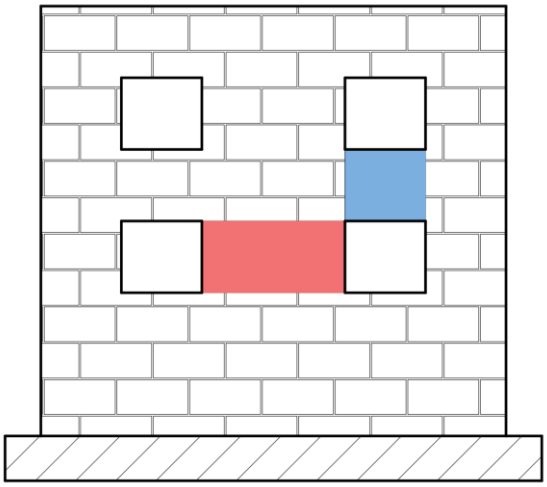

Figure 2.1 – Perforated Masonry Walls

To investigate the behaviour of the masonry piers, Mayes et al. (Mayes et al., 1976a; Mayes et al. 1976b) launched an experimental campaign consisting of 17 double-pier specimens at the University of California, Berkeley. The objectives of the test were to determine the effect of applied axial stress, the rate of loading, the distribution and quantity of the horizontal reinforcement, the quantity of vertical reinforcement, and the effect of partial grouting on the strength and deformation properties of the piers. The double-pier specimens consisted of two piers connected to one another with heavily reinforced spandrels at the top and bottom of each pier (Fig. 2.2). The spacing between the two piers was 1.8 m. Each pier was constructed with 15-cm concrete masonry units

and nominally measured 1.6 m in height and 0.8 m in width. Details of the reinforcement scheme for each pier specimen are also illustrated in Fig. 2.2.

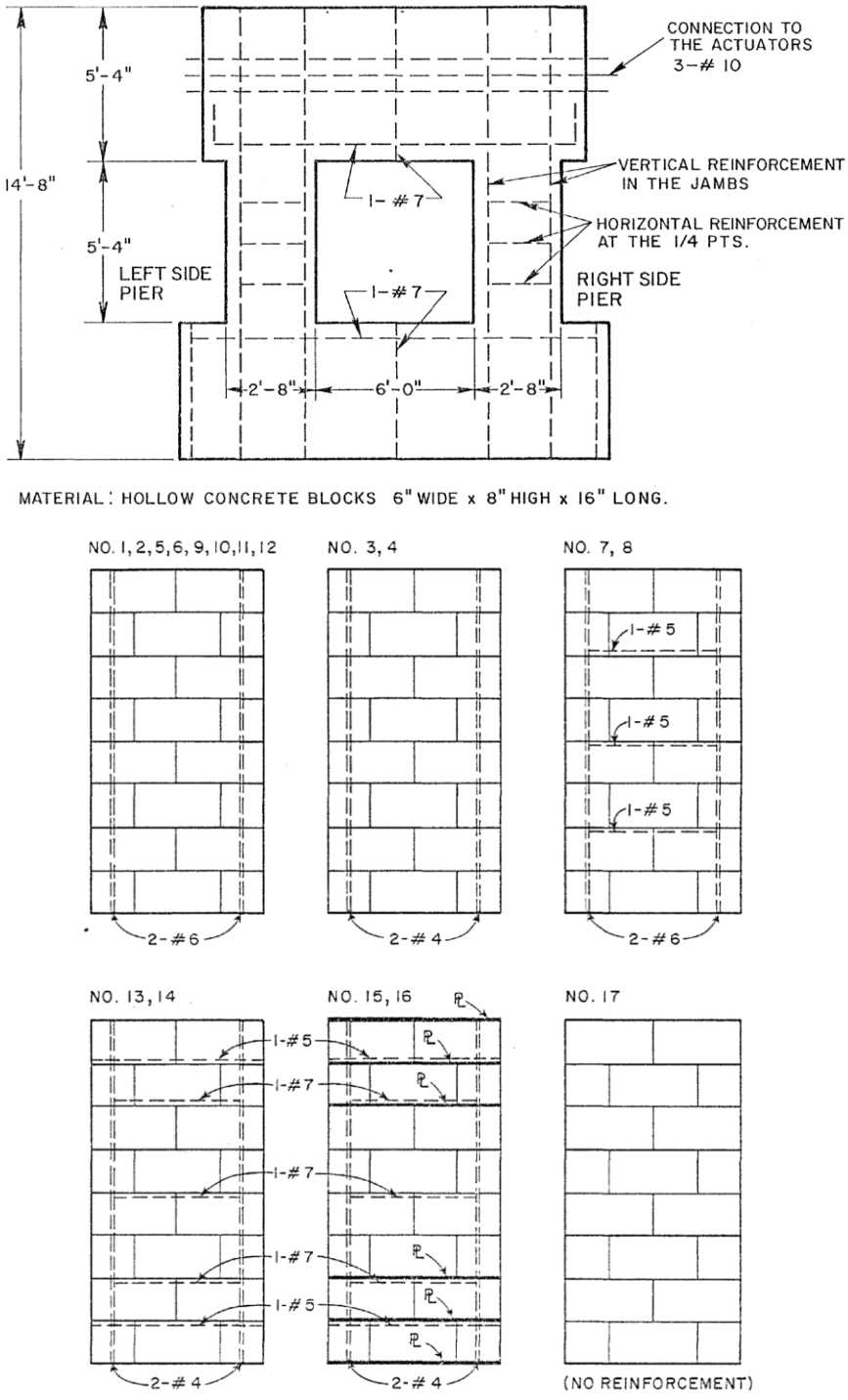

Figure 2.2 – Masonry Double-Pier Specimens Geometry and Reinforcement Details (Mayes et al., 1976a)

Figure 2.3 depicts the double-pier testing setup. Except for a single unreinforced specimen, all specimens were tested in pairs, with the first specimen tested under pseudo-static conditions while the second specimen was tested under dynamic conditions. The testing sequence of the specimens consisted of first applying an axial stress followed by the application of a cyclic lateral load at the top of the pier specimen. Rollers were placed along the top of the wall to prevent any rotation resulting in a fixed-fixed boundary condition. This was said to mimic the realistic condition provided by a reinforced concrete floor slab connected to the top of the wall system. The applied level of axial stress varied between 0 MPa and 3.45 MPa, with 13 out of the 17 specimens featuring an applied axial stress of either 0.86 MPa or 1.73 MPa.

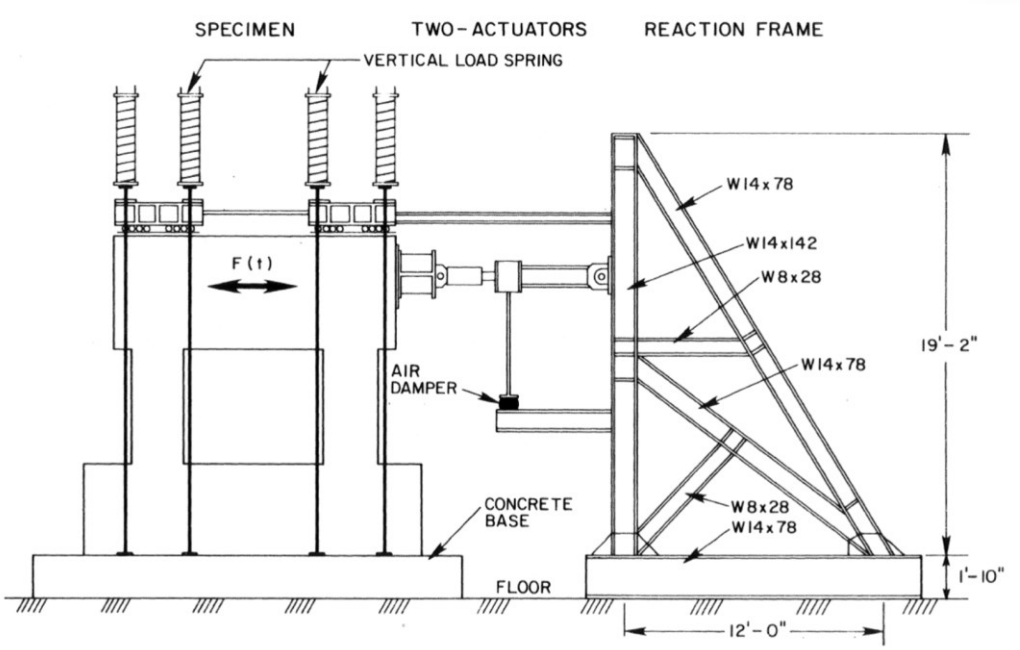

Figure 2.3 – Double-Pier Test Setup (Mayes et al., 1976a)

Observations from the test indicated that three modes of failure are possible: diagonal tension shear failure, flexural failure, and a combined flexure-shear failure. The most common failure observed was diagonal tension shear failure. Results from the tests indicated that the shear capacity of the piers is heavily influenced by the quantity of horizontal reinforcement, with the authors stating that the increase in shear capacity is approximately equivalent to the total area of horizontal steel multiplied by the yield

strength of the steel. An increase in applied axial stress was also found to increase the shear capacity of the piers. Partially-grouted specimens were observed to fail at lower levels of applied lateral load when compared to FG specimens. However, it was found that both specimens failed at similar values of applied shear stress. The inclusion of bed-joint reinforcement in the form of steel plates was found to significantly improve the ductility of the system but did not contribute to an increase in shear capacity.

With the double-pier testing concluded, attention was turned to a more extensive single-pier testing campaign. The overall campaign encompassed the testing of 63 single-pier specimens under fixed-fixed boundary conditions (Hidalgo et al., 1978; Chen et al., 1978; Hidalgo et al., 1979, Sveinsson et al., 1981). Of the 63 specimens tested, 17 pier specimens were constructed with 20-cm concrete masonry units, 28 were constructed with clay brick, and the remaining 18 were constructed as double-wythes. The main objective of the program mirrored the double-pier testing program in which relationships between design parameters and the resulting shear and deformation capacities of the pier specimens were sought. Investigated design parameters include the type of masonry construction (concrete masonry unit, clay brick, and double-wythe), height-width ratio, type of grouting, the quantity and distribution of the horizontal reinforcement, and the quantity of vertical reinforcement. Unlike the previous double-pier tests, however, the applied axial stress and loading rate were held constant.

Testing of the 63 specimens was subdivided into three groups based on the height-width ratios of the piers tested. Investigated height-width ratios include 0.5, 1.0, and 2.0. Figure 2.4 below depicts the test setup used for all single-pier specimens. All pier specimens were tested in an identical sequence in which an axial stress of 0.38 MPa was applied and then held while a lateral load was applied cyclically to the top of the pier until failure occurred. Steel columns were placed between the foundation and top beam to restrict the rotation of the pier, thus simulating fixed-fixed boundary conditions.

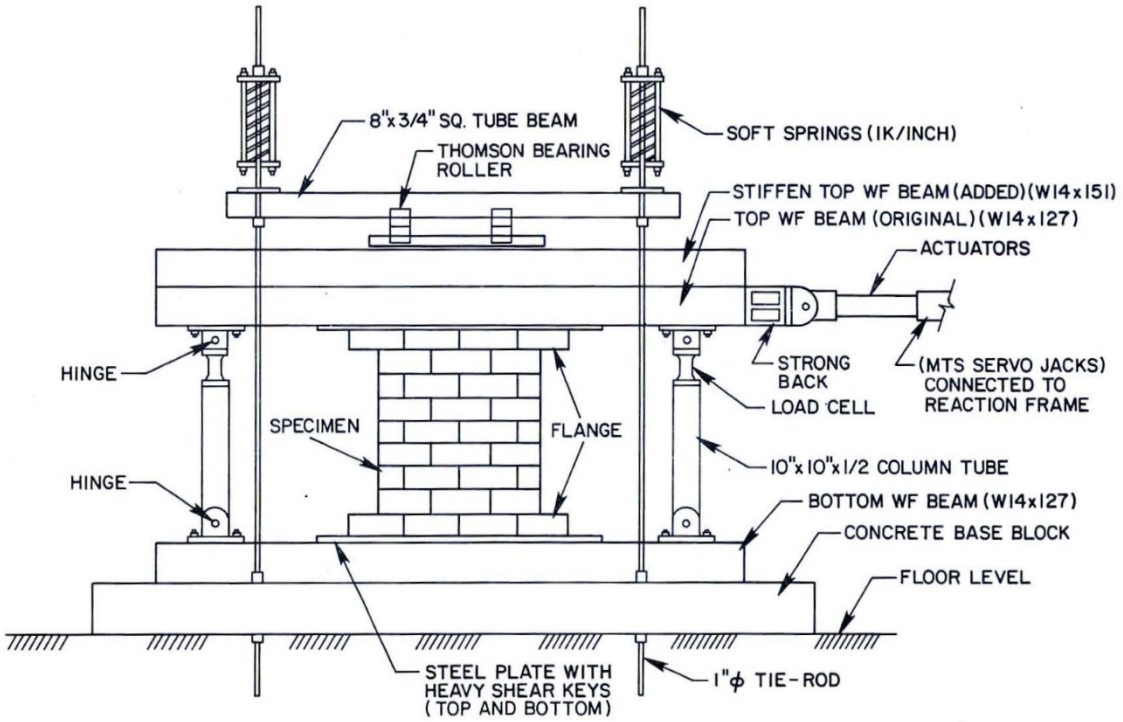

Figure 2.4 – Single-Pier Test Setup (Sviensson et al., 1981)

The first series of tests conducted by Hidalgo et al. (Hidalgo et al., 1978) involved the testing of 14 masonry pier specimens (nine clay brick and five double-width) with a height-width ratio of 2.0. It is noted that no concrete block specimens were included in this series. Pier specimens in this series nominally measured 2.0 m in height and 1.0 m in width. Conclusions from the series were rather inconclusive as many parameters found to influence the shear strength of clay brick piers did not influence the shear strength of the double-wythe piers. For instance, it was observed that an increase in horizontal reinforcement increased the shear capacity of clay brick pier specimens but had a negligible effect on the shear capacity of the double-wythe pier specimens.

The second series of tests conducted by Chen et al. (Chen et al., 1978) investigated a height-width ratio of 1.0 and involved the testing of 31 masonry pier specimens (eleven concrete block masonry, thirteen clay brick, and seven double-wythe). Pier specimens in this series nominally measured 1.4 m in height and 1.2 m in width. Reinforcing detailing of the concrete masonry unit specimens can be found in Fig. 2.5 below. All concrete masonry unit specimens tested displayed a shear mode of failure characterized by early

flexural cracks near the tension heel followed by diagonal cracking. Of the 11 concrete block specimens tested, seven were fully-grouted, and four were partially-grouted. While it was observed that all partially-grouted specimens resisted less load than their fully-grouted counterparts, the ultimate shear stress of the partially-grouted specimens was up to 22% larger when compared to fully-grouted specimens. Regarding the effect of horizontal reinforcement, it was generally observed that the addition of horizontal reinforcement to the pier system increased the shear capacity of the specimen when compared to unreinforced specimens. No significant increase in shear capacity was found when increasing the quantity of vertical reinforcement.

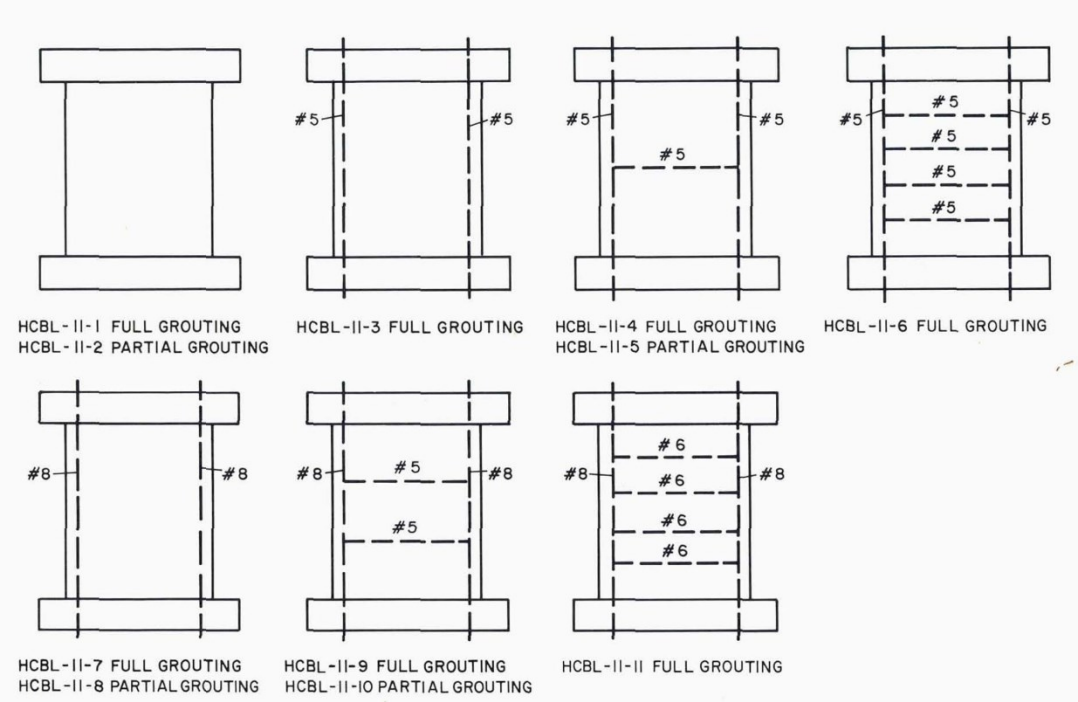

Figure 2.5 – Single-Pier Specimen Reinforcing Details (Chen et al., 1978)

In the final test series, Hidalgo et al. (Hidalgo et al., 1979) conducted 18 masonry pier tests (six concrete masonry unit, six clay brick, and six double-wythe) with a height-width ratio of 0.5. Pier specimens in this series nominally measured 1 m in height and 2 m in width. Reinforcement detailing of the concrete masonry unit specimens can be found in Fig. 2.6 below. All 6 of the concrete masonry unit specimens tested were FG and exhibited a shear-type failure, with four specimens failing in diagonal tension shear and

the remaining two failing in sliding shear. The authors reported that after the first diagonal crack, the lateral resistance of the wall was mainly carried through diagonal compressive struts bounded by the diagonal cracks. This behaviour was also reported by Park and Pauley (1975). Similar to Chen et al., it was observed that the quantity of horizontal reinforcement has an influence on the shear capacity of the pier specimen, with the conclusion that the addition of horizontal reinforcement generally results in increased shear strength. It was reported, however, that after a certain threshold, increased amounts of horizontal reinforcement resulted in a lower shear capacity.

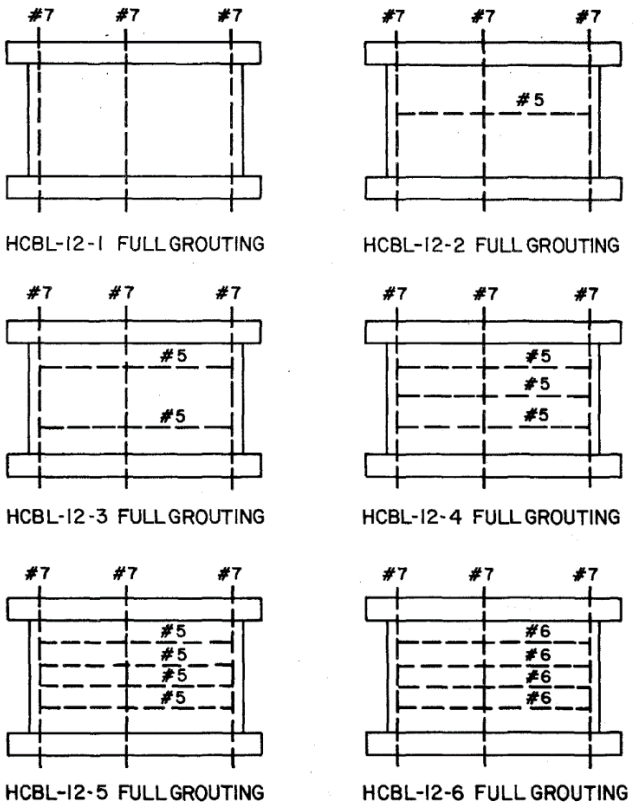

Figure 2.6 – Single-Pier Specimen Reinforcing Details (Hidalgo et al., 1979)

While testing the single-pier specimens, the authors noticed a deficiency in the testing setup in which the steel columns used to restrain the rotation at the top of the wall would induce additional compressive stresses on the test specimens. This resulted in an applied axial stress roughly 3 and 5 times larger than specified for the Chen et al. (1979) and Hidalgo et al. (1979) studies, respectively. To provide a more reliable testing dataset,

Sveinsson et al. (1985) conducted an additional 32 single-pier tests using a modified test setup (Fig. 2.7). In this modified setup, the axial load was applied through two actuators which would simultaneously control the rotation along the top of the wall to ensure the fixed-fixed (double-curvature) boundary condition.

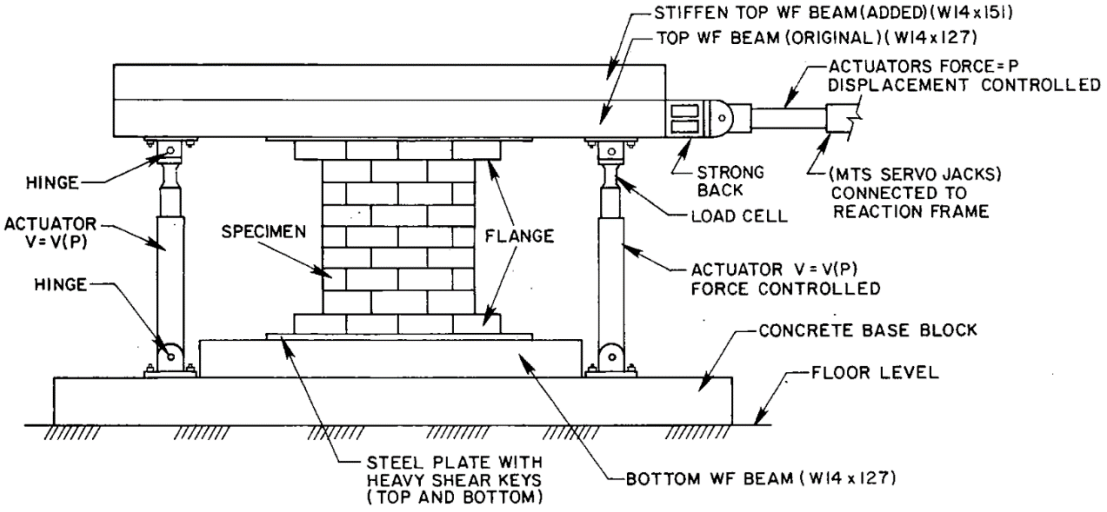

Figure 2.7 – Modified Single-Pier Test Setup (Sviensson et al., 1985)

Of the 32 specimen's pier specimens tested by Sviensson et al. (1985), 12 consisted of 20-cm concrete masonry units, 13 consisted of clay bricks, while the remaining 5 were double-wythes. All pier specimens were fully grouted and nominally measured 1.2-m in height and 1.0-m in width. Both the vertical and horizontal reinforcement quantities and distributions were varied between specimens. Reinforcement details of the concrete masonry unit specimens can be found in Fig. 2.8 below. Additional parameters investigated include the anchorage of the horizontal reinforcement (90º bends, 180º hooks, and steel embedment plates) and the placement of dur-o-wal reinforcement in select specimens which resembled modern-day bed-joint reinforcement. Testing of the wall was conducted in the same manner as the previous tests in which an axial stress was applied and held while a cyclic lateral load was applied to the top of the pier specimen. The magnitude of applied axial stress ranged from 1.72 MPa to 2.76 MPa.

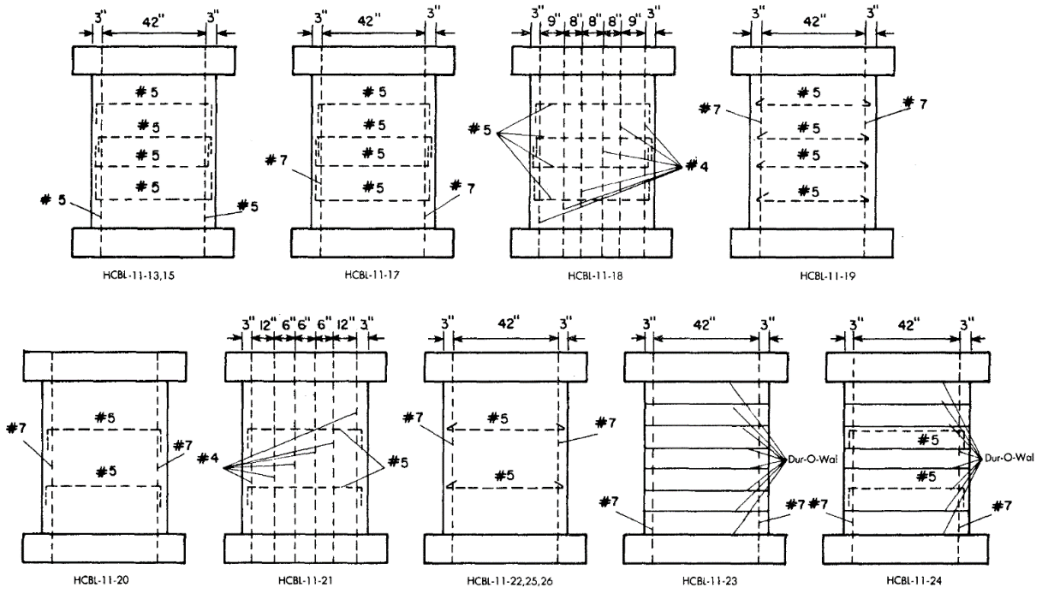

Figure 2.8 – Single-Pier Specimen Reinforcing Details (Sviensson et al., 1985)

Test observations indicated that the shear-resisting mechanisms of the piers were similar to that reported in Hidalgo et al. (1979) in compressive struts would form throughout the pier diagonals after cracking was initiated. The authors reported that if the specimen contained adequate amounts of horizontal reinforcement, the initial cracks did not open further under the increasing lateral load, but rather additional cracks would form, resulting in a ductile shear failure. Specimens featuring a light amount of horizontal reinforcement or inadequate anchorage exhibited a more brittle shear failure mode as the initial crack would continuously widen under the increasing axial load. Sliding shear failure and flexural failure were also observed for specimens featuring low amounts of vertical reinforcement and specimens under light axial loads, respectively.

The applied axial stress was reported to be the most influential factor impacting the shear capacity of the specimens. Specimens under higher axial loads would exhibit an increase in shear capacity at the expense of ductility. Regarding the effect of the horizontal reinforcement on the shear capacity of the specimens, the authors noted that only the concrete masonry unit specimens appeared to be influenced. Results from the tests indicated that doubling the amount of horizontal reinforcement increased the shear capacity of the pier by 16%. Similar to the results reported by Chen et al. (1979),

increasing the amount of vertical reinforcement resulted in an insignificant change in the shear capacity of the concrete masonry unit specimens.

Anchorage of the shear reinforcement was found to impact both the strength and deformation capacity of the specimens. The authors reported that specimens with 180º hooks were able to sustain higher lateral loads and increased deformations than those featuring 90º bends, as the 90º bends would straighten out during loading resulting in the gradual loss of anchorage. While testing was limited, the authors concluded that shear reinforcement consisting of reinforcing bars grouted within the masonry cells (bond beam reinforcement) outperformed shear reinforcement consisting of wire mesh placed within the mortar joints (bed-joint reinforcement) as no increase in shear capacity was observed with bed joint reinforcement. However, bed joint reinforcement was observed to improve the ductility of the specimen.

2.2.2 Kanagawa University Experimental Research Program

Matsumura (1987, 1988) tested a total of 90 masonry shear walls, of which 60 were constructed with hollow concrete masonry unit walls while the remaining 30 were constructed with clay brick. Two testing methods were adopted. The first method was to test the walls vertically with cantilever boundary conditions. The second method involved laying the wall specimens down horizontally and applying vertical shear loads like the restrained deep beam tests. Details of the two test methods are shown in Fig. 2.9 below.

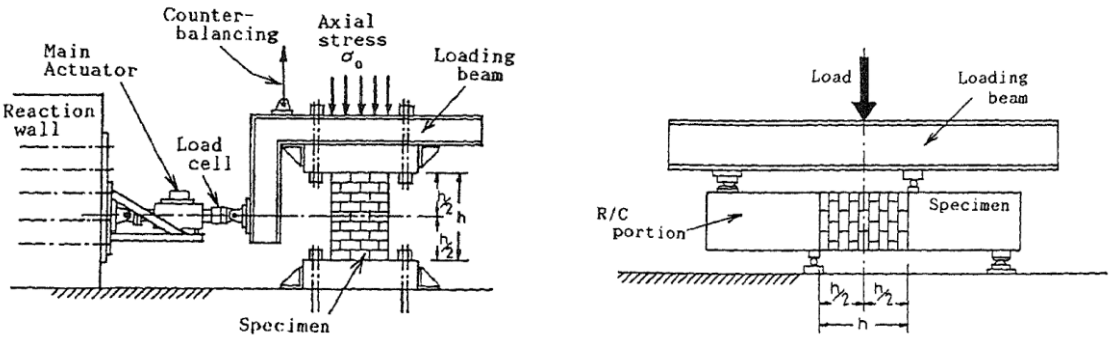

Figure 2.9 – Test Setup (Matsumura, 1988)

Parameters investigated included the widths of the masonry units (15-cm and 20-cm units), the applied axial stress, the horizontal shear reinforcement ratio, and the wall aspect ratio. The results indicated that the positive relationship between the prism strength and the maximum shear strength is not linear. Instead, the maximum shear capacity increased approximately proportionate to the square root of the prism strength. The axial stress, on the other hand, appeared to have a positive linear relationship with the maximum shear strength. The maximum shear strength appeared to increase as the horizontal reinforcement ratio increased. The normalized shear strength (ultimate shear strength divided by the square root of prism strength) was found to decrease as the aspect ratio increased.

Okamoto et al. (1987) tested a total of 35 masonry shear wall specimens (25 walls constructed with concrete masonry units, six walls constructed with clay bricks, and three walls constructed with reinforced concrete) under cyclic lateral loading. Five parameters were considered, including the axial stress, the size and spacing of the shear reinforcement, the size of the flexural reinforcement, the shear span ratio, and the presence of spiral confining reinforcement in the compression toe of the wall. All wall specimens were tested under fixed-fixed (double-curvature) boundary conditions. The results indicated that the maximum shear capacity increased as the axial stress increased while the relationship was not linear. The amount of shear reinforcement, however, did not appear to impact the ultimate shear strength. Also, the ultimate shear strength increased as the wall aspect ratio decreased.

2.2.3 Tests Conducted at the University of Colorado

Shing et al. (Shing et al., 1989; Shing et al., 1990a; Shing et al., 1990b; Shing et al., 1991) tested a total of 24 fully-grouted cantilever masonry walls under a combination of axial and cyclic/monotonic loading at the University of Colorado. Two types of masonry units (i.e., 15-cm hollow concrete masonry units and 10-cm hollow clay bricks) were used to construct the wall specimens. All the wall specimens tested measured 1.8 m in both height and width, resulting in an aspect ratio of 1.0. Due to the limitations on the number of specimens, three parameters were varied for the experimental study. The selected

parameters included the quantity of vertical reinforcement (vertical reinforcement ratios (ρ_v) considered include 0.38%, 0.54% and 0.74%), the quantity of horizontal reinforcement (horizontal reinforcement ratios (ρ_h) considered include 0.14% and 0.24%) and the magnitude of applied axial stress (0 MPa, 0.69 MPa, and 1.86 MPa). A schematic of the test set-up is presented in Fig. 2.10 below:

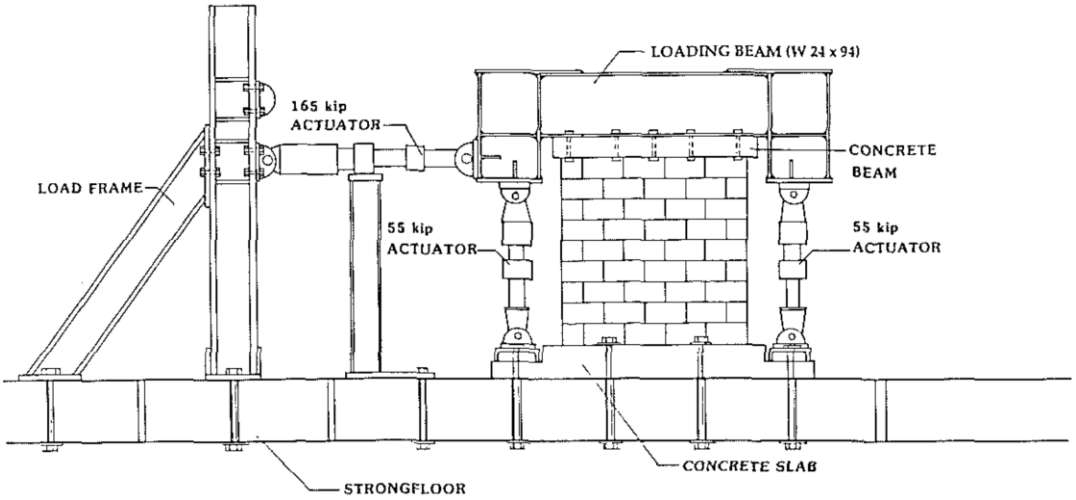

Figure 2.10 – Experimental Test Setup (Shing et al., 1989)

According to Shing et al., the normalized shear strength (the maximum shear stress divided by the square root of the compressive strength of masonry) increased from 4.2 (ρ_v = 0.74%; ρ_h = 0.14%) when zero axial compressive stress was applied, to between 3.0 (ρ_v = 0.38%; ρ_h = 0.14%) and 4.4 (ρ_v = 0.74%; ρ_h = 0.14%) for applied an axial stress of 0.69 MPa, and then to between 4.3 (ρ_v = 0.38%; ρ_h = 0.14%) and 6.0 (ρ_v = 0.74%; ρ_h = 0.24%) when 1.86 MPa of axial stress was applied. The results indicated that the shear capacity of the specimens increased as the axial compressive stress increased and when the vertical reinforcement ratio increased. However, the influence of the horizontal reinforcement ratio on the shear capacity of the specimens appeared to be inconsistent, as the first increase in horizontal reinforcement led to a negligible increase in in-plane shear capacity. However, a further second increase resulted in a shear capacity increase of approximately 20%.

The influence of different masonry unit types on the shear capacity was also negligible. Even though the material properties of hollow clay bricks were much different from hollow concrete blocks, the performances were similar. Meanwhile, the results regarding different load histories (i.e., cyclic versus monotonic loading) indicated that cyclic loading led to a lower shear strength.

2.2.4 Development of In-Plane Shear Strength Equations

The experimental data and observations of the conducted tests were subsequently used to derive semi-empirical expressions for predicting the in-plane shear capacity of reinforced masonry walls. The first attempts at creating expressions were that of Matsumura (1988) and Shing et al. (1990b), who formulated expressions based on the mechanics of the shear mechanisms observed and performed regression techniques with the data produced from their respective studies. The overall goal was to replace the current design standard expressions provided by the Uniform Building Code (ICBO,1988), which Shing et al. described as oversimplistic. The proposed equations by Matsumura and Shing et al. are presented by Eqns. 2.1 and 2.2, respectively. It is noted that the presented equations by Matsumura and Shing et al. are in metric and imperial units, respectively.

$$V_{u,\text{Matsumura}} = \frac{7td}{8}\left[k_u k_p \left(\frac{0.76}{(h/d)+0.7} + 0.012\right)\sqrt{f'_m} + 0.18\gamma\delta\sqrt{\rho_h f_{yh} f'_m} + 0.2\sigma_o\right] \quad (2.1)$$

$$V_{u,\text{Shing et al.}} = \left(0.0018\rho_v f_{yv} + 2\right)A\sqrt{f'_m} + \left(\frac{l-2d'}{s} - 1\right)A_h f_{yh} + (0.0018\sigma_o)A\sqrt{f'_m} \quad (2.2)$$

Where t is the thickness of the wall, d is the effective width of the wall (distance from the extreme compressive fibre to the outermost tensile reinforcement), k_u is a reduction factor due to the effects of flexure on the tensile reinforcement, k_p is a grouting factor (equal to 1.0 for fully-grouted walls and 0.64 for partially-grouted walls), h is the height of the wall, f'_m is the compressive strength of the masonry assemblage, γ is a grout confinement factor, δ is a loading factor, ρ_h is the shear reinforcement ratio, f_{yh} is the

yield strength of the shear reinforcement, σ_o is the applied axial stress, ρ_v is the vertical reinforcement ratio, f_{yv} is the yield strength of the vertical reinforcement, A is the net cross-sectional area of the wall, l is the width of the wall, d' is the distance of the extreme vertical reinforcement from the edge of the wall, s is the vertical spacing of the shear reinforcement, and A_h is the area of shear reinforcement.

An examination of equations reveals that both expressions predict the shear capacity of the masonry as the algebraic sum of the shear resistance contributed by the masonry, the shear reinforcement, and the axial stress acting on the wall. Differences also exist between the two expressions. For instance, the expression proposed by Matsumura heavily relies on data regression to determine the shear-resisting contributions of both the masonry and the shear reinforcement and does not consider the influence of the vertical reinforcement. Conversely, Shing et al. employed data regression to solely determine the contribution of the masonry to resist shear, while the contribution of the shear reinforcement was determined from a mechanics-based approach in which a 45º shear crack angle was assumed based on experimental observations. Other key distinctions between the two expressions include the incorporation of vertical reinforcement to the shear contribution of the masonry in the proposed equation by Shing et al. and the inclusion of a grouting parameter into the equation proposed by Matsumura, which extends the validity of the equation to partially-grouted walls.

2.2.5 Current Design Expressions

The development of the current design expressions largely stemmed from the general observations of the three experimental programs listed above. First, the effect of applied axial stress was found to considerably influences the shear capacity, failure mode, and ductility of the wall systems. All experimental programs noted that as the applied axial stress increased, an increase in shear capacity and a reduction in ductility were observed. In addition, the mode of failure would shift from flexural to diagonal tension shear or a combination of flexure and shear depending on the applied axial stress. Sveinsson et al. (1985) explained that the applied compression field must first be overcome to develop tensile stresses in the system. This, in turn, delays both the yielding of the flexural

reinforcement (hence the shift from flexural to shear failure and reduction in the ductility of the system) and the development of principle tensile stresses along the diagonal cracks resulting in an increased shear capacity. Shing et al. (1990b) added that the applied axial stress reduced crack openings allowing for enhanced aggregate interlock, which contributes to the increased shear-resisting capability of the masonry.

All studies concluded that increasing the quantity of horizontal reinforcement improves the post-cracked ductility of the wall specimens while only providing marginal increases in shear capacity. This was reinforced by Shing et al. (1990b), reporting that doubling the quantity of horizontal reinforcement in a specimen only resulted in a 6% increase in shear capacity. The increase in ductility was said to be attributed to the idea that horizontal reinforcement does not activate until after shear cracking occurs. While the horizontal reinforcement acts to bind the crack together as it opens (hence the increase in ductility), the masonry has already passed its maximum shear contribution resulting in only minor increases in capacity. This idea was consistent with the fully-grouted wall experiments conducted by Anderson and Priestley (1992). The effect of vertical reinforcement was found to be inconsistent between studies. Shing et al. (1990b) reported that increasing the amount of vertical reinforcement increases the shear capacity of the wall due to additional dowel action. However, Sveinsson et al. (1985) listed this increase as negligible.

From the several completed experimental studies, Fattal and Todd (1991) compared the performance of several proposed and existing in-plane shear capacities with the experimental dataset to determine the most suitable expression. Within the study, the performance of the expressions proposed by Shing et al. (1990b), Matsumura (1988), the Uniform Building Code (1988), and Okamoto et al. (1987) to predict the shear capacity of 62 experimentally tested fully-grouted wall specimens from the experimental studies listed above was explored. It was found that the expression proposed by Matsumura (1988) produced the best correlation with the experimental results. However, it was noted to lack the consistency required for design. The accuracy of the proposed equation by Shing et al. (1990b) was found to be comparable to that of Matsumura (1998) but was

said to overpredict the shear-resisting contribution of the shear reinforcement. Equations from the 1988 version of the Uniform Building Code and Okamoto et al. (1987) were found to be the least successful in predicting the shear capacity of the experimental specimens. The poor performance of the 1988 version of the Uniform Building Code was expected, however as the goal of the supplied equation was also to provide a conservative lower bound for the shear capacity rather than to provide an accurate prediction. The study also noted that none of the expressions were able to precisely predict the ultimate shear strength of all the specimens and that additional testing is required to expand the experimental database.

The cumulative work of the TCCMAR ultimately translated into a design expression (presented in imperial and metric units in Eqns. 2.3a and 2.3b, respectively) to predict the in-plane shear capacity of masonry that first appeared in the 1994 version of the National Earthquake Hazards Reduction Program (NEHRP, 1994a) recommended design provisions and became the basis of both TMS and CSA equations. The form of the equation follows that provided by Shing et al. (1990b) and Matsumura (1988) as the shear capacity of the masonry wall is expressed as a linear summation of shear resistance provided by the masonry, the horizontal reinforcement, and the applied axial load. The NEHRP commentary mentioned that the aspect ratio term within the masonry component was adapted from Anderson and Priestley (1992), while the axial load term was adapted from Blondet et al. (1989). The aspect ratio was selected over the height-width ratio as it simultaneously includes the boundary conditions of the wall (see Fig. 2.11 below). The NEHRP commentary also mentioned that although many TCCMAR members were inclined to include an additional term corresponding to the shear resistance provided by the vertical reinforcement, further investigations are needed as the majority of walls tested in the studies above only featured jamb reinforcement.

$$V_{\text{NEHRP,I}} = \left[4.0 - 1.75\left(\frac{M_u}{V_u d_v}\right)\right] A_{nv}\sqrt{f'_m} + 0.5\left(\frac{A_v}{s}\right) f_y d_v + 0.25 P_u \qquad (2.3a)$$

$$V_{\text{NEHRP,M}} = 0.166\left[2.0 - 1.75\left(\frac{M_u}{V_u d_v}\right)\right] A_{nv}\sqrt{f'_m} + 0.5\left(\frac{A_v}{s}\right) f_y d_v + 0.25 P_u \qquad (2.3b)$$

Where M_u is the factored moment, V_u is the factored shear, d_v is the effective depth, P_d is the axial compressive load A_v is the total area of shear reinforcement, f_y is the yield strength of the shear reinforcement, A_{nv} is the net shear area of the masonry.

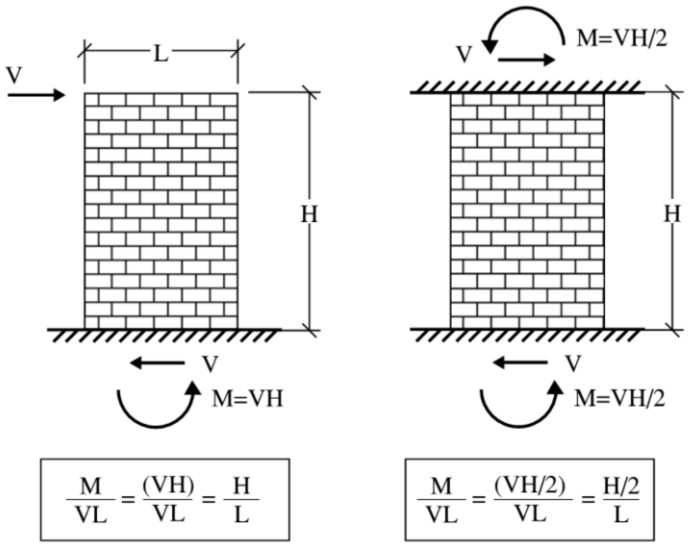

Figure 2.11 – Inclusion of Boundary Conditions in the Aspect Ratio (Hung, 2018)

Little has been done over the past 30 years to improve the equation from its original state. To address the overestimation of the horizontal reinforcement contribution present in the expression proposed by Shing et al. (1990b), both Canadian and American design expressions place a reduction factor (0.6 and 0.5, respectively) on the contribution of the horizontal reinforcement. The validity of applying a 0.5 reduction factor in the TMS 402/602 standard was later addressed by Davis (2008). The study involved performing a statistical analysis over a dataset similar to that of Fattal and Todd (1991) but with the added inclusion of the recent experimental results of FG wall tests performed by Voon and Ingham (2006). Based on fitting the expression to the database of experimentally tested specimens, Davis reported that the best fit was achieved when adding a 0.5 reduction factor to the horizontal reinforcement contribution. The physical significance of this reduction can be attributed to the idea that not all of the horizontal reinforcement intercepting the diagonal crack yields upon failure due to inadequate development length (Ghanem et al. 1992, 1993). The resulting unfactored in-plane shear strength expressions specified in CSA S304-14 and TMS 402/602-22 are shown by Eqns. 2.3 and 2.4,

respectively. It is noted that the presented equation in CSA and TMS are in metric and imperial units, respectively.

$$V_{u,\text{CSA}} = \left(0.16\left(2 - \frac{M_f}{V_f d_v}\right)\sqrt{f'_m} b_w d_v + 0.25 P_d\right)\gamma_{g,\text{CSA}} + 0.60 A_v f_y \frac{d_v}{s} \quad (2.3)$$

$$V_{u,\text{TMS}} = \left(\left[4.0 - 1.75\left(\frac{M_u}{V_u d_v}\right)\right] A_{nv}\sqrt{f'_m} + 0.5\left(\frac{A_v}{s}\right) f_y d_v + 0.25 P_u\right)\gamma_{g,\text{TMS}} \quad (2.4)$$

Where M_f/M_u is the factored/strength level moment, V_f/V_u is the factored/strength level shear, d_v is the effective depth, b_w is the overall web width, P_d is the axial compressive load (taken as 0.9 multiplied by the acting dead load), $\gamma_{g,\text{CSA}}/\gamma_{g,\text{TMS}}$ are the grouting factors, A_v is the total area of shear reinforcement, f_y is the yield strength of the shear reinforcement, A_{nv} is the net shear area of the masonry, A_v is the area of the shear reinforcement, and P_u is the strength level axial load. It is also noted that both equations above are subjected to upper limits based on the aspect ratio of the wall to prevent compressive strut shear failure.

Both equations are based on the findings of TCCMAR and quantify the shear resistance as the algebraic sum of the shear resistance contributed by the masonry, the horizontal reinforcement, and the axial stress acting on the wall. Compared to one another, it is noted that both equations are the same in form, with different coefficients applied to each shear contribution term (Dillon, 2015; Erdogmus et al., 2021a; Erdogmus et al., 2021b). To address partially-grouted masonry construction, a grouting factor (γ_g), which acts as a reduction factor if the wall is partially-grouted, was added to the equations. An examination of the equations shows that each standard applies this reduction factor differently. In the Canadian standard, the grouting factor is only applied to the masonry and axial load contributions, while the American standard applies the term to the masonry, axial load, and horizontal reinforcement. The value of the grouting factor is also different across standards. Within the American standard ($\gamma_{g,\text{TMS}}$), the value of the grouting factor is always 0.7, while in the Canadian standard ($\gamma_{g,\text{CSA}}$) it is calculated as the ratio of effective cross-sectional area to gross cross-sectional area (A_e/A_g) or 0.5,

whichever is lesser. From this, it is clear that the current Canadian and American design provisions for predicting the in-plane shear capacity of reinforced masonry walls were not meant to be applied to partially-grouted walls, but rather their more simplistic FG wall counterpart as all experimentation and analytical analysis regarding the formulation was based exclusively on fully-grouted specimens.

2.3 Performance of Canadian and American In-Plane Shear Strength Provisions

The poor performance of the current in-plane shear equations specified in CSA S304-14 (CSA, 2014) and TMS 402/602-22 (MSJC, 2022) for predicting the shear strength of partially-grouted walls has been highlighted extensively in the past two decades. Increasing amounts of experimental and analytical evidence show that current expressions tend to significantly overestimate the shear capacity of partially-grouted walls and do not reflect experimentally observed behaviour (Voon and Ingham, 2006; Voon and Ingham, 2008; Nolph, 2010; Elmapruk, 2010; Haach et al., 2010; Minaie et al., 2010; Oan, 2013; Hoque, 2013; Dillon, 2015; Ramírez et al., 2016; Hung, 2018; Schultz et al., 2019; Izquierdo Duque, 2021).

2.3.1 Experimental Programs at the University of Auckland

Voon and Ingham (2006; 2008) conducted two experimental studies investigating reinforced concrete masonry shear walls at the University of Auckland. In the first study, Voon and Ingham (2006) tested a total of 10 concrete masonry wall specimens under cantilevered conditions. Of the ten specimens, eight specimens were fully-grouted, while the remaining two were partially-grouted. Parameters investigated include the applied axial stress (0 MPa, 0.25 MPa, and 0.50 MPa), the horizontal reinforcement ratio (0%, 0.01%, 0.05%, 0.06%, and 0.14%), and the aspect ratio (0.6, 1.0, 2.0). Standard 15-cm concrete masonry units were specified for all specimens. The loading sequence for all specimens entailed the application of the axial stress followed by a cyclic lateral load applied to the top of the specimen.

Results indicated that a change in the quantity of the shear reinforcement directly impacted the shear capacity of masonry shear walls. A 10% increase in shear strength

was observed when the quantity of the shear reinforcement increased by a magnitude of 5. Walls with similar horizontal reinforcement ratios but different reinforcing bar distributions were also compared. The results indicated that adopting closely distributed bars with a smaller diameter can result in ductile shear failure, while loosely distributed bars with a larger diameter will lead to brittle shear failure. The applied axial stress was proven to have a positive influence on the shear strength. Shear capacity increases of 13% and 22% were observed when the applied axial stress was increased from 0 MPa to 0.25 MPa and then from 0.25 MPa to 0.5 MPa, respectively. Regarding the grouting method, a 50% increase in shear capacity was observed for a specimen featuring five grouted flues as compared to an otherwise identical specimen with three grouted flues. The aspect ratio of masonry walls appeared to have a negative influence over the maximum shear strength. A 15% decrease was observed in the maximum shear strength when the aspect ratio increased from 1.0 to 2.0. However, it was noted that the decrease in shear strength could have been due to the changes in the net area and the compressive strength of the masonry. Future study that excludes the net area and the compressive strength of masonry was recommended in order to study the meaningful relationship between the aspect ratio of the walls and the maximum shear strength.

Two years later, Voon and Ingham (2008) launched a second experimental campaign in which eight partially grouted concrete masonry walls with openings were tested. Unlike the first study, specimens in the second study were tested solely under a cyclic lateral load (no axial stress was applied). Standard 15-cm concrete masonry units were specified for all specimens. The size of the wall openings was the main parameter investigated during the study. Openings sizes varied from small windows to large doorframes. Details of the eight specimens are presented in Fig. 2.12 below. Results indicated that the size of openings and the length of trimming reinforcement significantly affected the lateral strength of the walls. The current New Zealand masonry design standard NZS 4229 (NZS, 2004) noticeably overpredicts the strength of concrete masonry walls with small openings, however, the prediction becomes increasingly conservative as the height of openings increases.

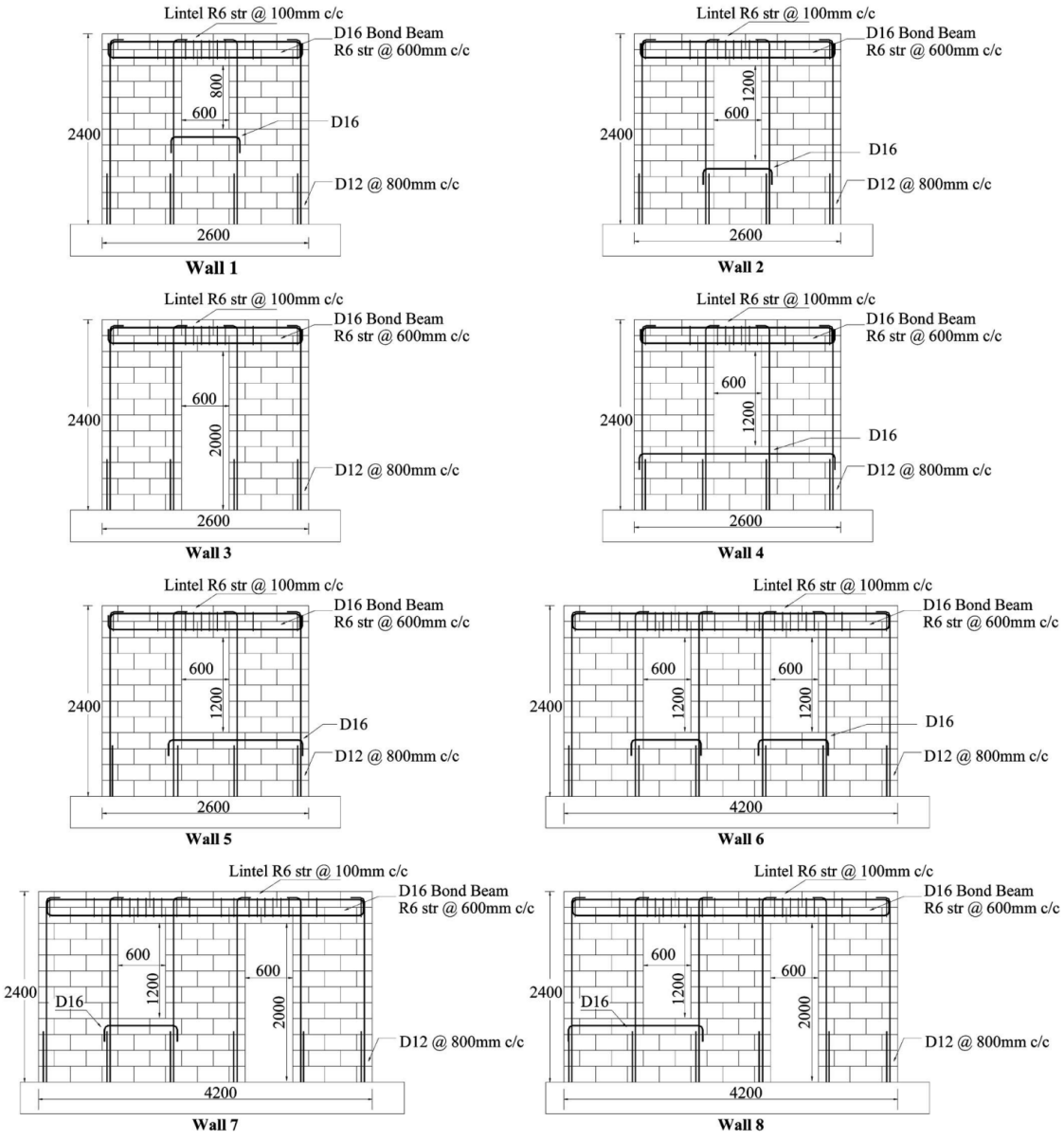

Figure 2.12 – Masonry Wall Specimens (Voon and Ingham, 2008)

2.3.2 Experimental Programs Conducted at Drexel University

Minaie et al. (2010) conducted a series of tests on four partially-grouted reinforced masonry shear walls at Drexel University. All specimens were subjected to combined axial and cyclic lateral loading. The parameters investigated included the boundary conditions (cantilevered and fixed-fixed) and mortar formulation (MC and portland

cement lime). The cantilever specimens featured aspect ratios of 1.37, and the fixed-fixed specimens had aspect ratios of 0.67. Standard 20-cm concrete masonry units were specified. Details of the test setup are presented in Fig. 2.13.

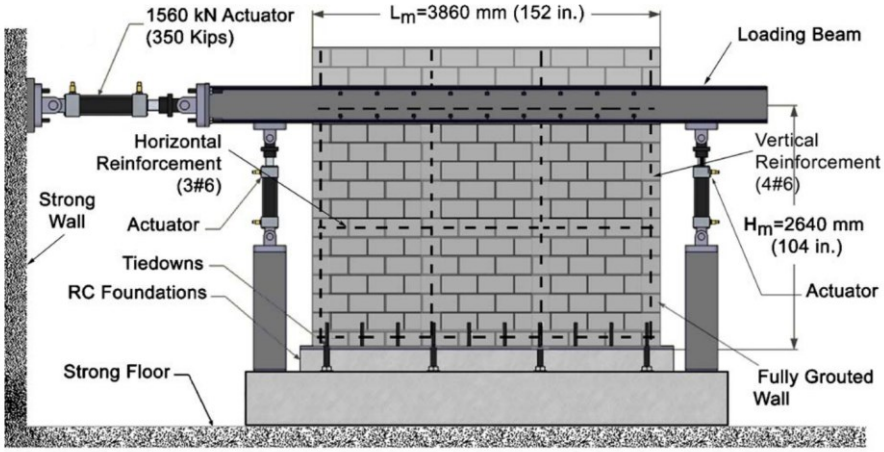

Figure 2.13 – Experimental Test Setup (Minaie et al., 2010)

Results from the test indicated that an increase in mortar strength (both compressive and bond) increases the overall shear capacity of the specimens. The influence of the boundary conditions was inconclusive, however, as the cantilever portland lime cement specimen was able to withstand a larger applied load as compared to the fixed-fixed specimen, but the reverse was found for the MC specimens. Table 2.1 presents a comparison of the experimentally obtained shear capacity with that predicted by TMS 402-08. Results from the table indicate that the standard is quite unconservative. Based on other available experimental results, Minaie et al. concluded the TMS 402-08 in-plane shear strength prediction expression becomes more unconservative as (a) the net area of shear walls increased, (b) the aspect ratio of the shear walls decreased below 1.0, and (c) the spacing of vertical and horizontal grout/reinforcement increased.

Table 2.1 – Experimental and Predicted Shear Capacities (Minaie et al., 2010)

Specimen	V_{Exp} (kN)	V_{TMS-08} (kN)	V_{Exp}/V_{TMS-08}
MC 1	190	556	0.34
MC 2	230	573	0.40
PCL 1	318	556	0.57
PCL 2	241	573	0.42

2.3.3 Experimental Programs Conducted at Washington State University

Elmapruk (Elmapruk, 2010; Elmapruk et al., 2020) and Nolph (Nolph, 2010; Nolph and ElGawady, 2012) at Washington State University tested a total of 11 partially-grouted walls and one fully-grouted wall under combined axial and cyclic lateral loading. Parameters explored included the distribution of vertical reinforcement (spacing investigated include 48 in., 32 in., and 24 in.), the quantity of shear reinforcement (between 0.085% and 0.254%), and the aspect ratio of the walls (0.56 and 1.00 for the walls tested by Elmapruk and Nolph, respectively). A fully-grouted wall specimen was also tested by Nolph for comparison purposes. Loading of each wall specimen consisted of the application of a constant axial stress of 0.1 MPa followed by a cyclic lateral load. A schematic of the testing setup is shown in Fig. 2.14 below.

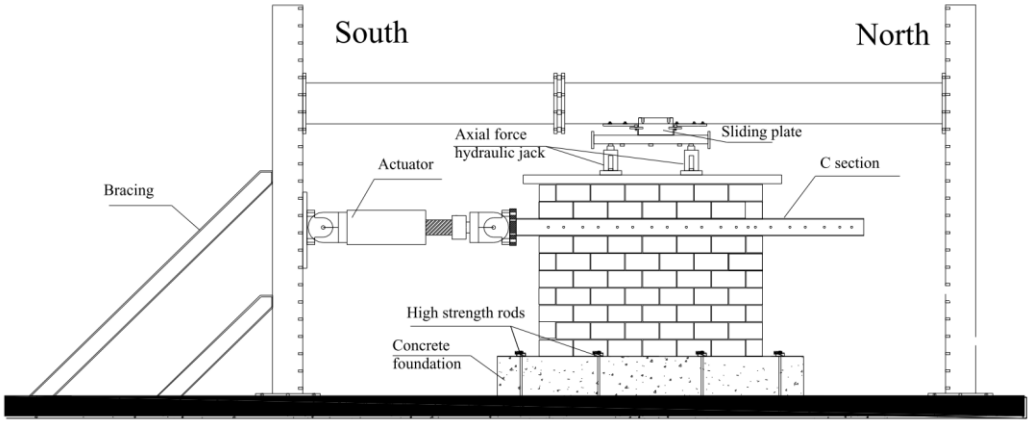

Figure 2.14 – Experimental Test Setup (Elmapruk, 2010)

From the test data, several conclusions were made. Regarding the quantity of horizontal reinforcement, Nolph reported that when increasing the horizontal reinforcement ratio from 0.085% to 0.120%, a 2.6% increase in shear capacity was observed. However, when the horizontal reinforcement ratio was further increased from 0.120% to 0.169%, the shear capacity of the specimens decreased by 11.8%. Similar inconclusive results were found by Elmapruk as the first increase in horizontal reinforcement ratio from 0.127% to 0.180% slightly decreased the shear capacity of the wall by 2.3%, while a second increase of the ratio from 0.180% to 0.254% increased the shear capacity by 14.0%. An

examination of the strains in the horizontal reinforcement suggested that this behaviour was attributed to the maximum contribution of horizontal reinforcement occurring after the peak lateral resistance of the wall, which is consistent with the findings of Shing et al. (1990b) and Priestley and Anderson (1992). In addition, it was noted that as the horizontal reinforcement ratio was increased, the strain in the horizontal reinforcement would decrease for partially-grouted wall specimens resulting in the horizontal reinforcement failing to yield for the majority of the specimens. This behaviour was not observed in the FG specimen with the same horizontal reinforcement ratio as strain readings indicated the specimen reached over 450% of the yield strain.

Referring to the influence of vertical reinforcement distribution, it was observed that by decreasing the grout core spacing (i.e., adding additional grout flutes while keeping the vertical reinforcement ratio constant), the shear capacity of the walls increased significantly. One particular reason listed was the observed notion that the addition of grout flutes resulted in the shear reinforcement yielding. In addition, it was noted that the shear reinforcement would yield closer to when the peak shear resistance of the masonry was reached, allowing for a greater superimposed strength.

2.3.4 Experimental Programs Conducted at the University of Calgary

Comprehensive masonry shear wall tests were carried out at the University of Calgary by both Oan (2013) and Hoque (2013). This entailed 66 concrete masonry walls tested under combined axial and monotonic lateral loading by Oan and 16 concrete masonry walls tested under cyclic and monotonic loading by Hoque. Referring to the Oan study, 51 out of the 66 specimens were partially-grouted while the remaining 15 were ungrouted. Standard 20-cm hollow concrete masonry blocks were specified for all specimens. Specimens nominally measured 1.2 m in height and 1.6 m in width, which resulted in an aspect ratio of 0.75. The vertical load was applied first, followed by the horizontal load, which was applied under displacement control at a rate of 0.1 mm/s. Parameters investigated in the initial stage of the experiment include the level of applied axial stress (2 MPa, 3 MPa, and 4 MPa), the horizontal reinforcement type (bond beam vs. bed-joint), the amount of horizontal reinforcement (0%, 0.04%, and 0.07%), and the effect of

grouting (partially grouted and ungrouted). The influence of the method of construction (i.e., the method of applying the bed joint reinforcement on either the dry masonry flange surface or embedded in the mortar) was also studied in a later phase. Figure 2.15 depicts the test setup of the experiment.

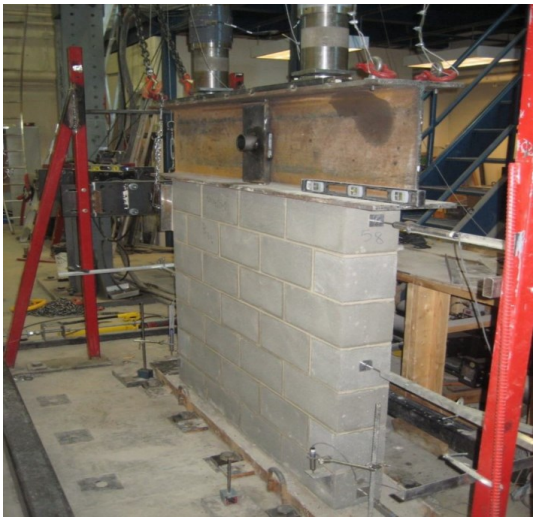

Figure 2.15 – Experimental Test Setup (Oan, 2013)

For partially-grouted specimens, an average increase of 32.5% on the maximum shear resistance was observed when the axial compressive stress increased from 2 MPa to 3 MPa, while only an average increase of 15.2% was observed when the axial stress increased from 3 MPa to 4 MPa. For ungrouted walls, a similar increase of 32.7% and 19.5% on the maximum shear resistance was observed when the axial compressive stress increased from 2 MPa to 3 MPa, and from 3 MPa to 4 MPa, respectively. Results indicated that different types of reinforcement had different impact levels on the shear resistance of the walls. Using large-diameter horizontal reinforcement resulted in a significant decrease in the shear resistance of the specimens, while no such decrease was observed when smaller-diameter horizontal reinforcement was specified. Vertical reinforcement, on the other hand, appeared to have no impact on the shear strength of the walls. The best performance (i.e., highest shear strength) was observed when specimens were reinforced with both vertical and horizontal reinforcement (grid reinforcement). When the net area acting to resist the lateral load was taken into consideration, ungrouted

walls were found to have a higher shear strength than partially-grouted walls. Results were also compared with the Canadian masonry design code CSA S304.1 (2004), which was proven to be overly unconservative.

Referring to the study by Hoque, all specimens were constructed with 20-cm concrete masonry units and were partially-grouted. The main parameters investigated include the spacing of the bond beams (400 mm, 600 mm, and 800 mm), the reinforcement anchorage type in the bond beam (180° hooks, 90° hooks, straight bars, shear studs), the dowel and splice position (top and bottom splice), and the variation in load history (monotonic and cyclic loading). Results indicated that there was no significant difference in shear capacity over the changes in the various parameters. However, bond beam reinforcement was reported to noticeably reduce cracking.

2.3.5 Analytical Programs Conducted Brigham Young University

Dillon (2015) developed a database consisting of 353 masonry shear wall specimens with the goal of using regression techniques to propose a new design equation to predict the in-plane shear capacity of partially-grouted masonry walls. Out of the 353 wall specimens, 171 were fully-grouted, and 182 were partially-grouted. Regarding the different types of masonry units, 252 database specimens were constructed with concrete masonry units, while the remaining 101 were constructed with clay brick. Of the 353 specimens, 47 specimens were tested under monotonic loading, 304 specimens were tested under cyclic loading, and the remaining 2 specimens were tested under simulated seismic loading. Three approaches were explored to develop a new shear strength prediction model: (1) Modify the existing TMS 402-13 (2013) in-plane shear strength equation to account for the differences in nominal strength and uncertainty between fully-grouted and partially-grouted walls; (2) develop a new shear equation for both fully-grouted and partially-grouted walls to replace and improve the current TMS equation; and (3) develop a strut-and-tie methodology for masonry structures. The results from the modified TMS model indicated that the TMS (2013) shear strength equation is unconservative for partially-grouted walls (TMS predicted strengths are 73% of the weighted mean of experimental values). Also, the current grouting factor of 0.75

appeared to be correct. The TMS-13 expression was also found to correlate better with fully-grouted walls, likely because the equation was developed based on findings from fully-grouted wall tests.

A linear regression model was then developed using the database to predict the shear strength of masonry walls. Results verified that the shear strength of masonry walls is related to the square root of the masonry compressive strength. It was found that the shear strength of walls was better correlated to the reciprocal of the aspect ratio rather than the aspect ratio itself. Results indicated that the notion that the horizontal reinforcement is directly involved in resisting the lateral shear force commonly reported in multiple studies is invalid. The proposed linear regression model showed an improvement in the variance of the predictions when compared to the TMS 402-13 provisions, as the proposed model contained coefficients that were specifically developed for partially-grouted walls.

Buxton (2017) later tested six half-scale multi-storey masonry shear walls. Three of the specimens tested featured door openings, while the remaining specimens featured window openings. All the specimens had the same overall dimensions with an aspect ratio of 1.25. Half-size 10-cm concrete masonry units were specified. Details of the test setup are presented in Fig 2.16.

Figure 2.16 – Experimental Test Setup (Buxton, 2017)

Results from the test were compared against TMS 402-16 (MSJC, 2016) provisions. It is noted that the TMS 402 equations do not account for wall openings. Two methods were adopted to address this issue. Method 1 was to neglect the openings and treat the entire wall as a single masonry shear wall without openings, while method 2 was to assume the two sides of the opening are two independent walls connected by masonry beams. It was found in both methods that the TMS provisions were extremely unconservative, with the predicted shear capacity reaching as far as 324% of the experimentally determined capacity.

2.3.6 Analytical Programs Conducted at the University of Alberta

Furthermore, an analytical study by Hung (2018) demonstrated the wide inconsistency of both CSA S304-14 (CSA, 2014) and TMS 402/602-16 (MSJC, 2016) in predicting the in-plane shear capacity of 292 experimentally tested specimens failing in diagonal tension shear (Fig. 2.17). Through the development of an artificial neural network (ANN), Hung also reported that the amount of vertical reinforcement does appear to influence the shear capacity of PG walls, although modestly. Hung concluded that while the power of ANNs could be utilized to further develop expressions for the in-plane shear capacity of PG walls, the current database needs to be expanded, either through experimental testing or FE modelling.

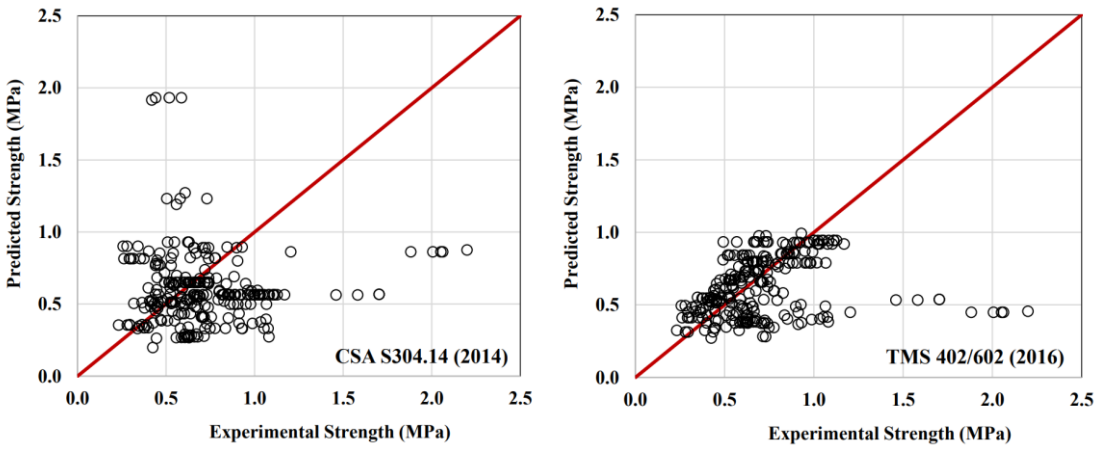

Figure 2.17 – Model Predictions (a) CSA S304-14 (b) TMS 402-16 (Hung, 2018)

Using the same database as Hung (2018), Izquierdo Duque (2021) employed stepwise regression and model tree techniques (Fig. 2.18) to determine the most significant design parameters contributing to the strength of PG masonry walls. While many of the design parameters currently included in the shear strength design provisions, such as applied axial stress and the aspect ratio, were found to influence the shear capacity, Izquierdo noted that the developed models (Fig. 2.19) predicted both the distribution of the vertical reinforcing bars and the quantity of the interior vertical reinforcing bars as key contributors to the in-plane shear strength. In addition, the model did not include any parameters related to the shear reinforcement, suggesting that the quantity of shear reinforcement does not play a significant role in contributing to the in-plane shear capacity of PG walls. Both the findings related to the vertical and shear reinforcement were consistent with experimental observations of Elmapruk (2010) and Nolph (2010).

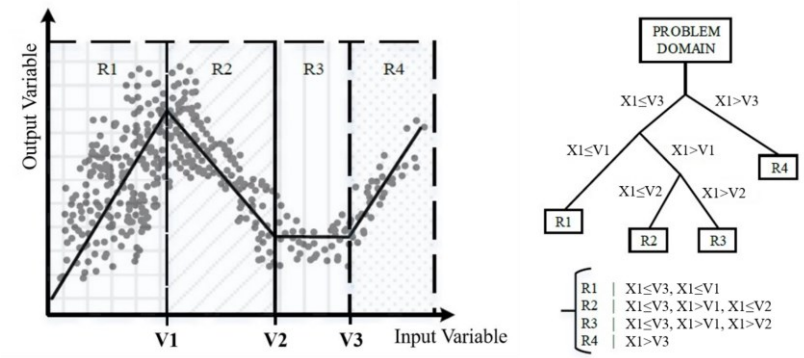

Figure 2.18 – Model Tree Structure (Mohsenijam, 2019)

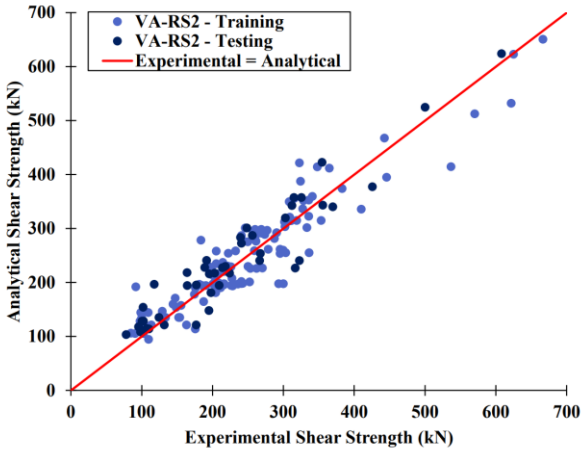

Figure 2.19 – Model Tree Shear Strength Prediction (Izquierdo Duque, 2021)

2.4 Reinforced Concrete Approaches to Predicting In-Plane Shear Capacity

The challenges associated with specifying adequate and consistent design provisions for predicting in-plane shear capacity is a problem also encountered in reinforced concrete (RC). However, unlike masonry, RC has remained the focal point of extensive experimental and analytical campaigns over the last half-century resulting in multiple robust methods to capture the in-plane shear strength of RC wall structures. Common methodologies to analyze RC elements under shear include those of nonlinear elasticity, plasticity, total-strain formulations, and fracture mechanics (Salazar Lopez, 2019). Perhaps the most well-known are the total-strain formulation Modified Compression Field Theory (MCFT) and the plasticity-based Strut-and-Tie Modelling (STM), as their introduction in the late 1980s revolutionized the RC shear design methodologies presented in both the Canadian and American RC design provisions (CSA A23.3-19 and ACI Code 318-19, respectively).

2.4.1 Modified Compression Field Theory

Referring to the MCFT (Vecchio and Collins, 1986), the shear response of an RC biaxial membrane element subjected to in-plane shear and axial stress can be determined by solving a system of 15 nonlinear equations (Fig. 2.20) derived based on equilibrium, strain compatibility between the concrete and reinforcing bars, predicting the shear resistance of the concrete due to aggregate interlock, and the nonlinear stress-strain relationships defining the compressive and tensile responses of both the concrete and reinforcing bars. Assumptions made within the formulation of the methodology include that there is only a single stress state corresponding to a particular strain state (loading is history independent), the stress and the strain are averaged over areas of the element, a perfect bond exists between the concrete and steel reinforcement, and the reinforcing grid is smeared over the element. To analyze the shear capacity, a value of principle tensile strain over the crack is selected and used to calculate both the shear stress and shear strain within the element. This process is repeated for increasing values of principle tensile strain until failure is deemed by either (1) the slipping of the crack due to the average tensile forces in the concrete exceeding the maximum resistance of the concrete and

reinforcement (diagonal tension shear failure), (2) the crushing of the concrete along the diagonal strut due to the principle compressive stresses in the concrete exceeding the compressive capacity of the concrete (compressive strut failure), or (3) the yielding of the reinforcement along the crack opening. The versatility of the MCFT element has also allowed for the incorporation into many finite element programs, such as VecTor2 and Response-2000 to predict the response of large-scale RC structures.

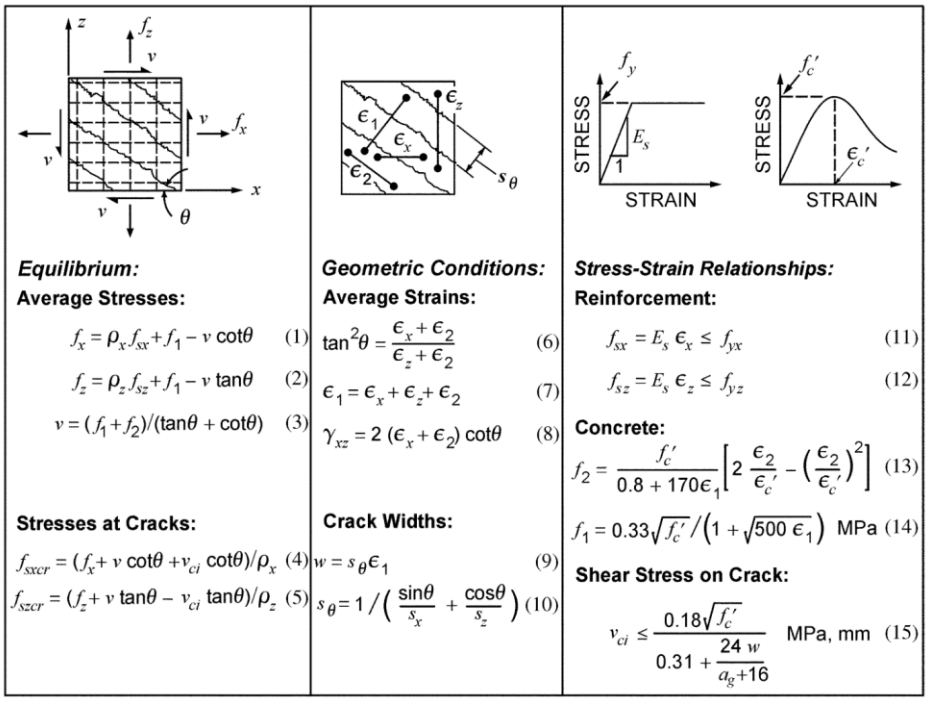

Figure 2.20 –Modified Compression Field Theory Equations (Bentz et al., 2006)

The mechanics-based transparency of the MCFT later resulted in the development of a simplified version (referred to as SMCFT) (Bentz et al. 2006), which is currently featured in the Canadian RC design provisions (CSA A23.3-19) to predict the shear capacity of RC elements in flexural regions. The simplifications came from applying concrete shear strength principles taken from AASHTO LRFD Bridge Design Specifications (2004), assuming no clamping stresses (hence the applicability only to flexural regions), assuming the steel reinforcement is yielding, and the development of simplified equations to relating the strength factor (β) and the diagonal crack angle (θ) to values of horizontal strain (ε_x).

These simplifications ultimately resulted in the reduction from 15 nonlinear equations specified by the MCFT to 4 non-iterative equations in which the shear strength of the RC member can be determined by calculating a strength factor, the angle of the diagonal cracks, and the horizontal strain. A stress limit corresponding to one-quarter of the peak compressive strength of the concrete ($0.25f_c'$) is also placed to ensure compressive strut failure does not occur.

2.4.2 Strut-and-Tie Modelling

An alternate design methodology to predict the strength of reinforced-concrete elements is the strut-and-tie model (STM), first proposed by Schlaich et al. (1987). Based upon the lower-bound theorem of plasticity, STM methodology involves analyzing the flow of tensile and compressive stresses within an element, in addition to any intersections between the stress paths (Fig. 2.21), referred to as tensile ties, compressive struts, and nodal zones, respectively. The method is especially suited in regions of concentrated forces and geometric discontinuities to determine concrete proportions (National Highway Institute, 2017). If the stress in all of the tensile ties, compressive struts, and nodal zones is found to be less than their factored material capacity, the structure is deemed safe. Conversely, if the stress exceeds the capacity in any of the elements, the structure is deemed to have failed. The simplicity of the method was recognized in 2002 when STM provisions were first implemented in the ACI 318 provisions (ACI, 2002). It is noted, however, that the prediction capability of the STM is very sensitive to the geometry and magnitude of the assumed stress paths, as incorrect paths can result in an unconservative estimation of the true strength of the structure. Extensive research has been devoted to the development of RC STMs with the correct stress paths for a variety of RC structures rigorously calibrated with a large pool of experimental and analytical studies (Schlaich and Anagnostou, 1990; Schlaich and Schafer, 1991; Hwang et al., 2001; Yun, 2006; To et al., 2009; Yun and Ramírez, 2016; Ismail et al. 2017, He et al. 2020).

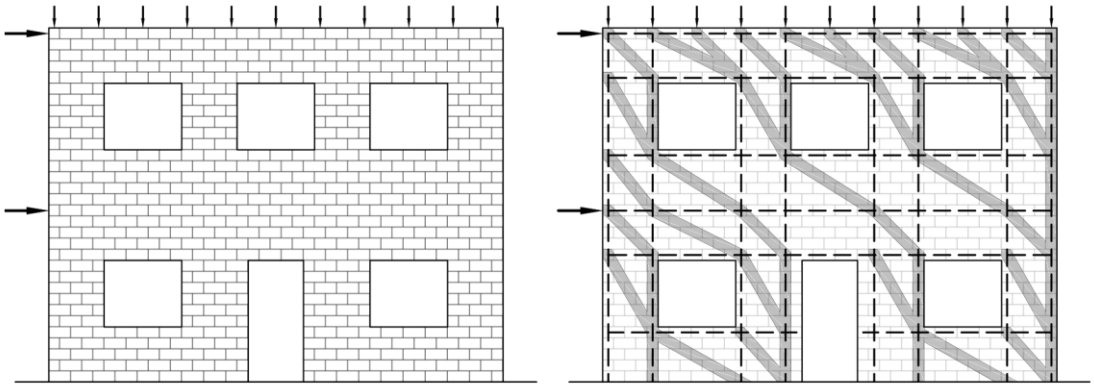

Figure 2.21 – Flow of Stresses in Strut-and-Tie Modelling (Dillon, 2015)

2.4.3 Applications of MCFT and STM to Masonry Structures

With concrete sharing many inherent behavioural characteristics to that of masonry, approaches to developing shear-related design provisions for masonry walls may focus on adapting the MCFT or STM methodology to masonry. Examination of the concrete-specific MCFT and STM methodologies reveals that a clear understanding of the material behaviour is required – for partially-grouted masonry construction; however, this is challenging due to its heterogeneous nature and the presence of geometric and material discontinuities.

Of the few attempted applications of either MCFT or STM to masonry, the majority of the success has been concentrated around fully-grouted walls systems, while the few attempts of applying either methodology to partially-grouted walls have produced unsatisfactory results (Nolph, 2010; Elmapruk, 2010; Dillon, 2015; Tuchscherer, 2016). This can be attributed to the similarities shared by reinforced concrete and FG masonry construction. A number of experimental programs have focused on assessing the shear behaviour of FG walls to develop performance-based design provisions (Banting and El-Dakhakhni 2012; Banting 2013; El-Dakhakhni et al. 2013; Seif ElDin and Galal 2017). One consistent finding from such experiments is that when all cells are filled with grout, the wall assemblage is bound together, thus reducing the planes of weakness found between the masonry units and mortar layers. Fully-grouted wall elements can thus be considered a homogenous isotropic element, provided that the anisotropic nature of the masonry assemblage is considered – for instance, the relationship between the

compressive strength and the direction of the applied stresses relative to the bed joints (Liu et al. 2006; Banting 2013). Thus, researchers were successfully able to derive acceptable versions of both the MCFT (Banting, 2013) and STM (Dillon, 2015) methodologies for FG wall systems.

Similar advancements have not been achieved for partially-grouted walls, despite the fact that partially-grouted masonry construction is widely used in low- to mid-seismic regions due to its economic advantages and lower seismic mass. As discussed above, the behaviour of partially-grouted walls is complex due to the lack of continuous grouting within the cells of the masonry. The voids in the wall result in sudden geometric discontinuities, and therefore the wall assemblage cannot be treated as a uniform isotropic element. This restricts the use of smeared crack approaches employed in MCFT, where the strains and stresses are averaged over an equivalent, homogeneous continuum. As an alternative, the use of the STM arises as a viable method since the main requirement is a clear idea of the flow of stresses inside the wall, which can be accomplished via experimental testing or numerical modelling. Research conducted on the application of STM methodology to partially-grouted walls will be discussed in further detail in Section 5.2.

2.5 Finite Element Micro-Modelling of Masonry Walls

From the above discussion, the application of an STM methodology to partially-grouted masonry walls would appear to be an interesting candidate for predicting their strength against in-plane loads. Unfortunately, several fundamental aspects of the behaviour of masonry remain largely unknown such as the interactions between the stress paths and the voids, the shape and geometry of the compressive struts, and nodal locations within the masonry. Within the literature, there is a consistent theme that the complexities associated with analytically examining PG walls are too vast and that the only plausible solution to quantify the shear capacity of masonry wall systems is through experimental testing (Banting and El-Dakhakhni 2012; Banting 2013; El-Dakhakhni et al. 2013). This is problematic when considering the significant financial cost and time commitment associated with experimental testing. Fortunately, advancements in computational power

and efficient finite element formulations and solution algorithms offer an alternative to testing.

Research conducted in South America and Europe over the last five years has led to the development of masonry micro-models specific to partially-grouted masonry that have satisfactorily captured the global and local responses of partially-grouted shear walls (Sandoval and Arnau 2017; Calderon et al. 2017; Ferretti et al. 2018). Micro-models treat each component of the masonry assemblage (masonry unit, mortar, and grout) independently (Fig. 2.22) with a cohesive interfacial bond existing between each material (Lourenço et al., 1995; Lourenço and Rots, 1997). While providing a more accurate representation of the masonry structure, these micro-models come at a high cost of time, both in development and computation. In addition, the number of parameters required to accurately represent the masonry structure in a micro-model is quite large, of which many are unknown. It is by this reasoning that micro-models have only been employed by a handful of researchers while considered completely unfeasible in design scenarios (Mojsilovic, 2011).

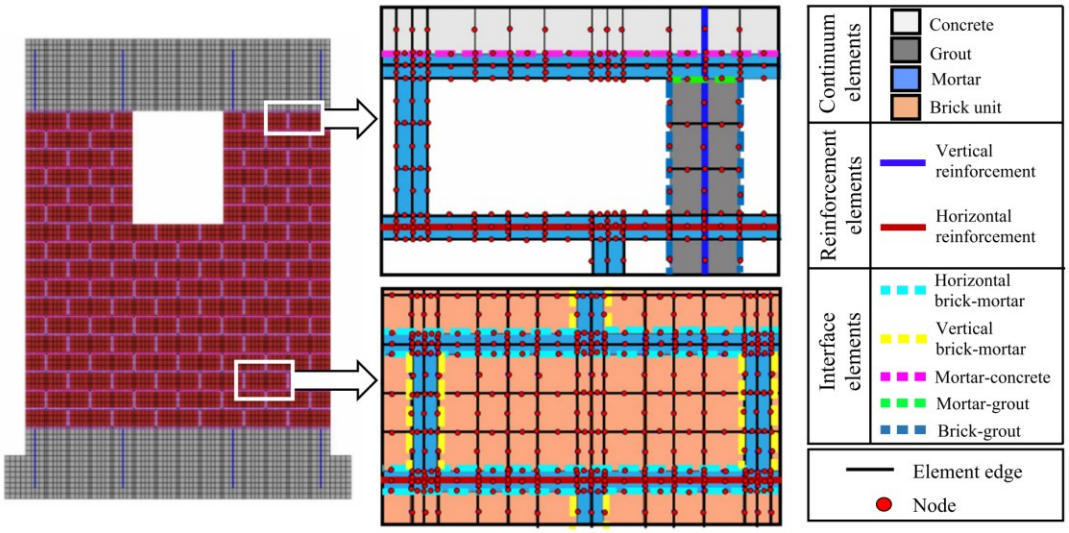

Figure 2.22 – Modelling Approach for PG Masonry Walls (Calderón et al. 2017)

Preliminary results using micro-models have demonstrated the validity of this approach as the models were able to replicate the load-displacement plots, failure modes, and cracking patterns of experimentally tested PG walls under in-plane loading within

reasonable accuracy (Calderón et al., 2017; Sandoval and Arnau, 2017). Referring to the study conducted by Calderon et al. (2017), the micro-model was able to predict the peak lateral load of three experimentally tested PG walls featuring openings within 10% (Fig. 2.23a). The micro-model was also able to capture the ultimate displacement and the degradation in stiffness of the experimental specimens. Failure modes and stress paths (Fig 2.23b) were also captured. A major limitation of these models, however, consists of the fact that they are unable to capture the cyclic behaviour of masonry elements subjected to in-plane loads. This is because of the total strain approach used in the numerical model similar to MCFT, in which the material behaviour is path-independent and thus insensitive to loading protocol and accumulated damage.

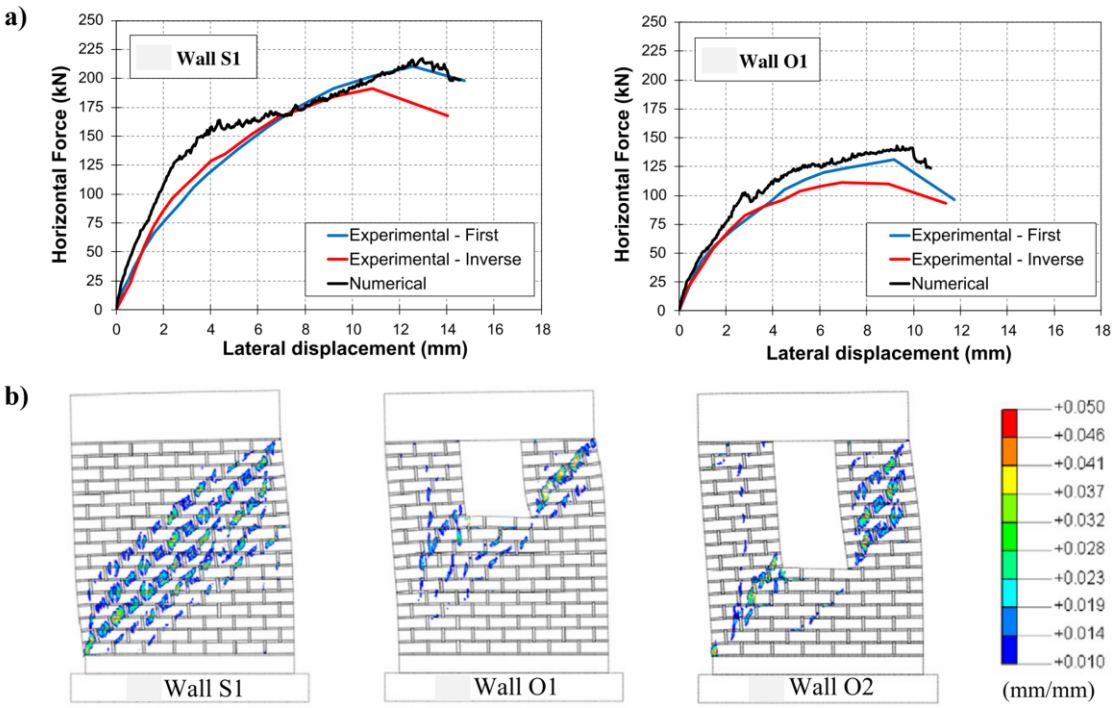

Figure 2.23 – Finite Element Micro-Model (a) Load-Displacement Plot (b) Stress Paths (Calderón et al., 2017)

The results in Fig. 2.23 suggest that a PG-specific micro-model has the capability to successfully capture the stress distribution, cracking, geometry discontinuity, and the roles of the reinforcement in PG walls, making micro-modelling a candidate tool to aid in adapting the STM methodology to PG wall systems. It is noted that the state-of-the-

art for partially-grouted masonry shear wall micro-models involves walls made with perforated clay bricks. Therefore, there is a need to develop models specific to the wall typologies used in North America, which utilize concrete blocks with large cells.

2.6 Literature Review Summary

This chapter presented the historical development of the in-plane shear design provisions specified in the Canadian and American masonry standards, CSA S304-14 (CSA, 2014) and TMS 402/602-16 (MSJC, 2022), respectively. The performance of the supplied equations to predict the in-plane shear capacity and accurately replicate experimentally observed behaviour was then examined. For the majority of studies, it was found that the provisions are quite inconsistent in the prediction of the in-plane strength and particularly unconservative for walls with low aspect ratios or large quantities of horizontal reinforcement. The equations also fail to capture experimentally-observed behaviour, such as the lack of yielding of the horizontal reinforcement. To determine an alternative methodology to predict the in-plane shear capacity of partially-grouted walls, methodologies currently employed for reinforcement concrete were presented. While the Modified Compression Field Theory was deemed unsuitable due to several assumptions made that are invalid for partially-grouted systems, it was found that a strut-and-tie methodology can be adapted to partially-grouted masonry systems if proper insights regarding the behaviour of the compressive struts, tensile ties, and nodal zones were explored. To accomplish this, a detailed finite element micro-model was explored as such a model, while time-consuming and difficult to develop, is capable of providing the insights required for a strut-and-tie methodology adaptation to partially-grouted masonry wall systems.

3.0 FINITE ELEMENT MICRO-MODELLING OF MASONRY WALLS

3.1 Introduction

This chapter presents the development and validation of a finite element model capable of capturing the in-plane shear capacity of partially-grouted masonry walls. All models were developed in the finite element software ABAQUS (Dassault Systems, 2022).

3.2 Micro-Model Development

3.2.1 Types of Masonry Models

Three primary types of masonry models exist. The first, referred to as a macro-model, is the most simplistic as it assumes the masonry assemblage to act as a single homogenous entity with material properties corresponding to those obtained from masonry prisms. Meso-models attempt to add interface characteristics to the system by defining discontinuous elements between the masonry units. The mortar is not modelled explicitly in meso-models as the mortar properties are included within the discontinuous element formulation. Micro-models are perhaps the most complex as each material component of the masonry is modelled individually with the interfaces existing between each component also defined. While macro-models have been shown to be valid options when attempting to predict the monotonic behaviour of the wall system (Hung, 2018; Ba Rahim, 2023) a micro-model was specified for this study as it is expected the interfaces existing between the components will have a significant impact on the stress paths within the wall.

3.2.2 Model Formulation

The basis of the detailed micro-model is to incorporate the non-prismatic characteristic of the masonry wall system while restricting the model to two dimensions to ensure computational efficiency. To accomplish this task, the wall geometry was separated into two layers of uniform thickness, namely, a ‘masonry layer’ consisting of the masonry unit flanges stacked between segments of mortar and a ‘grout layer’ consisting of the masonry unit webs, grout cores, vertical reinforcement, and horizontal reinforcement (Fig. 3.1).

Linear quadrilateral continuum elements with full integration and a fine mesh density were specified for the masonry units, mortar, grout cores, foundations, and capping beam. It is noted that quadratic elements were explored; however, the substantial increase in runtime was not substantiated by the results, as the peak load predicted by linear and quadratic simulations were typically within 1% of one another. Linear beam elements were specified for both the vertical and horizontal reinforcement.

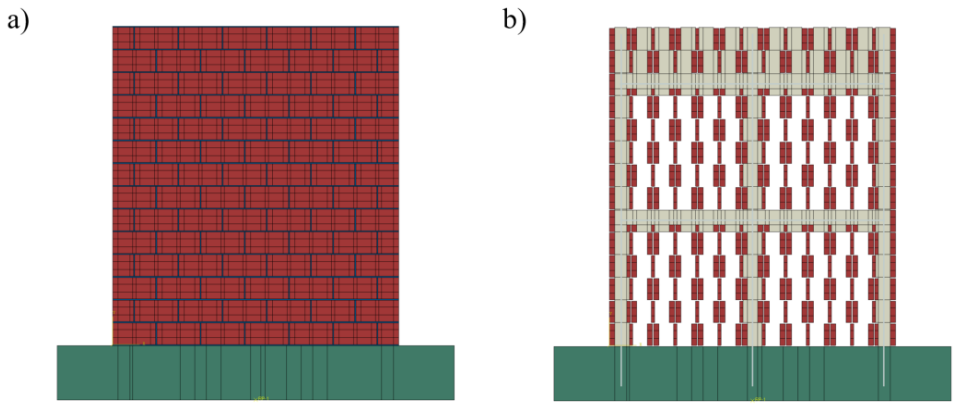

Figure 3.1 – Masonry Model Layers (a) Masonry Layer (b) Grout Layer

Contact interfaces existing between the masonry flanges and mortar layers and between the grout cores and masonry webs were defined by combining a Mohr-Coulomb friction law with a surface-based cohesion model. The behaviour of the combined model is characterized by a linear elastic traction-separation law based on the stiffness of the cohesion and a damage criterion based on the ratios of applied normal and shear stresses to their respective maximum limits. Once a damage limit state has been reached, the cohesive properties of the interface deteriorate exponentially until the interface is solely governed by the Mohr-Coulomb friction law. It is important to note that the combining Mohr-Coulomb friction law with the cohesive model is necessary to introduce the compressive pressure dependency of the peak shear strength for the interface, as a cohesion model alone does not feature this dependency.

To couple the masonry layer with the grout layer, embedment constraints were specified. In this constraint, the translational degrees of freedom of an embedded set of elements (the masonry web elements) are constrained to that of a set of host region elements (the

masonry flange elements). This results in the embedded elements retaining their position with respect to the host elements upon loading. Referring back to the two-layer system, the embedment constraints were specified to (1) embed both the horizontal and vertical reinforcing bars within the solid grout elements and (2) embed the masonry unit web elements within the masonry unit flanges. From this, mechanical loading applied to the grout core would be transferred to the masonry webs via defined contact between the grout cores and masonry webs, which would then be transferred from the masonry webs to the masonry flanges due to the embedment constraint.

3.2.3 Material Models

Two material plasticity models were selected for the model. The first is a von Mises plasticity model used to define the elastic and strain hardening behaviours of the steel reinforcement, while the second is the history-dependent Concrete Damage Plasticity (CDP) model (Lubliner et al., 1989; Lee and Fenves, 1998) to model the highly nonlinear masonry unit, mortar, and grout materials. Similar to other plasticity-based models, the CDP model defines the biaxial response of the material based on a defined uniaxial stress-strain response for both the tension and compression. The model also requires five additional field parameters. These parameters, in no particular order, are the dilation angle, the eccentricity, the ratio of biaxial compressive yield stress to the uniaxial yield stress, the ratio of the second stress invariant on the tensile mean, and the viscosity parameter. The first two parameters (dilation angle and eccentricity) are specified to account for the dilatancy phenomenon in which cementitious materials (masonry unit, mortar, and grout) experience an increase in volumetric strain under shear deformation, ultimately prohibiting the use of an associated flow rule. Instead, a non-associated flow rule based on the Drucker-Prager hyperbolic function is employed within the CDP model. This function requires the definition of the typically linear relationship of the effective stress envelope in the normal stress–shear stress (p-q) plane. Here the dilation angle defines the slope of this linear relationship while the eccentricity smooths out the asymptote when the shear stress approaches zero, allowing for the creation of a smooth and continuous hyperbolic function that is always uniquely defined. Values of dilation

angle and eccentricity were taken as 30º and 0.1, respectively, due to recommendations by various other researchers in the masonry field (Mohsin, 2005; Kmiecik and Kaminski, 2011; Genikomsou and Polak, 2014, Michal and Andrzej, 2015; Nasiri and Liu, 2017; Darmayadi and Satyarna, 2019). The ratio of equal biaxial compression to uniaxial compression was taken as 1.16 (the default value for concrete materials), while the ratio of the second stress invariant on the tensile mean was taken as 2/3 (also widely considered the default value for concrete materials). Finally, the viscosity parameter was set as 0.0002. This value was determined through a series of simulations in which the viscosity parameter was continuously increased until a noticeable change in the load-displacement response of the wall was observed, as higher values of viscosity drastically reduce the runtime of the analysis at the cost of accuracy. The reasoning for the save in runtime at the cost of accuracy is that the viscosity parameter relaxes the rigid conditions of the yield surface and allows for the determined stress state to lay outside of the yield surface rather than on or within it. It should be noted that due to the nature of the visco-plastic regularization employed, the model response becomes dependent on the pseudo-timestep, even during static analysis.

The uniaxial compressive behaviour of all the masonry materials was assumed to initially follow the Hognestad parabola (1951) defined by Eqn. 3.1a and presented in Fig 3.2 until the peak compressive strength. The selection for this model was based on the versatility it provides as the complete uniaxial compressive stress-strain response of the material can be defined with only two parameters, namely, the peak compressive stress of the specimen and either the corresponding strain at which the peak stress is encountered or the initial elastic modulus of the material. While values of peak compressive stress were typically provided throughout the research studies explored, values of elastic modulus and/or peak strain for the masonry units, grout, and mortar are scarcer within the literature. From this, the elastic modulus of the masonry unit, mortar, and grout was calculated based on a research study focused on the behaviour of concrete masonry assemblages (Ross, 2013), the Canadian concrete design provisions (CSA A23.3-19), and the American masonry design provisions (TMS 402/602-16), respectively. The post-peak compressive behaviour of the masonry units, mortar, and grout was defined using the

stress-strain model proposed by Priestley and Elder (1983), which is a modified version of the Kent and Park (1971) concrete stress-strain model (Eqn. 3.1b). Unlike the Hognestad model, which assumes the softening follows a quadratic response, the Priestley and Elder model assumes a linear softening profile.

$$\sigma_c = f_c\left[2\left(\frac{\varepsilon_c}{\varepsilon_p}\right) - \left(\frac{\varepsilon_c}{\varepsilon_p}\right)^2\right] \qquad \varepsilon_c \le \varepsilon_p \tag{3.1a}$$

$$\sigma_c = f_c\left[1 - \frac{0.5}{\frac{3 + 145 f_c \varepsilon_p}{145 f_c - 1000} - \varepsilon_p}\left(\varepsilon_c - \varepsilon_p\right)\right] \qquad \varepsilon_p < \varepsilon_c \le \varepsilon_{cr} \tag{3.1b}$$

Where σ_c is the uniaxial stress in compression, ε_c is the uniaxial strain in compression, E_c is the compressive elastic modulus of the material, f_c is the peak compressive strength of the material, ε_p is the strain corresponding to the peak compressive strength of the material, and ε_{cr} is the crushing strain of the material.

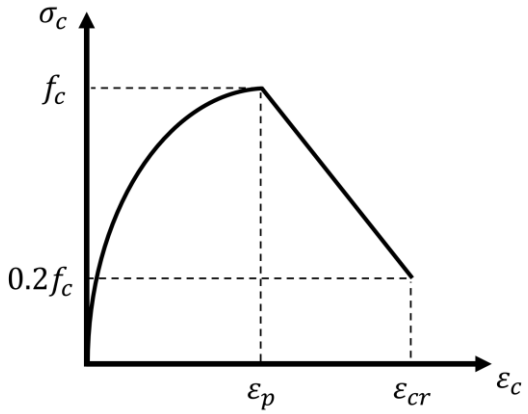

Figure 3.2 – Uniaxial Compressive Response of the Masonry Units, Mortar, and Grout

The tensile response of the grout was expressed by the tensile model proposed by Vecchio and Collins (1986) in which the tensile response remains linear elastic until rupture occurs (Eqn. 3.2a) followed by tension softening (Eqn. 3.2b) as depicted in Fig. 3.3a. The tensile response of the masonry unit and mortar were assumed to follow the model proposed by Nayal and Rasheed (2006) presented in Fig. 3.3b. The major difference between the two

tensile models is the rate of tensile degradation, as the Vecchio and Collins (1986) model features a slower rate of tensile degradation as compared to the model proposed by Nayal and Rasheed (2006). This is due to the idea that the Vecchio and Collins (1986) model assumes there is steel reinforcement present within the cementitious material, which, when applied to the micro-model, is valid for the grout cores but invalid for the masonry unit and mortar. It is noted that fractured energy approaches were explored to define the tensile response (CEB-FIP Model Code 1990, 1993), however, the approach was abandoned as convergence issues arose.

$$\sigma_t = E_t \varepsilon_t \qquad \sigma_t \leq f_r \tag{3.2a}$$

$$\sigma_t = \frac{f_r}{1 + \sqrt{200\varepsilon_t}} \qquad \sigma_t > f_r \tag{3.2b}$$

Where σ_t is the uniaxial stress in tension, ε_t is the uniaxial strain in tension, E_t is the elastic modulus in tension, and f_r is the rupture stress.

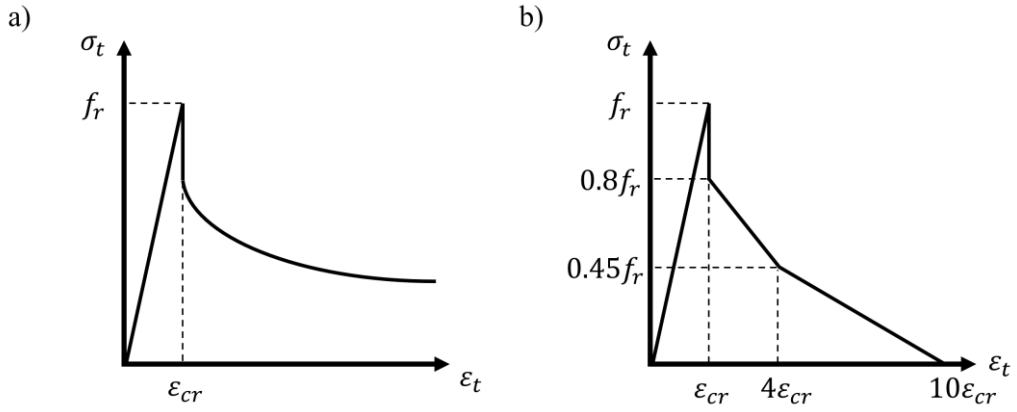

Figure 3.3 – Uniaxial Tensile Response of the (a) Grout (b) Masonry Unit and Mortar

The final parameters defined in the CDP model are two scalar damage parameters and two stiffness recovery factors that are used to account for the reduction in stiffness as cementitious materials degrade under cyclic loading. The two scalar damage parameters (d_c and d_t for compression and tension, respectively) are featured in many damage-based concrete models (Mazars, 1986) and applied by reducing the elastic modulus of the

material by a factor of d_c and d_t in compression and tension, respectively. The implementation of these parameters is similar to that of the uniaxial true stress-plastic strain curve in that specific values of the damage parameter are defined for specific regions of inelastic strain. Compressive and tensile damage parameters specified within the model were calculated based on the expressions provided by Obaidat (2017) and Birtel and Mark (2006), respectively. The stiffness recovery factors (w_c and w_t for compression and tension, respectively) control if stiffness is regained when the material shifts from compression to tension or vice-versa. Figure 3.4 illustrates the cyclic behaviour of the CDP model and the role of both the damage and stiffness recovery factors.

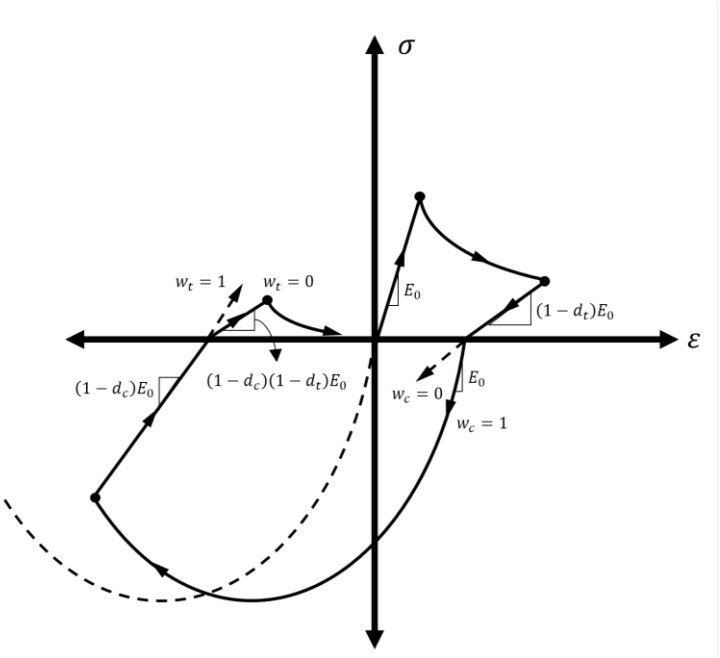

Figure 3.4 – Cyclic Response of the Concrete Damage Plasticity Model

3.2.4 Model Limitations

Due to the two-dimensional definition of the micro-model, a plane stress assumption was made. While considered valid for this model as the thickness of the wall into the page is considered quite thin compared to the plane of the wall, this analysis type limits the capability of the model to capture any out-of-plane behaviour. To capture such performance, a three-dimensional model would need to be implemented.

Due to inadequate mechanical definitions of the masonry unit–mortar and masonry unit–grout interfaces, the cyclic performance of the model is limited in accuracy. This is due to the inability of the implemented interface model to capture any reduction in stiffness that occurred by the material during loading. To accurately define the correct cyclic behaviour of the interface, custom interface models would need to be developed (Zeng et al., 2021), which was considered outside the scope of this study as the peak load of the specimens can be reasonably obtained from a monotonic pushover analysis.

3.3 Finite Element Micro-Model Validation – South American Studies

The culmination of the discussed detailed micro-modelling methodology was initially validated with South American studies conducted by Sandoval and Arnau (2017) and Calderon et al. (2017). These studies were selected as they represent a select handful of studies that contain all the parameters needed to define both the shear interfaces existing between the masonry units, mortar, and grout and the material properties of the masonry components.

3.3.1 Sandoval and Arnau (2017)

The validity of the cohesive contact-based interfaces was tested by modelling experimental tests conducted by Sandoval and Arnau (2017) involving a series of triplet and diagonal tension tests, as shown in Figs. 3.5 and 3.6, respectively. The triplet tests act to ensure that the shear response of the implemented interface is adequate, while the diagonal tension tests verify the combined axial and shear performance of the interface in addition to the concrete damage plasticity model. The models were developed following the methodology above and using material parameters specified in the study. As grout was absent from both the triplet and diagonal tension test specimens, only a masonry layer was defined within each respective model. A displacement-controlled and force-controlled static analysis were specified for the triplet and diagonal tension tests, respectively.

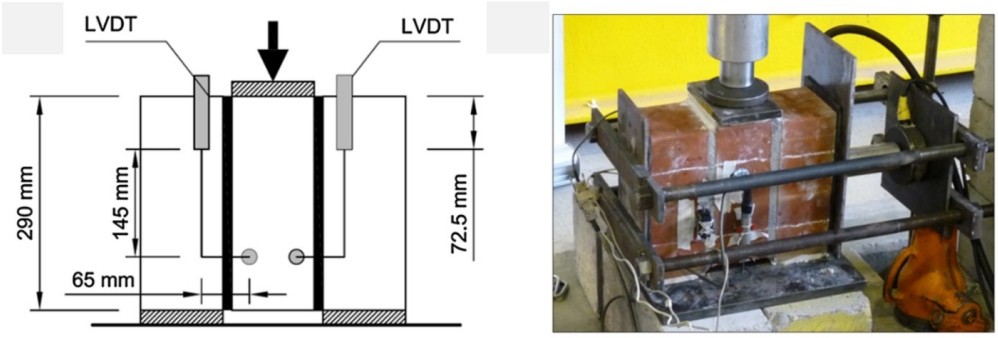

Figure 3.5 – Triplet Test Experimental Setup (Sandoval and Arnau, 2017)

Figure 3.6 – Diagonal Tension Tests (Sandoval and Arnau, 2017)

The results of the micro-model in predicting the traction-separation response of the triplet tests and the load-displacement response of the diagonal tension tests are presented in Figs. 3.7 and 3.8, respectively. A comparison of the experimental responses to that predicted by the micro-model demonstrates the validity of the implemented contact-based interface, as a good correlation is generally observed. Referring to the triplet tests, it is observed that the micro-model is able to capture the initial stiffness of the interface reasonably well until a shear stress of approximately 1 MPa. After 1 MPa, however, the stiffness of the interface, as predicted by the micro-model, decreases until the peak load is reached. This is a result of using a Mohr-Coulomb friction law to artificially include the dependence of axial compressive stress in the stiffness calculation of the cohesive interface.

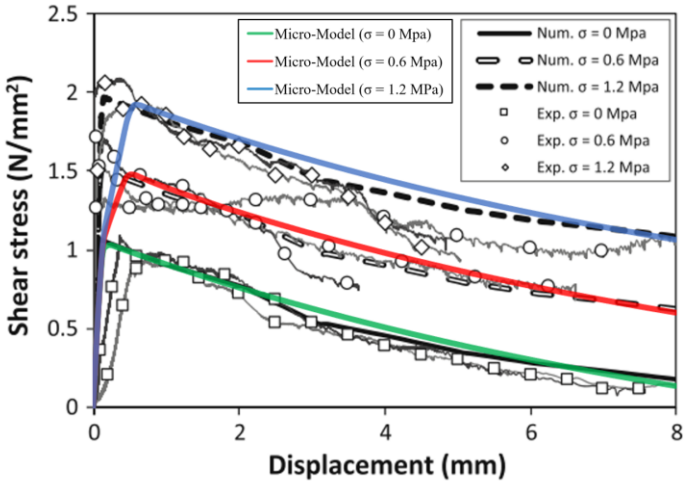

Figure 3.7 – Triplet Test Shear Stress-Displacement Plots

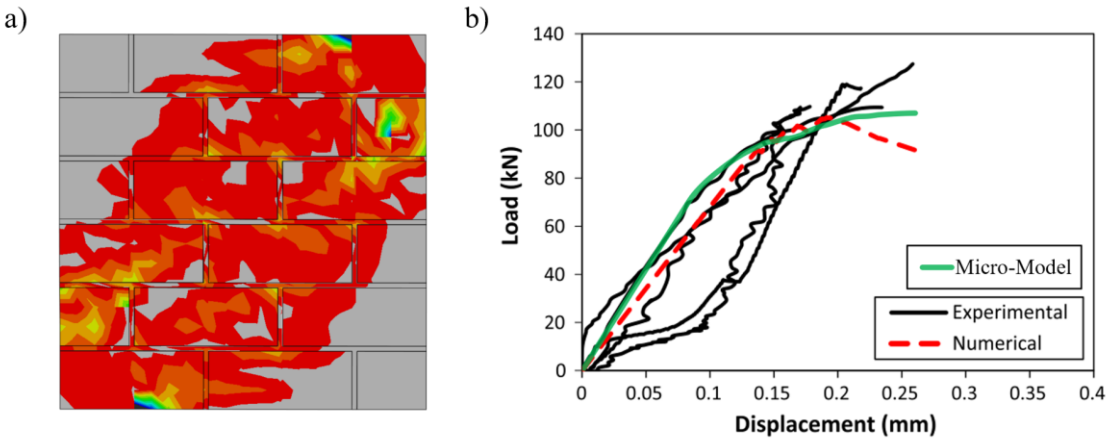

Figure 3.8 – Diagonal Tension Test Results (a) Model (b) Load-Displacement Plot

3.3.2 Calderón et al. (2017)

Validation of the methodology as a whole was conducted by micro-modelling three cantilevered partially-grouted masonry walls experimentally tested by Calderón et al. (2017) under combined cyclic lateral loading. Details of the test setup are presented in Fig. 3.9 below.

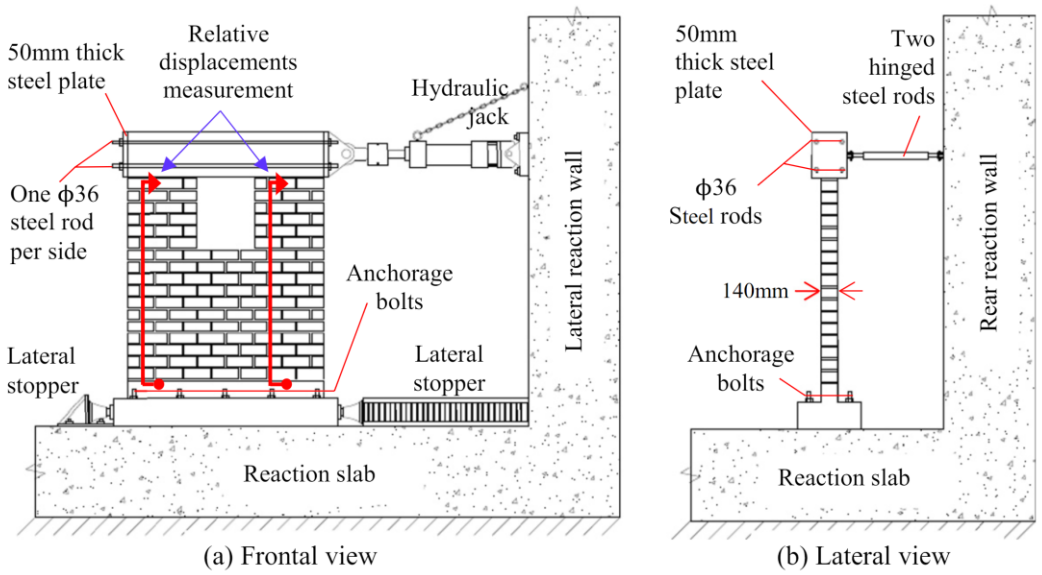

Figure 3.9 – Experimental Setup (Calderón et al., 2017)

All test specimens were constructed with perforated clay brick specimens. The first specimen was a solid wall, while the remaining two specimens contained wall openings of varied sizes. All specimens were reinforced vertically and horizontally, with details of the reinforcing schemes presented in Fig. 3.10 below.

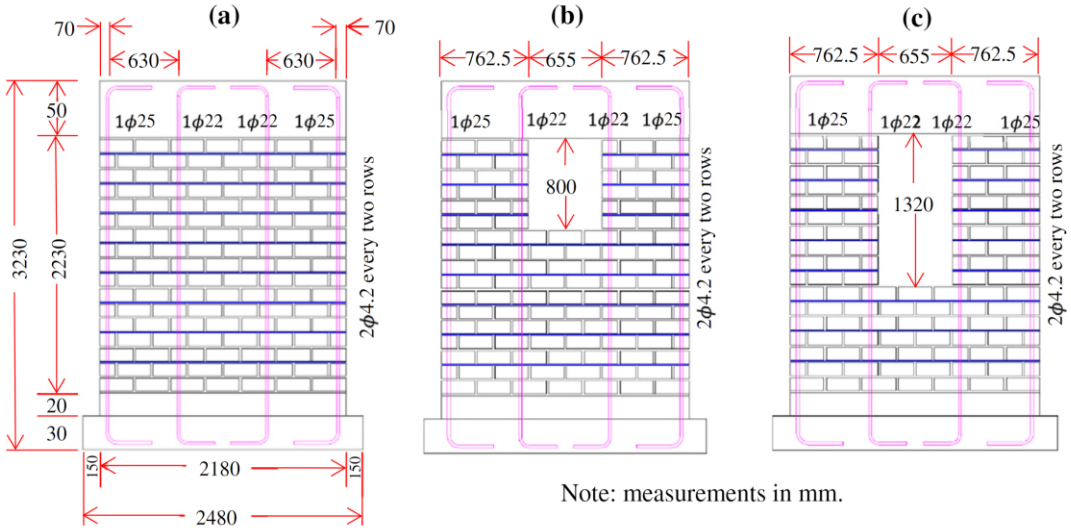

Figure 3.10 – Clay Brick Test Specimens (a) S1 (b) O1 (c) O2 (Calderón et al., 2017)

As all three specimens featured grout flutes where vertical reinforcement was present, the two-layer system described in the model development section was implemented. All material and interfacial properties specified were obtained from the study. A static analysis was performed that consisted of applying a gravity load in an initial step (to account for self-weight) followed by a displacement-controlled lateral load in the second step.

Load-displacement plots of the experimental tests, the micro-model developed by Calderón et al. (2017), and the developed micro-model are shown in Figs. 3.11 to 3.13 below with the green line representing the currently developed micro-model. It is observed that the developed micro-model exhibits a greater correlation compared to the total-strain model produced by Calderón et al. (2017). This can perhaps be attributed to the plasticity-based approach adopted, as more complex behavioural characteristics of the cementitious material (e.g., dilatancy effects) are captured. As the development of the micro-model created by Calderón et al. (2017) was not discussed apart from the implemented material and interfacial properties, it is difficult to speculate further on the differences between the two models. Comparing the predicted response of the developed micro-model to the experimental response, a good correlation is generally observed, with the exception of the slightly stronger behaviour exhibited by the micro-model when compared to two experimental tested specimens. This can be attributed to the monotonic loading specified by the micro-model as compared to the cyclical loading experienced by the specimens. As each reverse cycle induced new tensile cracks, the compressive capacity of the specimens began to wane, resulting in a deteriorated load-displacement response. In regard to the peak load, it was observed that the micro-model is able to capture the peak load relatively well, as differences were less than 5% in all three comparisons. Figure 3.14 illustrates the formation of compressive struts (measured as the minimal principal stresses) at peak load, further validating the choice of a micro-model to aid in an STM development.

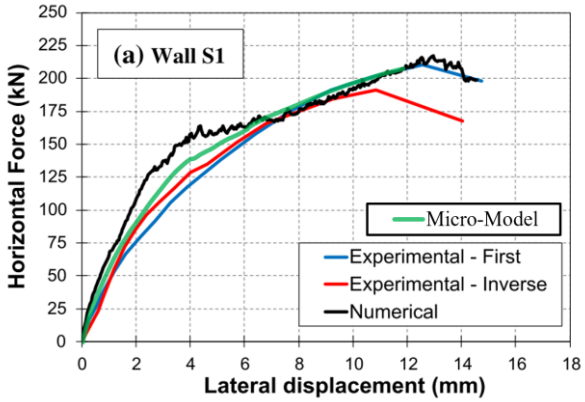

Figure 3.11 – Load-Displacement Comparison (Calderón - S1)

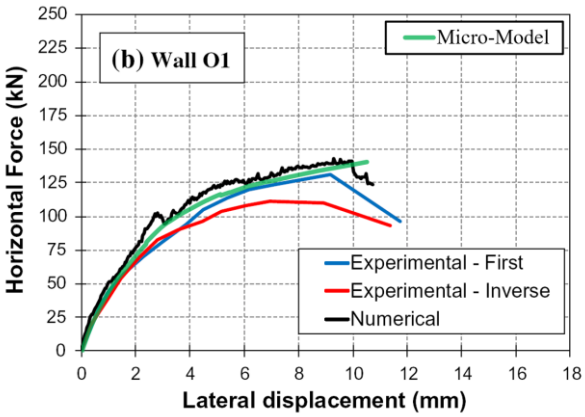

Figure 3.12 – Load-Displacement Comparison (Calderón - O1)

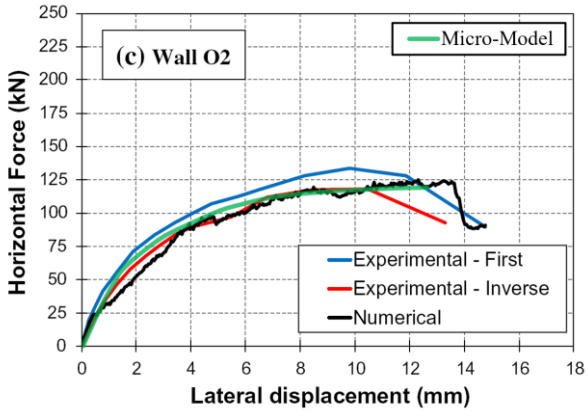

Figure 3.13 – Load-Displacement Comparison (Calderón - O2)

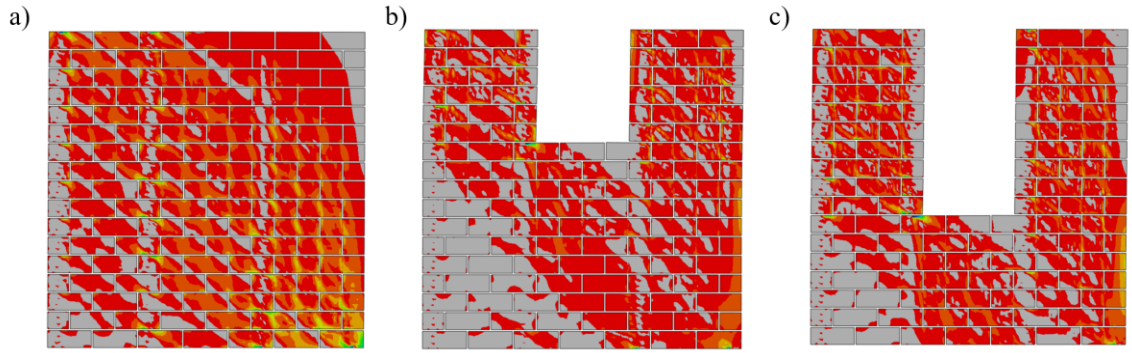

Figure 3.14 – Compressive Struts (a) S1 (b) O1 (c) O2

3.4 Experimental Determination of Concrete Block Shear Interfaces

With the methodology of the proposed micro-model validated with South American experimental studies, attention was turned to North American studies. Prior to proceeding, experimental testing was conducted to determine the required mechanical properties of shear interfaces of concrete block units, as the studies conducted in South America featured perforated clay bricks. The mechanical properties of the masonry-mortar shear interface were determined by conducting joint shear strength tests as defined in BS EN1052-3 (2002) on masonry triplet specimens. The test consists of applying a level of precompression normal to the bed joint of the masonry triplet, followed by the application of a load normal to the head joint of the middle unit in the triplet. From this, a relationship relating the applied shear stress to the interface displacement (traction-separation response) can be determined for varying levels of precompression. Several researchers (Haach, 2009; Sandoval and Arnau, 2016; Bolaños, 2020) have adopted this test configuration to study the shear bond properties of the mortar joints.

3.4.1 Experimental Setup and Test Specimens

All specimens were masonry triplets which consist of three hollow masonry units laid in a stack bond pattern. Five levels of precompression encompassing a range considered typical in partially-grouted walls (0 MPa, 1.0 MPa, 1.5 MPa, 2.0 MPa, and 2.5 MPa) were investigated. Three tests were conducted for each level of precompression, resulting in a total of 15 tested specimens. All triplet specimens were constructed using standard 20-cm masonry units and Type S mortar by a professional mason. Details of the

experimental setup can be found in Figs. 3.15 and 3.16 below. Four horizontal jacks, each with a 50 kN capacity, were used to employ the precompression, which was then held constant as a 500 kN vertical jack imposed the shear displacement until failure, defined by the slipping of the middle unit with respect to the end units, occurred. Fiberboard was placed between the points of contact between the triplet specimens and the loading apparatus to ensure stress concentrations did not occur. The applied horizontal and vertical loads were measured via load cells, while the shear displacements were measured using a linear variable displacement transducer (LVDT). Locations of the LVDTs are also shown in Fig. 3.15.

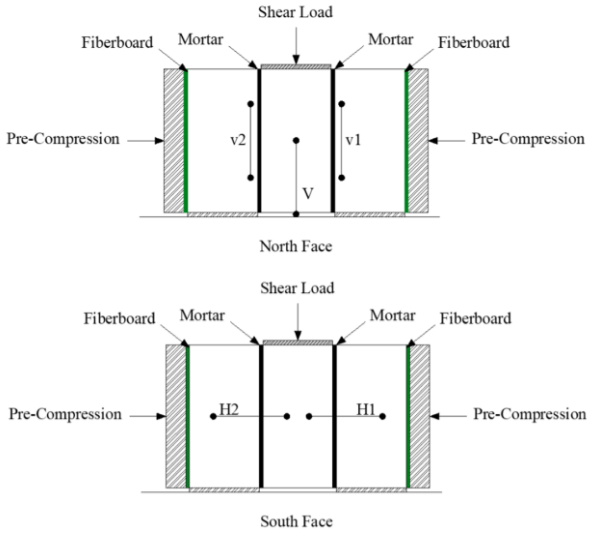

Figure 3.15 – Triplet Test Experimental Setup

Figure 3.16 – Conducted Triplet Test

3.4.2 Experimental Results

The shear stress–displacement response for all 15 specimens is presented in Fig. 3.17 below. From the plot, it is observed that the maximum shear stress increases with increased levels of precompression. In addition, all 15 specimens displayed similar levels of initial shear stiffness prior to the peak load. The traction-separation behaviour of the specimens can be represented by three distinct branches. The first is a linear elastic regime in which the cohesive bond between the masonry and mortar remains completely intact and governs the response. After the peak load is reached, the cohesive bond begins to deteriorate exponentially until the third branch, consisting of a plateau, is reached. When the plateau is reached, the cohesive bond between the masonry-mortar interface has completely deteriorated, with the only remaining shear resistance attributed to dry friction.

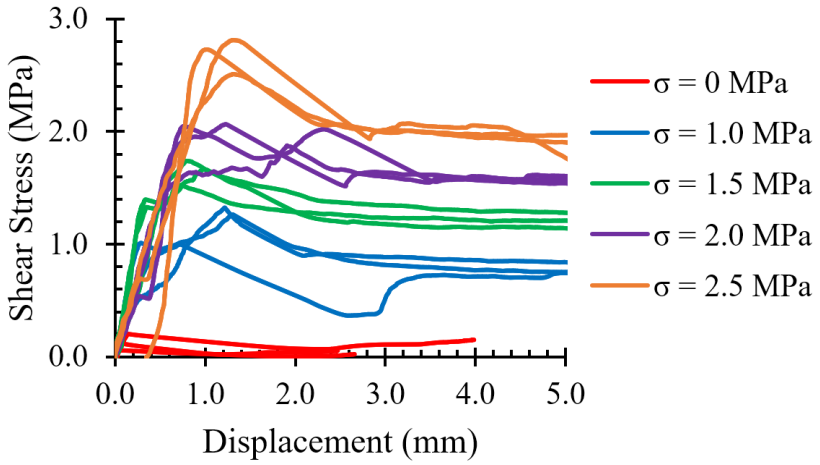

Figure 3.17 – Triplet Test Shear Stress – Joint Displacement Results

To determine the idealized linear Mohr-Coulomb friction law governing the interface, data points of peak load as a function of precompression are plotted (Fig. 3.18). By performing a linear regression analysis on the data, the initial cohesion and coefficient of friction of the interface (corresponding to the y-intercept and slope of the linear Mohr-Coulomb response, respectively) were determined to be 0.139 MPa and 0.999, respectively.

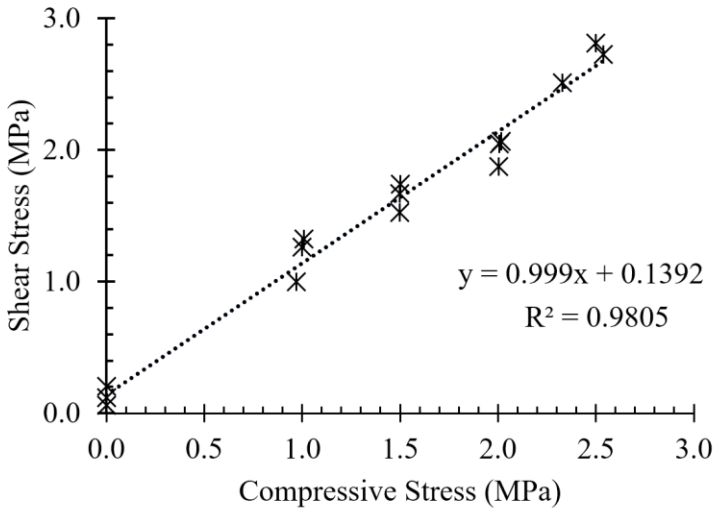

Figure 3.18 – Triplet Test Block-Mortar Mohr-Coulomb Idealization

3.4.3 Finite Element Simulation of the Triplet Tests

The triplet tests were simulated using the micro-modelling methodology in an attempt to reproduce the experimentally determined behaviour (Fig. 3.19a). It was found, however, that the initial coefficient of friction related to the elastic cohesive behaviour (0.999) did not match that of the coefficient of friction experienced by the interfaces after the deterioration occurred (calculated on average as 0.777 based on the mechanics of dry friction). This effect can be seen by comparing the shear stress-displacement plots of Figs. 3.19b and 3.19c. Referring to Fig. 3.19b, an implemented value of 0.999 results in an accurate prediction of the peak shear capacity of the interface; however, the post-peak region is noticeably overestimated. Figure 3.19c demonstrates that this post-peak behaviour can be better accounted for by specifying the lower coefficient of friction (0.777); however, the peak shear strength of the interface is not captured.

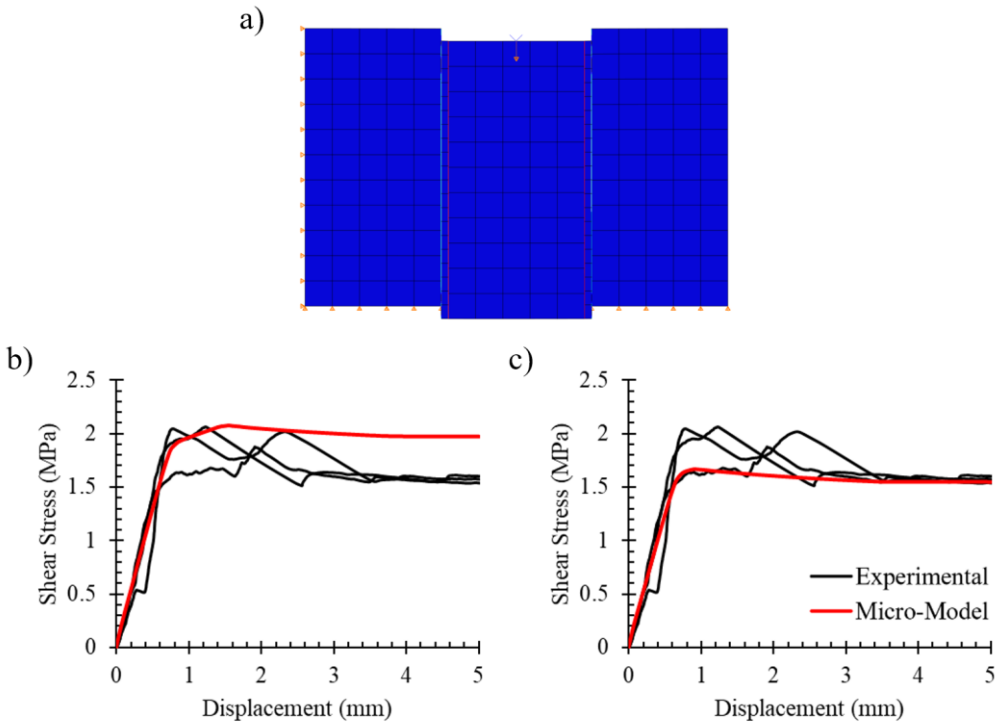

Figure 3.19 – Triplet Test Simulation (a) Model (b) Friction Coefficient of 0.999 (c) Friction Coefficient of 0.777

To account for both the peak shear capacity and the post-peak response of the interface, the lower coefficient of friction was specified with an artificially increased value of cohesion (from 0.139 MPa to 0.25 MPa). Unfortunately, such a modification must be made to adequately capture this complex response within a simplistic contact. The implication of this modification on the traction-separation behaviour is shown in Fig. 3.20 below, in which the shear stress-displacement plots for all levels of precompression as predicted by the micro-model are compared to the experimental results. Referring to Fig 3.20, it is observed that the artificial increase in cohesion allows for both the peak and post-peak behaviour of the shear interface to be reasonably captured. It is noted that for the highest level of precompression (2.5 MPa), the validity of this approach is limited. However, these high stresses are rarely encountered as applied axial stresses are typically below 0.5 MPa.

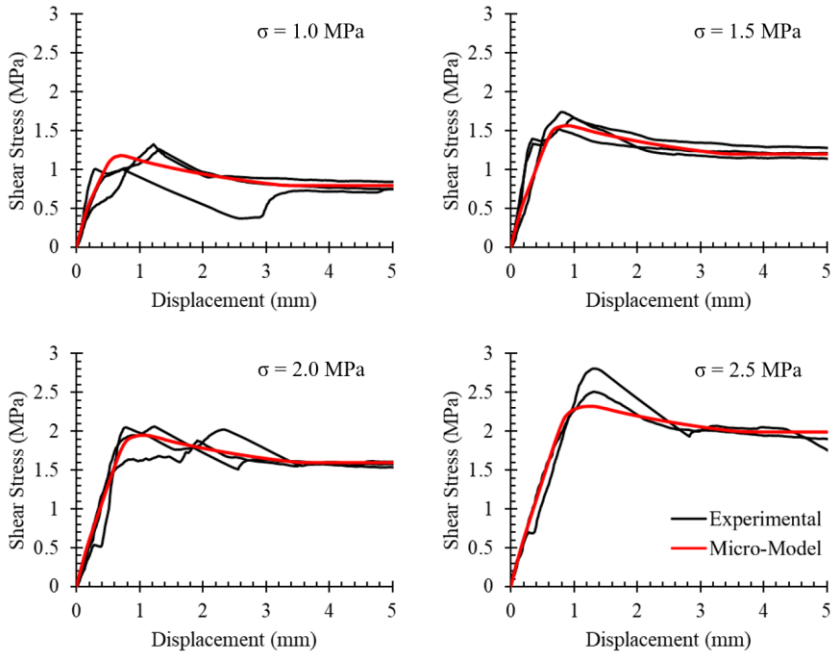

Figure 3.20 – Triplet Test Simulation with Modified Interface Properties

3.5 Finite Element Micro-Model Validation – North American Studies

To determine the performance of the micro-model in capturing the behaviour of North American partially-grouted wall systems, four experimental studies were selected from the literature. These studies are those of Nolph (2010), Elmapruk (2010), Minaie et al. (2010), and Ba Rahim et al. (2022). The rationale for the selection of these studies was that variations of key design parameters are accounted for, as highlighted in Table 3.1. It is noted that although Nolph (2010) and Elmapruk (2010) did not independently investigate the influence of the aspect ratio, their combined studies provide the insight necessary to form conclusions.

Table 3.1 – Key Design Parameters Investigated

Study	Axial Stress	Aspect Ratio	Reinforcement Spacing		Reinforcement Quantity		Boundary Conditions
			Vert.	Hor.	Vert.	Hor.	
Nolph (2010)	-	X	X	-	X	X	-
Elmapruk (2010)	-	X	X	-	X	X	-
Minaie et al. (2010)	-	-	-	-	-	-	X
Ba Rahim et al. (2022)	X	X	-	X	-	-	-

3.5.1 Minaie et al. (2010)

Minaie et al. (2010) was the first study simulated. Details of the study were discussed in detail in Section 2.3.2. Varied parameters between specimens include the mortar type (MC and PCL) and the wall boundary conditions (cantilevered and fixed-fixed). Material properties specified in the micro-model are displayed in Table 3.2 below. It is noted that the yield strength of the steel reinforcement was not specified, so a value of 400 MPa was assumed based on the results of similar studies.

Table 3.2 – Material Properties (Minaie)

Material	Peak Compressive Strength (MPa)	Yield Strength (MPa)
Masonry Units	13.8	-
Mortar (MC)	12.6	-
Mortar (PCL)	25.8	-
Grout	22.0	-
Reinforcing Steel	-	400 (Assumed)

Figure 3.21 depicts the general two-layered micro-model developed for the four simulations. A general fixed base boundary condition was specified for all four models by restraining the base of the concrete foundation from translating in both the horizontal and lateral directions. Loading was applied in a two-step static analysis. In the first step, an axial stress was applied to the top of the model and held during the second step, in which a lateral displacement was specified at several nodes roughly 400 mm apart. This spacing represents the placement of the steel bolts specified to fasten the steel loading beam to the wall system. The vertical degrees of freedom of the nodes where the lateral displacement was applied were left free to allow for rotation along the top of the wall, thus simulating the cantilever boundary conditions for two of the four specimens. For the two walls with specific fixed-fixed boundary conditions, the vertical displacement of the laterally displaced nodes was constrained to zero.

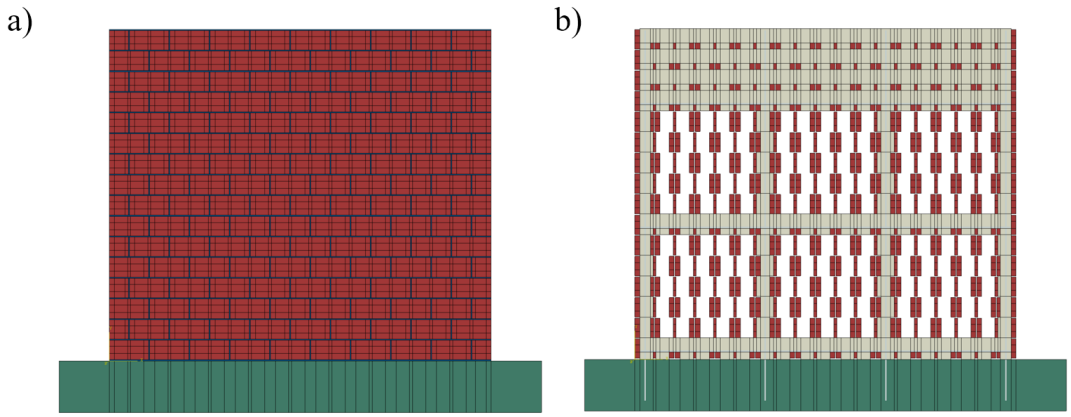

Figure 3.21 – Micro-Model (a) Masonry Layer (b) Grout Layer (Minaie)

Figures 3.22 to 3.25 below compare the applied load–wall drift response obtained from the finite element micro-model to that obtained from experimental testing for the four specimens. In general, a good correlation is observed between the two models in terms of ultimate load capacity and initial stiffness. Referring to the ultimate load capacity, it was found that the micro-model tended to slightly overestimate the ultimate load capacity for all the specimens tested. This is expected, however, due to the likelihood that the cyclic testing of the wall specimens prohibited the wall from reaching the same peak load that would have been obtained if a monotonic loading had been specified. Differences between the experimentally obtained peak load (V_{Exp}) and that predicted by the micro-model (V_{FE}) were generally acceptable within the range of 11%, as shown in Table 3.3. The exception, however, was that of Specimen MC1, in which the model over-predicted the strength of the specimen by 22%. This was also the only specimen in which the micro-model predicted the yielding of the vertical reinforcement prior to failure, which is visually evident by the large drifts the wall was able to withstand, as displayed in Fig. 3.22. As significant details such as vertical reinforcement anchorage, yield strength, and failure modes were not reported in the study, it is challenging to determine the source of the overestimation.

Referring to the two specimens tested under fixed-fixed boundary conditions, it is interesting to note the load-displacement plateaus shortly after the peak load was reached. Results from the micro-model indicated that, at this point, the interfaces were

significantly damaged, resulting in a frictional sliding response which is consistent with findings reported in the study. It is also observed that the micro-model is able to capture the initial elastic stiffness of the wall specimens within a reasonable degree. As the loading increases, however, the model begins to overestimate the stiffness. This is expected, however, as the cyclic loading of the experiments would continuously degrade the stiffness of the wall specimens, which is not captured in the monotonic loading of the micro-model.

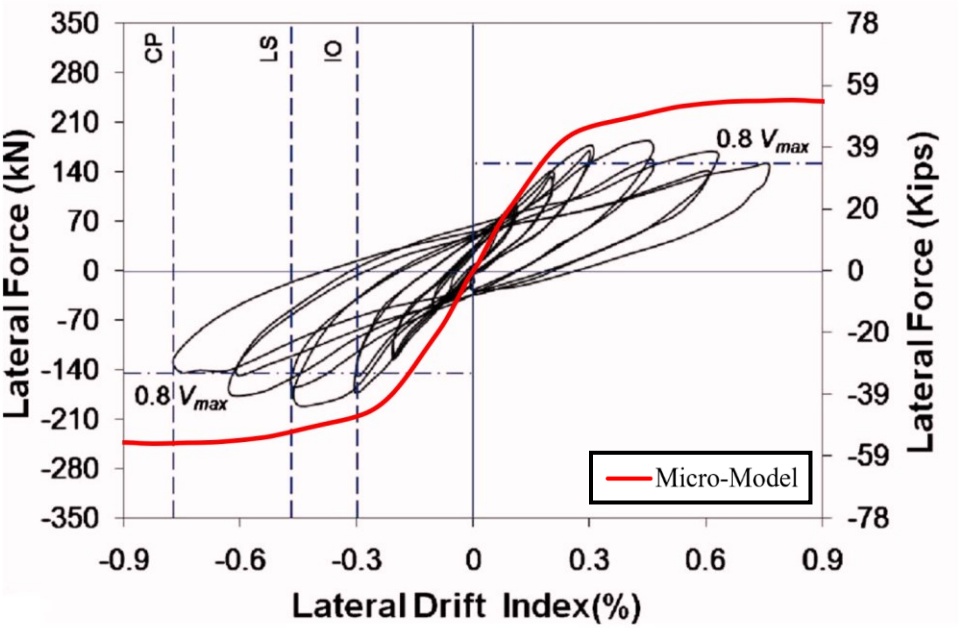

Figure 3.22 – Applied Load-Wall Drift Comparison (Minaie - MC1)

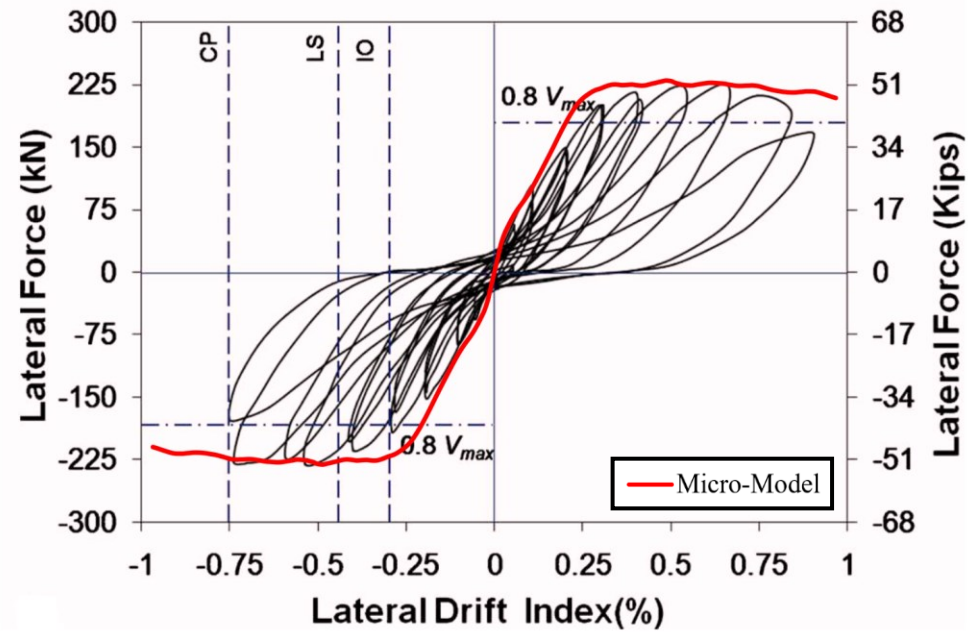

Figure 3.23 – Applied Load-Wall Drift Comparison (Minaie - MC2)

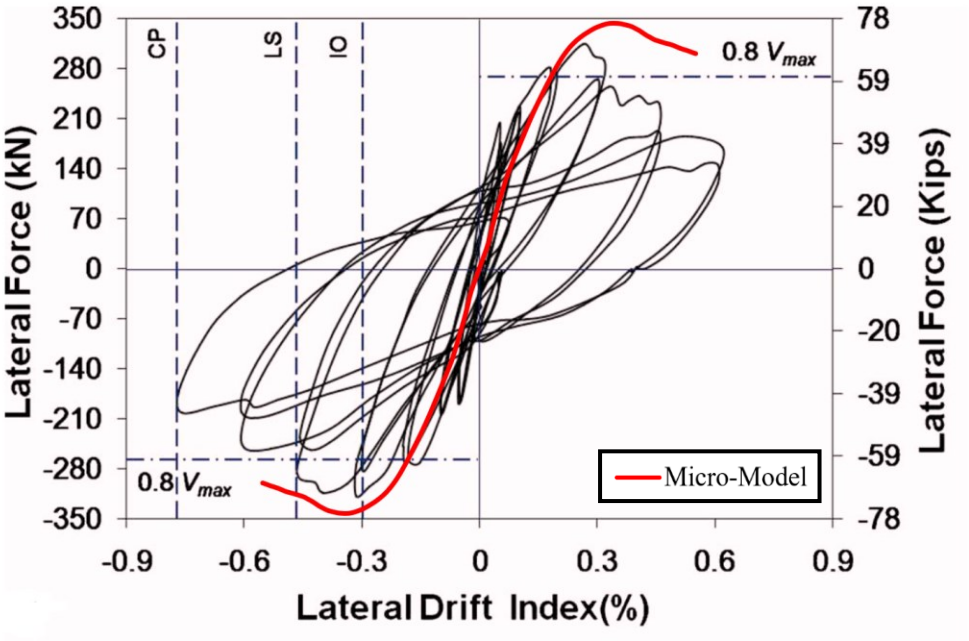

Figure 3.24 – Applied Load-Wall Drift Comparison (Minaie - PCL1)

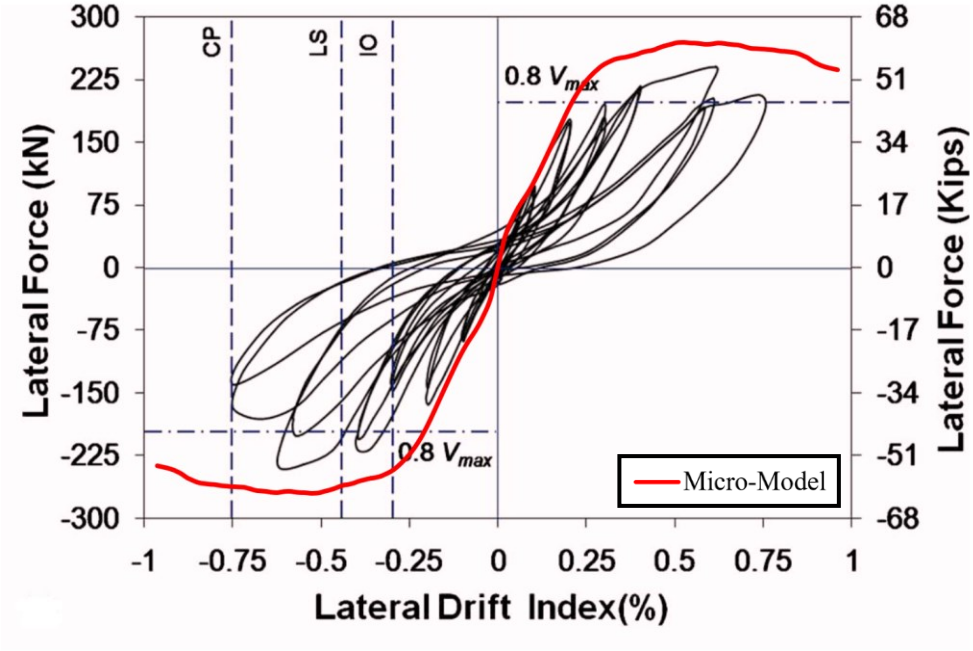

Figure 3.25 – Applied Load-Wall Drift Comparison (Minaie - PCL2)

Table 3.3 – Micro Model Results Comparison (Minaie)

Specimen	V_{Exp} (kN)	V_{FE} (kN)	V_{Exp}/V_{FE}
MC1	190	243	0.78
MC2	230	232	0.99
PCL1	318	344	0.92
PCL2	241	271	0.89

3.5.2 Nolph (2010) & Nolph and ElGawady (2012)

The second experimental study selected in the micro-model validation process was conducted by Nolph (2010). Details of the study were discussed in detail in Section 2.3.3. Varied parameters between specimens include the quantity and distribution of both the horizontal and vertical reinforcement. Material properties specified in the micro-model are displayed in Table 3.4 below. While the peak strength of the mortar was not specified in the report, the value obtained from Elmapruk (2010) was selected as the two studies were conducted in conjunction. To test the cyclic performance of the micro-model, an

additional cyclic simulation was conducted for Specimen PG085-48, which is considered to be the specimen featuring the most typical design parameters.

Table 3.4 – Material Properties (Nolph)

Material	Peak Compressive Strength (MPa)	Yield Strength (MPa)
Masonry Units	18.1	-
Mortar	14.9	-
Grout	29.2	-
Steel (#5 Bar)	-	439
Steel (#6 Bar)	-	439

Figure 3.26 depicts the general two-layered micro-model developed for the specimens featuring a vertical reinforcement spacing of 1200 mm. A general fixed base boundary condition was specified for all four models by restraining the base of the concrete foundation from translating in both the horizontal and lateral directions. Loading was applied in a two-step static analysis. In the first step, an axial stress of 0.1 MPa was applied to the top of the model and held during the second step, in which a lateral displacement was specified at several nodes roughly 400 mm apart. This spacing represents the placement of the steel bolts specified to fasten the steel loading beam to the wall system, similar to the Minaie et al. (2010) study. The vertical degrees of freedom of the nodes where the lateral displacement was applied were left free to allow for rotation along the top of the wall, thus simulating the cantilever boundary conditions.

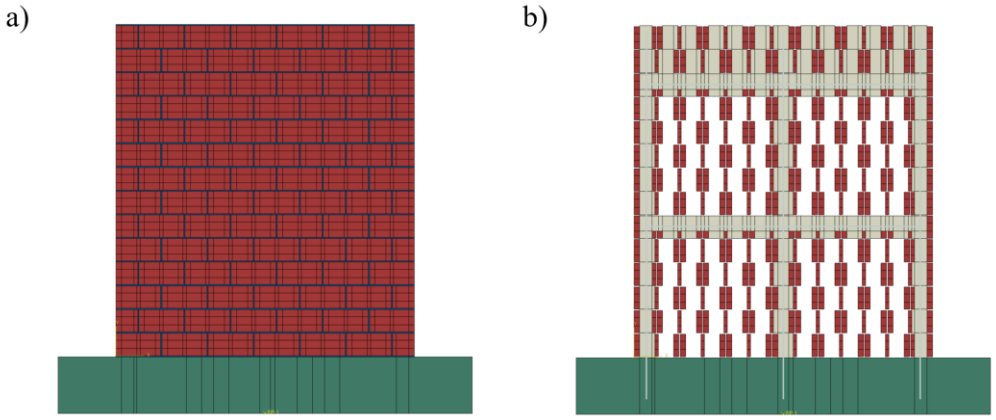

Figure 3.26 – Micro-Model (a) Masonry Layer (b) Grout Layer (Nolph)

Figures 3.27 to 3.30 below compare the applied load–wall drift response obtained from the finite element micro-model to that obtained from experimental testing for the four specimens. Overall, the micro-model displayed a good correlation with the experimental data in predicting both the initial stiffness and ultimate load capacity. Predictions of the ultimate load capacity ranged between 5% to 14%, as indicated in Table 3.5. Unlike the Minaie et al. (2010) study, however, the micro-model consistently under-predicted the ultimate load capacity of the specimens. This was expected as no strain-hardening definition was included for the flexural reinforcement, which was indicated to yield for the majority of the specimens. The exception to this was Specimen PG169-48, in which no yielding of the flexural reinforcement occurred. In this instance, the micro-model was able to capture the ultimate load capacity to within 5%.

Regarding the initial stiffness prediction, a good correlation between the experimental results and those predicted by the micro-model was observed. The exception to this was Specimen PG085-24, in which the initial stiffness predicted by the micro-model is noticeably larger than the experimental findings. This can be attributed to the authors noting that Specimen PG085-24 was damaged during initial transportation into the loading frame, resulting in the cracking of several interfaces prior to testing and, ultimately, a lower initial stiffness than what would be expected. The micro-model also did not predict any yielding of the horizontal reinforcement at peak load, which is consistent with the reported findings. This is an important observation as both the Canadian and American masonry design provisions assume the yielding of the reinforcement. Additional discussions on this aspect will be presented in detail in Section 4.2.3.

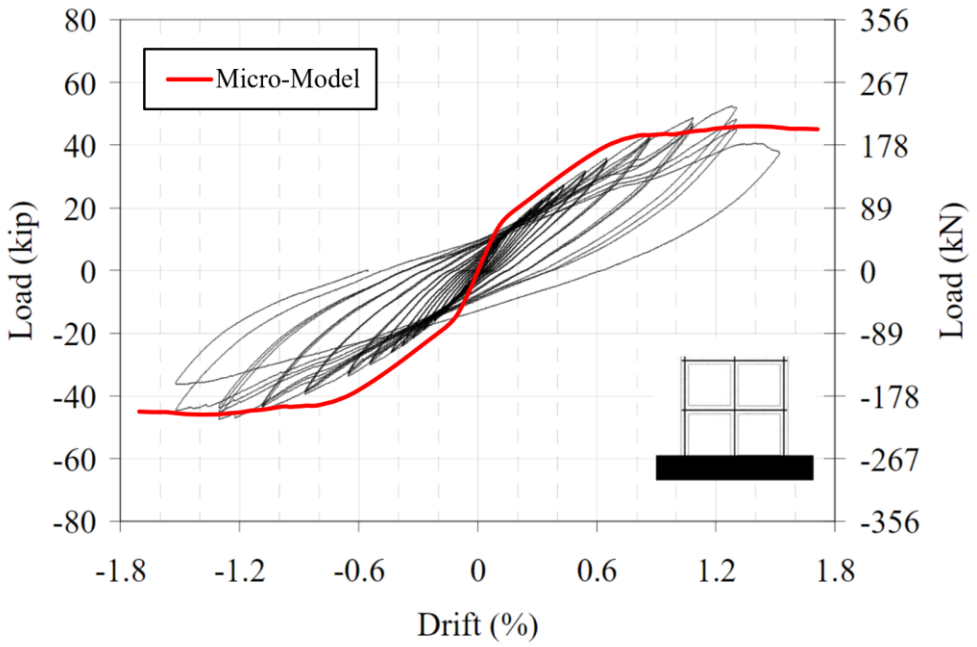

Figure 3.27 – Applied Load-Wall Drift Comparison (Nolph – PG085-48)

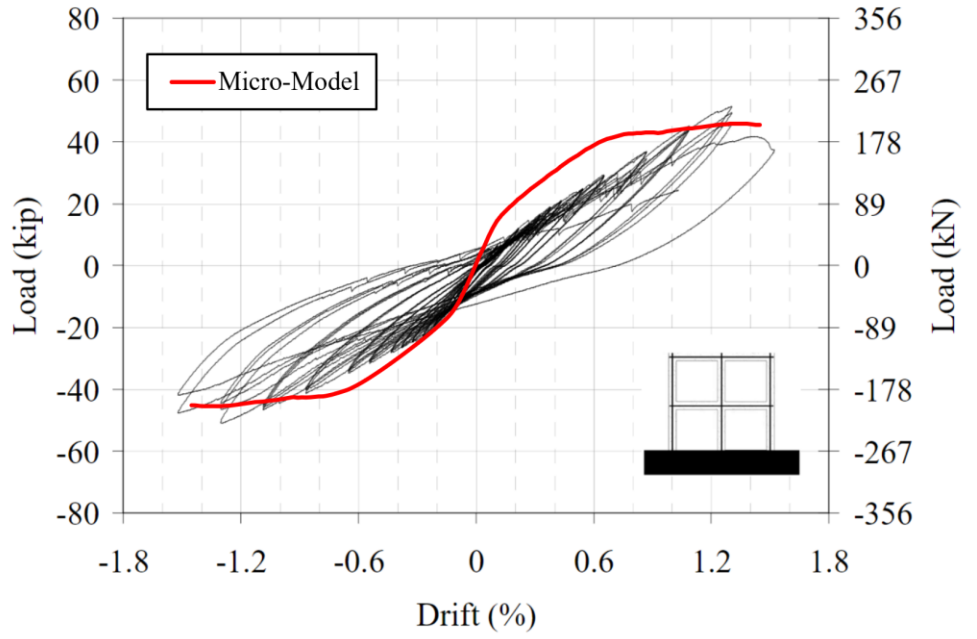

Figure 3.28 – Applied Load-Wall Drift Comparison (Nolph – PG127-48)

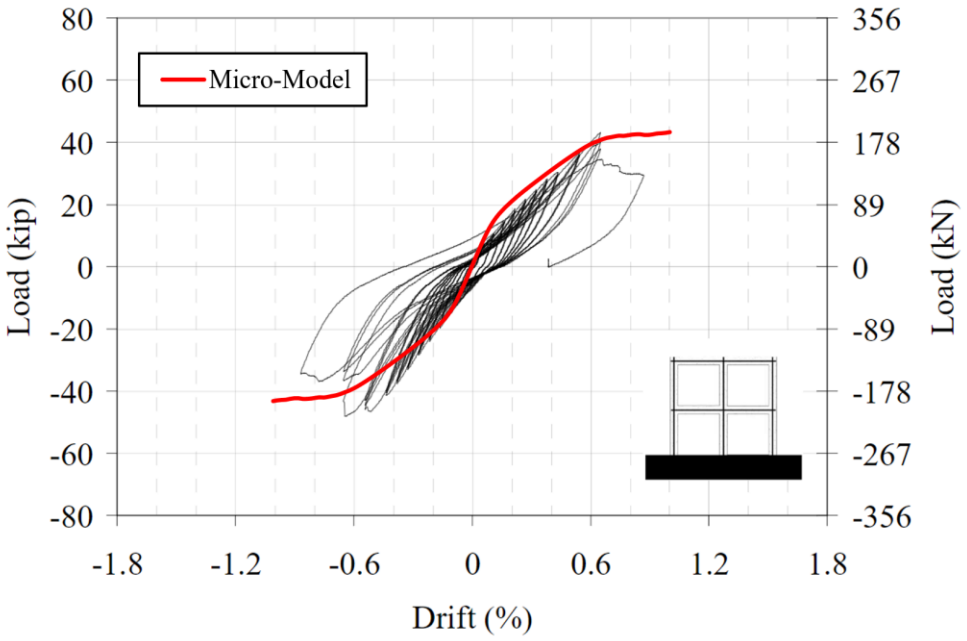

Figure 3.29 – Applied Load-Wall Drift Comparison (Nolph – PG169-48)

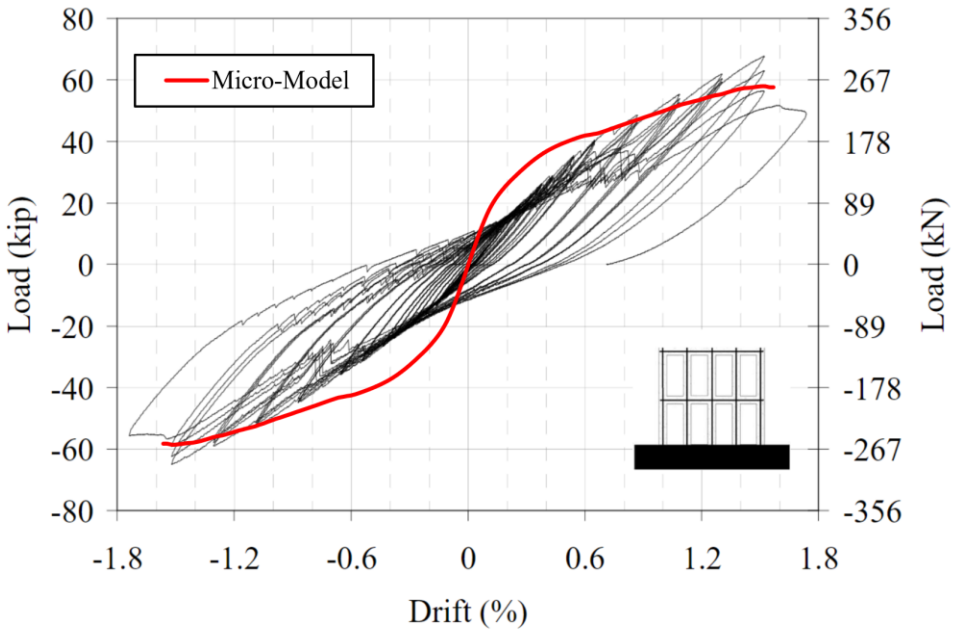

Figure 3.30 – Applied Load-Wall Drift Comparison (Nolph – PG085-24)

Table 3.5 – Micro Model Results Comparison (Nolph)

Specimen	V_{Exp} (kN)	V_{FE} (kN)	V_{Exp}/V_{FE}
PG085-48	222	204	1.09
PG120-48	228	203	1.12
PG169-48	203	193	1.05
PG085-24	295	259	1.14

Figure 3.31 presents the cyclic applied load-drift response of Specimen PG085-48. Overall, the performance of the model to predict the response is quite satisfactory, provided that the defined interfaces and implemented steel plasticity models do not account for the cyclic degradation of the materials. The neglection of these cyclic models is quite noticeable when comparing the unloading behaviour of the experimental results to that of the micro-model, as the stiffness of the experimental response is significantly lower than that of the micro-model. It is expected that additional testing regarding the material properties and interface characteristics will allow for the insight required to accurately define the cyclic response of the materials, and ultimately provide a micro-model capable of capturing the cyclic behaviour of partially-grouted masonry walls.

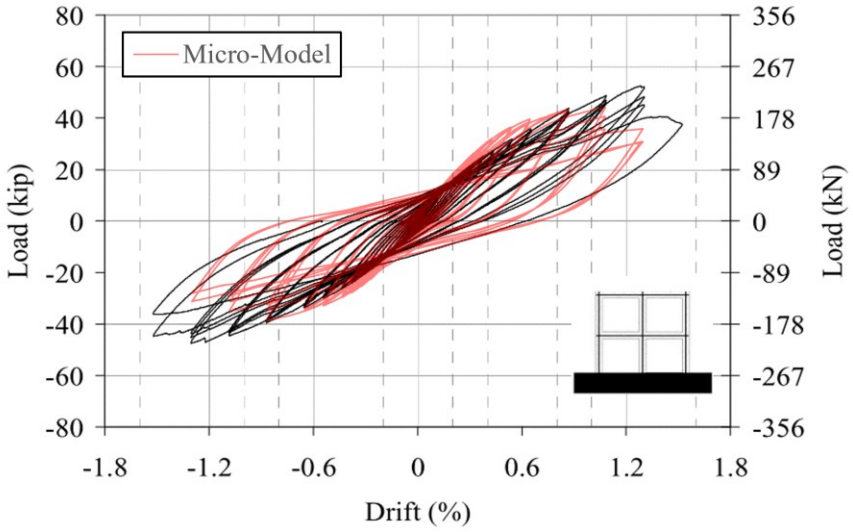

Figure 3.31 – Cyclic Applied Load-Wall Drift Comparison (Nolph – PG085-48)

3.5.3 Elmapruk (2010) & Elmapruk et al. (2020)

The third experimental study selected in the micro-model validation process was conducted by Elmapruk (2010). Details of the study were discussed in detail in Section 2.3.3. Varied parameters between specimens include the quantity of horizontal and vertical reinforcement in addition to the spacing of the vertical reinforcement. As the study was conducted in collaboration with Nolph (2010), the reinforcing schemes, applied axial loads, and boundary conditions of the specimens are identical between the two studies, resulting in additional comparisons regarding the influence of the aspect ratio to be made. Material properties specified in the micro-model are displayed in Table 3.6 below. While the peak strength of the masonry unit was not specified in the report, the value obtained from Nolph (2010) was selected.

Table 3.6 – Material Properties (Elmapruk)

Material	Peak Compressive Strength (MPa)	Yield Strength (MPa)
Masonry Units	18.1	-
Mortar	14.9	-
Grout	35.9	-
Steel (#5 Bar)	-	452
Steel (#6 Bar)	-	427

Figure 3.32 depicts the general two-layered micro-model developed for the specimens featuring a vertical reinforcement spacing of 1200 mm. A general fixed base boundary condition was specified for all four models by restraining the base of the concrete foundation from translating in both the horizontal and lateral directions. Loading was applied in a two-step static analysis. In the first step, an axial stress of 0.1 MPa was applied to the top of the model and held during the second step, in which a lateral displacement was specified at several nodes roughly 400 mm apart. This spacing represents the placement of the steel bolts specified to fasten the steel loading beam to the wall system. The vertical degrees of freedom of the nodes where the lateral displacement was applied were left free to allow for rotation along the top of the wall, thus simulating the cantilever boundary conditions.

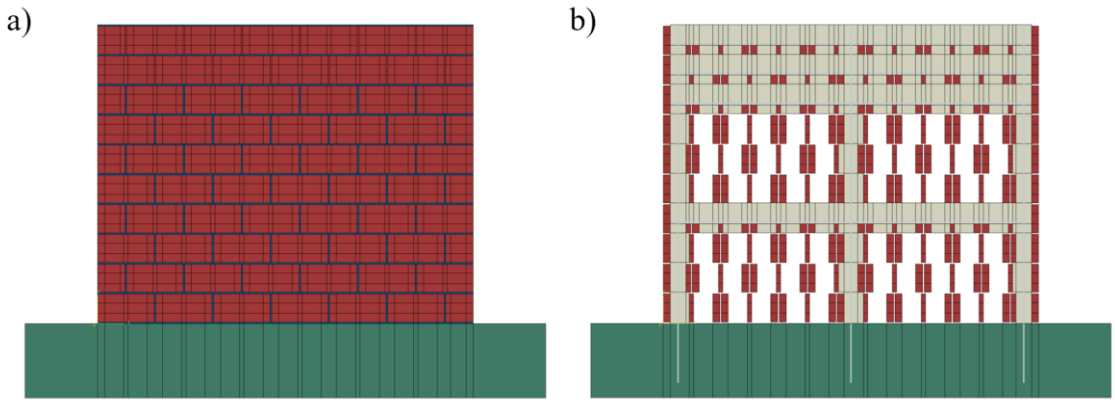

Figure 3.32 – Micro-Model (a) Masonry Layer (b) Grout Layer (Elmapruk)

Figures 3.33 to 3.38 below compare the applied load–wall drift response obtained from the finite element micro-model to that obtained from experimental testing for the six specimens. The performance of the micro-model to predict the initial stiffness and ultimate load capacity was similar to the Nolph (2010) predictions in that a good correlation was observed for all specimens. Referring to Table 3.7, ultimate load strength predictions were within 9% of the experimentally reported results, with four of the six predictions within 3% of the experimentally reported results. Unlike previous results where the micro-model would begin to predict a higher lateral stiffness after cracking occurred, in this study, the opposite appears to be true in which the micro-model appears to underestimate the stiffness for the majority of the specimens prior to peak load. This underestimation of the stiffness is most likely attributed to the interface model defined, as a similar behaviour was observed in Fig. 3.7 above in which the interface begins to lose stiffness prior to peak load. The micro-model was consistent with experimental findings in that no yielding of the horizontal reinforcement was observed.

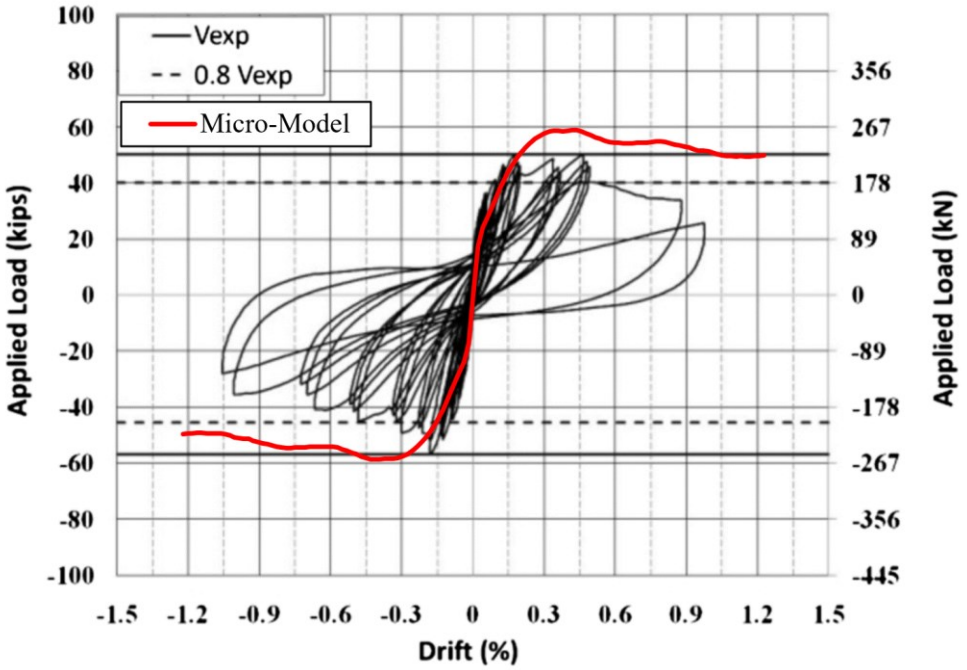

Figure 3.33 – Applied Load-Wall Drift Comparison (Elmapruk – PG127-48)

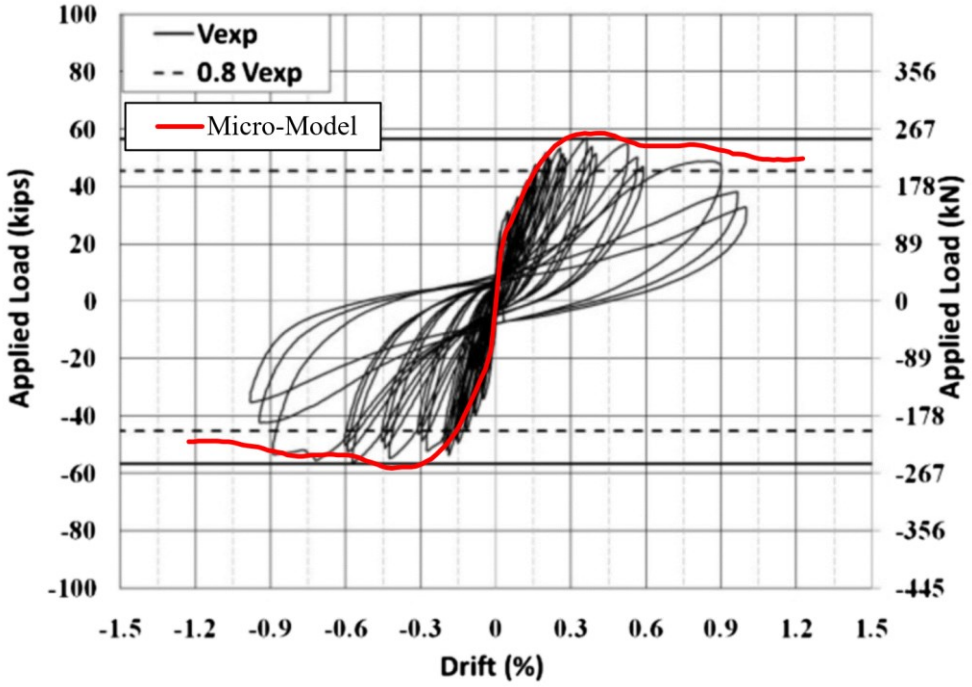

Figure 3.34 – Applied Load-Wall Drift Comparison (Elmapruk – PG127-48I)

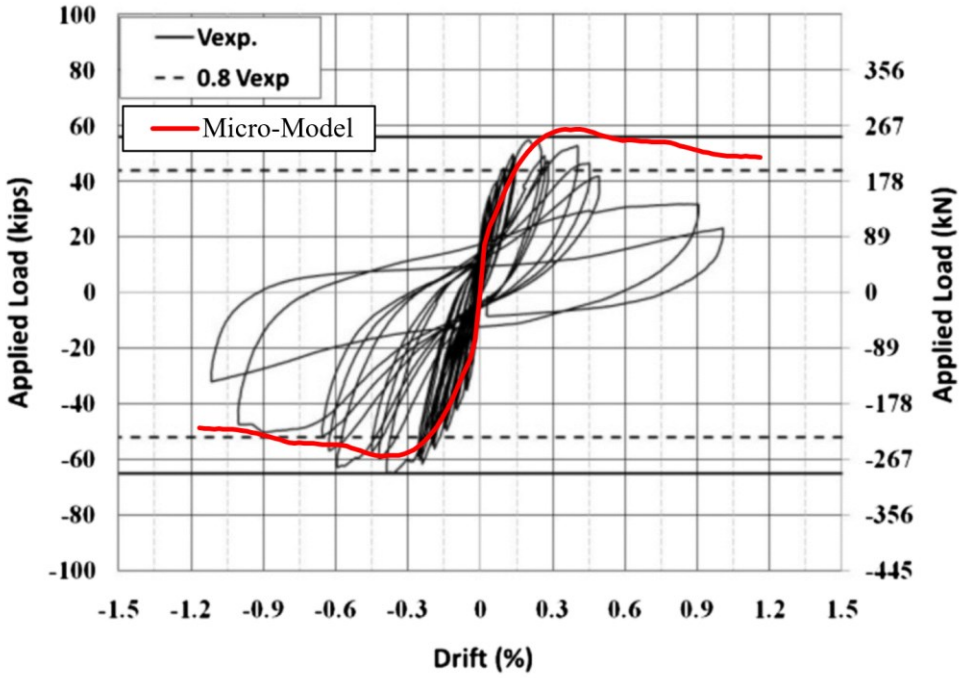

Figure 3.35 – Applied Load-Wall Drift Comparison (Elmapruk – PG180-48)

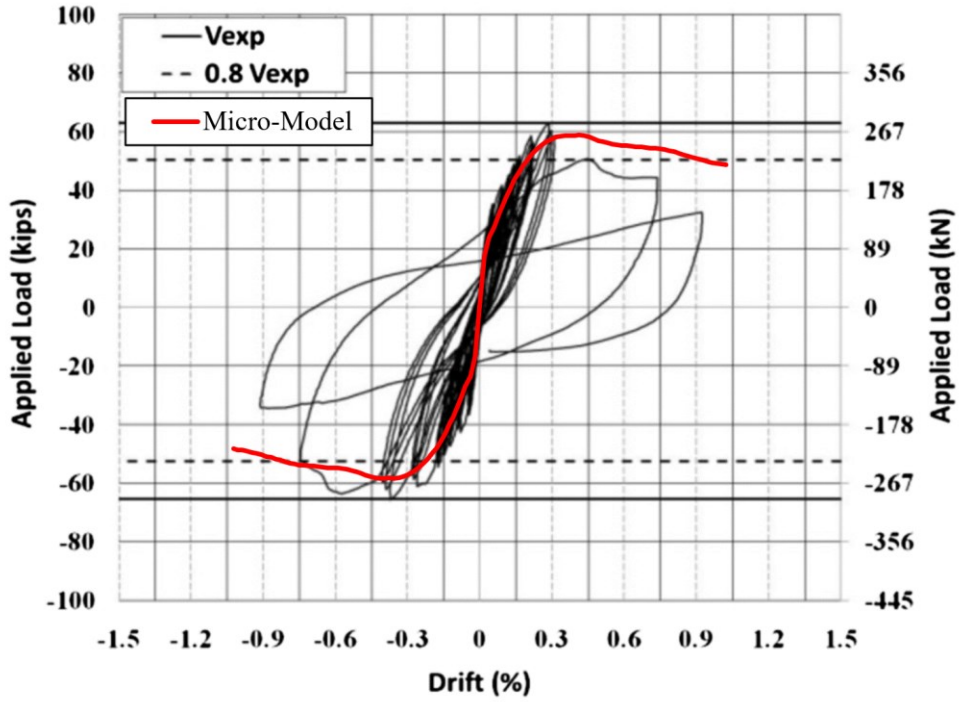

Figure 3.36 – Applied Load-Wall Drift Comparison (Elmapruk – PG254-48)

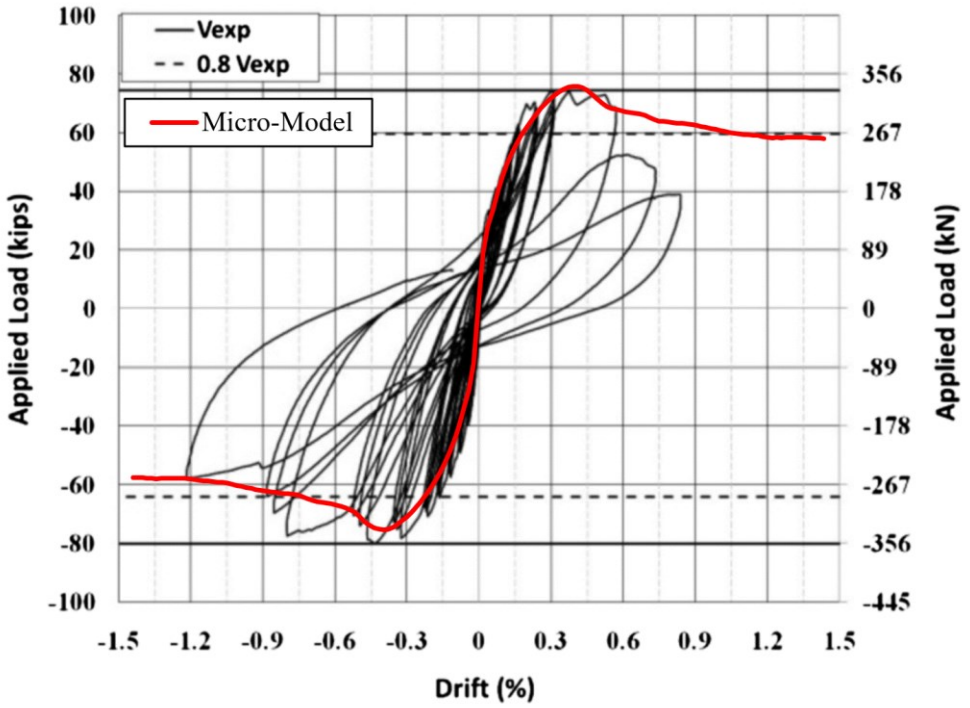

Figure 3.37 – Applied Load-Wall Drift Comparison (Elmapruk – PG127-32)

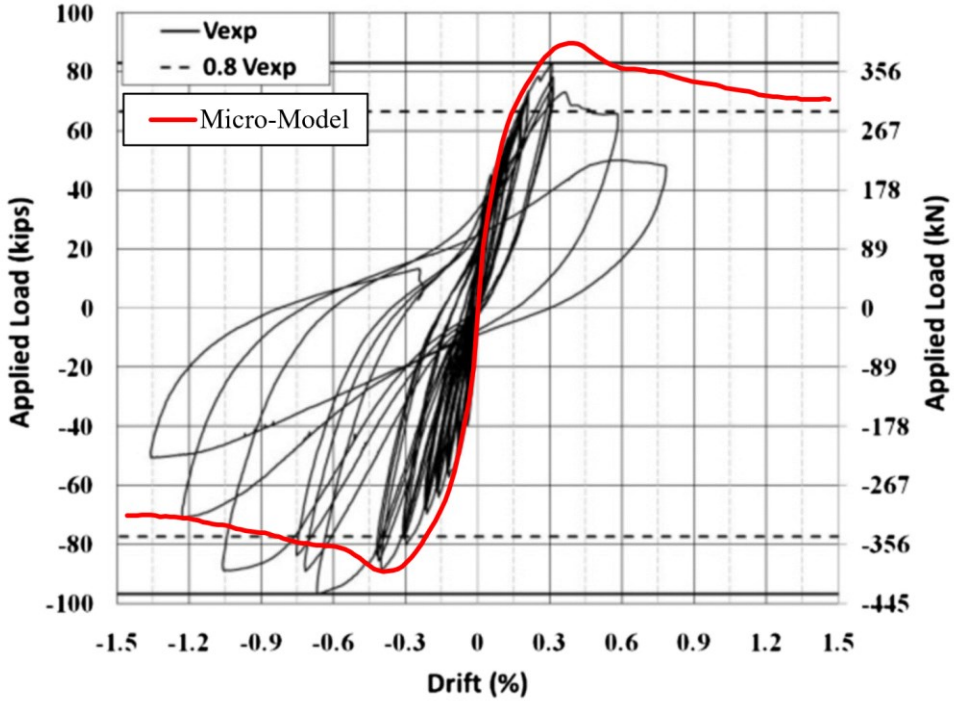

Figure 3.38 – Applied Load-Wall Drift Comparison (Elmapruk – PG127-24)

Table 3.7 – Micro Model Results Comparison (Elmapruk)

Specimen	V_{Exp} (kN)	V_{FE} (kN)	V_{Exp}/V_{FE}
PG127-48	238	260	0.92
PG127-48I	252	260	0.97
PG180-48	266	261	1.02
PG254-48	286	262	1.09
PG127-32	344	334	1.03
PG127-24	400	398	1.01

3.5.4 Ba Rahim et al. (2022)

The final experimental study selected in the micro-model validation process was that conducted by Ba Rahim et al. (2022). The study involved the testing of 4 cantilevered partially-grouted masonry wall specimens under combined axial and cyclic lateral loading. Figure 3.39 below depicts the experimental setup. Varied parameters in the study included both the aspect ratio of the wall and the type of horizontal reinforcement specified. All specimens were 2.6 m in height, with two of the wall specimens measuring 2.6 m in width while the other two measured 1.4 m in width. This corresponds to aspect ratios of 1.00 and 1.86. Between the two specimens of equal height, the type of horizontal reinforcement was varied, with one specimen featuring bond-beam reinforcement while the other featured bed-joint reinforcement. Details of the reinforcing schemes are presented in Fig. 3.40. Material properties specified in the micro-model are displayed in Table 3.8 below.

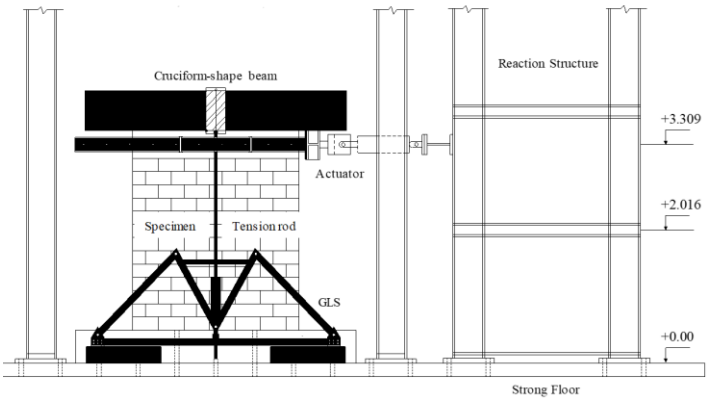

Figure 3.39 – Test Setup (Ba Rahim, 2023)

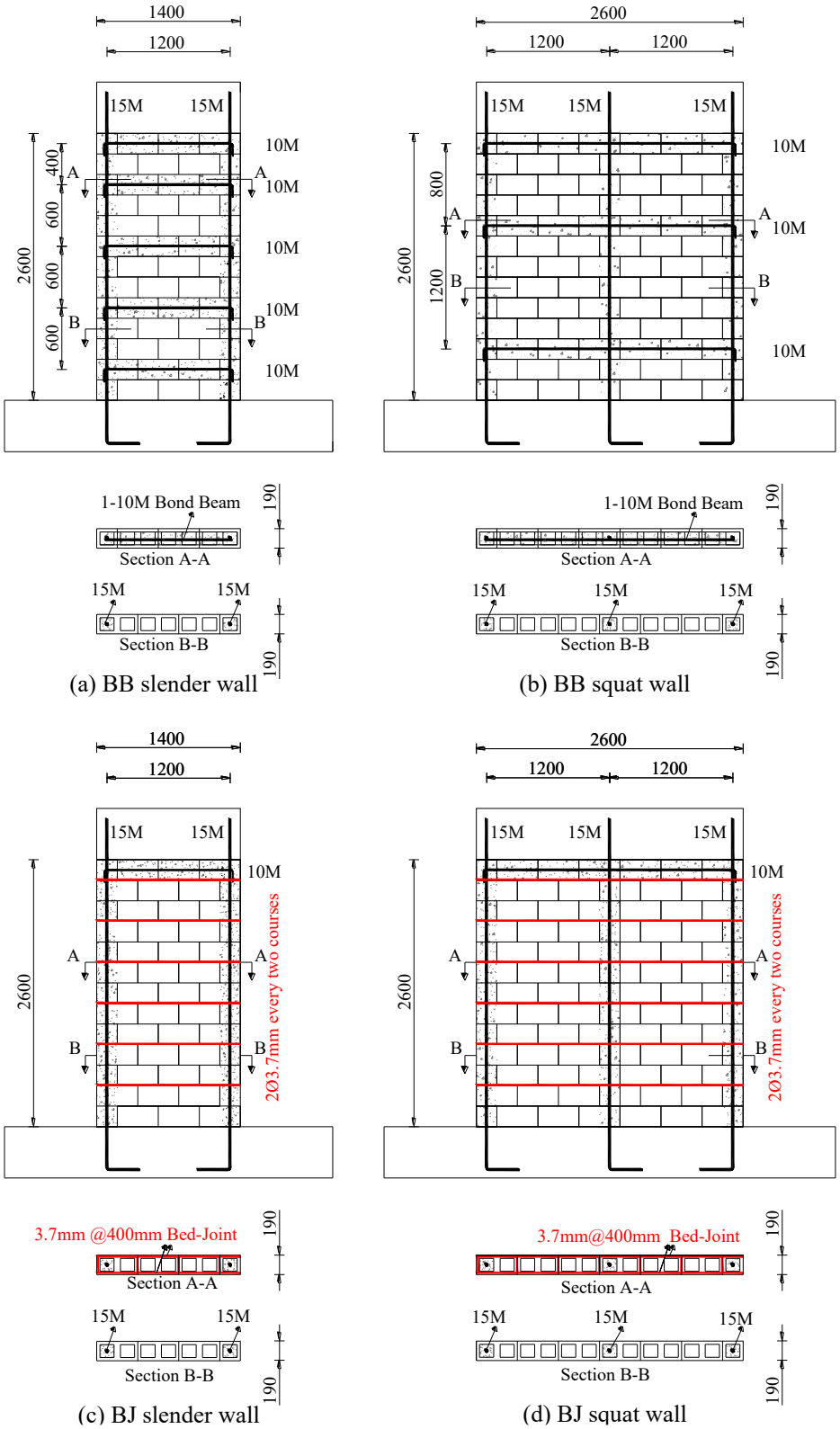

Figure 3.40 – Test Specimens (Ba Rahim, 2023)

Table 3.8 – Material Properties (Ba Rahim)

Material	Peak Compressive Strength (MPa)	Yield Strength (MPa)
Masonry Units	31.2	-
Mortar	14.8	-
Grout	30.6	-
Steel (V)	-	455
Steel (H)	-	521
Steel (Bed-Joint)	-	617

Figure 3.41 depicts the general two-layered micro-model developed for squat all containing the bond beam reinforcement. A general fixed base boundary condition was specified for all four models by restraining the base of the concrete foundation from translating in both the horizontal and lateral directions. Loading was applied in a two-step static analysis. In the first step, an axial stress of 1.98 MPa was applied to the top capping beam and held during the second step, in which a cyclic lateral displacement was specified at several nodes roughly 400 mm apart. The vertical degrees of freedom of the nodes where the lateral displacement was applied were left free to allow for rotation along the top of the wall, thus simulating the cantilever boundary conditions. Bed-joint reinforcement was added in two of the models using an embedment constraint similar to the bond beam reinforcement constraint featured in the previous studies. In this case, however, the bed-joint reinforcement would be embedded within the mortar elements rather than the grout elements.

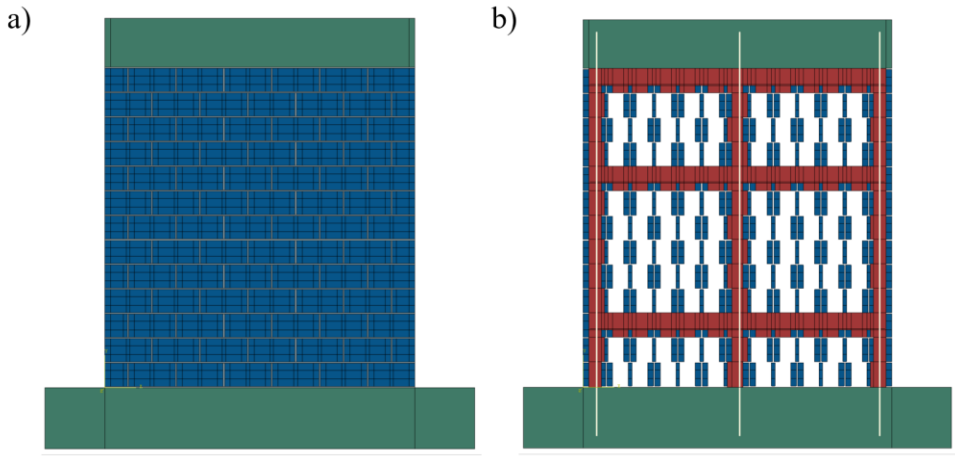

Figure 3.41 – Micro-Model (a) Masonry Layer (b) Grout Layer (Ba Rahim)

Figures 3.42 to 3.45 below compare the applied load–wall drift response obtained from the finite element micro-model to that obtained from experimental testing for the four specimens. The performance of the model to predict the ultimate load capacity of the four specimens would be considered adequate as differences between the predictions and experimental results ranged between 7% to 12%, as presented in Table 3.9. And while the initial stiffness was predicted within reasonable accuracy, the micro-model tended to noticeably overestimate the stiffnesses of the bond beam specimens just prior to peak load. This could be due to the inadequate anchorage of the horizontal reinforcement, as indicated by the significant pinching effects displayed in the experimental results. Due to the constraints of the micro-model, perfect anchorage is assumed. Thus, if bond slip occurred, the model would not be able to capture such behaviour. As this behaviour was not prevalent in specimens featuring bed-joint reinforced, it further reinforces bond slip as a reasonable explanation for the difference in predicted and experimental responses.

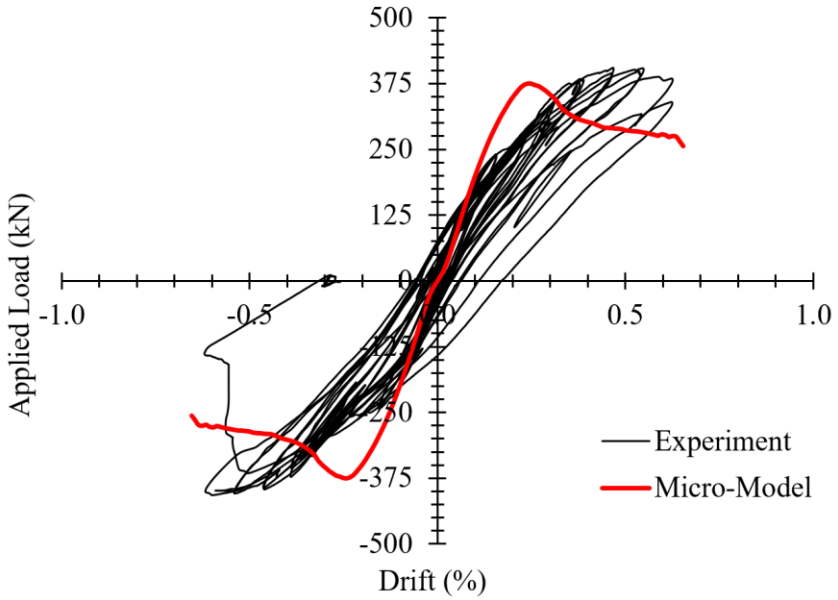

Figure 3.42 – Applied Load – Wall Drift Comparison (BB Squat)

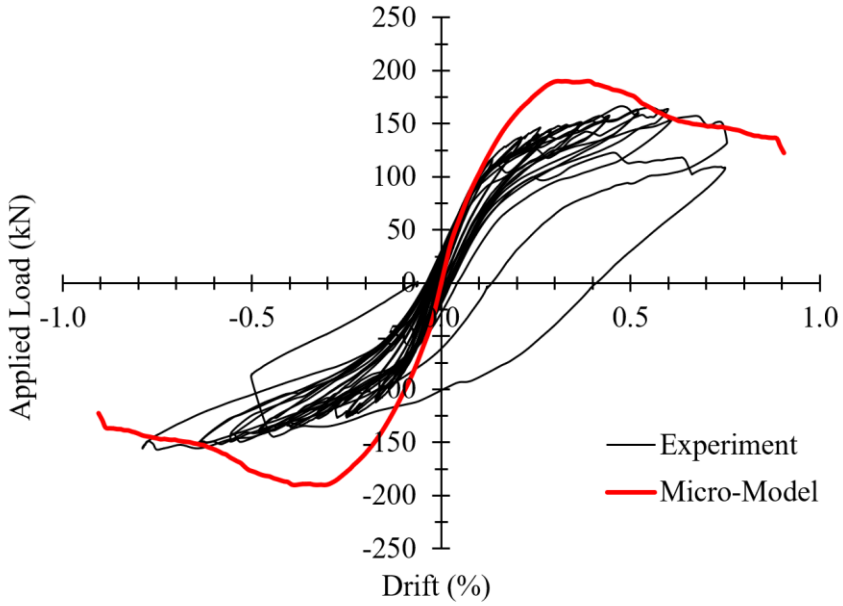

Figure 3.43 – Applied Load – Wall Drift Comparison (BB Slender)

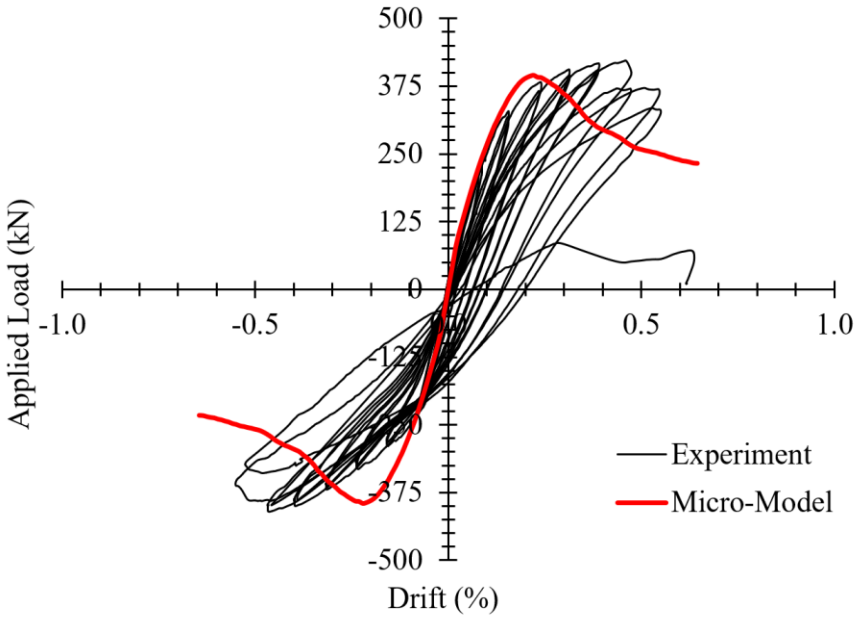

Figure 3.44 – Applied Load – Wall Drift Comparison (BJ Squat)

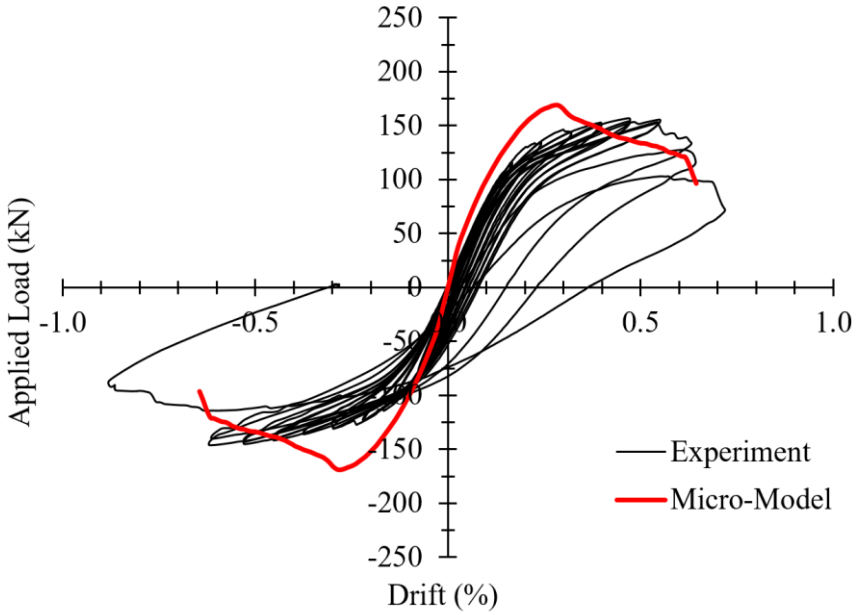

Figure 3.45 – Applied Load – Wall Drift Comparison (BJ Slender)

Table 3.9 – Micro Model Results Comparison (Ba Rahim)

Specimen	V_{Exp} (kN)	V_{FE} (kN)	V_{Exp}/V_{FE}
BB Squat	405	375	1.08
BB Slender	167	190	0.88
BJ Squat	422	395	1.07
BJ Slender	157	169	0.93

3.6 Finite Element Micro-Model Summary

In this chapter, the development of the finite element micro-model specific to North American partially-grouted masonry walls was developed. The model was then validated with four experimental studies. Differences between the predicted ultimate load capacity of the micro-model and that experimentally obtained were within 12% for all specimens, with the exception of a single specimen (MC2) from the Minaie et al. (2010) study, which showcased a difference of 22%. Overall, the performance of the micro-model to predict the in-plane shear capacity of partially-grouted specimens with varied aspect ratios applied axial stresses, quantities and spacings of both the horizontal and vertical reinforcement, horizontal reinforcement types, and boundary conditions was deemed acceptable.

4.0 PARAMETRIC STUDY

4.1 Introduction

This chapter presents the findings from a conducted parametric analysis. Within the analysis, over 1,600 simulations were conducted using the developed micro-model with the goal of determining the influence of the effective height-to-width (aspect) ratio, applied axial stress, quantities and spacings of both horizontal and vertical reinforcement, and horizontal reinforcement types on the in-plane load capacity of partially-grouted masonry walls. The complete dataset and plots of the completed analysis are available in Appendices A and B, respectively.

4.2 Parametric Model Definition

All simulations were conducted in a two-step static analysis in which an axial stress would be applied and held in the first step (if a non-zero axial stress was specified), followed by a continuously increasing lateral displacement applied to a capping beam fastened to the top of the masonry wall until failure occurred. This process closely resembles that used for all four validation studies presented in the previous chapter.

4.2.1 Fixed Parameters

Fixed parameters entail the parameters that were not varied between simulations. In this study, the strength of the masonry materials (masonry units, mortar, and grout), the thickness of the masonry unit, the width of the masonry wall, and the wall boundary conditions were held constant. Values of the fixed parameters are presented in Table 4.1 below. The rationale for holding the strength parameters constant can be attributed to the notion that modern design methodologies tend to associate the shear strength contribution of the masonry material to the masonry prism strength and not the individual strengths of the masonry constituents (which is what the developed micro-model is formulated around). Although empirical equations have been developed to relate the strength of the individual components to the strength of the prism (Dillon, 2015; Liu, 2023), additional research is required to ensure a meaningful comparison between the in-plane load

capacity of the masonry wall as predicted by the micro-model to the prism strength of the masonry.

Table 4.1 – Parametric Study - Fixed Parameters

Fixed Parameters	Value
Masonry Unit Strength	20 MPa
Mortar Compressive Strength	15 MPa
Grout Compressive Strength	30 MPa
Yield Strength of the Steel Reinforcement	400 MPa
Masonry Unit Thickness	190 mm
Wall Width	2600 mm
Boundary Condition	Cantilever

Regarding the choice of a cantilevered boundary condition, the choice was made to mimic modern-day construction. As was mentioned by Bennett (2013), modern masonry systems often feature movement joints which decouple the monolithic masonry system into a series of individual wall segments under single curvature conditions, as shown in Fig. 4.1 below. This change in construction is also prevalent in the literature as masonry wall specimens tested in the 1970s and 1980s tended to specify fixed-fixed (double curvature, Fig. 4.1a) boundary conditions, while experimental programs conducted in the 2000s and beyond tend to specify cantilever (single curvature, Fig. 4.1b) boundary conditions.

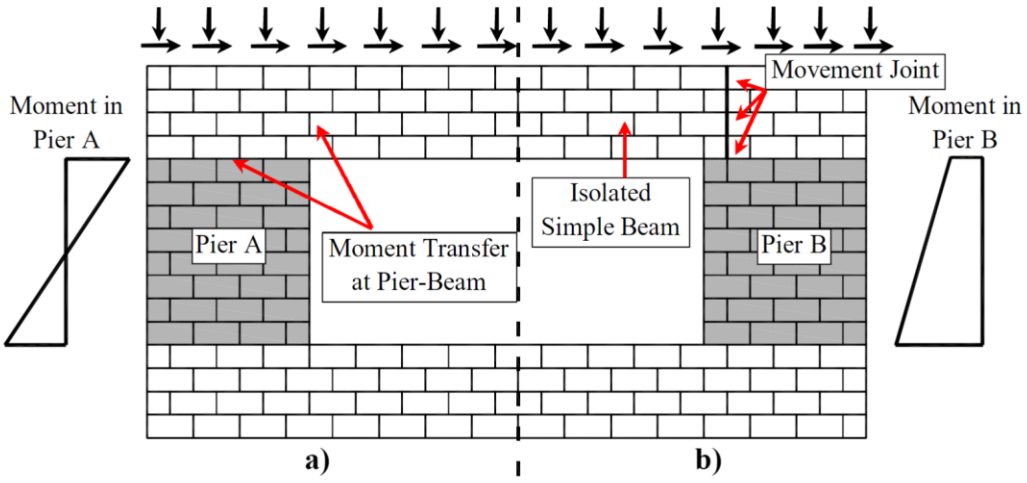

Figure 4.1 – Masonry Wall Boundary Conditions (a) Fixed-Fixed (b) Cantilevered (Banting, 2013)

4.2.2 Independent Parameters

Independent parameters considered of those varied between simulations. In this study, the independent parameters considered of the wall aspect ratio, applied axial stress, horizontal reinforcement spacings, horizontal reinforcement sizes, vertical reinforcement spacings, vertical reinforcement size, and the inclusion of bed-joint reinforcement. Table 4.2 below illustrates the independent parameters and the values investigated.

Table 4.2 – Independent Parameters

Independent Parameters	Values Investigated
Aspect Ratio	0.62, 0.92, 1.24
Applied Axial Stress	0 MPa, 0.1 MPa, 0.25 MPa, 0.50 MPa, 1.0 MPa, 1.5 MPa
Horizontal Reinforcement Spacing*	400 mm, 800 mm, 1200 mm
Horizontal Reinforcement Size	10M (100 mm^2), 15M (200 mm^2), 20M (300 mm^2)
Vertical Reinforcement Spacing	600 mm, 800 mm, 1200 mm
Vertical Reinforcement Size	20M (300 mm^2), 25M (500 mm^2), 30M (700 mm^2)
Bed-Joint Reinforcement	No, Yes**

* Only varied for an aspect ratio of 0.92

** Bed-Joint reinforcement consisted of 21.5 mm^2 spaced every 400 mm

Investigated values of horizontal and vertical reinforcement sizes were selected based on a combination of industrial experience and those selected within the literature. From this, the sizes of horizontal reinforcing bars ranged between 10M (100 mm^2) and 20M (300 mm^2), while the size of the vertical reinforcing bars ranged between 20M (300 mm^2) and 30M (700 mm^2). Aspect ratios were achieved by varying the height of the wall specimens. As the widths of all wall specimens were held constant at 2.6 m, wall heights of 1.6 m, 2.4 m, and 3.2 m were selected to achieve aspect ratios of 0.62, 0.92, and 1.24, respectively.

The spacings of the horizontal and vertical reinforcement were selected to ensure uniform spacing between all bond beams/grout cores over the entire span of the wall. It is for this reason that multiple spacings of horizontal reinforcing bars (bond beams) were only varied for wall heights of 2.4 m. For instance, if a horizontal rebar spacing of 1200 mm

was applied to the 1.6 m tall wall specimens, there would be a 400 mm gap between the bond beam and capping beam or foundation. Figures 4.2 through 4.6 below illustrate the different combinations of horizontal and vertical reinforcement spacings investigated.

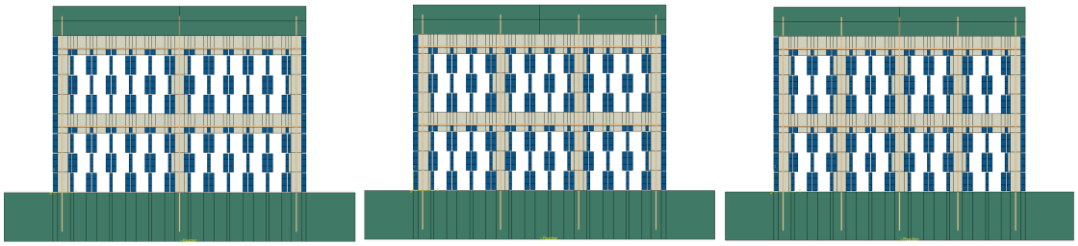

Figure 4.2 – Grout Core Spacings (1.6 m Wall Height)

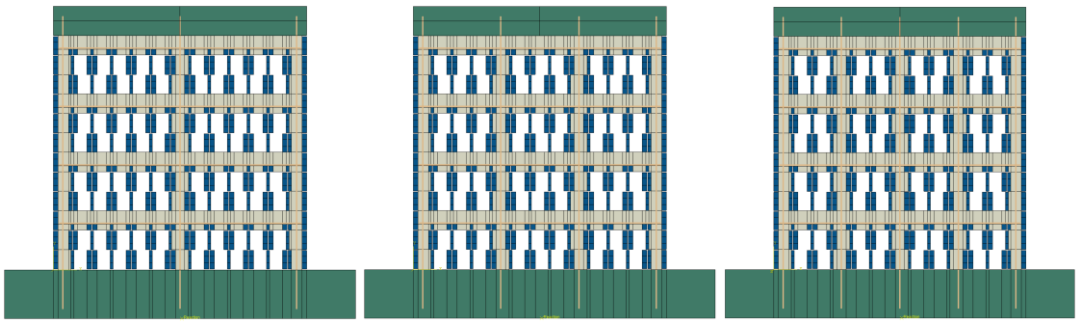

Figure 4.3 – Grout Core Spacings (2.4 m Wall Height, 0.4 m Bond Beam Spacing)

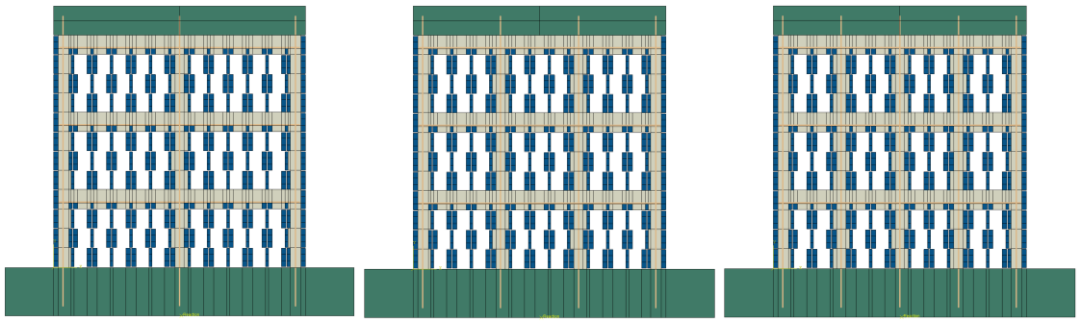

Figure 4.4 – Grout Core Spacings (2.4 m Wall Height, 0.6 m Bond Beam Spacing)

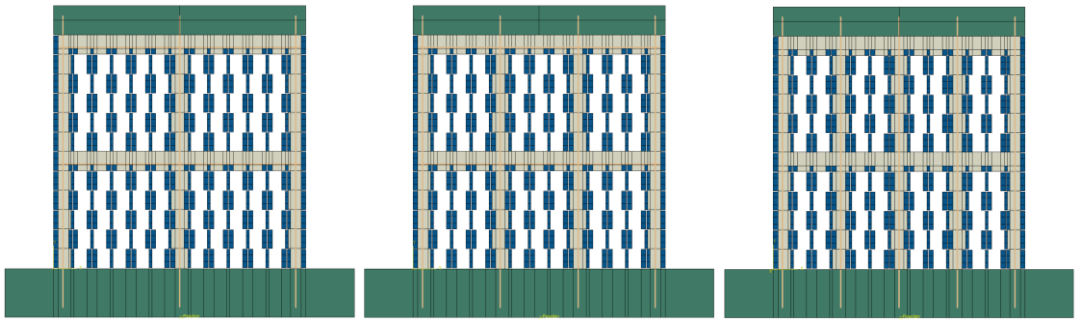

Figure 4.5 – Grout Core Spacings (2.4 m Wall Height, 1.2 m Bond Beam Spacing)

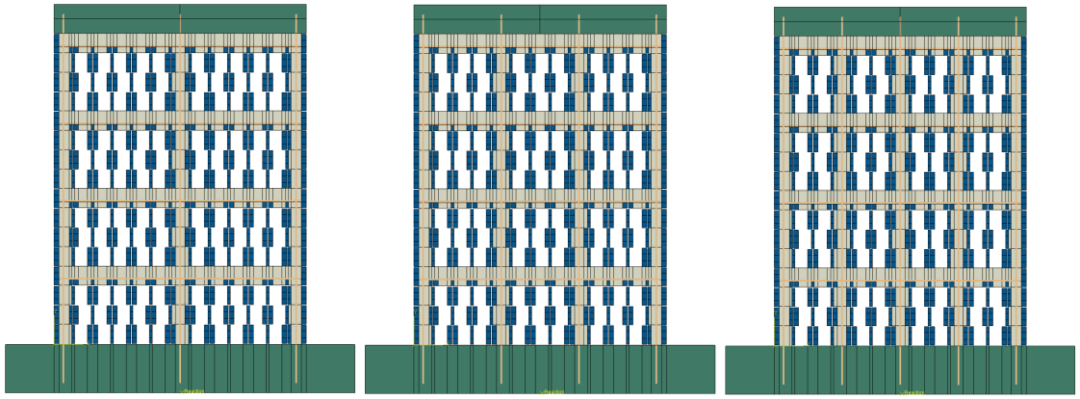

Figure 4.6 - Grout Core Spacings (3.2 m Wall Height)

4.2.3 Dependent Parameter

The dependent parameter in the conducted parametric study is the ultimate load capacity of the wall specimens. This was evaluated as the peak load the specimen was able to achieve before softening occurred. If the model did not converge prior to reaching this peak load, the analysis was disregarded. Of the 1,620 analyses conducted, 1608 (99.3%) were able to achieve peak load. As some combinations of variables may result in a flexural failure (e.g., a tall wall featuring low amounts of vertical reinforcement under light axial loads), it is important to note that the ultimate load capacity of the specimen may not necessarily be the in-plane shear capacity. However, since the goal of the study is to provide insights regarding common design parameters and not develop a shear capacity equation, this is acceptable. If the database is to be used in a future regression analysis to determine an in-plane shear design equation, an initial scrutinization of the data must be conducted to ensure only walls failing in diagonal tension shear are included.

4.3 Effect of Independent Parameters on the In-Plane Shear Capacity

The discussions below pertain to the influence of several design parameters on the in-plane load capacity of the simulated specimens. Unless otherwise stated, all walls presented in the comparison plots are identical in all aspects allowing for a meaningful comparison.

4.3.1 Aspect Ratio (Wall Geometry)

Figure 4.7 below compares the influence of different aspect ratios on the in-plane load capacity of the specimens. It is observed in all cases that a lower aspect ratio resulted in an increased in-plane load capacity. However, the magnitude of the increase is coupled with other effects. The influence of the aspect ratio also appears to be coupled with the applied axial stress. Decreasing the aspect ratio from 1.24 to 0.62 of a wall with applied axial stress of 0.1 MPa resulted in a 16% increase in load capacity, while when the aspect ratio of the same wall but under higher axial stress of 1.5 MPa was decreased from 1.24 to 0.62, a substantially higher 28% increase in in-plane load capacity was observed. The magnitude of the increase also appears to be rather independent of the spacing of the vertical reinforcement. Comparing the increase in load capacity when lowering the aspect ratio from 1.24 to 0.62 of specimens under an axial stress of 0.1 MPa, it is observed that the increase in load capacity was 16% and 17% for the specimens featuring a vertical reinforcement spacing of 600 mm and 1200 mm, respectively.

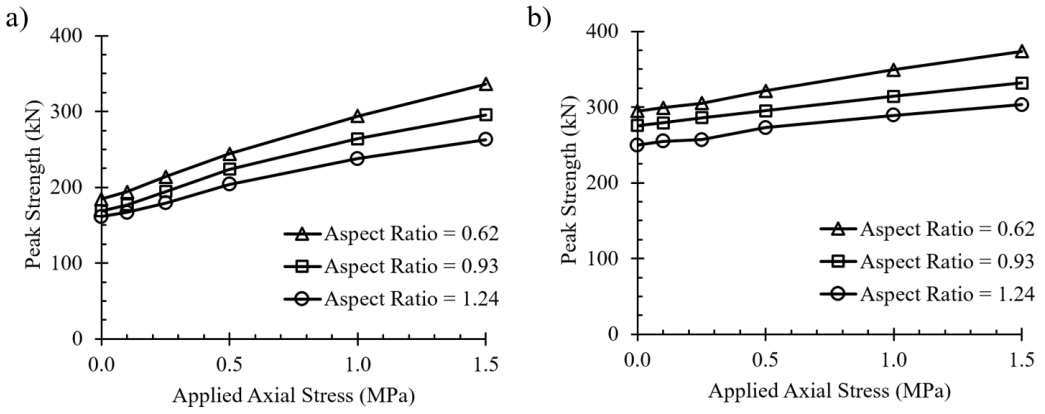

Figure 4.7 – Influence of Aspect Ratio on the In-Plane Load Capacity (a) Vertical Spacing = 600 mm (b) Vertical Spacing = 1200 mm

Results from the micro-model indicated that this increase in load capacity with a decreased aspect ratio could be attributed to the notion that more compressive struts enter directly into the foundation of the walls as opposed to the leading edge for walls with smaller aspect ratios. Referring to Fig. 4.8, which depicts the compressive struts of two walls with varied aspect ratios, it is observed that the wall with a smaller aspect ratio has the majority of compressive struts enter directly into the foundation from the top of the wall. However, the wall with the larger aspect ratio only has only a select few of struts enter directly into the foundation, none of which start at the top of the wall. For walls with larger aspect ratios, having more struts enter the leading edge of the wall resulting in significant stress concentrations and, ultimately, failure at a lower applied load.

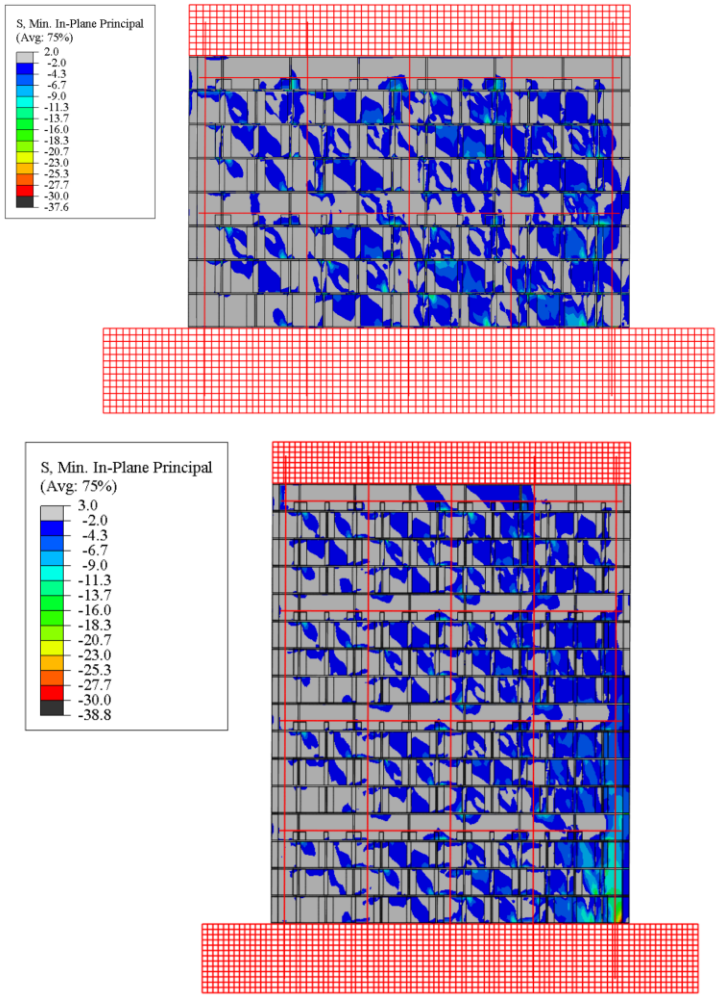

Figure 4.8 – Compressive Stress Trajectories (a) Aspect Ratio = 0.62 (b) Aspect Ratio = 1.24

4.3.2 Applied Axial Stress

In all cases, it was found that an increase in applied axial stress results in a higher load capacity. It is noted, however, that there was a noticeable decrease in ductility was observed when the applied axial stress was increased. Figure 4.9 below illustrates the increase in load capacity with increased levels of axial stress for varied values of both horizontal and vertical reinforcement spacing. The magnitude of the increase in load capacity appears to be coupled with the vertical reinforcement spacing. For instance, when increasing the applied levels of axial stress from 0.1 MPa to 1.5 MPa, wall specimens with a vertical reinforcement spacing of 600 mm exhibited a 21% increase in load capacity, while walls with a vertical reinforcement spacing of 1200 mm exhibited a 73% increase in load capacity. This is substantiated by noticing the increase in load capacity with increased levels of axial stress appears to be linear for walls with closely spaced vertical reinforcing bars but nonlinear for walls with widely spaced vertical reinforcing bars. When comparing specimens with varied horizontal reinforcement spacing, it is noticed that the horizontal reinforcement spacing has a negligible effect on how the applied axial stress influences the load capacity. Additional comments regarding the effect of horizontal reinforcement are presented in the following section. The notion of having an increased load capacity upon increasing the axial load is valid from a mechanics standpoint as the increased axial load increases the aggregate interlock and, in turn, the load capacity of the wall.

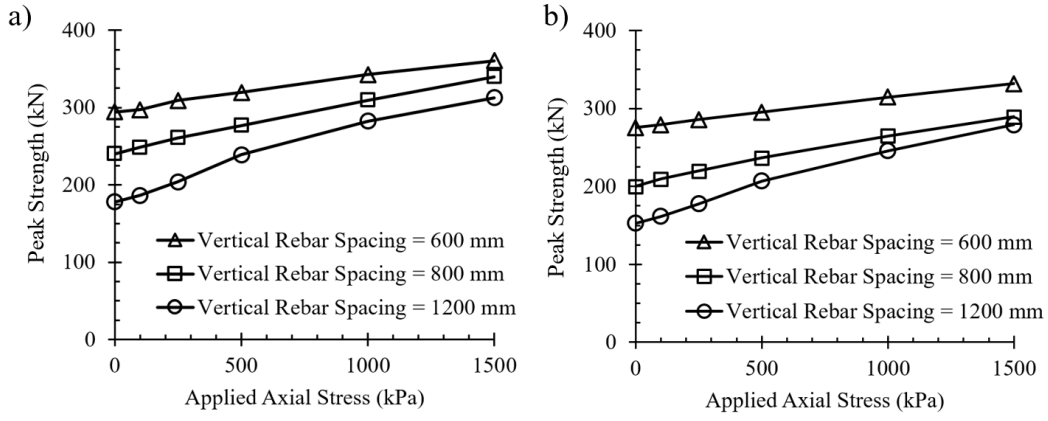

Figure 4.9 – Effect of Applied Axial Stress on the In-Plane Load Capacity (a) Horizontal Spacing = 400 mm (b) Horizontal Spacing = 1200 mm

4.3.3 Horizontal Reinforcement (Spacing, Size, and Type)

While a positive correlation is shown between the amount of horizontal reinforcement and the in-plane load capacity, it is observed that this correlation can be attributed to the spacing of the horizontal reinforcement and not the size of the horizontal reinforcing bars. To illustrate this, consider the two scenarios depicted in Fig. 4.10 below. Both scenarios feature two identical walls in which the horizontal reinforcing ratio is increased. In scenario 1, the size of the reinforcing bars is increased from 10M to 20M bars which in turn increases the reinforcing ratio of the wall from 0.07% to 0.20%. In the second scenario, the size of the reinforcing bars is kept constant but the spacing of the reinforcement is decreased from 1200 mm to 400 mm, allowing for additional bond beams within the wall system. This decrease in spacing results in an increase in horizontal reinforcing ratio from 0.09% to 0.18%.

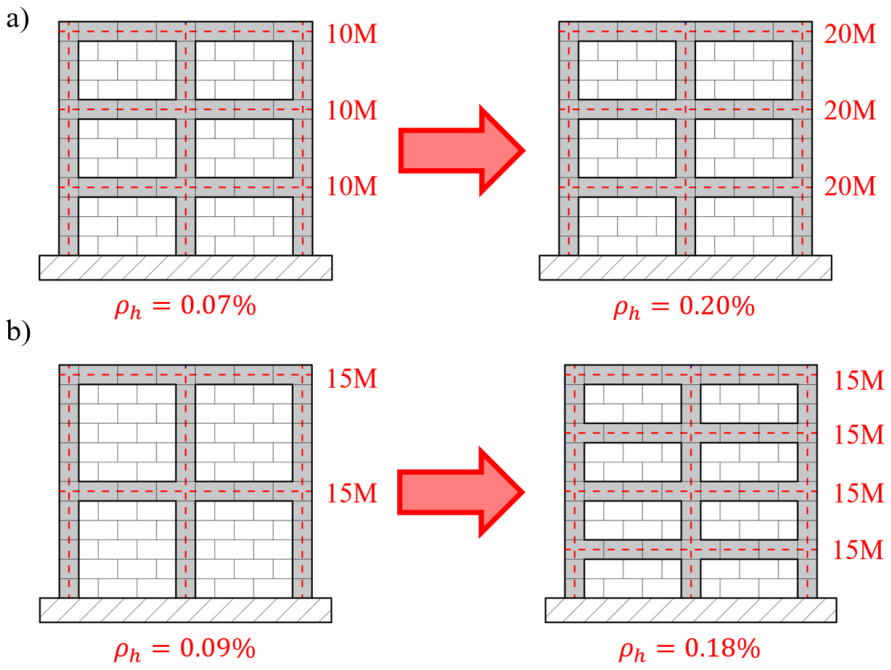

Figure 4.10 – Increasing Horizontal Reinforcing Ratio (a) Increasing Horizontal Bar Size (b) Decreasing Horizontal Bar Spacing

Figure 4.11 below illustrates the effect both of the scenarios above have on the in-plane load capacity of the wall system. Referring to Fig. 4.10a, the size of the horizontal reinforcement appears to have an insignificant impact on the in-plane load capacity.

Based on the micro-model results, this is due to stresses in the horizontal reinforcement remaining below their yield capacity when peak load is achieved, even for the smallest reinforcing bar size. Referring to Fig. 4.11b however, it is seen that decreasing the horizontal reinforcement spacing contributes to an increase in load capacity. For example, comparing the in-plane load capacity of the specimens under 0.1 MPa of axial stress in Fig. 4.11b, it is seen that decreasing the spacing from 1200 mm to 400 m results in a 19% increase in load capacity. From a mechanics standpoint, this can be expected as the presence of additional bond beams results in additional nodes along the leading edge of the wall with the ability to redistribute the forces from the incoming compressive struts back to the trailing end of the wall, similar to the mechanisms of stirrups in reinforced concrete.

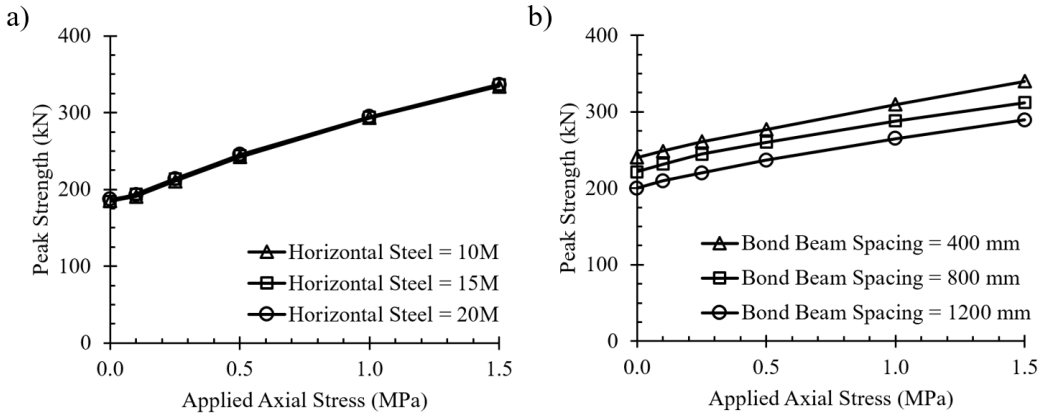

Figure 4.11 – Impact of Horizontal Reinforcement on the In-Plane Load Capacity (a) Reinforcement Quantity (b) Reinforcement Spacing

The influence of bed-joint reinforcement was found to have an insignificant result on the in-plane load capacity of all specimens tested. Referring to Figs. 4.12 and 4.13 below, it is observed that there is very little influence of the bed-joint reinforcement for walls of different aspect ratios or walls with varied horizontal reinforcement spacings. Based on the results of the micro-model, this is largely in part to the bed-joint reinforcement not being able to form nodes at the intersections of the compressive struts, thus lacking the ability to redistribute forces in the same manner as a bond beam. It is noted, however, that specimens with bed-joint reinforcement were observed to have a greater ability to

maintain their ultimate load capacities compared to those without bed-joint reinforcement. Also, the specimens containing bed-joint reinforcement also featured bond beams which may have acted as the primary horizontal reinforcing resister leaving the effect of the bed-joint reinforcement null. It is also noted that bed-joint reinforcement employed in practice contains additional steel links running perpendicular to the wall plane and connecting the two steel wires present on each masonry flange. This could help resist the tensile splitting of the masonry units that commonly occur at the compression toe and enhance the load capacity of the wall system. However, since the micro-model was constrained to two dimensions, it is unable to capture any resistance provided by the bed-joint reinforcement perpendicular to the wall plane.

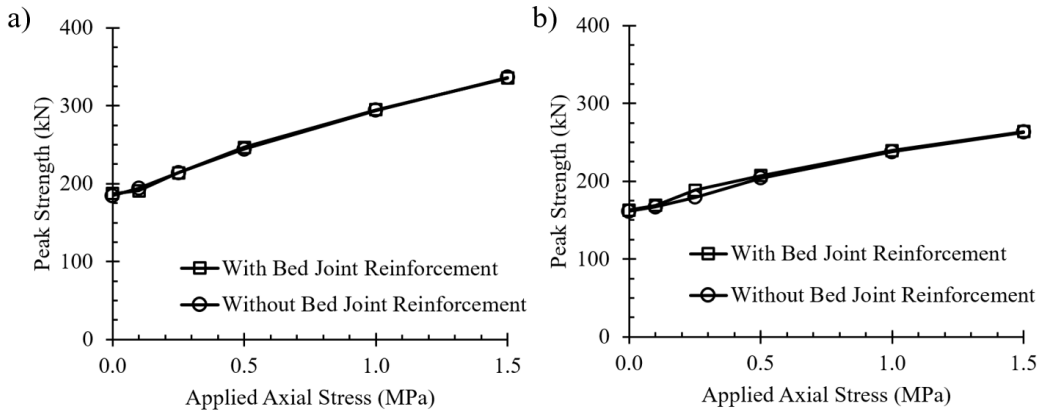

Figure 4.12 – Influence of Bed-Joint Reinforcement on the In-Plane Load Capacity (a) Aspect Ratio = 0.62 (b) Aspect Ratio = 1.24

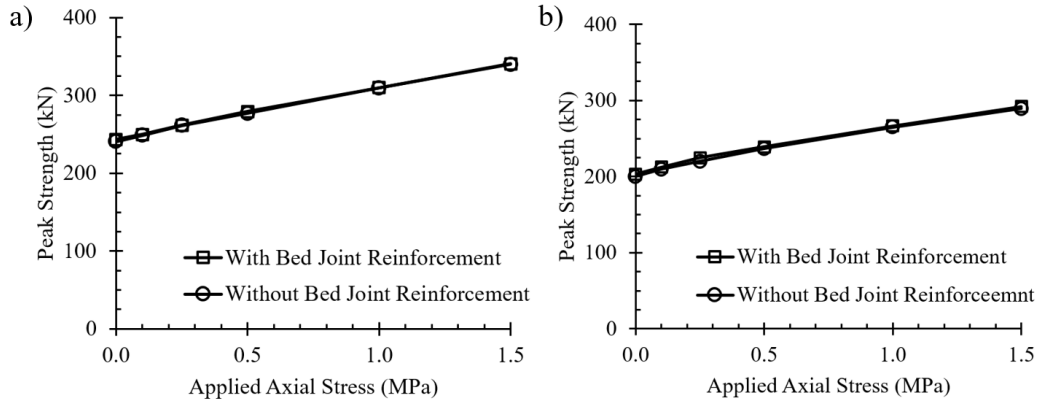

Figure 4.13 – Influence of Bed-Joint Reinforcement on the In-Plane Load Capacity (a) Horizontal Bar Spacing = 400 mm (b) Horizontal Bar Spacing = 1200 mm

4.3.4 Vertical Reinforcement (Spacing and Size)

Unlike the horizontal reinforcement, where the quantity appeared to be insignificant as the load capacity was seemingly dependent on solely the horizontal spacing, both the vertical reinforcement spacing, and quantity were found to play a role in influencing the in-plane load capacity. This is illustrated in a similar manner as before in which two scenarios were compared (Fig. 4.14). In the first scenario, the size of the vertical reinforcing bars was increased from 20M to 30M resulting in an increase in vertical reinforcing ratio from 0.18% to 0.43%. In the second scenario, the size of the vertical reinforcement was kept constant, however, the vertical reinforcement spacing was decreased from 1200 mm to 600 mm resulting in an increase in vertical reinforcing ratio from 0.30% to 0.51%.

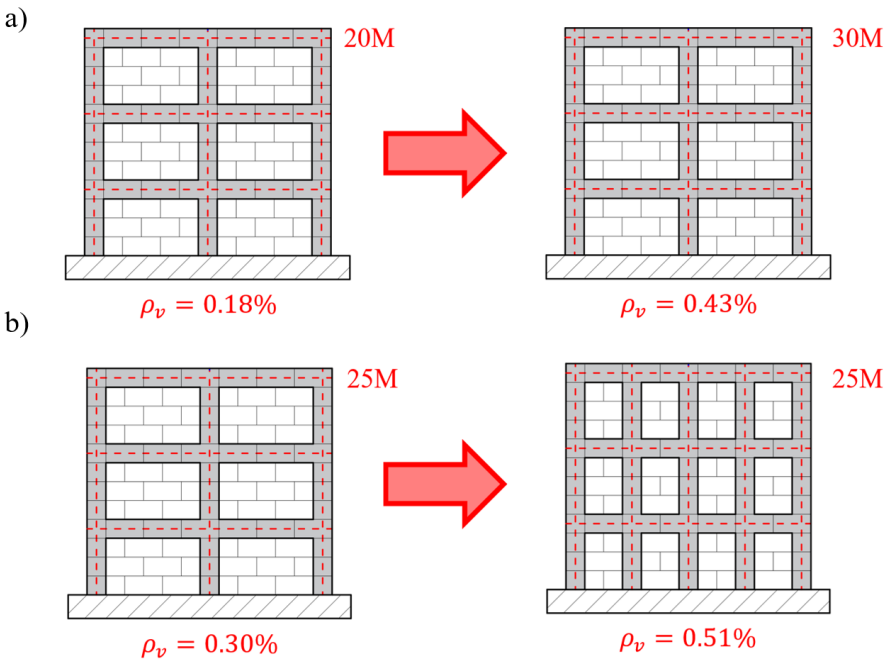

Figure 4.14 – Increasing Vertical Reinforcing Ratio (a) Increasing Vertical Bar Size (b) Decreasing Vertical Bar Spacing

Referring to the role of the vertical reinforcement quantity, as shown in Fig. 4.15, it is observed that the influence of vertical reinforcement quantity decreases as the applied axial stress is increased. For instance, increasing the total vertical reinforcement size from 20M to 30M in a wall with an aspect ratio of 0.62, an 11% increase in load capacity

is observed when an axial stress of 0.1 MPa is applied; however, only an 0.5% increase is observed when an axial stress of 1.5 MPa is applied. This relationship also appears to be coupled with the aspect ratio of the wall, as when the same comparison is made for wall specimens with an aspect ratio of 1.24, the increase in in-plane load capacity is 25% and 4% for walls under applied axial stresses of 0.1 MPa and 1.5 MPa, respectively. Both of these findings make physical sense in that as the applied axial load is increased, the compression field acting on the wall must first be overcome to activate the vertical steel. Regarding the aspect ratio, it has already been discussed the idea that the higher the aspect ratio, the more stress concentrations appear at the compression toe of the wall. From equilibrium, these compressive forces must be balanced by the tensile forces within the vertical steel at the tension heel of the wall resulting in an increased demand for the vertical steel reinforcing bar.

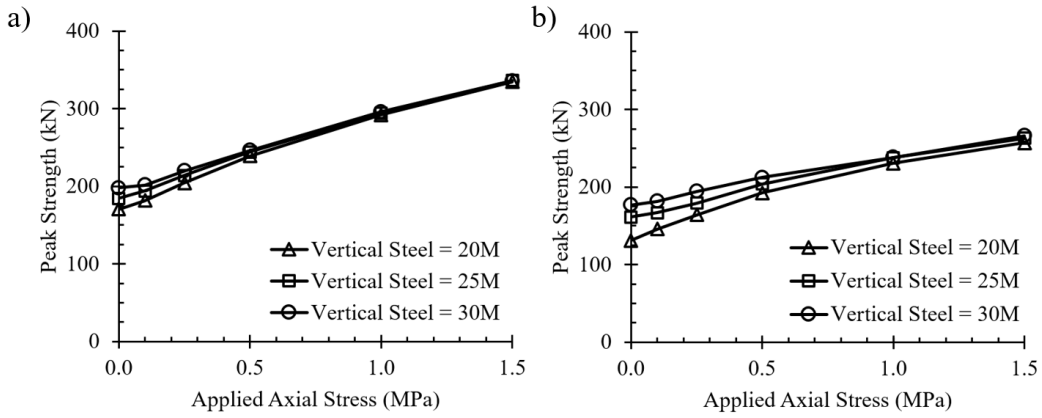

Figure 4.15 – Impact of Vertical Reinforcement Quantity on the In-Plane Load Capacity (a) Aspect Ratio = 0.62 (b) Aspect Ratio = 1.24

The spacing of the vertical reinforcement, and in turn, the spacing of the grout cores, also appears to have a significant contribution to the in-plane load capacity, as shown in Fig. 4.16. The magnitude of the contribution depends largely on the level of applied stress, as the influence appears to decrease as the level of axial stress is increased. For instance, decreasing the spacing of the vertical reinforcement from 1200 mm to 600 mm in a wall with an aspect ratio of 0.62, an 54% increase is observed when an axial stress of 0.1 MPa is applied; however, only an 11% increase is observed when an axial stress of 1.5 MPa is applied. This trend, however, appears to be independent of aspect ratio. Referring back

to the comparison above, if the aspect ratio of the wall was decreased from 1.24 to 0.62, the increases in in-plane load capacity would be 53% and 15% for applied axial stress levels of 0.1 MPa and 1.5 MPa, respectively. The mechanism involved that results in this increase is described in detail in Section 5.2.1.

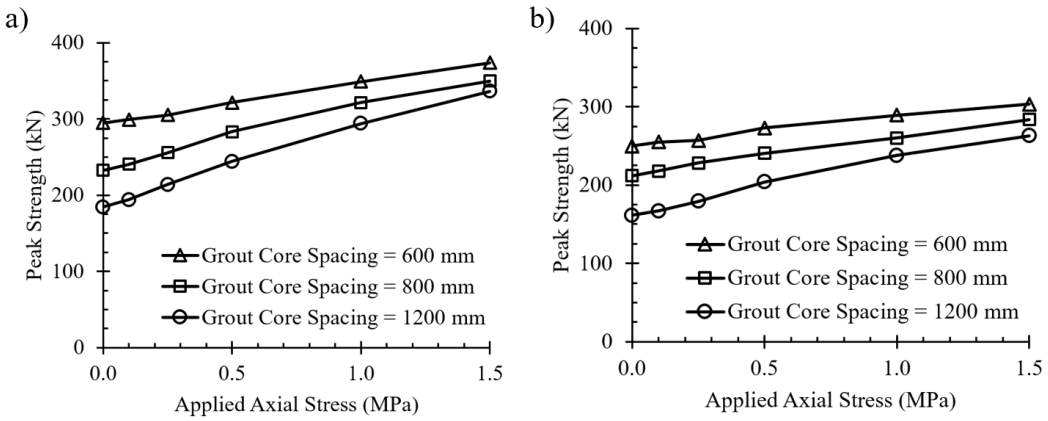

Figure 4.16 – Impact of Vertical Reinforcement Spacing on the In-Plane Load Capacity (a) Aspect Ratio = 0.62 (b) Aspect Ratio = 1.24

4.4 Parametric Study Summary

In this chapter, a parametric study was conducted. The study involved over 1,600 simulations of partially-grouted masonry walls under combined axial and lateral loads. The goal of the study was to determine the influence of applied axial stress, aspect ratio, quantity and distribution of both horizontal and vertical reinforcement, and the type of horizontal reinforcement on the in-plane load capacity of the wall specimens. Results indicated that an increased load capacity could be achieved if (a) the aspect ratio is decreased, (b) the applied axial stress is increased, or (c) the spacing of either the horizontal or vertical reinforcement is decreased. While increases in load capacity were observed for increased values of vertical reinforcement quantities, this was limited to walls under light levels of axial compression or walls with high aspect ratios. Both bed-joint reinforcement and the size of horizontal reinforcement were found to play an insignificant role in influencing the in-plane load capacity.

5.0 DEVELOPMENT OF MASONRY-SPECIFIC STRUT-AND-TIE MODEL

5.1 Introduction

This chapter presents the development of a strut-and-tie methodology specific to partially-grouted masonry walls. Findings from the micro-model were used to facilitate the adaptation. The finalized methodology, which is presented in a simple stepwise format, is then verified with experimental findings available in the literature. Finally, the ability of the methodology to reproduce experimentally and analytically determined behaviour is presented and discussed.

5.2 Development of Masonry-Specific Strut-and-Tie Design Provisions

5.2.1 Previous Attempts

While several studies within the literature discuss the application of strut-and-tie models to partially-grouted masonry wall systems (Voon and Ingham, 2008; Nolph, 2010; Elmapruk, 2010; Dillon, 2015; Tuchscherer, 2016), all attempts with the exception of that from Dillon (2015) did not fully represent a complete strut-and-tie methodology but rather an equivalent truss model. Both models consider the structure as a series of compressive struts and tensile ties; however, strut-and-tie models are more comprehensive as nodal zones (the location at which compressive struts and/or tensile ties intersect) must be checked to ensure the nodal stresses are within an acceptable limit and that sufficient anchorage is provided for the tensile ties. In addition, a strut-and-tie model specifies that no two compressive struts may overlap one another. The difference between the two models is visually demonstrated below as Fig. 5.1a depicts an idealized truss model, while Fig. 5.1b depicts a strut-and-tie model. In contrast, the strut-and-tie methodology employed by Dillon (2015) was true to the original form proposed by Schlaich et al. (1987). Lacking the experimental or analytical evidence to facilitate such an adaptation of the methodology to partially-grouted structures, many of the assumptions made by Dillon (2015) were based on practical experience and limited experimental studies. Discussions of these assumptions and how they correlate with micro-model findings are presented below.

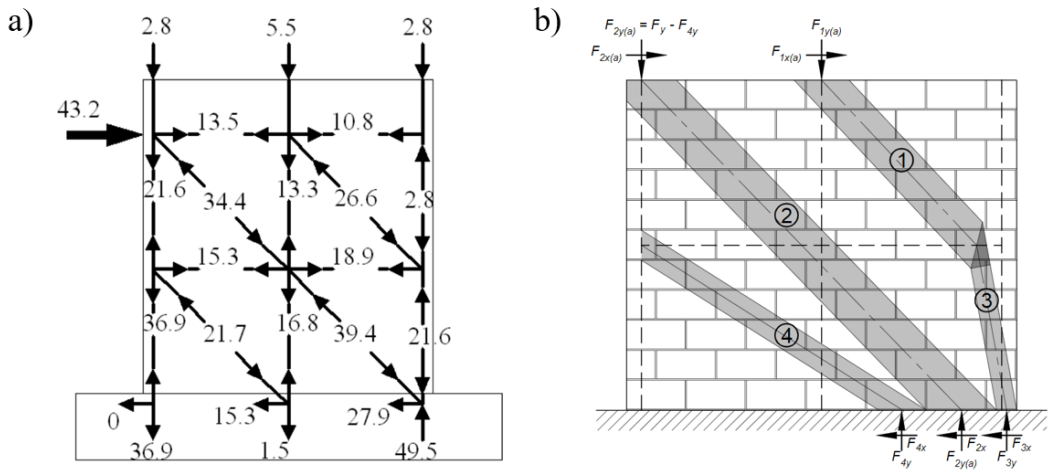

Figure 5.1 – Model Types (a) Equivalent Truss (Nolph, 2010) (b) Strut-and-Tie (Dillon, 2015)

5.2.2 Compressive Struts

Figures 5.2 to 5.5 below depict the generally observed minimum principal stress trajectories for partially-grouted wall systems at peak load. Prevalent in all of the figures is the notion that the compressive struts in the ungrouted panels are bounded by the step cracks surrounding the masonry units resulting in constant strut angles of 45º. This is quite interesting as all previous attempts to adapt the strut-and-tie methodology to masonry systems have assumed that the compressive struts can act at a variety of angles, as shown in Fig. 5.6. This finding is also extremely valuable from a design standpoint as the determination of the compressive strut angles are typically an unknown and need to be solved for using iterative methods.

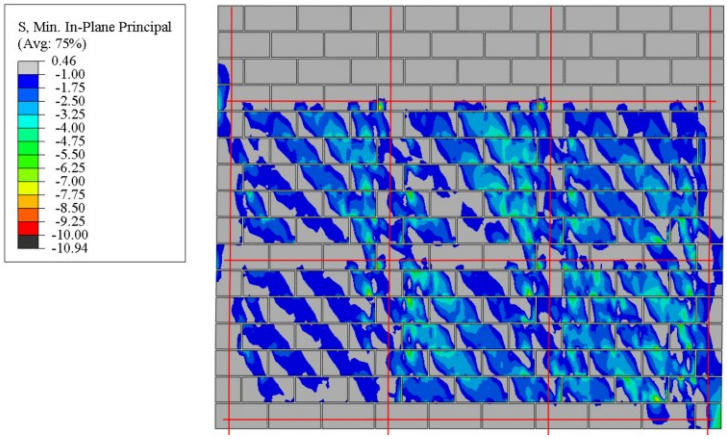

Figure 5.2 – Compressive Struts in Partially-Grouted Masonry Walls (Minaie)

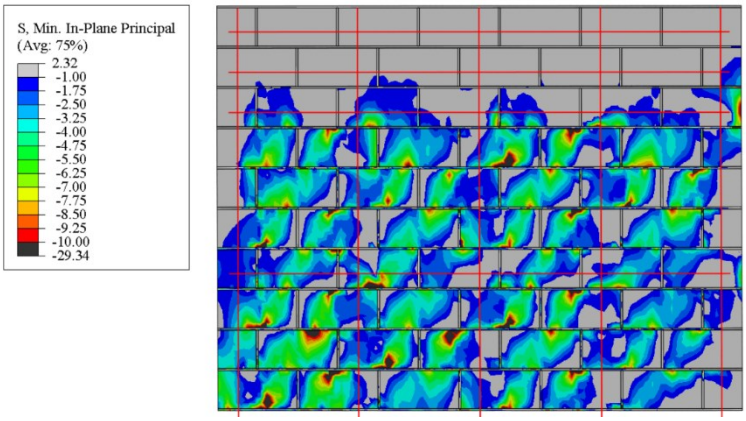

Figure 5.3 – Compressive Struts in Partially-Grouted Masonry Walls (Elmapruk)

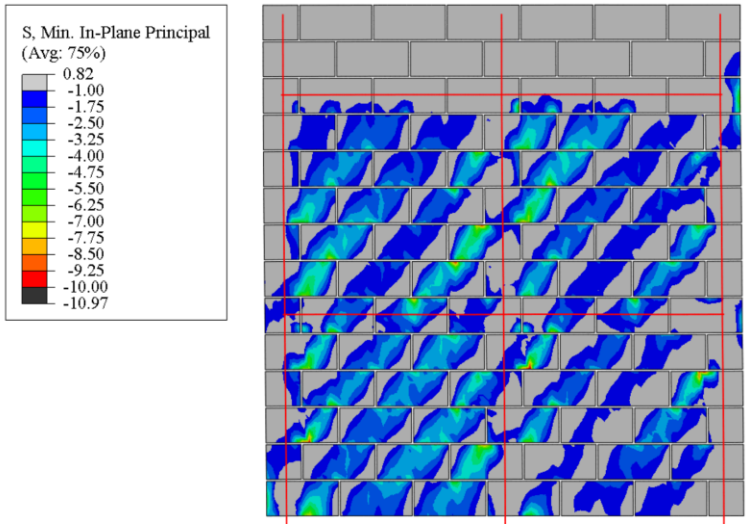

Figure 5.4 – Compressive Struts in Partially-Grouted Masonry Walls (Nolph)

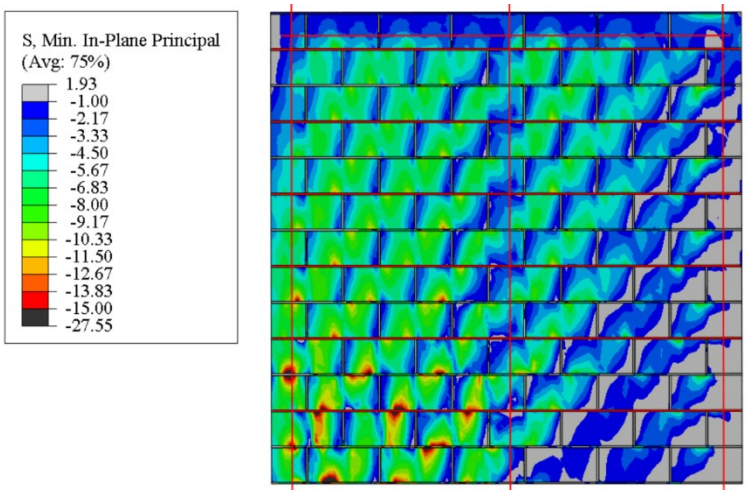

Figure 5.5 – Compressive Struts in Partially-Grouted Masonry Walls (Ba Rahim)

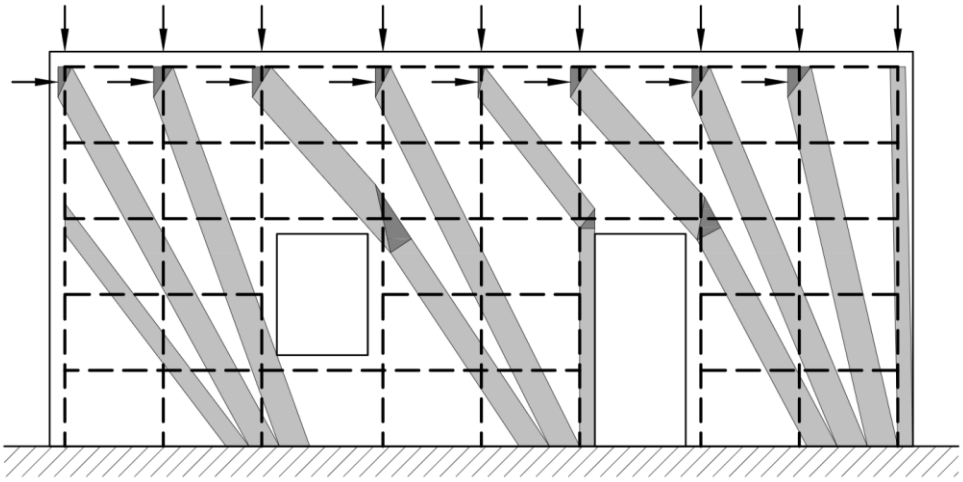

Figure 5.6 – Varied Masonry Compression Strut Angles (Dillon, 2015)

The only exception to the 45-degree strut angles observed is that of the compressive struts encountered within the grout core spanning the compression edge of the wall. In this zone, the struts appear to be near vertical (approximately 85 degrees) and act to redirect the incoming 45-degree compressive struts of the ungrouted panel to the compression toe of the wall. From the stress trajectories, it is also observed that the ungrouted strut widths appears to be constrained by the size of the units, as the compressive struts generally do not cross the head joints. This behaviour is rational as multiple experimental studies reported that step cracking occurs along these head joints resulting in the inability to transfer compressive stresses. From this, the maximums compressive strut widths of the ungrouted panels can be approximated as the height of the masonry unit.

Based on the stress trajectories, four types of struts were identified, as shown in Fig. 5.7. The first is the lead strut which is a nearly vertical strut contained solely in the grout core along the compression edge of the wall. The second type is referred to as bent struts, which originate at the top of the wall and proceed down the wall at a 45-degree angle until entering the compression edge grout core. At this point, the strut is redirected downwards towards the compression toe of the wall. It is noted for such a redirection to occur, some of the strut force must be redistributed to either the vertical reinforcing steel or, if present, the horizontal reinforcing steel. The third type, referred to as top struts,

originates at the top of the wall and proceeds downwards at a 45-degree angle, similar to bent struts. The difference, however, is that the strut is able to proceed directly into the foundation of the wall prior to intercepting the compression edge grout core. The final type of strut, edge struts, are those originating along the tension edge of the wall, which then proceed downward at a 45-degree angle until entering the foundation. It is noted that it is possible for an edge strut to intercept the compression edge grout core prior to reaching the foundation; however, this can be treated as a special case of a bent strut. Details regarding the design calculations of each of the four strut types will be discussed in more detail in Section 5.3.

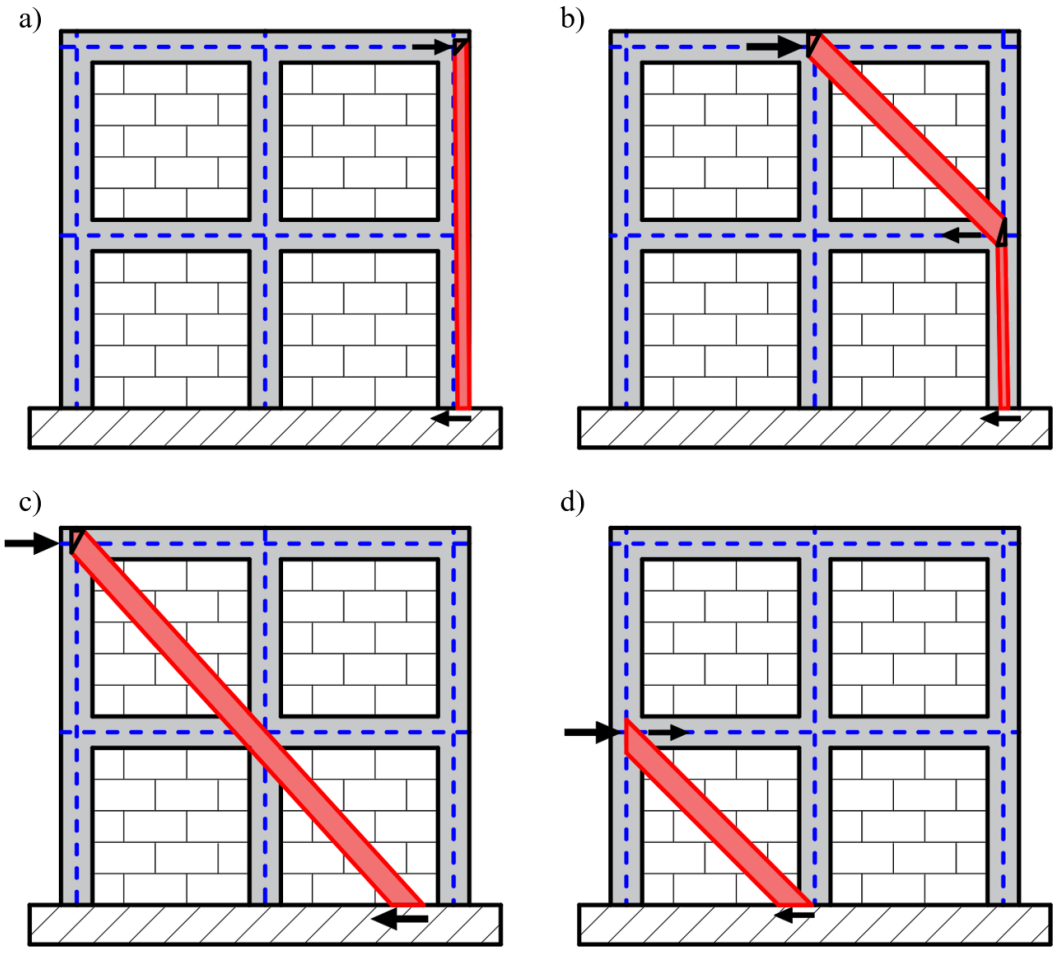

Figure 5.7 – Identified Strut Types (a) Lead (b) Bent (c) Top (d) Edge

Results from the micro-model also provide insights regarding the magnitudes of the compressive struts. Referring to the trajectories presented in Fig. 5.4, the magnitudes of

the compressive struts appear to be dependent on if the strut crosses the interior vertical reinforcing bar. A stress magnitude of approximately 4.0 MPa and 5.5 MPa was observed for the struts that did not cross the vertical reinforcing bar and the struts that did cross the reinforcing bar, respectively. Compared to the reported ungrouted prism strength of 11.3 MPa, this corresponds to a strut magnitude of approximately 35% and 50% of the ungrouted prism strength for struts that do not cross and cross a vertical reinforcing bar, respectively. These ratios of ungrouted strut magnitudes to the ungrouted prism strength appear consistent when applied to the observed stress trajectories of other studies. To represent this behaviour, the following maximum strut capacity equation proposed by Dillon (2015) is adapted to calculate the maximum allowable stress of the struts:

$$f_s = 0.8\beta_S\beta_A f'_m \tag{5.1}$$

Where f_s is the maximum compressive strength of the struts, the 0.8 is added to maintain consistency with other masonry design provisions, β_s is an efficiency factor, β_A is the strut inclination factor, and f'_m is the peak compressive strength of the masonry prism.

The first reduction factor, β_S, is termed the strut efficiency factor and is used to account for the reduction in compressive capacity present due to transverse tensile stresses that account for the transverse tensile stresses that occur when the compressive strut bulge. This is illustrated in Fig. 5.8 below as the expansion of the strut in both the fan-shaped strut and bottle-shaped induce transverse tensile stresses due to Poisson effects. Based on the micro-model findings, it was observed that the struts are largely constrained by the geometry of the masonry wall resulting in an overall prismatic strut behaviour. However, within each individual masonry unit, it is observed that slight bulging occurs. The bulging is controlled around areas of vertical reinforcement as the steel present in the grout column acts to resist the induced transverse tensile stresses. From this, different values of the strut efficiency factor are proposed based on the number of interior grout cores the strut intercepts (Table 5.1). The initial value of 0.75 was adopted from the American concrete design provisions ACI 318-19 (ACI, 2019), which is then increased by increments of 0.10 for every additional grout core intercepted until a maximum value of

1.00 is reached. For the grouted compressive strut that runs solely through the compression edge grout cores, a constant value of 0.75 is specified.

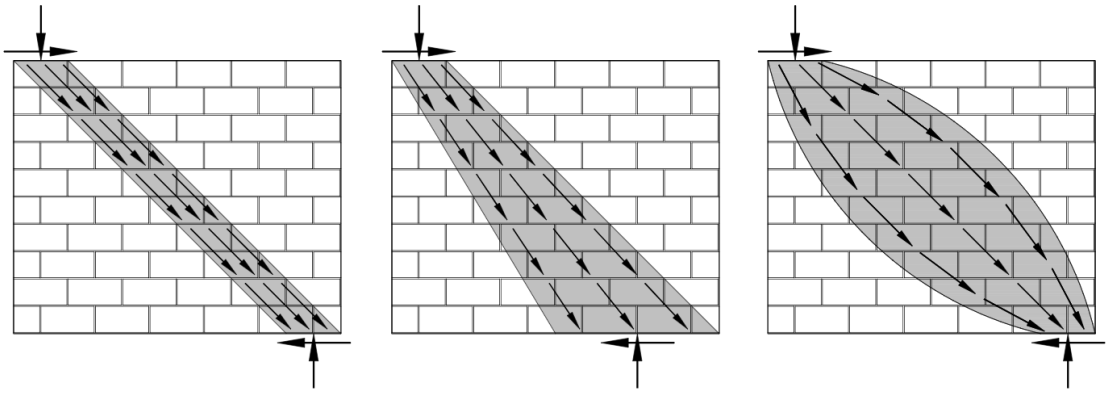

Figure 5.8 – Different Strut Types (Dillon, 2015)

Table 5.1 – Proposed Strut Efficiency Factors

Interior Grout Cores Intercepted	Proposed Strut Efficiency Factor (β_S)
0	0.75
1	0.85
2	0.95
3+	1.00

The second reduction factor (β_A) is termed the strut inclination factor and is used to account for the decrease in masonry compressive strength for loads that are not applied perpendicular to the bed joints of the masonry. Figure 5.9 below depicts both the theoretical strength reduction factors and proposed strength reduction factors that reduce the strength of the masonry material based on the inclination angle of the applied loads. For an inclination angle of 0 degrees, there is no reduction as the load is applied perpendicular to the bed joints, as would be the case when experimentally determining the strength of the masonry prism. As the angle increases, the reduction becomes more apparent. As the ungrouted compressive struts were generally inclined at an angle of 45 degrees, a constant strut inclination reduction factor of 0.6 is specified. This value is below the theoretical strength; however, the value is simplistic to employ and conservative. As grouted struts present in the compression edge grout core are almost vertical, a strut inclination reduction factor of 1.00 is specified.

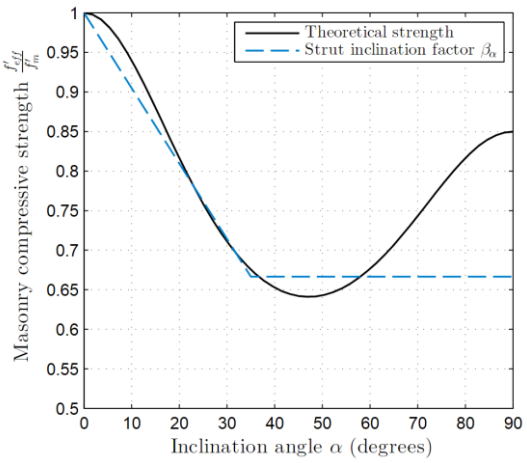

Figure 5.9 – Strut Capacity Reductions (Dillon, 2015)

When applying both of these factors to a compressive strut featured in the Nolph (2010) specimen presented in Fig. 5.4, it is found that the maximum compressive strength of an ungrouted strut that does not and does intercept a grout core is 4.05 MPa and 5.15 MPa, respectively, which closely matches the values predicted by the micro-model.

5.2.3 Tensile Ties

As the masonry components of the wall are assumed to have negligible strength in tension, the only tensile ties present in the model are that of the steel reinforcement. This results in simplistic stress calculations, as the stresses in the tensile ties can be found by dividing the tensile forces by the cross-sectional areas of the reinforcement. Anchorage requirements of the tensile ties were adapted from the development recommendations listed in the TMS 402-22 (MSJC, 2022) provisions, as illustrated in Fig. 5.10.

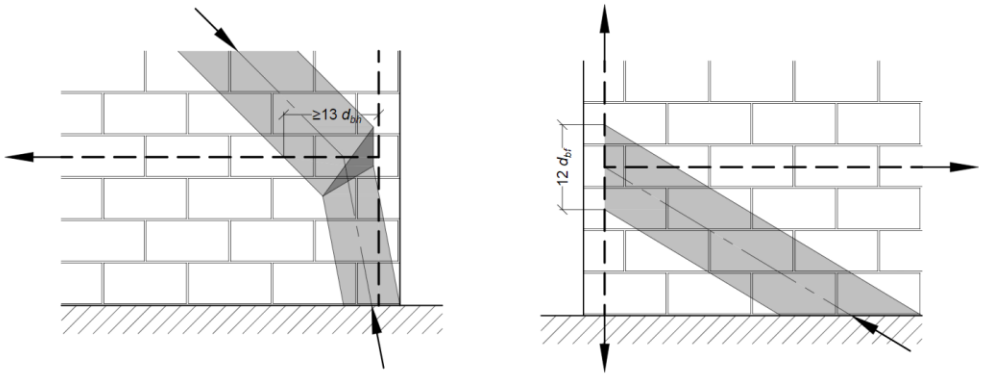

Figure 5.10 – Anchorage Requirements of the Tensile Ties (Dillon, 2015)

5.2.4 Nodal Zones

Referring to the stress trajectories of Fig. 5.4 above, it is seen that the majority of nodes form along the perimeter of the walls. Along both the top of the wall and along the tensile edge of the wall, nodes appear to form at approximately 400 mm increments and result in the creation of a compressive strut. This is interesting as the formation of compressive struts defined in previous studies was limited to the top of the wall (Voon and Ingham, 2008; Nolph, 2010; Elmapruk, 2010; Dillon, 2015). The presence of nodes along the tensile edge of the wall can be attributed to the loading mechanism of the wall. While reinforced concrete walls are loaded primarily from the top of the structure, partially-grouted masonry walls are primarily loaded through the grout core. When the trailing grout core is laterally displaced, contact is initiated between the grout core and the masonry units along the tensile edge of the wall. This behaviour is analogous to that of masonry in-fill walls in which the source of mechanical loading is the contact between the frame and the masonry in-fill wall. On the compression edge of the wall, compressive struts enter the grout core and are redirected toward the foundation of the wall. The location at which this redirection occurs will be the location of the node. Furthermore, analysis of the stress distributions in the reinforcing bars (Fig. 5.11) indicates that nodes are additionally formed at the intersections of bond beams and grout cores. This can be seen as sudden increases and decreases in the steel stresses are observed at these intersections allowing for the conclusion that portions of the stress have been redistributed to the masonry.

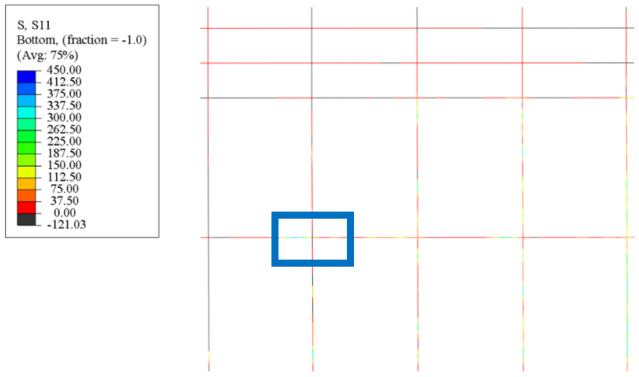

Figure 5.11 – Identified Nodal Zones

Nodes play an important role in a strut-and-tie analysis as the capacity of each node must be checked alongside the capacities of the struts and ties. The capacity of each node is dependent on the number of struts and ties intercepting the node. For instance, a node featuring predominantly tensile ties will have a smaller capacity than that containing predominantly compressive struts, as the tensile ties reduce the compressive capacity of the node. Fortunately, for partially-grouted walls, the stress calculations of the nodes are less influential. This can be attributed to the majority of the compressive struts within the wall system occurring in the ungrouted regions and thus are defined by the ungrouted compressive capacity. Nodes, on the other hand, exist in the grouted regions and thus are defined by the noticeably larger grouted compressive capacity. In addition, the ungrouted struts are defined by the cross-sectional area of the masonry flanges, while the nodal cross-sectional area is defined by the thickness of the masonry wall, which is approximately 3-times larger when compared to the masonry flanges. The combined increased stress capacity and larger cross-sectional area of the nodes, when compared to the ungrouted compressive struts, results in a system in which the nodal calculations rarely govern the capacity of the system.

5.3 Strut-and-Tie Design Procedure

The proposed strut-and-tie design methodology can be summarized in 5 transparent and mechanics-based steps. As an iterative process is required to find the optimal solution (discussed below), MATLAB code (MathWorks, 2022) is provided in Appendix C to determine the forces of the struts and ties for the majority of strut types encountered. It is noted that 45-degree strut angles and strut widths equivalent to the height of the masonry units were specified for all ungrouted struts.

Step 1: Determine the Location of all Nodal Zones

The first step in the methodology is determining the locations at which compressive struts originate. From the parametric analysis, it was observed that nodes form along both the top of the wall and along the tensile edge and are spaced in increments of 400 mm. This is conducted in a two-step process in which initial nodes are placed at the top of each

grout core, followed by the additional placement of nodes spaced at 400 mm increasements between the grout cores. It is noted that the tension heel of the wall is known to exhibit flexural cracks; thus, no nodes are to be placed within the bottom four courses of the wall. An example of determined initial nodes is presented below in Fig. 5.12, in which the red circles are the identified nodal locations. When the nodal locations along the top of the wall are determined, the applied axial stress can be converted into a series of points loads based on tributary area and then applied to each node along the top of the wall.

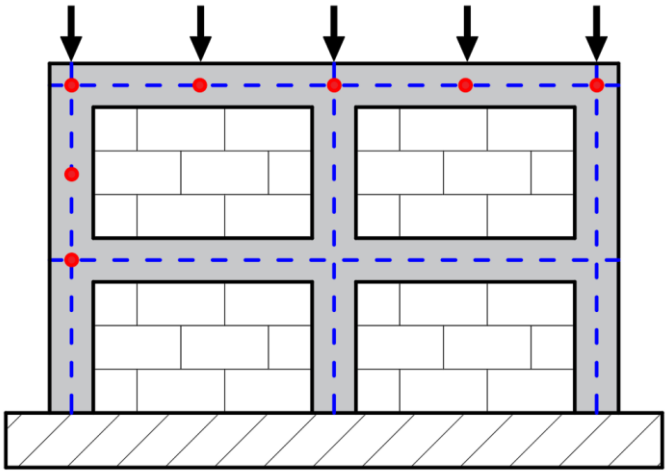

Figure 5.12 – Strut-and-Tie Model (Step 1)

Step 2: Calculate the Stresses/Forces and Width of the Lead Strut

Step 2 involves the calculation of the lead strut, which runs from the node located at the top of the compression side grout core to the foundation of the wall (Fig. 5.13). As the strut is completely within the grout core, grouted masonry properties are used for all calculations. Based on the particle equilibrium of the top node, there are three unknown forces and a known axial load. The three unknown forces include the vertical reinforcing bar, the applied lateral load, and the strut force. These three forces can be determined using the two equilibrium equations and the constraint equation that the strut force must be less than or equal to the calculated maximum strut capacity. Within this system of equations, the geometry of the strut is also required to determine both the angle at which

the strut acts (for the equilibrium equations) and the width of the strut (for the constraint equation).

To begin the calculations, an initial strut angle is assumed, which allows for the calculations to occur. Once complete, the strut width is calculated and checked against the geometry of the wall. If the strut exits the masonry structure, the assumed strut angle is deemed invalid, and the process is repeated until the strut remains inside the grout core. As multiple values of strut angles will produce valid solutions, the solution in which the compressive strut enters the foundation at precisely the edge of the wall (optimal solution as presented in Fig. 5.13) is selected.

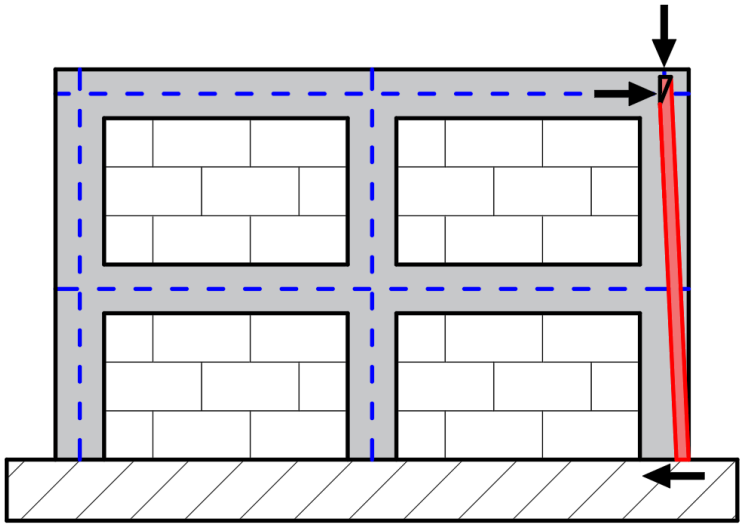

Figure 5.13 – Strut-and-Tie Model (Step 2)

Step 3: Calculate the Stresses/Forces and Widths of the Bent Struts

Step 3 is the most difficult step of the overall process and involves the calculations of the forces and widths of the bent struts. This involves a two-part process in which the initial strut originating at the top is first calculated, followed by the redirect strut within the grout core. Grouted and ungrouted masonry properties were specified for the initial and redirected strut, respectively. The challenge is presented in that the redirected strut is restricted from crossing the previously calculated lead or bent struts. An additional challenge exists in determining the interactions of the bent strut with additional nodes in

the system. Referring to Fig. 5.14a, it is observed that the bent strut originates at the top of a grout core and enters the compressive grout core at the location of a bond beam. From this, extra calculations exist in that the forces in the reinforcement of the interior grout core at the top node and the forces in the bond beam reinforcement must also be calculated. Thus, for struts in which interaction exists between the struts and the inter grout cores or bond beams, the capacity constraint equation must be simultaneously employed within the equilibrium equations. The bent strut presented in Fig. 5.14b does not encounter this problem, however, as it does not originate at the top of a grout core nor intersect the bond beam at a nodal location. From this, all of the forces within the system can be calculated using the equilibrium equations solely, with the capacity constraint checked afterwards.

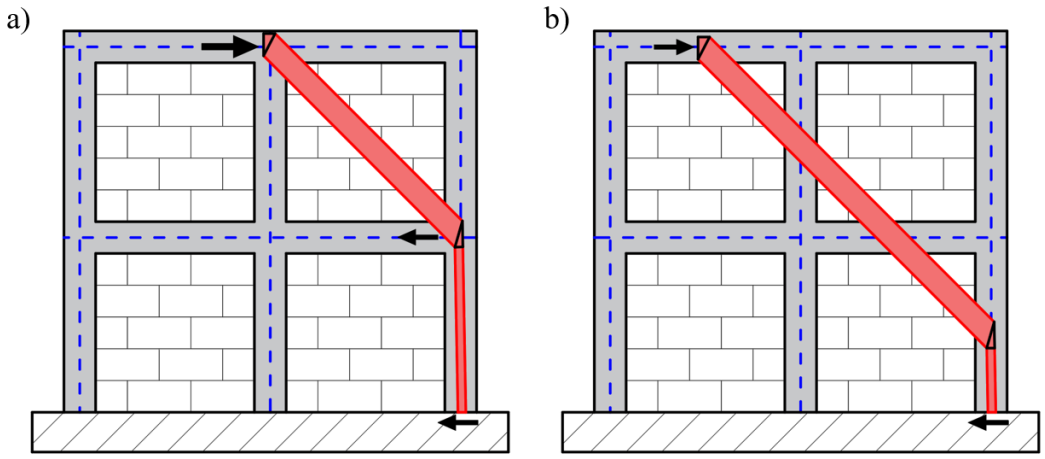

Figure 5.14 – Bent Strut Types (a) Intersects Grout Cores and/or Bond Beams (b) Does Not Intersect Grout Cores and/or Bond Beams

Once all the properties of the bent struts have been calculated, the compression toe must be checked to ensure all redirected compressive struts remain in the grout core and do not intersect. If it is found that the total horizontal width of all struts presents in the compressive grout core, the analysis must be re-run utilizing different combinations of redirected strut angles and forces until a valid solution is found. If no solution exists for a particular force level, it is assumed that the wall has already failed prior to reaching the level of the applied load. A valid solution is presented in Fig. 5.15 below.

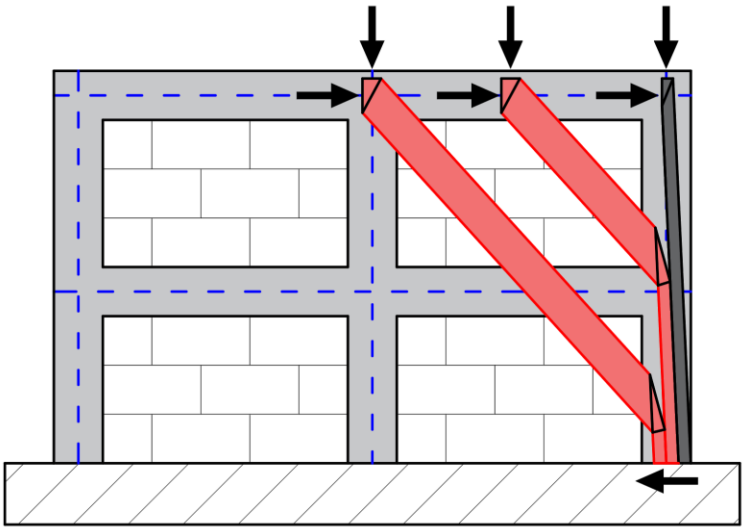

Figure 5.15 – Strut-and-Tie Model (Step 3)

Step 4: Calculate the Stresses/Forces of the Top Struts

Step 4 involves the calculation of all struts originating at the top of the wall but entering the foundation prior to reaching the compressive grout core (Fig. 5.16).

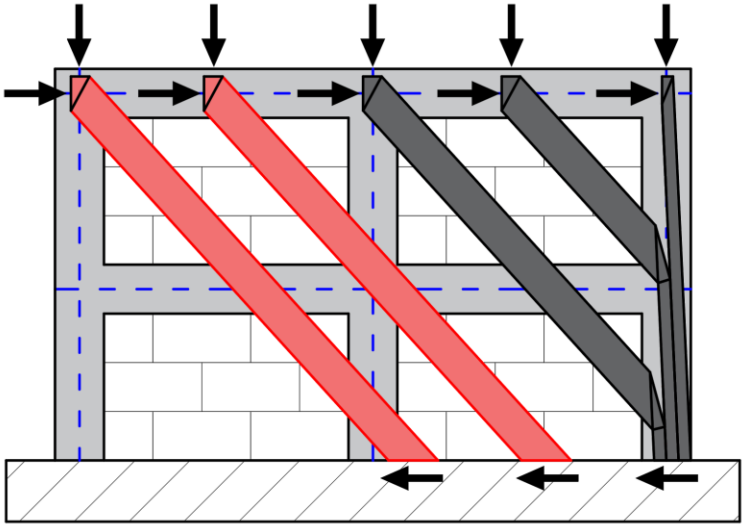

Figure 5.16 – Strut-and-Tie Model (Step 4)

As no top struts enter the compressive grout core, only the ungrouted properties of the masonry are used during the calculations. The calculations of these struts are simpler than that of the compressive struts, as geometric considerations do not need to be accounted for as the maximum strut width is limited to the height of the unit as described

above, and no strut redirection occurs. As the nodes are ensured to be spaced at least 400 mm apart, the crossing of the compressive struts cannot occur. Care must be taken to consider if these struts feature any interaction with any grout cores (Fig. 5.17a) or with any bond beams (Fig. 5.17b). If such interactions exist, the capacity constraint equation must be simultaneously employed within the equilibrium conditions. If no interactions exist, then the nodal systems can be solved from the equilibrium equations alone.

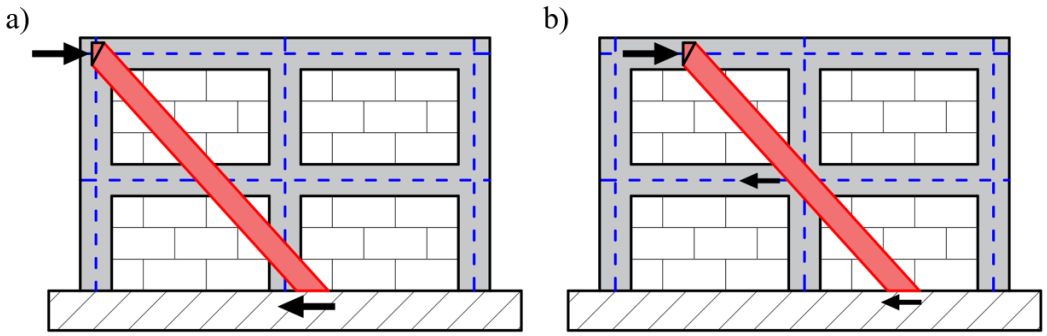

Figure 5.17 – Top Strut Types (a) Intersects Grout Cores and/or Bond Beams (b) Does Not Intersect Grout Cores and/or Bond Beams

Step 5: Calculate the Stresses/Forces of the Edge Struts

The final step involves the calculations of all of the edge struts, as shown in Fig. 5.18 and the final determination of the in-plane shear capacity of the partially-grouted wall.

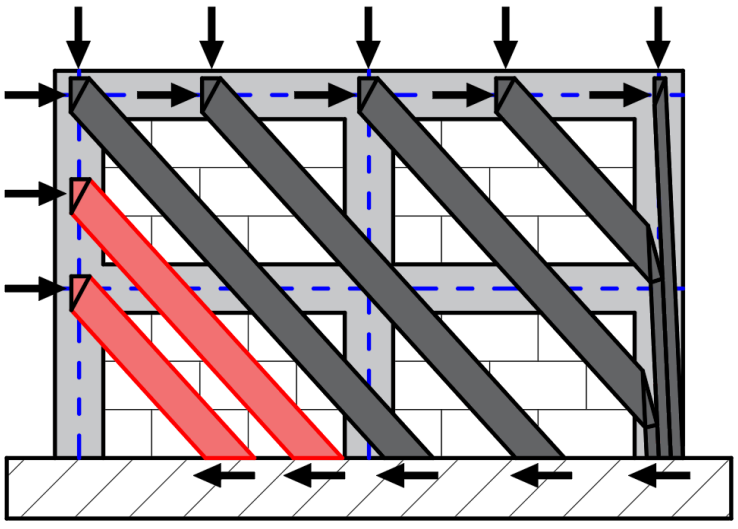

Figure 5.18 – Strut-and-Tie Model (Step 5)

Two possible types of edge struts exist. The first type is an edge strut that initiates at the location of a bond beam (Fig. 5.19a), while the second type is an edge strut that does not initiate at the location of a bond beam (Fig. 5.19b). Unlike the previous strut types, the calculation of these struts requires the capacity constraint equation, as they both have three unknown forces. These unknowns are the strut force, the vertical reinforcing bar force, and the applied lateral load, as the forces within the bond beam have been calculated in previous steps. As the presence of the compressive struts continuously increases the forces present in the vertical reinforcing bar, an additional check must be conducted to determine if yielding occurs. If yielding does occur, then the force of the compressive strut must be decreased.

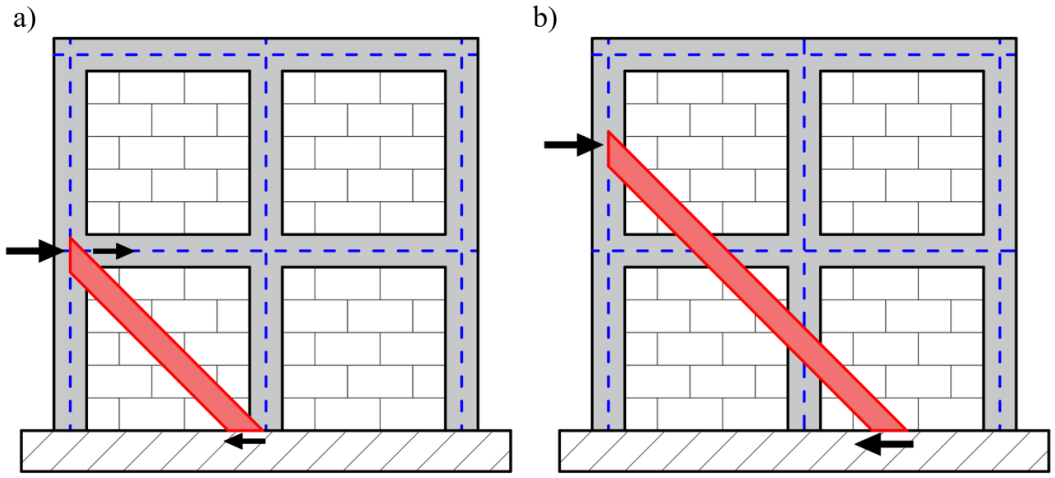

Figure 5.19 – Edge Struts (a) Intersects Bond Beam (b) Does Not Intersect Bond Beam

With all calculations complete, the in-plane shear capacity of the wall can be determined as the sum of the horizontal components of the shear forces present at the bottom of the wall (shown as the leftward pointed arrows in Fig. 5.18) or the sum of the applied loads (shown as the rightward pointed arrows in Fig. 5.18). If a discrepancy exists between the two summations, the structure is not in equilibrium, and an error exists. If found to be in equilibrium, then the model is deemed valid as (a) the structure is in equilibrium, (b) no compressive struts intersect one another, (c) no compressive strut or tensile tie exceeds their respective yield limit, and (d) all nodal stresses are less than their factored capacities.

It is also noted that multiple solutions exist as the capacity constraint may be satisfied for many combinations of the applied load. For a simplistic way to find the maximum capacity, it is recommended to assume all compressive struts are at their full compressive capacity.

5.4 Strut-and-Tie Model Validation

The developed partially-grouted strut-and-tie methodology was validated with two experimental studies available in the literature. The combination of these studies allows for the determination of the methodology to predict the shear capacity under varied aspect ratios, and distributions and quantities of both vertical and horizontal reinforcement. Tables 5.2 and 5.3 below show the shear capacity prediction of the strut-and-tie model (V_{STM}), along with unfactored predictions from both CSA S304-14 (V_{CSA}) and TMS 402-16 (V_{TMS}), and the experimentally obtained capacity (V_{Exp}). Overall, the performance of the strut-and-tie methodology is quite reasonable given its simplicity, as the difference between the experimentally determined shear capacity and the shear capacity predicted by the strut-and-tie methodology was within 6% and 9% for the specimens in the Nolph (2010) and Elmapruk (2010) studies, respectively. As the variations between the strut-and-tie predicted and experimentally determined shear capacities are all under 10%, these variations can be attributed to the natural variations existing in the masonry material and interface properties. The strut-and-tie model also predicted that the horizontal reinforcing bars do not yield at peak load, which is consistent with experimental findings.

Table 5.2 – Strut-and-Tie Results (Nolph)

Specimen	V_{Exp} (kN)	V_{CSA} (kN)	$\frac{V_{\mathrm{Exp}}}{V_{\mathrm{CSA}}}$	V_{TMS} (kN)	$\frac{V_{\mathrm{Exp}}}{V_{\mathrm{TMS}}}$	V_{STM} (kN)	$\frac{V_{\mathrm{Exp}}}{V_{\mathrm{STM}}}$
PG085-48	222	358	0.86	255	0.87	218	1.02
PG127-48	228	306	0.75	255	0.89	218	1.05
PG169-48	204	313	0.65	255	0.80	218	0.94
PG085-32	260	275	0.95	278	0.94	249	1.04
PG085-24	293	281	1.05	301	0.98	276	1.06
Mean	-	-	0.85	-	0.90	-	1.02
COV	-	-	0.19	-	0.08	-	0.05

Table 5.3 - Strut and-Tie Results (Elmapruk)

Specimen	V_{Exp} (kN)	V_{CSA} (kN)	$\frac{V_{Exp}}{V_{CSA}}$	V_{TMS} (kN)	$\frac{V_{Exp}}{V_{TMS}}$	V_{STM} (kN)	$\frac{V_{Exp}}{V_{STM}}$
PG127-48	238	314	0.76	306	0.78	262	0.91
PG127-48I	252	314	0.80	306	0.82	262	0.96
PG180-48	266	365	0.73	306	0.87	262	1.02
PG254-48	286	438	0.65	306	0.93	262	1.09
PG127-32	344	328	1.05	322	1.07	335	1.03
PG127-24	400	332	1.20	362	1.10	416	0.96
Mean	-	-	0.87	-	0.93	-	0.99
COV	-	-	0.25	-	0.14	-	0.06

Referring to the different prediction methods above, it is found that overall, the Canadian standard (CSA S304-14) exhibits the worst performance based on the mean and coefficient of variation of the calculated experimental to predicted ratios of shear capacity. This can mainly be attributed to the assumption that the horizontal steel yields at peak load (which was experimentally determined to be untrue), resulting in an overprediction of shear strength. The exception is that of specimen PG085-24, in which the capacity was underpredicted. This can perhaps be attributed to the closely spaced grout cores resulting in behaviour more reminiscent of fully-grouted walls upon which the equations were derived around. The TMS 402-16 equation, although featuring an improved performance when compared to CSA S304-14, suffers from the same problem in that the horizontal steel is predicted to yield at peak load resulting in an overprediction of in-plane shear capacity. The improved performance, however, is not attributed to the actual in-plane shear capacity equation (which performed similarly to that of CSA S304) but rather the maximum limit placed on the in-plane shear capacity prediction to prevent compressive strut failure. For the widely spaced grout cores, this limit was found o govern the in-plane shear prediction, which is why a constant prediction is presented for multiple specimens even when the horizontal reinforcement quantity was increased.

5.5 Influence of Key Design Parameters from the Strut-and-Tie Methodology

Results from the literature and parametric study indicate that the in-plane shear strength of partially-grouted masonry walls is influenced by the aspect ratio, size and distribution

of the vertical reinforcement, the distribution of the horizontal reinforcement, and the applied axial load. The size of horizontal reinforcement was found to play little role in contributing to the shear capacity. Below discusses the ability of the strut-and-tie model to reproduce such behaviour.

5.5.1 Wall Geometry (Aspect Ratio)

Increasing the aspect ratio of the wall was found to decrease the shear capacity of the wall. This trend is also captured by the proposed strut-and-tie methodology, as the larger the aspect ratio of the wall, the less compressive struts enter directly into the foundation (i.e., more bent struts over top struts). This quickly results in the concentration of strut stresses in the compression grout core and the inability of the redirected compressive struts to remain in the compressive grout core. As mentioned above, the forces in the struts must then be lowered to ensure this geometric constraint. By lowering the aspect ratio, however, more struts are converted from bent struts to top structs, which are able to directly enter the foundation without entering the compressive grout core. Being independent of the compressive grout core geometry, these top struts are able to develop larger strut forces which allow for a higher in-plane shear capacity of the wall system.

5.5.2 Horizontal Reinforcement

The findings of the parametric study indicated that only the spacing of the horizontal reinforcement influences the in-plane shear capacity and that the size of the reinforcement plays an insignificant role. This behaviour is also represented in the strut-and-tie model. Referring to the spacing of the reinforcement, it is seen that the more bond beams present in the wall, the more incoming forces from the compressive struts can be redistributed to the tensile edge of the wall resulting in lower redirected strut forces. These lower forces then relax the geometric conditions of the compressive grout core as the lower forces result in lower strut widths. The size of the reinforcement only impacts the amount of force that is able to be redirected to the tensile side of the wall. As the incoming strut forces are typically small compared to the capacity of the reinforcing bars, yielding is quite unlikely and, thus, is rarely the governing factor. This was observed in the

experimental validation above as the horizontal reinforcement was found to not yield for all the specimens considered.

5.5.3 Vertical Reinforcement

Increasing the size of the reinforcement and decreasing the spacing of the reinforcement was found to increase the in-plane shear capacity of the wall. This behaviour is accounted for in the model in two ways. The first involves the nodes present at the top of the wall. If the node is located on the top of a grout core, the vertical reinforcing steel is considered in the particle equilibrium. This allows for larger strut forces to develop, resulting in larger shear capacities. Of course, this is coupled with the role of the horizontal reinforcement if the strut is a bent strut, as the compressive grout core must be able to withstand these larger forces. The second way is the idea that the presence of additional grout cores allows for a higher strut efficiency factor which also allows for higher strut forces to be developed.

5.5.4 Applied Axial Stress

Applied axial stress was found to be the most influential parameter contributing to the in-plane shear capacity. As the applied axial stress increases, so does the in-plane shear capacity. This is represented in the model in the same way as the vertical reinforcement above, as the presence of additional vertical forces on the top nodes of the wall allows for larger compressive struts to form. Unlike the vertical reinforcement, which only applies to nodes featuring a grout core, the applied axial load impacts every node along the top of the wall, possibly explaining why an increased axial load was found to be more influential than the grout core spacing. If the applied axial stress is too large, the capacity equation of the compressive strut will not be met, resulting in a predicted compressive strut failure.

5.6 Strut-and-Tie Development Summary

In this chapter, the development and experimental validation of the strut-and-tie modelling methodology for partially grouted masonry walls are presented. The model was formed by considering the foundational principles guiding the strut-and-tie

methodology developed for reinforced concrete structures and making the necessary adaptations to partially-grouted masonry walls based on micro-model findings. Such findings include the locations of nodal zones, the geometry of the compressive struts, and the stress magnitudes of the compressive struts. The proposed methodology was then validated with experimental findings to assess the prediction capacity of the methodology. For all specimens considered, the methodology was able to capture the in-plane shear strength within 10%. The strut-and-tie model was also found to accurately account for the influence of different key design parameters on the in-plane shear strength.

6.0 CONCLUSIONS AND RECOMMENDATIONS

This chapter provides a summary, conclusions, and recommendations from the study of developing a strut-and-tie methodology to predict the in-plane shear capacity of partially-grouted North American masonry walls.

6.1 Summary

The objective of developing a strut-and-tie methodology to predict the in-plane shear capacity of partially-grouted North American masonry walls was achieved by the following:

1. Developing a detailed finite element micro-model to accurately predict the in-plane shear capacity and assess the behaviour of partially-grouted concrete-block masonry walls:
   - A detailed finite element micro-model was developed using the commercially available software ABAQUS (Dassault Systems, 2022) to predict the in-plane shear capacity of shear-critical partially-grouted walls.
   - The model featured a two-layer system in which the flanges of the masonry units and mortar would be contained in one layer while the masonry webs, grout, and steel reinforcement would be contained in another layer. These layers would then be coupled together through a series of constraints.
   - Material nonlinearity of the masonry units, mortar, and grout was accounted for through the implementation of the plasticity-based concrete damage plasticity (CDP) model.
   - Interface characteristics between the masonry units – mortar and masonry units – grout were implemented through the combined use of a surface-based cohesion model and a Mohr-Coulomb friction law to couple the interface shear capacity with the applied compressive loads.
   - Validation of the micro-model was performed by comparing the applied load–wall drift responses of the micro-model with several studies available in the literature. These include Calderón et al. (2017), Minaie et al. (2010), Nolph

(2010), Elmapruk (2010), and Ba Rahim et al. (2022). From this, the model was verified to be able to capture the in-plane shear capacity of partially-grouted walls with varied aspect ratios, applied axial loads, quantity and distributions of horizontal and vertical reinforcement, types of horizontal reinforcement, and boundary conditions.

2. Conducting an extensive parametric study to determine the influence of key design parameters (applied axial stress, aspect ratio, etc.) on the in-plane load capacity and to provide insight into the mechanical response of the wall:
   - Using the developed micro-model, an extensive parametric analysis involving over 1,600 simulations was conducted.
   - Fixed parameters in the study included the strength properties of the masonry assemblage (masonry units, mortar, and grout), the strength of the steel reinforcement, the thickness and width of the masonry wall, and the wall boundary conditions.
   - Independent parameters consisted of the aspect ratio/wall weight (3 variations), horizontal reinforcement size (3 variations), horizontal reinforcement spacings (3 variations), vertical reinforcement size (3 variations), vertical reinforcement spacings (3 variations), applied axial stress (6 variations), and bed-joint reinforcement (2 variations).
   - The sole dependent parameter in the analysis was the in-plane load capacity of the wall specimen.
   - Results from the study were used to determine the influence of each key design parameter on the in-plane load capacity of the wall.
3. Development of a strut-and-tie model to predict the in-plane shear capacity of partially-grouted masonry wall systems:
   - Findings, the developed micro-model and parametric analysis were used in combination to provide behavioural insights required to facilitate a strut-and-tie adaptation of the reinforced concrete systems to partially-grouted masonry systems.

- From the model, the in-plane shear capacity of partially-grouted masonry walls can be predicted.
- Insights explored include the strut and tie locations, compressive strut angles, compressive strut magnitudes, and nodal locations.
- The finalized methodology was summarized in an easy-to-follow guide to be readily adapted to existing masonry design provisions.
- The proposed methodology was validated with two experimental studies from the literature (Nolph, 2010; Elmapruk, 2010) to ensure validity.
- Mechanics of the proposed methodology were compared against a combination of experimental findings and the results of the parametric study to determine if the model can capture the observed influence of different parameters on the in-plane shear capacity.

6.2 Conclusions

Conclusions from the analytical modelling of partially-grouted masonry walls are as follows. It is noted that these conclusions are valid for shear-critical partially-grouted masonry walls constructed with concrete masonry units and featuring steel reinforcement.

- Experimental triplet tests indicated the mechanical behaviour of the masonry unit–mortar interface closely follows a Mohr-Coulomb friction model.
- The developed micro-modelling methodology was able to capture the ultimate load capacities within 10% for the majority of experimentally tested specimens with varied aspect ratios, applied axial loads, quantities and spacings of horizontal and vertical reinforcing bars, and horizontal reinforcing types. Furthermore, the model was able to capture several experimentally observed behavioural characteristics, such as the lack of yielding of the horizontal reinforcement and initial stiffnesses of the specimens.
- Decreasing the aspect ratio of the wall results in a significant increase in-plane shear capacity. This is due to the majority of the compressive struts formed at the top of the wall being able to travel directly into the foundation as opposed to concentrating at the compression toe of the wall.

- Increasing the horizontal reinforcing spacing results in a noticeable increase in-plane shear capacity. This is due to the additional nodes formed along the leading edge of the wall allowing for incoming compressive strut forces to be redistributed back to the trailing edge of the wall analogues to the mechanisms of stirrups in reinforced concrete.
- Increasing the size of the horizontal reinforcement bars has an insignificant effect on the in-plane shear capacity. This is attributed to the horizontal reinforcing bars not yielding at peak load.
- Increasing the spacing of the vertical reinforcement results in a significant increase in the in-plane shear capacity.
- While increasing the size of the vertical reinforcing bars does influence the in-plane shear capacity, the effect is dependent on the magnitude of applied axial stress and the aspect ratio of the wall. For walls under light amounts of axial stress, increasing the size of the vertical reinforcing bars noticeably increases the in-plane shear capacity of the wall. However, for walls under high levels of applied axial stress, increasing the size of the vertical reinforcement has a negligible influence on the in-plane shear capacity as the steel does not yield. The influence of increasing the size of the vertical reinforcement on the in-plane shear capacity is more prevalent in walls with higher aspect ratios as the behaviour becomes more flexural.
- Bed-joint reinforcement was found to have a negligible influence on the in-plane shear capacity.
- Stress trajectories produced from the micro-model indicate that the compressive struts in the masonry wall are constrained between the head joints and act at 45-degree angles.
- Locations where compressive struts initiate suggest that the behaviour of partially-grouted masonry walls may be reminiscent of masonry infill walls in which the grout cores act as the concrete frame.
- Levels of stress in the reinforcing steel indicated that nodes are formed at the intersections of bond beams and grout cores.

- The developed strut-and-tie methodology for partially-grouted masonry walls was found to predict the in-plane shear capacity of several experimentally tested walls within 10%.
- The mechanics of the developed strut-and-tie model are capable of predicting the influence of different design parameters (listed above) on the in-plane shear strength of the wall.

6.3 Recommendations and Future Research

This study aimed to develop a strut-and-tie model to predict the in-plane shear capacity of partially-grouted concrete block masonry walls. As this was the initial work of a much larger project, there are several recommendations for future work based on the outcomes of this thesis:

- Future development of masonry micro-models should explore the creation of three-dimensional models. As mentioned in the thesis, there are several aspects that could not be captured due to the two-dimensional constrain of the models. Examples include the role of bed-joint reinforcement links perpendicular to the plane of the wall, possible bond-slip of the horizontal and vertical reinforcement, and the ability of compressive struts to interact with the interior grout cores of the wall.
- Future micro-model simulations should aim to develop more detailed interface models designed to capture the degradation of the interfaces under cyclic loading. In addition to predicting the in-plane shear capacity of partially-grouted walls, there exists a substantial need to quantify the ductility and energy dissipation of partially-grouted to begin the development of performance-based seismic design provisions.
- Additional testing of triplet tests should be conducted to determine the mechanical characteristics of the masonry unit–mortar interfaces at additional levels of precompression. In addition, testing should be conducted to determine the mechanical properties of the masonry unit–grout interfaces.

- The parametric study should be vastly expanded upon to include additional aspect ratios, applied axial loads, and the quantities and distributions of horizontal and vertical reinforcement. New parameters that should be included are the wall boundary conditions, material strengths of the masonry units, mortar, grout, and steel reinforcement, and non-uniform spacings of the horizontal and vertical reinforcing bars.
- Future research should explore using the parametric study database to conduct linear and nonlinear regression analysis to aid in the development of a new in-plane shear capacity equation. While the author supports the notion that the complete in-plane shear capacity cannot be captured with a single equation, these simplistic equations are useful for quick and easy calculations in design offices.
- The developed strut-and-tie methodology should be expanded to include the capability to predict the inelastic deflections of the wall specimens. This can be achieved by implementing the stress-strain characteristics of the masonry materials into the compressive struts and tensile ties.
- Additional research should be used to verify the role of anchorage in the strut-and-tie model and the capacity of the nodal zones.

REFERENCES

AASHTO LRFD. (2004). “Bridge Design Specifications and Commentary,” 3rd Edition, Washington, D.C.: American Association of State Highway Transportation Officials.

Abdulla, K., Cunningham, L., and Gille, M. (2017). “Simulating Masonry Wall Behaviour using a Simplified Micro-Model Approach.” Engineering Structures, 151(2017), 349-365.

Alshebani, M. and Sinha, S. (2000). “Stress-Strain Characteristics of Brick Masonry Under Cyclic Biaxial Compression.” Journal of Structural Engineering, 129(9), 1004-1007.

American Concrete Institute (ACI) Committee. (2002). “Building Code Requirements for Structural Concrete.” ACI 318-02. Farmington Hills, MI: American Concrete Institute.

American Concrete Institute (ACI) Committee. (2019). “Building Code Requirements for Structural Concrete.” ACI 318-19. Farmington Hills, MI: American Concrete Institute.

Anderson, D., and Priestley, M. (1992). “In Plane Shear Strength of Masonry Walls.” Proc. 6th Canadian Masonry Symposium (CMS), 223–234. Saskatoon, Canada.

Ba Rahim, A., Pettit, C., Cruz-Noguez, C., Hung, J. (2020). “An Analysis Model for Partially Grouted Masonry Shear Walls using Macro-Modelling.” Proc. Canadian Society of Civil Engineers (CSCE) 2020 Annual Conference.

Ba Rahim, A. (2023). “Shear Strength of Partially-Grouted (PG) Masonry Shear Walls: Experimental and Analytical Studies.” Ph.D. Dissertation, University of Alberta, Alberta, Canada.

Ba Rahim, A., Cruz-Noguez, C., and Pettit, C. (2022). “Experimental Testing of Partially Grouted Masonry Shear Walls with Different Horizontal Reinforcement Types.” Proc. Canadian Society of Civil Engineers (CSCE) 2022 Annual Conference.

Banting, B. (2013). “Seismic Performance Quantification of Concrete Block Masonry Structural Walls with Confined Boundary Elements and Development of the Normal Strain-Adjusted Shear Strength Expression (NSSSE).” Ph.D. Dissertation, McMaster University, Ontario, Canada.

Banting, B., and El-Dakhakhni, W. (2012). “Force- and Displacement-Based Seismic Performance Parameters for Reinforced Masonry Structural Walls with Boundary Elements.” Journal of Structural Engineering, 138(12), 1477–1491.

Bedeir, H., Marwan, S., Hussein, O., and Osama, H. (2017). “A Force-Based Macro-Model for Reinforced Concrete Masonry Walls Subjected to Quasi-Static Lateral Loading.” Proc. 13th Canadian Masonry Symposium (CMS). Halifax, Canada.

Bentz, E. (2000). “Sectional Analysis of Reinforced Concrete Members.” Ph.D. Dissertation, University of Toronto, Ontario, Canada.

Bentz, E., Vecchio, F., and Collins, M. (2006). “Simplified Modified Compression Field theory for Calculating Shear Strength of Reinforced Concrete Elements.” ACI Structural Journal, 103(4), 614-624.

Birtel, V. and Mark, P. (2006). “Parameterised Finite Element Modelling of RC Beam Shear Failure.” Proc. 2006 ABAQUS User’s Conference.

Blondet, J., Mayes, R., Kelly, T., Villablanca, R., and Klingner, R. (1989). “Performance of Engineered Masonry in the Chilean Earthquake of March 3, 1985: Implications for U.S. Design Practice.” PMFSEL Report No. 89-2, National Science Foundation.

Bolaños, P. (2020). “Edificaciones De Albañileria Armada.” M.Sc. Thesis, Pontificia Universidad Catolica De Chile Escuela De Ingenieria Analisis, Chile.

Bolhassani, M., Hamid, A., Lau, A., and Moon, F. (2015). “Simplified Micro Modeling of Partially Grouted Masonry Assemblages.” Construction and Building Materials, 83(2015), 159-173.

British Standards (BSI). (2002). “Methods of Test for Masonry – Part 3: Determination of Initial Shear Strength.” BS EN 1052-3:2002, BSI, London, England.

Brown, R. and Melander, J. (2001). “Flexural Bond Strength of Masonry Parallel to the Bed Joints.” Proc. 9th Canadian Masonry Symposium (CMS). Fredericton, Canada.

Buxton, J. (2017). “Strut-and-Tie Modeling of Multistory, Partially-Grouted, Concrete Masonry Shear Walls with Openings.” M.Sc. Thesis, Brigham Young University, Utah, USA.

Calderón, S., Sandoval, C., and Arnau, O. (2017). “Shear Response of Partially-Grouted Reinforced Masonry Walls with a Central Opening: Testing and Detailed Micro-Modelling.” Engineering structures, 118(2017), 122-137.

Calderón, S., Milani, G., and Sandoval, C. (2021). “Simplified Micro-Modeling of Partially-Grouted Reinforced Masonry Shear Walls with Bed-Joint Reinforcement: Implementation and Validation.” Engineering structures, 234(2021), 111987.

Calderón, S., Sandoval, C., Araya-Letelier, G., Inzunza, E., and Arnau, O. (2021). “Influence of Different Design Parameters on the Seismic Performance of Partially-Grouted Masonry Shear Walls.” Engineering structures, 239(2021), 112058.

Calderón, S., Sandoval, C., Araya-Letelier, G., Inzunza, E., and Milani, G. (2021). “Quasi-Static Testing of Concrete Masonry Shear Walls with Different Boundary Conditions.” Engineering structures, 38(2021), 102201.

Calderón, S., Milani, G., and Sandoval, C. (2021). “Simplified Micro-Modeling of Partially-Grouted Reinforced Masonry Shear Walls with Bed-Joint Reinforcement: Implementation and Validation.” Engineering structures, 234(2021), 111987.

Canadian Standards Association (CSA). (2019). “Design of Concrete Structures.” CSA A23.3-19, CSA, Mississauga, Canada.

Canadian Standards Association (CSA). (2014). “Design of Masonry Structures.*” CSA S304-14 (R2019),* CSA, Mississauga, Canada.

CEB-FIP Model Code 1990. (1993). Desing Code. London, T. Telford.

Cecchi, A. and Di Marco, R. (2002). “Homogenized Strategy Toward Constitutive Identification of Masonry.” Journal of Engineering Mechanics, 128(6), 688-697.

Chen, S., Hidalgo, P., Mayes, R., Clough, R., and McNiven, H. (1978). "Cyclic Loading Tests of Single Masonry Piers – Volume 2: Height to Width Ratio of 1." Report No. UCB/EERC-78-28, Earthquake Engineering Research Center, University of California Berkeley, USA.

Darmayadi, D. and Satyarno, I. (2019). "Finite Element Modeling of Masonry Wall with Mortar 1pc:4 Lime:10 Sand under Later Force." Proc. MATEC Web of Conferences 258, 05019.

Davis, C. (2008). "Evaluation of Design Provisions for In-Plane Shear in Masonry Walls." M.Sc. Thesis, Washington State University, Washington, USA.

Dhanasekar, M. and Haider, W. (2010). "Effect of Spacing of Reinforcement on the Behaviour of Partially-Grouted Masonry Shear Walls." Advances in Structural Engineering, 14(2), 281-293.

Dickie, J. and Lissel, S. (2009). "Comparison of In-Plane Masonry Shear Models." Proc. 11th Canadian Masonry Symposium (CMS). Toronto, Canada.

Dillon, P. (2015). "Shear Strength Prediction Methods for Grouted Masonry Shear Walls." Ph.D. Dissertation, Brigham Young University, Utah, USA.

El-Adaway, I., Breakah, T., and Khedr, S. (2011). "Brick Masonry and Sustainable Construction." Proc. Integrating Sustainability Practices in the Construction Industry. Kansas City, MO: Construction Institute of ASCE.

El-Dakhakhni, W., Banting, B., and Miller, S. (2013). "Seismic Performance Parameter Quantification of Shear-Critical Reinforced Concrete Masonry Squat Walls." Journal of Structural Engineering, 139(June), 957–973.

El-Hashimy, T., Ezzeldin, M., Tait, M., and El-Dakhakhni, W. (2019). "Out-of-Plane Performance of Reinforced Masonry Shear Walls Constructed with Boundary Elements." Journal of Structural Engineering, 145(8), 04019073.

Elmapruk, J. (2010). "Shear Strength of Partially Grouted Squat Masonry Shear Walls." M.Sc. Thesis, Washington State University, Washington, USA.

Elmapruk, J., ElGawady, M., and Hassanli, R. (2020). “Experimental and Analytical Study on the Shear-Strength of Partially Grouted Masonry Walls.” Journal of Structural Engineering, 146(8), 04020147.

Elmeligy, O., Aly, N., and Galal, K. (2021). “Sensitivity Analysis of the Numerical Simulations of Partially Grouted Reinforced Masonry Shear Walls.” Engineering Structures, 245(2021), 112876.

Erdogmus, E., Cruz-Noguez, C., Ledent, P., Lane, J., Hughes, K., Banting, B., and Thompson, J. (2021a). “Parametric Study on Reinforced Masonry Shear Walls Resisting In-Plane Loads: A Comparison of CSA S304-14 and TMS 402-16.” Proc. 14th Canadian Masonry Symposium (CMS). Montreal, Canada.

Erdogmus, E., Dutrisac, H., Thompson, J., and Banting, B. (2021b). “Comparison of Selected CSA S304-14 and TMS 42-16 Reinforced Masonry Design Provisions and Material Properties.” 14th Canadian Masonry Symposium (CMS). Montreal, Canada.

Facconi, L., Plizzari, G., and Vecchio, F. (2013). “Disturbed Stress Field Model for Unreinforced Masonry.” Journal of Structural Engineering, 140(4), 4013085.

Fattal, S. (1993a). “The Effect of Critical Parameters on the Behavior of Partially-Grouted Masonry Shear Walls under Lateral Loads.” NISTIR Report No. 5116. National Institute of Standards and Technology. Gaithersburg, USA.

Fattal, S. (1993b). “Research Plane for Masonry Shear Walls.” NISTIR Report No. 5117. National Institute of Standards and Technology. Gaithersburg, USA.

Fattal, S. (1995). “Strength of Partially-Grouted Masonry Shear Walls under Lateral Loads.” NISTIR Report No. 5147. National Institute of Standards and Technology. Gaithersburg, USA.

Fattal, S., and Todd, D. (1991). “Ultimate Strength of Masonry Shear Walls: Prediction vs. Test Results.” NISTIR 4633, Building and Fire Research Laboratory, Gaithersburg, USA.

Fonseca, F. and Dillon, P. (2017). “Analysis of Masonry Shear Walls using Strut-and-Tie

Models." Proc. 13th Canadian Masonry Symposium (CMS). Halifax, Canada.

Fortes, E., Parsekian, G., and Fonseca, F. (2015). "Relationship between the Compressive Strength of Concrete Masonry and the Compressive Strength of Concrete Masonry Units." Journal of Materials in Civil Engineering, 27(9), 04014238.

Fouchal, F., Lebon, F., Raffa, M., and Vairo, G. (2014). "An Interface Model Including Cracks and Roughness Applied to Masonry." The Open Journal of Civil Engineering, 8(2014), 263-271.

Furtaw, C. and Hamid, A. (2004). "Fire Rating and Performance Based Design of Concrete Masonry Walls." Proc., 2004 Structures Congress. Nashville, TN: Structural Engineering Institute of ASCE.

Genikomsou, A., and Polak, M. (2014). "Finite Element Analysis of a Reinforced Concrete Slab-Column Connection using ABAQUS." Proc. Structures Congress 2014. Boston, USA.

Ghanem, G., Essawy, A., and Hamid, A. (1992). "Effect of Steel Distribution on the Behavior of Partially Reinforced Masonry Walls." Proc. 6th Canadian Masonry Symposium (CMS), 365–376. Saskatoon, Canada.

Ghanem, G., Salama, A., Elmagd, S., and Hamid, A. (1993). "Effect of Axial Compression on the Behavior of Partially Reinforced Masonry Shear Walls." Proc. 6th North American Masonry Conference, 1145–1157. Philadelphia, USA.

Giambanco, G., Rizzo, S., and Spallino, R. (2001), "Numerical Analysis of Masonry Structures via Interface Models." Computer Methods in Applied Mechanics and Engineering, 190(2001), 6493-6511.

Haach, V., Vasconcelos, G., and Lourenço, P. (2010). "Experimental Analysis of Reinforced Concrete Block Masonry Walls Subjected to In-Plane Cyclic Loading." Journal of Structural Engineering, 136(4), 452-462.

Hamid, A. (1978). "Behaviour Characteristics of Concrete Masonry." Ph.D. Dissertation, McMaster University, Ontario, Canada.

Hamid, A., Chandrakeerthy, S., and Elnawawy, O. (1992). “Flexural Tensile Strength of Partially Grouted Concrete Masonry.” Journal of Structural Engineering, 118(2), 3377-3392.

Hamid, A. and Drysdale, R. (1981). “Proposed Failure Criteria for Concrete Block Masonry under Biaxial Stresses.” Journal of the Structural Division, 107(8), 1675-1687.

He, Z., Liu, Z., Wang, J., and Ma, Z. (2020). “Development of Strut-and-Tie Models using Load Path in Structural Concrete.” Journal of Structural Engineering, 146(5), 06020004-1.

Hidalgo, P., Mayes, R., McNiven, H., and Clough, R. (1978). “Cyclic Loading Tests of Single Masonry Piers – Volume 1: Height to Width Ratio of 2.” Report No. UCB/EERC-78-27, Earthquake Engineering Research Center, University of California Berkeley, USA.

Hidalgo, P., Mayes, R., McNiven, H. and Clough, R. (1979). “Cyclic Loading Tests of Single Masonry Piers – Volume 3: Height to Width Ratio of 0.5.” Report No. UCB/EERC-78-12, Earthquake Engineering Research Center, University of California Berkeley, USA.

Hognestad, E. (1951). “A Study of Combined Bending Axial Load in Reinforced Concrete Members.” Bulletin Series No. 399 (Vol. 49), Urbana: Engineering Experimental Station, The University of Illinois.

Hoque, N. (2013). “In-Plane Cyclic Testing of Reinforced Concrete Masonry Walls to Assess the Effect of Varying Reinforcement Anchorage and Boundary Conditions.” M.Sc. Thesis, University of Calgary, Alberta, Canada.

Hung, J. (2018). “Artificial Neural Network Model for Analysis of In-Plane Shear Strength of Partially Grouted Masonry Shear Walls.” M.Sc. Thesis, University of Alberta, Alberta, Canada.

Hwang, S., Fang, W., Lee, H., and Yu, H. (2001). “Analytical Model for Predicting Shear Strength of Squat Walls.” Journal of Structural Engineering, 127(1), 43-50.

International Council of Building Officials (ICBO). (1988). Uniform Building Code (UBC). International Council of Building Officials, Whittier, California, U.S.A.

Isfeld, A., Muller, A., Hagel, M., and Shrive, N. (2019). "Analysis of Safety of Slender Concrete Masonry Walls in Relation to CSA S304-14." Canadian Journal of Civil Engineering, 46(5), 424-438.

Isfeld, A., Rizaee, S., Hagel, M., Kahed, M., and Shrive, N. (2017). "Testing and Finite Element Modelling of Concrete Block Masonry in Compression." Proc. 13th Canadian Masonry Symposium (CMS). Halifax, Canada.

Ismail, K., Guadagnini, M., and Pilakoutas, K. (2017). "Strut-and-Tie Modeling of Reinforced Concrete Deep Beams." Journal of Structural Engineering, 144(2), 04017216-1.

Izquierdo Duque, K. (2021). "Statistical Prediction Methods for the In-Plane Shear Strength of Partially Grouted Masonry Walls." M.Sc. Thesis, University of Alberta, Alberta, Canada.

Kassem, W. and Elsheikh, A. (2010). "Estimation of Shear Strength of Structural Shear Walls." Journal of Structural Engineering, 136(10), 1215-1224.

Kent, D. and Park, R. (1971). "Flexural Members with Confined Concrete." Journal of the Structural Division, 97(7), 1969-1990.

Kmiecik, P. and Kaminski, M. (2011). "Modelling of Reinforced Concrete Structures and Composite Structures with Concrete Strength Degradation taken into Consideration." Archives of Civil and Mechanical Engineering, XI (2011) No. 3.

Koutras, A. and Shing, P. (2020), "Seismic Behavior of a Partially Grouted Reinforced Masonry Structure: Shake-Table Testing and Numerical Analysis." Earthquake Engineering and Structural Dynamics, 49(2020), 1115-1136.

Lee, J. and Fenves, G. (1998). "Plastic-Damage Model for Cyclic Loading of Concrete Structures." Journal of Engineering Mechanics, 124(8), 892–900.

Légeron, F., Paultre, P., and Mazars, J. (2005). "Damage Mechanics Modeling of

Nonlinear Seismic Behavior of Concrete Structures." Journal of Structural Engineering, 131(6), 946-955.

Liu, W. (2023). "Concrete Masonry Compressive Strength Prediction using Mechanics-based Modelling and Gaussian Process Regression with Error Evaluation based on Experimental Data" M.Sc. Thesis, University of Alberta, Alberta, Canada.

Liu, L., Tang, D., and Zhai, X. (2006). "Failure Criteria for Grouted Concrete Block Masonry under Biaxial Compression." Advances in Structural Engineering, 9(2), 229–239.

Lourenço, P. and Rots, J. (1997). "Multisurface Interface Model for Analysis of Masonry Structures." Journal of Engineering Mechanics, 123(7), 660–668.

Lourenço, P., Rots, J., and Blaauwendraad, J. (1995). "Two Approaches for the Analysis of Masonry Structures: Micro and Macro-Modeling." HERON, 40(4), 313– 340.

Lopez, J., Oller, S., Onate, E., and Lubliner, J. (1999). "A Homogenous Constitutive Model for Masonry." International Journal for Numerical Methods in Engineering, 46(1999), 1651-1671.

Lubliner, J., Oliver, J., Oller, S., and Onate, E. (1989). "A Plastic-Damage Model for Concrete." International Journal of Solids and Structures, 25(3), 299–326.

Maleki, M., Drysdale, R., Hamid, A., and El-Damatty, E. (2009). "Behaviour of Partially Grouted Reinforced Masonry Shear Walls – Experimental Study." Proc. 11th Canadian Masonry Symposium (CMS). Toronto, Canada.

Masonry Standards Joint Committee (MSJC). (2011). "Building Requirements and Specifications for Masonry Structures." TMS 402/602-11. Longmont, CO: Masonry Society.

Masonry Standards Joint Committee (MSJC). (2016). "Building Requirements and Specifications for Masonry Structures." TMS 402/602-16. Longmont, CO: Masonry Society.

Masonry Standards Joint Committee (MSJC). (2022). "Building Requirements and

Specifications for Masonry Structures." TMS 402/602-22. Longmont, CO: Masonry Society.

MatLab, (2022). MatLab R2022a. MathWorks. Natick, USA.

Matsumura, A. (1987). "Shear Strength of Reinforced Hollow Unit Masonry Walls." Proc. 4th North American Masonry Conference (NAMC).

Matsumura, A. (1988). "Shear Strength of Reinforced Masonry Walls." Proc., 9th World Conf. on Earthquake Engineering, Vol. 7, 121–126. Tokyo, Japan.

Mayes, R. and Clough, R. (1975a). "A Literature Survey – Compressive, Tensile, Bond and Shear Strength of Masonry." Report No. EERC-75-15, Earthquake Engineering Research Center, University of California Berkeley, USA.

Mayes, R. and Clough, R. (1975b). "State-of-the-Art in Seismic Shear Strength of Masonry – An Evaluation and Review." Report No. EERC-75-21, Earthquake Engineering Research Center, University of California Berkeley, USA.

Mayes, R., Omote, Y., and Clough, R. (1976a). "Cyclic Shear Tests of Masonry Piers Volume 1 – Test Results." Report No. EERC-76-8, Earthquake Engineering Research Center, University of California Berkeley, USA.

Mayes, R., Omote, Y., and Clough, R. (1976b). "Cyclic Shear Tests of Masonry Piers Volume 2 – Analysis of Test Results." Report No. EERC-76-16, Earthquake Engineering Research Center, University of California Berkeley, USA.

Mazars, J. (1986). "A Description of Micro and Macroscale Damage of Concrete Structure." Engineering Fracture Mechanics, 25, 729–737.

Meli, R. (1972). "Behaviour of Masonry Walls Under Lateral Loads." Proc. 5th World Conference on Earthquake Engineering (WCEE). Rome, Italy.

Michal, S. and Andrzej, W. (2015). "Calibration of the CDP Model Parameters in Abaqus." Proc. 2015 World Congress on Advances in Structural Engineering and Mechanics. Incheon, Korea.

Minaie, E. (2009). "Behavior and Vulnerability of Reinforced Masonry Shear Walls."

Ph.D. Dissertation, Drexel University, Pennsylvania, USA.

Minaie, E., Mota, M., Moon, F., and Hamid, A. (2010). "In-Plane Behavior of Partially Grouted Reinforced Concrete Masonry Shear Walls." Journal of Structural Engineering, 136(9), 1089–1097.

Mohsenijam, A. (2019). "Advanced Regression Based Analytics for Steel Fabrication Productivity Modeling." Ph.D. Dissertation, University of Alberta, Alberta, Canada.

Mohsin, E. (2005). "Support Stiffness Effect on Tall Load Bearing Masonry Walls." Ph.D. Dissertation, University of Alberta, Alberta, Canada.

Mojsilovic, N. (2011). "Strength of Masonry Subjected to In-Plane Loading: A Contribution." International Journal of Solids and Structures, 48, 865–873.

Muttoni, A., Fernández Ruiz, M., and Niketic, F. (2015). "Design Versus Assessment of Concrete Structures Using Stress Fields and Strut-and-Tie Models." ACI Structural Journal, 112(5), 605-616.

National Earthquake Hazards Reduction Program (NEHRP). (1994a). "NEHRP Recommended Provisions for Seismic Regulations for New Buildings – Part 1: Provisions." Building Seismic Safety Council, Washington, D.C.

National Earthquake Hazards Reduction Program (NEHRP). (1994b). "NEHRP Recommended Provisions for Seismic Regulations for New Buildings – Part 2: Commentary." Building Seismic Safety Council, Washington, D.C.

Nasiri, E. and Liu, Y. (2017). "Development of a Detailed 3D FE Model for Analysis of the In-Plane Behaviour of Masonry Infilled Concrete Frames." Engineering Structures. 143 (2017): 603-616.

National Highway Institute. (2017). "Strut-and-Tie Modeling (STM) for Concrete Structures." Report No. FHWA-NHI-17-071. Arlington, VA.

Nayal, R. and Rasheed, H. (2006). "Tension Stiffening Model for Concrete Beams Reinforced with Steel and FRP Bars." Journal of Materials in Civil Engineering, 18(6), 831-841.

Nolph, S. (2010). “In-Plane Shear Performance of Partially Grouted Masonry Shear Walls.” M.Sc. Thesis, Washington State University, Washington, USA.

Nolph, S. and ElGawady, M. (2012). “Static Cyclic Response of Partially Grouted Masonry Shear Walls.” Journal of Structural Engineering, 138(7), 864-879.

Nunn, R., Miller, M., and Hegemier, G. (1978). “Grout-Block Bond Strength in Concrete Masonry.” Report No. UCSD/AMES/TR-78-001, University of California San Diego, USA.

NZS. (2004). “Design of reinforced concrete masonry structures.” NZS 4230, Standards Association of New Zealand, Wellington, New Zealand.

Oan, A. (2013). “Diagonal Shear of Partially Grouted Concrete Masonry Panels.” M.Sc. Thesis, University of Calgary, Alberta, Canada.

Obaidat, A. M. (2017). “Compressive Behavior of C-Shaped Confined Masonry Boundary Elements.” Ph.D. Dissertation, Concordia University, Québec, Canada.

Okamoto, S., Yamazaki, Y., Kaminosono, T., Teshigawara, M., and Hirashi, H. (1987). “Seismic Capacity of Reinforced Masonry Walls and Beams.” Proc. of the 18th Joint Meeting of the U.S.-Japan Cooperative Program in Natural Resource Panel on Wind and Seismic Effects, NBSIR 87-3540, National Institute of Standards and Technology, Gaithersburg, pp. 307- 319.

Pan, H. (2018). “Modelling In-Plane Shear in Partially Reinforced Concrete Masonry.” M.Sc. Thesis, University of Calgary, Alberta, Canada.

Park, R. and Paulay, T. (1975). “Reinforced Concrete Structures.” John Wiley & Sons, Inc.

Pettit, C. (2020). “Effect of Rotational Base Stiffness on the Behaviour of Loadbearing Masonry Walls.” M.Sc. Thesis, University of Alberta, Alberta, Canada.

Priestley, M. (1977). “Seismic Resistance of Reinforced Concrete-Masonry Shear Walls with High Steel Percentages.” Bulletin of the New Zealand National Society for Earthquake Engineering, 10(1), 1-16.

Priestley, M. and Bridgeman, D. (1974). “Seismic Resistance of Brick Masonry Walls.” Bulletin of the New Zealand National Society for Earthquake Engineering, 7(4), 167-187.

Priestley, M. and Elder, D. (1982). “Cyclic Loading Tests of Slender Concrete Masonry Shear Walls.” Bulletin of the New Zealand National Society for Earthquake Engineering, 15(1), 3-21.

Priestley, M. and Elder, D. (1983). “Stress-Strain Curves for Unconfined and Confined Concrete Masonry.” ACI Structural Journal, May-June 1983, 192-201.

Priestley, M., Verma, R., and Xiao, Y. (1994). “Seismic Shear Strength of Reinforced Concrete Columns.” Journal of Structural Engineering, 120(8), 2310-2329.

Ramírez, P., Sandoval, C., and Almazán, J. (2016). “Experimental Study on In-Plane Cyclic Response of Partially Grouted Reinforced Concrete Masonry Shear Walls.” Engineering Structures, 126, 598–617.

Rizaee, S. (2015). “Assessing Bond Beam Horizontal Reinforcement Efficacy with Different End Anchorage Conditions in Concrete Block Masonry Shear Walls.” M.Sc. Thesis, University of Calgary, Alberta, Canada.

Robazza, B., Brzev, S., Yang, T., Elwood, T., Anderson, D., and McEwen, B. (2018). “Out-of-Plane Behavior of Slender Reinforced Masonry Shear Walls under In-Plane Loading: Experimental Investigation.” Journal of Structural Engineering, 144(3), 04018008.

Ross, M. (2013). “Recalibration of the Unit Strength Method for Determining the Compressive Strength of Grouted Concrete Masonry.” M.Sc. Thesis, University of Alberta, Alberta, Canada.

Salazar Lopez, J. (2019). “Implementation and Verification of Simple Concrete Biaxial Models Under Monotonic, Cyclic, and Dynamic Loading.” M.Sc. Thesis, University of Alberta, Alberta, Canada.

Sandoval, C. and Arnau, O. (2017). “Experimental Characterization and Detailed Micro-

Modeling of Multi-Perforated Clay Brick Masonry Structural Response." Materials and Structures, (2017) 50:34.

Sandoval, C., Calderón, S, and Almazán, J. (2018). "Experimental Cyclic Response Assessment of Partially Grouted Reinforced Clay Brick Masonry Walls." Bulletin of Earthquake Engineering, 15(2018), 3127-3152.

Schlaich, J., Schäfer, K., and Jennewein, M. (1987). "Towards a Consistent Design of Structural Concrete." PCI Journal, 32(3), 74-150.

Schlaich, J. and Schäfer, K. (1991). "Design and Detailing of Structural Concrete using Strut-and-Tie Models." The Structural Engineer, 69(6), 113-125.

Schlaich, M. and Anagnostou, G. (1990). "Stress Fields for Nodes of Strut-and-Tie Models." Journal of Structural Engineering, 116(1), 13-23.

Schneider, R. (1959). "Lateral Load Tests on Reinforced Grouted Masonry Shear Walls." Report No. 70-101, University of Southern California Engineering Center.

Schultz, A. (1994). "NIST Research Program on the Seismic Resistance of Partially-Grouted Masonry Shear Walls." NISTIR Report No. 5481. National Institute of Standards and Technology.

Schultz, A. and Johnson, C. (2019). "Seismic Resistance Mechanisms in Partially Grouted Shear Walls with New Design Details." Proc. 13th North American Masonry Conference, Salt Lake City, UT, USA, 1274–1286.

Scrivener, J. (1966). "Concrete Masonry Wall Panel Tests with Predominant Flexural Effects." New Zealand Concrete Construction, July 1966.

Scrivener, J. (1969). "Static Racking Tests on Concrete Masonry Walls." Designing, Engineering, and Constructing with Masonry Products, May 1969.

Seif ElDin, H. (2016). "In-Plane Shear Behaviour of Fully Grouted Reinforced Masonry Shear Walls." Ph.D. Dissertation, Concordia University, Québec, Canada.

Seif ElDin, H. and Galal, K. (2017). "In-Plane Seismic Performance of Fully Grouted Reinforced Masonry Shear Walls." Journal of Structural Engineering, 143(7),

04017054.

Shedid, M., Drysdale, R., and El-Dakhakhni, W. (2008). “Behavior of Fully Grouted Reinforced Concrete Masonry Shear Walls Failing in Flexure: Experimental Results.” Journal of Structural Engineering, 134(11), 1754-1767.

Shedid, M., El-Dakhakhni, W., and Drysdale, R. (2010). “Characteristics of Rectangular, Flanges, and End-Confined Reinforced Concrete Masonry Shear Walls for Seismic Design.” Journal of Structural Engineering, 136(12), 1471-1482.

Shing, P., Noland, J., Klamerus, E., and Spaeh, H. (1989). “Inelastic Behavior of Concrete Masonry Shear Walls.” Journal of Structural Engineering, 115(9), 2204-2225.

Shing, P. Schuller, M., and Hoskere, V. (1990a). “Flexural and Shear Response of Reinforced Masonry Walls.” ACI Structural Journal, 87(6), 646-656.

Shing, P., Schuller, M., and Hoskere, V. (1990b). “In-Plane Resistance of Reinforced Masonry Shear Walls.” Journal of Structural Engineering, 116(3), 619-640.

Shing, P., Noland, J., Spaech, H., Klamerus, E., and Schuller, M. (1991). “Response of Single-Storey Reinforced Masonry Shear Walls to In-Plane Lateral Loads.” U.S. – Japan Coordinated Program for Masonry Building Research Report No. 3.1(a)-2, University of Colorado at Boulder, USA.

Singhal, V. and Rai, D. (2017). “Strut-and-Tie Model for Predicting the Shear Capacity of Confined Masonry Walls With and Without Openings.” Proc. 16th World Conference on Earthquake Engineering (WCEE). Santiago, Chile.

Siyam, M., El-Dakhakhni, W., Banting, B., and Drysdale, R. (2016). “Seismic Response Evaluation of Ductile Reinforced Concrete Block Structural Walls. II: Displacement and Performance-Based Design Parameters.” Journal of Structural Engineering, 30(4), 04015067.

Stavridis, A., Ahmadi, F., Mavros, M., Shing, P., Klingner, R., and McLean, D. (2016). “Shake-Table Tests of a Full-Scale Three-Story Reinforced Masonry Shear Wall Structure.” Journal of Structural Engineering, 142(10), 04016074.

Sveinsson, B., Mayes, R., and McNiven, H., (1981). “Evaluation of Seismic Design Provisions for Masonry in the United States.” Report No. UCB/EERC-81-10, Earthquake Engineering Research Center, University of California Berkeley, USA.

Sveinsson, B., McNiven, H., and Sucuoglu, H. (1985). “Cyclic Loading Tests of Masonry Piers – Volume 4: Additional Tests with Height to Width ratio of 1.” Report No. UCB/EERC-85-15, Earthquake Engineering Research Center, University of California Berkeley, USA.

Technical Coordinating Committee for Masonry Research. (1986). “Summary report: U.S. Coordinated Program for Masonry Building Research.” Report No. 11.1-1. UNJR Panel on Wind & Seismic Effects.

To, N., Sritharan, S., and Ingham, J. (2009). “Strut-and-Tie Nonlinear Cyclic Analysis of Concrete Frames.” Journal of Structural Engineering, 135(10), 1259-1268.

Tomazevic, M., and Lutman, M. (1988). “Seismic Resistance of Reinforced Masonry Walls.” Proc. 9th World Conference on Earthquake Engineering (WCEE). Tokyo, Japan.

Tomanzevic, M., Lutman, M., and Petkovic, L. (1996). “Seismic Behavior of Masonry Walls: Experimental Simulation.” Journal of Structural Engineering, 122(9), 1040-1047.

Tuchscherer, R. (2016). “Strut-and-Tie Capacity of Partially-Grouted CMU Shear Walls.” Proc. Geotechnical and Structural Engineering Congress 2016, 177-189.

Vargas, L., Sandoval, C., Bertolesi, E., and Calderón, S. (2022). “Seismic Behavior of Partially Grouted Masonry Shear Walls Containing Openings: Experimental Testing.” Engineering Structures, 278(2023), 115549.

Vecchio, F. and Collins, M. (1986). “The Modified Compression-Field Theory for Reinforced Concrete Elements Subjected to Shear.” ACI Structural Journal, 83(2), 219-231.

Voon, K. and Ingham, J. (2006). “Experimental In-Plane Shear Strength Investigation of

Reinforced Concrete Masonry Walls." Journal of Structural Engineering, 132(3), 400-408.

Voon, K. and Ingham, J. (2007). "Design Expression for the In-Plane Shear Strength of Reinforced Concrete Masonry." Journal of Structural Engineering, 133(5), 706-713.

Voon, K. and Ingham, J. (2008). "Experimental In-Plane Investigation of Reinforced Concrete Masonry Walls with Openings." Journal of Structural Engineering, 134(5), 758–768.

Wright, G., Kowalsky, M., and Ingham, J. (2007). "Shake Table Testing of Posttensioned Concrete Masonry Walls with Openings." Journal of Structural Engineering, 133(11), 1551-1559.

Yancey, C., Fattal, S., and Dikkers, R. (1991). "Review of Research Literature on Masonry Shear Walls." NISTIR Report No. 4512. National Institute of Standards and Technology. Gaithersburg, USA.

Yun, Y. (2006). "Strength of Two-Dimensional Nodal Zones in Strut-Tie Models." Journal of Structural Engineering, 132(11), 1764-1783.

Yun, Y. and Ramírez, J. (2016). "Strength of Concrete Struts in Three-Dimensional Strut-Tie Models." Journal of Structural Engineering, 142(11), 04016117-1.

Zeng, B., Li, Y., and Cruz-Noguez, C. (2021). "Modeling and Parameter Importance Investigation for Simulating In-Plane and Out-of-Plane Behaviors of Un-Reinforced Masonry Walls." Engineering Structures, 248(2021), 113233.

APPENDIX A: PARAMETRIC ANALYSIS RESULTS (DATA)

The complete dataset of the conducted parametric analysis is presented in Table A.1.

Table A.1 – Parametric Analysis Data

Wall Height (mm)	Aspect Ratio	Reinforcement Spacing (mm)		Reinforcement Size		Bed-Joint Reinforcement	Reinforcement Ratio		Axial Stress (kPa)	Load Capacity (kN)
		Horizontal	Vertical	Horizontal	Vertical		Horizontal	Vertical		
1600	0.62	800	1200	20M	10M	No	0.00183	0.00066	0	171.3
1600	0.62	800	1200	20M	10M	No	0.00183	0.00066	100	178.5
1600	0.62	800	1200	20M	10M	No	0.00183	0.00066	250	202.7
1600	0.62	800	1200	20M	10M	No	0.00183	0.00066	500	238.9
1600	0.62	800	1200	20M	10M	No	0.00183	0.00066	1000	291.0
1600	0.62	800	1200	20M	10M	No	0.00183	0.00066	1500	333.4
1600	0.62	800	1200	20M	10M	Yes	0.00183	0.00123	0	174.4
1600	0.62	800	1200	20M	10M	Yes	0.00183	0.00123	100	182.9
1600	0.62	800	1200	20M	10M	Yes	0.00183	0.00123	250	204.5
1600	0.62	800	1200	20M	10M	Yes	0.00183	0.00123	500	239.8
1600	0.62	800	1200	20M	10M	Yes	0.00183	0.00123	1000	291.9
1600	0.62	800	1200	20M	10M	Yes	0.00183	0.00123	1500	334.2
1600	0.62	800	1200	20M	15M	No	0.00183	0.00132	0	170.7
1600	0.62	800	1200	20M	15M	No	0.00183	0.00132	100	181.6
1600	0.62	800	1200	20M	15M	No	0.00183	0.00132	250	204.3
1600	0.62	800	1200	20M	15M	No	0.00183	0.00132	500	239.1
1600	0.62	800	1200	20M	15M	No	0.00183	0.00132	1000	292.2
1600	0.62	800	1200	20M	15M	No	0.00183	0.00132	1500	334.5
1600	0.62	800	1200	20M	15M	Yes	0.00183	0.00189	0	175.2
1600	0.62	800	1200	20M	15M	Yes	0.00183	0.00189	100	183.6
1600	0.62	800	1200	20M	15M	Yes	0.00183	0.00189	250	205.6
1600	0.62	800	1200	20M	15M	Yes	0.00183	0.00189	500	242.9
1600	0.62	800	1200	20M	15M	Yes	0.00183	0.00189	1000	293.4
1600	0.62	800	1200	20M	15M	Yes	0.00183	0.00189	1500	333.8
1600	0.62	800	1200	20M	20M	No	0.00183	0.00199	0	170.9
1600	0.62	800	1200	20M	20M	No	0.00183	0.00199	100	181.1
1600	0.62	800	1200	20M	20M	No	0.00183	0.00199	250	205.9
1600	0.62	800	1200	20M	20M	No	0.00183	0.00199	500	242.1

Wall Height (mm)	Aspect Ratio	Reinforcement Spacing (mm)		Reinforcement Size		Bed-Joint Reinforcement	Reinforcement Ratio		Axial Stress (kPa)	Load Capacity (kN)
		Horizontal	Vertical	Horizontal	Vertical		Horizontal	Vertical		
1600	0.62	800	1200	20M	20M	No	0.00183	0.00199	1000	293.3
1600	0.62	800	1200	20M	20M	No	0.00183	0.00199	1500	335.4
1600	0.62	800	1200	20M	20M	Yes	0.00183	0.00256	0	175.8
1600	0.62	800	1200	20M	20M	Yes	0.00183	0.00256	100	184.8
1600	0.62	800	1200	20M	20M	Yes	0.00183	0.00256	250	206.7
1600	0.62	800	1200	20M	20M	Yes	0.00183	0.00256	500	243.8
1600	0.62	800	1200	20M	20M	Yes	0.00183	0.00256	1000	293.8
1600	0.62	800	1200	20M	20M	Yes	0.00183	0.00256	1500	336.4
1600	0.62	800	1200	25M	10M	No	0.00305	0.00066	0	184.9
1600	0.62	800	1200	25M	10M	No	0.00305	0.00066	100	191.0
1600	0.62	800	1200	25M	10M	No	0.00305	0.00066	250	210.9
1600	0.62	800	1200	25M	10M	No	0.00305	0.00066	500	242.3
1600	0.62	800	1200	25M	10M	No	0.00305	0.00066	1000	293.3
1600	0.62	800	1200	25M	10M	No	0.00305	0.00066	1500	334.2
1600	0.62	800	1200	25M	10M	Yes	0.00305	0.00123	0	184.9
1600	0.62	800	1200	25M	10M	Yes	0.00305	0.00123	100	192.4
1600	0.62	800	1200	25M	10M	Yes	0.00305	0.00123	250	212.5
1600	0.62	800	1200	25M	10M	Yes	0.00305	0.00123	500	243.6
1600	0.62	800	1200	25M	10M	Yes	0.00305	0.00123	1000	293.9
1600	0.62	800	1200	25M	10M	Yes	0.00305	0.00123	1500	333.9
1600	0.62	800	1200	25M	15M	No	0.00305	0.00132	0	184.7
1600	0.62	800	1200	25M	15M	No	0.00305	0.00132	100	193.9
1600	0.62	800	1200	25M	15M	No	0.00305	0.00132	250	213.8
1600	0.62	800	1200	25M	15M	No	0.00305	0.00132	500	244.4
1600	0.62	800	1200	25M	15M	No	0.00305	0.00132	1000	294.1
1600	0.62	800	1200	25M	15M	No	0.00305	0.00132	1500	336.1
1600	0.62	800	1200	25M	15M	Yes	0.00305	0.00189	0	187.3
1600	0.62	800	1200	25M	15M	Yes	0.00305	0.00189	100	190.9
1600	0.62	800	1200	25M	15M	Yes	0.00305	0.00189	250	214.0
1600	0.62	800	1200	25M	15M	Yes	0.00305	0.00189	500	246.4

Wall Height (mm)	Aspect Ratio	Reinforcement Spacing (mm)		Reinforcement Size		Bed-Joint Reinforcement	Reinforcement Ratio		Axial Stress (kPa)	Load Capacity (kN)
		Horizontal	Vertical	Horizontal	Vertical		Horizontal	Vertical		
1600	0.62	800	1200	25M	15M	Yes	0.00305	0.00189	1000	294.7
1600	0.62	800	1200	25M	15M	Yes	0.00305	0.00189	1500	335.2
1600	0.62	800	1200	25M	20M	No	0.00305	0.00199	0	187.1
1600	0.62	800	1200	25M	20M	No	0.00305	0.00199	100	192.8
1600	0.62	800	1200	25M	20M	No	0.00305	0.00199	250	213.7
1600	0.62	800	1200	25M	20M	No	0.00305	0.00199	500	245.5
1600	0.62	800	1200	25M	20M	No	0.00305	0.00199	1000	294.9
1600	0.62	800	1200	25M	20M	No	0.00305	0.00199	1500	336.6
1600	0.62	800	1200	25M	20M	Yes	0.00305	0.00256	0	187.0
1600	0.62	800	1200	25M	20M	Yes	0.00305	0.00256	100	193.6
1600	0.62	800	1200	25M	20M	Yes	0.00305	0.00256	250	214.7
1600	0.62	800	1200	25M	20M	Yes	0.00305	0.00256	500	247.4
1600	0.62	800	1200	25M	20M	Yes	0.00305	0.00256	1000	295.7
1600	0.62	800	1200	25M	20M	Yes	0.00305	0.00256	1500	337.3
1600	0.62	800	1200	30M	10M	No	0.00427	0.00066	0	194.5
1600	0.62	800	1200	30M	10M	No	0.00427	0.00066	100	197.2
1600	0.62	800	1200	30M	10M	No	0.00427	0.00066	250	216.5
1600	0.62	800	1200	30M	10M	No	0.00427	0.00066	500	245.0
1600	0.62	800	1200	30M	10M	No	0.00427	0.00066	1000	294.1
1600	0.62	800	1200	30M	10M	No	0.00427	0.00066	1500	333.6
1600	0.62	800	1200	30M	10M	Yes	0.00427	0.00123	0	193.5
1600	0.62	800	1200	30M	10M	Yes	0.00427	0.00123	100	194.9
1600	0.62	800	1200	30M	10M	Yes	0.00427	0.00123	250	181.8
1600	0.62	800	1200	30M	10M	Yes	0.00427	0.00123	500	245.9
1600	0.62	800	1200	30M	10M	Yes	0.00427	0.00123	1000	294.9
1600	0.62	800	1200	30M	10M	Yes	0.00427	0.00123	1500	335.4
1600	0.62	800	1200	30M	15M	No	0.00427	0.00132	0	198.0
1600	0.62	800	1200	30M	15M	No	0.00427	0.00132	100	201.8
1600	0.62	800	1200	30M	15M	No	0.00427	0.00132	250	219.8
1600	0.62	800	1200	30M	15M	No	0.00427	0.00132	500	246.1

Wall Height (mm)	Aspect Ratio	Reinforcement Spacing (mm)		Reinforcement Size		Bed-Joint Reinforcement	Reinforcement Ratio		Axial Stress (kPa)	Load Capacity (kN)
		Horizontal	Vertical	Horizontal	Vertical		Horizontal	Vertical		
1600	0.62	800	1200	30M	15M	No	0.00427	0.00132	1000	295.9
1600	0.62	800	1200	30M	15M	No	0.00427	0.00132	1500	336.0
1600	0.62	800	1200	30M	15M	Yes	0.00427	0.00189	0	202.2
1600	0.62	800	1200	30M	15M	Yes	0.00427	0.00189	100	199.7
1600	0.62	800	1200	30M	15M	Yes	0.00427	0.00189	250	219.9
1600	0.62	800	1200	30M	15M	Yes	0.00427	0.00189	500	248.1
1600	0.62	800	1200	30M	15M	Yes	0.00427	0.00189	1000	297.3
1600	0.62	800	1200	30M	15M	Yes	0.00427	0.00189	1500	336.1
1600	0.62	800	1200	30M	20M	No	0.00427	0.00199	0	199.7
1600	0.62	800	1200	30M	20M	No	0.00427	0.00199	100	200.3
1600	0.62	800	1200	30M	20M	No	0.00427	0.00199	250	220.8
1600	0.62	800	1200	30M	20M	No	0.00427	0.00199	500	249.2
1600	0.62	800	1200	30M	20M	No	0.00427	0.00199	1000	297.0
1600	0.62	800	1200	30M	20M	No	0.00427	0.00199	1500	337.8
1600	0.62	800	1200	30M	20M	Yes	0.00427	0.00256	0	200.6
1600	0.62	800	1200	30M	20M	Yes	0.00427	0.00256	100	197.0
1600	0.62	800	1200	30M	20M	Yes	0.00427	0.00256	250	217.3
1600	0.62	800	1200	30M	20M	Yes	0.00427	0.00256	500	249.9
1600	0.62	800	1200	30M	20M	Yes	0.00427	0.00256	1000	296.6
1600	0.62	800	1200	30M	20M	Yes	0.00427	0.00256	1500	338.4
1600	0.62	800	800	20M	10M	No	0.00244	0.00066	0	217.7
1600	0.62	800	800	20M	10M	No	0.00244	0.00066	250	246.9
1600	0.62	800	800	20M	10M	No	0.00244	0.00066	500	274.4
1600	0.62	800	800	20M	10M	No	0.00244	0.00066	1000	316.6
1600	0.62	800	800	20M	10M	No	0.00244	0.00066	1500	346.3
1600	0.62	800	800	20M	10M	Yes	0.00244	0.00123	0	221.4
1600	0.62	800	800	20M	10M	Yes	0.00244	0.00123	100	228.9
1600	0.62	800	800	20M	10M	Yes	0.00244	0.00123	250	248.1
1600	0.62	800	800	20M	10M	Yes	0.00244	0.00123	500	276.9
1600	0.62	800	800	20M	10M	Yes	0.00244	0.00123	1000	317.1

Wall Height (mm)	Aspect Ratio	Reinforcement Spacing (mm)		Reinforcement Size		Bed-Joint Reinforcement	Reinforcement Ratio		Axial Stress (kPa)	Load Capacity (kN)
		Horizontal	Vertical	Horizontal	Vertical		Horizontal	Vertical		
1600	0.62	800	800	20M	10M	Yes	0.00244	0.00123	1500	346.4
1600	0.62	800	800	20M	15M	No	0.00244	0.00132	0	221.2
1600	0.62	800	800	20M	15M	No	0.00244	0.00132	100	231.4
1600	0.62	800	800	20M	15M	No	0.00244	0.00132	250	249.5
1600	0.62	800	800	20M	15M	No	0.00244	0.00132	500	277.8
1600	0.62	800	800	20M	15M	No	0.00244	0.00132	1000	319.2
1600	0.62	800	800	20M	15M	No	0.00244	0.00132	1500	348.8
1600	0.62	800	800	20M	15M	Yes	0.00244	0.00189	0	224.7
1600	0.62	800	800	20M	15M	Yes	0.00244	0.00189	100	235.1
1600	0.62	800	800	20M	15M	Yes	0.00244	0.00189	250	251.9
1600	0.62	800	800	20M	15M	Yes	0.00244	0.00189	500	280.9
1600	0.62	800	800	20M	15M	Yes	0.00244	0.00189	1000	320.3
1600	0.62	800	800	20M	15M	Yes	0.00244	0.00189	1500	350.0
1600	0.62	800	800	20M	20M	No	0.00244	0.00199	0	223.6
1600	0.62	800	800	20M	20M	No	0.00244	0.00199	100	232.1
1600	0.62	800	800	20M	20M	No	0.00244	0.00199	250	248.3
1600	0.62	800	800	20M	20M	No	0.00244	0.00199	500	280.5
1600	0.62	800	800	20M	20M	No	0.00244	0.00199	1000	321.1
1600	0.62	800	800	20M	20M	No	0.00244	0.00199	1500	351.0
1600	0.62	800	800	20M	20M	Yes	0.00244	0.00256	0	226.4
1600	0.62	800	800	20M	20M	Yes	0.00244	0.00256	100	236.6
1600	0.62	800	800	20M	20M	Yes	0.00244	0.00256	250	252.4
1600	0.62	800	800	20M	20M	Yes	0.00244	0.00256	500	283.4
1600	0.62	800	800	20M	20M	Yes	0.00244	0.00256	1000	321.9
1600	0.62	800	800	20M	20M	Yes	0.00244	0.00256	1500	352.2
1600	0.62	800	800	25M	10M	No	0.00406	0.00066	0	228.2
1600	0.62	800	800	25M	10M	No	0.00406	0.00066	100	237.7
1600	0.62	800	800	25M	10M	No	0.00406	0.00066	250	250.7
1600	0.62	800	800	25M	10M	No	0.00406	0.00066	500	278.1
1600	0.62	800	800	25M	10M	No	0.00406	0.00066	1000	318.5

Wall Height (mm)	Aspect Ratio	Reinforcement Spacing (mm)		Reinforcement Size		Bed-Joint Reinforcement	Reinforcement Ratio		Axial Stress (kPa)	Load Capacity (kN)
		Horizontal	Vertical	Horizontal	Vertical		Horizontal	Vertical		
1600	0.62	800	800	25M	10M	No	0.00406	0.00066	1500	345.2
1600	0.62	800	800	25M	10M	Yes	0.00406	0.00123	0	232.6
1600	0.62	800	800	25M	10M	Yes	0.00406	0.00123	100	240.8
1600	0.62	800	800	25M	10M	Yes	0.00406	0.00123	250	236.7
1600	0.62	800	800	25M	10M	Yes	0.00406	0.00123	500	281.3
1600	0.62	800	800	25M	10M	Yes	0.00406	0.00123	1000	318.9
1600	0.62	800	800	25M	10M	Yes	0.00406	0.00123	1500	346.7
1600	0.62	800	800	25M	15M	No	0.00406	0.00132	0	232.7
1600	0.62	800	800	25M	15M	No	0.00406	0.00132	100	240.6
1600	0.62	800	800	25M	15M	No	0.00406	0.00132	250	255.6
1600	0.62	800	800	25M	15M	No	0.00406	0.00132	500	283.2
1600	0.62	800	800	25M	15M	No	0.00406	0.00132	1000	321.4
1600	0.62	800	800	25M	15M	No	0.00406	0.00132	1500	349.7
1600	0.62	800	800	25M	15M	Yes	0.00406	0.00189	0	236.5
1600	0.62	800	800	25M	15M	Yes	0.00406	0.00189	100	242.1
1600	0.62	800	800	25M	15M	Yes	0.00406	0.00189	250	241.3
1600	0.62	800	800	25M	15M	Yes	0.00406	0.00189	500	286.8
1600	0.62	800	800	25M	15M	Yes	0.00406	0.00189	1000	321.2
1600	0.62	800	800	25M	15M	Yes	0.00406	0.00189	1500	350.4
1600	0.62	800	800	25M	20M	No	0.00406	0.00199	0	234.7
1600	0.62	800	800	25M	20M	No	0.00406	0.00199	100	244.8
1600	0.62	800	800	25M	20M	No	0.00406	0.00199	250	256.8
1600	0.62	800	800	25M	20M	No	0.00406	0.00199	500	286.3
1600	0.62	800	800	25M	20M	No	0.00406	0.00199	1000	322.5
1600	0.62	800	800	25M	20M	No	0.00406	0.00199	1500	352.4
1600	0.62	800	800	25M	20M	Yes	0.00406	0.00256	0	238.6
1600	0.62	800	800	25M	20M	Yes	0.00406	0.00256	100	247.3
1600	0.62	800	800	25M	20M	Yes	0.00406	0.00256	250	260.1
1600	0.62	800	800	25M	20M	Yes	0.00406	0.00256	500	288.9
1600	0.62	800	800	25M	20M	Yes	0.00406	0.00256	1000	322.7

Wall Height (mm)	Aspect Ratio	Reinforcement Spacing (mm)		Reinforcement Size		Bed-Joint Reinforcement	Reinforcement Ratio		Axial Stress (kPa)	Load Capacity (kN)
		Horizontal	Vertical	Horizontal	Vertical		Horizontal	Vertical		
1600	0.62	800	800	25M	20M	Yes	0.00406	0.00256	1500	352.5
1600	0.62	800	800	30M	10M	No	0.00569	0.00066	0	235.2
1600	0.62	800	800	30M	10M	No	0.00569	0.00066	100	243.2
1600	0.62	800	800	30M	10M	No	0.00569	0.00066	250	256.8
1600	0.62	800	800	30M	10M	No	0.00569	0.00066	500	281.2
1600	0.62	800	800	30M	10M	No	0.00569	0.00066	1000	318.4
1600	0.62	800	800	30M	10M	No	0.00569	0.00066	1500	345.7
1600	0.62	800	800	30M	10M	Yes	0.00569	0.00123	0	238.7
1600	0.62	800	800	30M	10M	Yes	0.00569	0.00123	100	248.3
1600	0.62	800	800	30M	10M	Yes	0.00569	0.00123	250	238.7
1600	0.62	800	800	30M	10M	Yes	0.00569	0.00123	500	284.3
1600	0.62	800	800	30M	10M	Yes	0.00569	0.00123	1000	319.6
1600	0.62	800	800	30M	10M	Yes	0.00569	0.00123	1500	346.0
1600	0.62	800	800	30M	15M	No	0.00569	0.00132	0	240.4
1600	0.62	800	800	30M	15M	No	0.00569	0.00132	100	248.7
1600	0.62	800	800	30M	15M	No	0.00569	0.00132	250	261.1
1600	0.62	800	800	30M	15M	No	0.00569	0.00132	500	286.2
1600	0.62	800	800	30M	15M	No	0.00569	0.00132	1000	322.4
1600	0.62	800	800	30M	15M	No	0.00569	0.00132	1500	348.7
1600	0.62	800	800	30M	15M	Yes	0.00569	0.00189	0	245.1
1600	0.62	800	800	30M	15M	Yes	0.00569	0.00189	100	253.1
1600	0.62	800	800	30M	15M	Yes	0.00569	0.00189	250	254.1
1600	0.62	800	800	30M	15M	Yes	0.00569	0.00189	500	289.9
1600	0.62	800	800	30M	15M	Yes	0.00569	0.00189	1000	322.4
1600	0.62	800	800	30M	15M	Yes	0.00569	0.00189	1500	351.2
1600	0.62	800	800	30M	20M	No	0.00569	0.00199	0	243.8
1600	0.62	800	800	30M	20M	No	0.00569	0.00199	100	252.6
1600	0.62	800	800	30M	20M	No	0.00569	0.00199	250	263.9
1600	0.62	800	800	30M	20M	No	0.00569	0.00199	500	289.0
1600	0.62	800	800	30M	20M	No	0.00569	0.00199	1000	324.4

Wall Height (mm)	Aspect Ratio	Reinforcement Spacing (mm)		Reinforcement Size		Bed-Joint Reinforcement	Reinforcement Ratio		Axial Stress (kPa)	Load Capacity (kN)
		Horizontal	Vertical	Horizontal	Vertical		Horizontal	Vertical		
1600	0.62	800	800	30M	20M	No	0.00569	0.00199	1500	352.8
1600	0.62	800	800	30M	20M	Yes	0.00569	0.00256	0	246.6
1600	0.62	800	800	30M	20M	Yes	0.00569	0.00256	100	256.0
1600	0.62	800	800	30M	20M	Yes	0.00569	0.00256	250	263.7
1600	0.62	800	800	30M	20M	Yes	0.00569	0.00256	500	292.3
1600	0.62	800	800	30M	20M	Yes	0.00569	0.00256	1000	324.9
1600	0.62	800	800	30M	20M	Yes	0.00569	0.00256	1500	353.3
1600	0.62	800	600	20M	10M	No	0.00305	0.00066	0	273.0
1600	0.62	800	600	20M	10M	No	0.00305	0.00066	100	282.0
1600	0.62	800	600	20M	10M	No	0.00305	0.00066	250	294.6
1600	0.62	800	600	20M	10M	No	0.00305	0.00066	500	310.6
1600	0.62	800	600	20M	10M	No	0.00305	0.00066	1000	339.5
1600	0.62	800	600	20M	10M	No	0.00305	0.00066	1500	368.0
1600	0.62	800	600	20M	10M	Yes	0.00305	0.00123	0	277.9
1600	0.62	800	600	20M	10M	Yes	0.00305	0.00123	100	280.0
1600	0.62	800	600	20M	10M	Yes	0.00305	0.00123	250	297.9
1600	0.62	800	600	20M	10M	Yes	0.00305	0.00123	500	314.6
1600	0.62	800	600	20M	10M	Yes	0.00305	0.00123	1000	343.7
1600	0.62	800	600	20M	10M	Yes	0.00305	0.00123	1500	371.3
1600	0.62	800	600	20M	15M	No	0.00305	0.00132	0	277.2
1600	0.62	800	600	20M	15M	No	0.00305	0.00132	100	284.6
1600	0.62	800	600	20M	15M	No	0.00305	0.00132	250	298.6
1600	0.62	800	600	20M	15M	No	0.00305	0.00132	500	315.0
1600	0.62	800	600	20M	15M	No	0.00305	0.00132	1000	344.3
1600	0.62	800	600	20M	15M	No	0.00305	0.00132	1500	372.4
1600	0.62	800	600	20M	15M	Yes	0.00305	0.00189	0	281.1
1600	0.62	800	600	20M	15M	Yes	0.00305	0.00189	100	288.9
1600	0.62	800	600	20M	15M	Yes	0.00305	0.00189	250	291.2
1600	0.62	800	600	20M	15M	Yes	0.00305	0.00189	500	318.9
1600	0.62	800	600	20M	15M	Yes	0.00305	0.00189	1000	349.4

Wall Height (mm)	Aspect Ratio	Reinforcement Spacing (mm)		Reinforcement Size		Bed-Joint Reinforcement	Reinforcement Ratio		Axial Stress (kPa)	Load Capacity (kN)
		Horizontal	Vertical	Horizontal	Vertical		Horizontal	Vertical		
1600	0.62	800	600	20M	15M	Yes	0.00305	0.00189	1500	375.5
1600	0.62	800	600	20M	20M	No	0.00305	0.00199	0	279.3
1600	0.62	800	600	20M	20M	No	0.00305	0.00199	100	288.0
1600	0.62	800	600	20M	20M	No	0.00305	0.00199	250	300.3
1600	0.62	800	600	20M	20M	No	0.00305	0.00199	500	318.2
1600	0.62	800	600	20M	20M	No	0.00305	0.00199	1000	348.8
1600	0.62	800	600	20M	20M	No	0.00305	0.00199	1500	375.8
1600	0.62	800	600	20M	20M	Yes	0.00305	0.00256	0	283.4
1600	0.62	800	600	20M	20M	Yes	0.00305	0.00256	100	282.2
1600	0.62	800	600	20M	20M	Yes	0.00305	0.00256	250	304.7
1600	0.62	800	600	20M	20M	Yes	0.00305	0.00256	500	322.2
1600	0.62	800	600	20M	20M	Yes	0.00305	0.00256	1000	352.3
1600	0.62	800	600	20M	20M	Yes	0.00305	0.00256	1500	379.3
1600	0.62	800	600	25M	10M	No	0.00508	0.00066	0	291.2
1600	0.62	800	600	25M	10M	No	0.00508	0.00066	100	286.5
1600	0.62	800	600	25M	10M	No	0.00508	0.00066	250	301.4
1600	0.62	800	600	25M	10M	No	0.00508	0.00066	500	316.5
1600	0.62	800	600	25M	10M	No	0.00508	0.00066	1000	344.0
1600	0.62	800	600	25M	10M	No	0.00508	0.00066	1500	368.5
1600	0.62	800	600	25M	10M	Yes	0.00508	0.00123	0	294.8
1600	0.62	800	600	25M	10M	Yes	0.00508	0.00123	100	298.0
1600	0.62	800	600	25M	10M	Yes	0.00508	0.00123	250	305.3
1600	0.62	800	600	25M	10M	Yes	0.00508	0.00123	500	320.7
1600	0.62	800	600	25M	10M	Yes	0.00508	0.00123	1000	348.2
1600	0.62	800	600	25M	10M	Yes	0.00508	0.00123	1500	372.1
1600	0.62	800	600	25M	15M	No	0.00508	0.00132	0	294.9
1600	0.62	800	600	25M	15M	No	0.00508	0.00132	100	299.1
1600	0.62	800	600	25M	15M	No	0.00508	0.00132	250	305.2
1600	0.62	800	600	25M	15M	No	0.00508	0.00132	500	321.6
1600	0.62	800	600	25M	15M	No	0.00508	0.00132	1000	349.1

Wall Height (mm)	Aspect Ratio	Reinforcement Spacing (mm)		Reinforcement Size		Bed-Joint Reinforcement	Reinforcement Ratio		Axial Stress (kPa)	Load Capacity (kN)
		Horizontal	Vertical	Horizontal	Vertical		Horizontal	Vertical		
1600	0.62	800	600	25M	15M	No	0.00508	0.00132	1500	373.7
1600	0.62	800	600	25M	15M	Yes	0.00508	0.00189	0	299.7
1600	0.62	800	600	25M	15M	Yes	0.00508	0.00189	100	304.8
1600	0.62	800	600	25M	15M	Yes	0.00508	0.00189	250	298.6
1600	0.62	800	600	25M	15M	Yes	0.00508	0.00189	500	325.3
1600	0.62	800	600	25M	15M	Yes	0.00508	0.00189	1000	353.0
1600	0.62	800	600	25M	15M	Yes	0.00508	0.00189	1500	377.0
1600	0.62	800	600	25M	20M	No	0.00508	0.00199	0	297.1
1600	0.62	800	600	25M	20M	No	0.00508	0.00199	100	302.6
1600	0.62	800	600	25M	20M	No	0.00508	0.00199	250	308.4
1600	0.62	800	600	25M	20M	No	0.00508	0.00199	500	325.3
1600	0.62	800	600	25M	20M	No	0.00508	0.00199	1000	352.4
1600	0.62	800	600	25M	20M	No	0.00508	0.00199	1500	377.0
1600	0.62	800	600	25M	20M	Yes	0.00508	0.00256	0	302.0
1600	0.62	800	600	25M	20M	Yes	0.00508	0.00256	100	307.8
1600	0.62	800	600	25M	20M	Yes	0.00508	0.00256	250	313.6
1600	0.62	800	600	25M	20M	Yes	0.00508	0.00256	500	328.1
1600	0.62	800	600	25M	20M	Yes	0.00508	0.00256	1000	355.5
1600	0.62	800	600	25M	20M	Yes	0.00508	0.00256	1500	380.4
1600	0.62	800	600	30M	10M	No	0.00711	0.00066	0	297.6
1600	0.62	800	600	30M	10M	No	0.00711	0.00066	100	303.3
1600	0.62	800	600	30M	10M	No	0.00711	0.00066	250	307.5
1600	0.62	800	600	30M	10M	No	0.00711	0.00066	500	321.2
1600	0.62	800	600	30M	10M	No	0.00711	0.00066	1000	345.9
1600	0.62	800	600	30M	10M	No	0.00711	0.00066	1500	369.4
1600	0.62	800	600	30M	10M	Yes	0.00711	0.00123	0	303.7
1600	0.62	800	600	30M	10M	Yes	0.00711	0.00123	100	306.9
1600	0.62	800	600	30M	10M	Yes	0.00711	0.00123	250	312.5
1600	0.62	800	600	30M	10M	Yes	0.00711	0.00123	500	326.1
1600	0.62	800	600	30M	10M	Yes	0.00711	0.00123	1000	349.6

Wall Height (mm)	Aspect Ratio	Reinforcement Spacing (mm)		Reinforcement Size		Bed-Joint Reinforcement	Reinforcement Ratio		Axial Stress (kPa)	Load Capacity (kN)
		Horizontal	Vertical	Horizontal	Vertical		Horizontal	Vertical		
1600	0.62	800	600	30M	10M	Yes	0.00711	0.00123	1500	373.6
1600	0.62	800	600	30M	15M	No	0.00711	0.00132	0	303.7
1600	0.62	800	600	30M	15M	No	0.00711	0.00132	100	306.8
1600	0.62	800	600	30M	15M	No	0.00711	0.00132	250	312.2
1600	0.62	800	600	30M	15M	No	0.00711	0.00132	500	327.1
1600	0.62	800	600	30M	15M	No	0.00711	0.00132	1000	351.1
1600	0.62	800	600	30M	15M	No	0.00711	0.00132	1500	374.8
1600	0.62	800	600	30M	15M	Yes	0.00711	0.00189	0	308.6
1600	0.62	800	600	30M	15M	Yes	0.00711	0.00189	100	310.4
1600	0.62	800	600	30M	15M	Yes	0.00711	0.00189	250	310.7
1600	0.62	800	600	30M	15M	Yes	0.00711	0.00189	500	331.6
1600	0.62	800	600	30M	15M	Yes	0.00711	0.00189	1000	355.4
1600	0.62	800	600	30M	15M	Yes	0.00711	0.00189	1500	378.7
1600	0.62	800	600	30M	20M	No	0.00711	0.00199	0	307.3
1600	0.62	800	600	30M	20M	No	0.00711	0.00199	100	305.7
1600	0.62	800	600	30M	20M	No	0.00711	0.00199	250	316.1
1600	0.62	800	600	30M	20M	No	0.00711	0.00199	500	331.6
1600	0.62	800	600	30M	20M	No	0.00711	0.00199	1000	356.6
1600	0.62	800	600	30M	20M	No	0.00711	0.00199	1500	378.7
1600	0.62	800	600	30M	20M	Yes	0.00711	0.00256	0	311.8
1600	0.62	800	600	30M	20M	Yes	0.00711	0.00256	100	316.3
1600	0.62	800	600	30M	20M	Yes	0.00711	0.00256	250	306.2
1600	0.62	800	600	30M	20M	Yes	0.00711	0.00256	500	334.8
1600	0.62	800	600	30M	20M	Yes	0.00711	0.00256	1000	358.7
1600	0.62	800	600	30M	20M	Yes	0.00711	0.00256	1500	382.7
2400	0.93	1200	1200	20M	10M	No	0.00183	0.00044	0	143.9
2400	0.93	1200	1200	20M	10M	No	0.00183	0.00044	100	151.7
2400	0.93	1200	1200	20M	10M	No	0.00183	0.00044	250	168.4
2400	0.93	1200	1200	20M	10M	No	0.00183	0.00044	500	201.6
2400	0.93	1200	1200	20M	10M	No	0.00183	0.00044	1000	242.6

Wall Height (mm)	Aspect Ratio	Reinforcement Spacing (mm)		Reinforcement Size		Bed-Joint Reinforcement	Reinforcement Ratio		Axial Stress (kPa)	Load Capacity (kN)
		Horizontal	Vertical	Horizontal	Vertical		Horizontal	Vertical		
2400	0.93	1200	1200	20M	10M	No	0.00183	0.00044	1500	275.3
2400	0.93	1200	1200	20M	10M	Yes	0.00183	0.00101	0	147.5
2400	0.93	1200	1200	20M	10M	Yes	0.00183	0.00101	100	155.4
2400	0.93	1200	1200	20M	10M	Yes	0.00183	0.00101	250	173.2
2400	0.93	1200	1200	20M	10M	Yes	0.00183	0.00101	500	204.9
2400	0.93	1200	1200	20M	10M	Yes	0.00183	0.00101	1000	244.4
2400	0.93	1200	1200	20M	10M	Yes	0.00183	0.00101	1500	277.5
2400	0.93	1200	1200	20M	15M	No	0.00183	0.00088	0	144.2
2400	0.93	1200	1200	20M	15M	No	0.00183	0.00088	100	151.8
2400	0.93	1200	1200	20M	15M	No	0.00183	0.00088	250	167.8
2400	0.93	1200	1200	20M	15M	No	0.00183	0.00088	500	201.5
2400	0.93	1200	1200	20M	15M	No	0.00183	0.00088	1000	244.4
2400	0.93	1200	1200	20M	15M	No	0.00183	0.00088	1500	276.6
2400	0.93	1200	1200	20M	15M	Yes	0.00183	0.00145	0	147.1
2400	0.93	1200	1200	20M	15M	Yes	0.00183	0.00145	100	118.8
2400	0.93	1200	1200	20M	15M	Yes	0.00183	0.00145	250	172.8
2400	0.93	1200	1200	20M	15M	Yes	0.00183	0.00145	500	206.7
2400	0.93	1200	1200	20M	15M	Yes	0.00183	0.00145	1000	244.7
2400	0.93	1200	1200	20M	15M	Yes	0.00183	0.00145	1500	277.9
2400	0.93	1200	1200	20M	20M	No	0.00183	0.00132	0	144.2
2400	0.93	1200	1200	20M	20M	No	0.00183	0.00132	100	152.0
2400	0.93	1200	1200	20M	20M	No	0.00183	0.00132	250	169.7
2400	0.93	1200	1200	20M	20M	No	0.00183	0.00132	500	201.7
2400	0.93	1200	1200	20M	20M	No	0.00183	0.00132	1000	243.5
2400	0.93	1200	1200	20M	20M	No	0.00183	0.00132	1500	277.2
2400	0.93	1200	1200	20M	20M	Yes	0.00183	0.00189	0	148.0
2400	0.93	1200	1200	20M	20M	Yes	0.00183	0.00189	100	151.9
2400	0.93	1200	1200	20M	20M	Yes	0.00183	0.00189	250	173.4
2400	0.93	1200	1200	20M	20M	Yes	0.00183	0.00189	500	206.5
2400	0.93	1200	1200	20M	20M	Yes	0.00183	0.00189	1000	244.9

Wall Height (mm)	Aspect Ratio	Reinforcement Spacing (mm)		Reinforcement Size		Bed-Joint Reinforcement	Reinforcement Ratio		Axial Stress (kPa)	Load Capacity (kN)
		Horizontal	Vertical	Horizontal	Vertical		Horizontal	Vertical		
2400	0.93	1200	1200	20M	20M	Yes	0.00183	0.00189	1500	278.2
2400	0.93	1200	1200	25M	10M	No	0.00305	0.00044	0	155.3
2400	0.93	1200	1200	25M	10M	No	0.00305	0.00044	100	161.2
2400	0.93	1200	1200	25M	10M	No	0.00305	0.00044	250	176.9
2400	0.93	1200	1200	25M	10M	No	0.00305	0.00044	500	205.7
2400	0.93	1200	1200	25M	10M	No	0.00305	0.00044	1000	246.7
2400	0.93	1200	1200	25M	10M	No	0.00305	0.00044	1500	279.8
2400	0.93	1200	1200	25M	10M	Yes	0.00305	0.00101	0	165.0
2400	0.93	1200	1200	25M	10M	Yes	0.00305	0.00101	100	134.5
2400	0.93	1200	1200	25M	10M	Yes	0.00305	0.00101	250	179.7
2400	0.93	1200	1200	25M	10M	Yes	0.00305	0.00101	500	209.1
2400	0.93	1200	1200	25M	10M	Yes	0.00305	0.00101	1000	247.3
2400	0.93	1200	1200	25M	10M	Yes	0.00305	0.00101	1500	280.7
2400	0.93	1200	1200	25M	15M	No	0.00305	0.00088	0	153.0
2400	0.93	1200	1200	25M	15M	No	0.00305	0.00088	100	161.5
2400	0.93	1200	1200	25M	15M	No	0.00305	0.00088	250	177.6
2400	0.93	1200	1200	25M	15M	No	0.00305	0.00088	500	206.9
2400	0.93	1200	1200	25M	15M	No	0.00305	0.00088	1000	245.8
2400	0.93	1200	1200	25M	15M	No	0.00305	0.00088	1500	279.3
2400	0.93	1200	1200	25M	15M	Yes	0.00305	0.00145	0	157.5
2400	0.93	1200	1200	25M	15M	Yes	0.00305	0.00145	100	165.6
2400	0.93	1200	1200	25M	15M	Yes	0.00305	0.00145	250	181.9
2400	0.93	1200	1200	25M	15M	Yes	0.00305	0.00145	500	210.1
2400	0.93	1200	1200	25M	15M	Yes	0.00305	0.00145	1000	246.7
2400	0.93	1200	1200	25M	15M	Yes	0.00305	0.00145	1500	280.1
2400	0.93	1200	1200	25M	20M	No	0.00305	0.00132	0	154.7
2400	0.93	1200	1200	25M	20M	No	0.00305	0.00132	100	161.7
2400	0.93	1200	1200	25M	20M	No	0.00305	0.00132	250	177.7
2400	0.93	1200	1200	25M	20M	No	0.00305	0.00132	500	207.9
2400	0.93	1200	1200	25M	20M	No	0.00305	0.00132	1000	245.5

Wall Height (mm)	Aspect Ratio	Reinforcement Spacing (mm)		Reinforcement Size		Bed-Joint Reinforcement	Reinforcement Ratio		Axial Stress (kPa)	Load Capacity (kN)
		Horizontal	Vertical	Horizontal	Vertical		Horizontal	Vertical		
2400	0.93	1200	1200	25M	20M	No	0.00305	0.00132	1500	281.0
2400	0.93	1200	1200	25M	20M	Yes	0.00305	0.00189	0	160.2
2400	0.93	1200	1200	25M	20M	Yes	0.00305	0.00189	100	165.0
2400	0.93	1200	1200	25M	20M	Yes	0.00305	0.00189	250	182.3
2400	0.93	1200	1200	25M	20M	Yes	0.00305	0.00189	500	209.4
2400	0.93	1200	1200	25M	20M	Yes	0.00305	0.00189	1000	246.9
2400	0.93	1200	1200	25M	20M	Yes	0.00305	0.00189	1500	280.0
2400	0.93	1200	1200	30M	10M	No	0.00427	0.00044	0	163.4
2400	0.93	1200	1200	30M	10M	No	0.00427	0.00044	100	169.9
2400	0.93	1200	1200	30M	10M	No	0.00427	0.00044	250	182.8
2400	0.93	1200	1200	30M	10M	No	0.00427	0.00044	500	210.0
2400	0.93	1200	1200	30M	10M	No	0.00427	0.00044	1000	248.4
2400	0.93	1200	1200	30M	10M	No	0.00427	0.00044	1500	279.9
2400	0.93	1200	1200	30M	10M	Yes	0.00427	0.00101	0	164.2
2400	0.93	1200	1200	30M	10M	Yes	0.00427	0.00101	100	177.4
2400	0.93	1200	1200	30M	10M	Yes	0.00427	0.00101	250	186.2
2400	0.93	1200	1200	30M	10M	Yes	0.00427	0.00101	500	212.8
2400	0.93	1200	1200	30M	10M	Yes	0.00427	0.00101	1000	248.9
2400	0.93	1200	1200	30M	10M	Yes	0.00427	0.00101	1500	280.0
2400	0.93	1200	1200	30M	15M	No	0.00427	0.00088	0	164.4
2400	0.93	1200	1200	30M	15M	No	0.00427	0.00088	100	169.5
2400	0.93	1200	1200	30M	15M	No	0.00427	0.00088	250	183.6
2400	0.93	1200	1200	30M	15M	No	0.00427	0.00088	500	212.1
2400	0.93	1200	1200	30M	15M	No	0.00427	0.00088	1000	247.4
2400	0.93	1200	1200	30M	15M	No	0.00427	0.00088	1500	280.2
2400	0.93	1200	1200	30M	15M	Yes	0.00427	0.00145	0	173.7
2400	0.93	1200	1200	30M	15M	Yes	0.00427	0.00145	100	183.2
2400	0.93	1200	1200	30M	15M	Yes	0.00427	0.00145	250	191.0
2400	0.93	1200	1200	30M	15M	Yes	0.00427	0.00145	500	213.2
2400	0.93	1200	1200	30M	15M	Yes	0.00427	0.00145	1000	249.6

Wall Height (mm)	Aspect Ratio	Reinforcement Spacing (mm)		Reinforcement Size		Bed-Joint Reinforcement	Reinforcement Ratio		Axial Stress (kPa)	Load Capacity (kN)
		Horizontal	Vertical	Horizontal	Vertical		Horizontal	Vertical		
2400	0.93	1200	1200	30M	15M	Yes	0.00427	0.00145	1500	280.8
2400	0.93	1200	1200	30M	20M	No	0.00427	0.00132	0	165.0
2400	0.93	1200	1200	30M	20M	No	0.00427	0.00132	100	169.8
2400	0.93	1200	1200	30M	20M	No	0.00427	0.00132	250	183.7
2400	0.93	1200	1200	30M	20M	No	0.00427	0.00132	500	211.4
2400	0.93	1200	1200	30M	20M	No	0.00427	0.00132	1000	201.2
2400	0.93	1200	1200	30M	20M	No	0.00427	0.00132	1500	280.0
2400	0.93	1200	1200	30M	20M	Yes	0.00427	0.00189	0	192.1
2400	0.93	1200	1200	30M	20M	Yes	0.00427	0.00189	100	172.6
2400	0.93	1200	1200	30M	20M	Yes	0.00427	0.00189	250	193.9
2400	0.93	1200	1200	30M	20M	Yes	0.00427	0.00189	500	212.4
2400	0.93	1200	1200	30M	20M	Yes	0.00427	0.00189	1000	251.1
2400	0.93	1200	1200	30M	20M	Yes	0.00427	0.00189	1500	282.4
2400	0.93	1200	800	20M	10M	No	0.00244	0.00044	0	185.1
2400	0.93	1200	800	20M	10M	No	0.00244	0.00044	100	195.9
2400	0.93	1200	800	20M	10M	No	0.00244	0.00044	250	210.8
2400	0.93	1200	800	20M	10M	No	0.00244	0.00044	500	228.6
2400	0.93	1200	800	20M	10M	No	0.00244	0.00044	1000	256.8
2400	0.93	1200	800	20M	10M	No	0.00244	0.00044	1500	287.3
2400	0.93	1200	800	20M	10M	Yes	0.00244	0.00101	0	187.6
2400	0.93	1200	800	20M	10M	Yes	0.00244	0.00101	100	198.7
2400	0.93	1200	800	20M	10M	Yes	0.00244	0.00101	250	214.8
2400	0.93	1200	800	20M	10M	Yes	0.00244	0.00101	500	233.3
2400	0.93	1200	800	20M	10M	Yes	0.00244	0.00101	1000	258.8
2400	0.93	1200	800	20M	10M	Yes	0.00244	0.00101	1500	288.9
2400	0.93	1200	800	20M	15M	No	0.00244	0.00088	0	186.2
2400	0.93	1200	800	20M	15M	No	0.00244	0.00088	100	196.7
2400	0.93	1200	800	20M	15M	No	0.00244	0.00088	250	212.2
2400	0.93	1200	800	20M	15M	No	0.00244	0.00088	500	231.5
2400	0.93	1200	800	20M	15M	No	0.00244	0.00088	1000	257.8

Wall Height (mm)	Aspect Ratio	Reinforcement Spacing (mm)		Reinforcement Size		Bed-Joint Reinforcement	Reinforcement Ratio		Axial Stress (kPa)	Load Capacity (kN)
		Horizontal	Vertical	Horizontal	Vertical		Horizontal	Vertical		
2400	0.93	1200	800	20M	15M	No	0.00244	0.00088	1500	287.9
2400	0.93	1200	800	20M	15M	Yes	0.00244	0.00145	0	188.1
2400	0.93	1200	800	20M	15M	Yes	0.00244	0.00145	100	199.4
2400	0.93	1200	800	20M	15M	Yes	0.00244	0.00145	250	215.9
2400	0.93	1200	800	20M	15M	Yes	0.00244	0.00145	500	234.7
2400	0.93	1200	800	20M	15M	Yes	0.00244	0.00145	1000	259.9
2400	0.93	1200	800	20M	15M	Yes	0.00244	0.00145	1500	288.1
2400	0.93	1200	800	20M	20M	No	0.00244	0.00132	0	186.2
2400	0.93	1200	800	20M	20M	No	0.00244	0.00132	100	197.3
2400	0.93	1200	800	20M	20M	No	0.00244	0.00132	250	213.5
2400	0.93	1200	800	20M	20M	No	0.00244	0.00132	500	232.7
2400	0.93	1200	800	20M	20M	No	0.00244	0.00132	1000	258.7
2400	0.93	1200	800	20M	20M	No	0.00244	0.00132	1500	286.4
2400	0.93	1200	800	20M	20M	Yes	0.00244	0.00189	0	188.5
2400	0.93	1200	800	20M	20M	Yes	0.00244	0.00189	100	200.2
2400	0.93	1200	800	20M	20M	Yes	0.00244	0.00189	250	216.3
2400	0.93	1200	800	20M	20M	Yes	0.00244	0.00189	500	235.5
2400	0.93	1200	800	20M	20M	Yes	0.00244	0.00189	1000	260.6
2400	0.93	1200	800	20M	20M	Yes	0.00244	0.00189	1500	288.4
2400	0.93	1200	800	25M	10M	No	0.00406	0.00044	0	199.0
2400	0.93	1200	800	25M	10M	No	0.00406	0.00044	100	207.9
2400	0.93	1200	800	25M	10M	No	0.00406	0.00044	250	220.0
2400	0.93	1200	800	25M	10M	No	0.00406	0.00044	500	234.1
2400	0.93	1200	800	25M	10M	No	0.00406	0.00044	1000	261.5
2400	0.93	1200	800	25M	10M	No	0.00406	0.00044	1500	287.3
2400	0.93	1200	800	25M	10M	Yes	0.00406	0.00101	0	202.5
2400	0.93	1200	800	25M	10M	Yes	0.00406	0.00101	100	211.2
2400	0.93	1200	800	25M	10M	Yes	0.00406	0.00101	250	223.1
2400	0.93	1200	800	25M	10M	Yes	0.00406	0.00101	500	237.3
2400	0.93	1200	800	25M	10M	Yes	0.00406	0.00101	1000	265.4

Wall Height (mm)	Aspect Ratio	Reinforcement Spacing (mm)		Reinforcement Size		Bed-Joint Reinforcement	Reinforcement Ratio		Axial Stress (kPa)	Load Capacity (kN)
		Horizontal	Vertical	Horizontal	Vertical		Horizontal	Vertical		
2400	0.93	1200	800	25M	10M	Yes	0.00406	0.00101	1500	289.5
2400	0.93	1200	800	25M	15M	No	0.00406	0.00088	0	200.1
2400	0.93	1200	800	25M	15M	No	0.00406	0.00088	100	209.5
2400	0.93	1200	800	25M	15M	No	0.00406	0.00088	250	219.9
2400	0.93	1200	800	25M	15M	No	0.00406	0.00088	500	236.6
2400	0.93	1200	800	25M	15M	No	0.00406	0.00088	1000	264.9
2400	0.93	1200	800	25M	15M	No	0.00406	0.00088	1500	289.3
2400	0.93	1200	800	25M	15M	Yes	0.00406	0.00145	0	203.1
2400	0.93	1200	800	25M	15M	Yes	0.00406	0.00145	100	212.4
2400	0.93	1200	800	25M	15M	Yes	0.00406	0.00145	250	224.9
2400	0.93	1200	800	25M	15M	Yes	0.00406	0.00145	500	239.1
2400	0.93	1200	800	25M	15M	Yes	0.00406	0.00145	1000	266.4
2400	0.93	1200	800	25M	15M	Yes	0.00406	0.00145	1500	291.9
2400	0.93	1200	800	25M	20M	No	0.00406	0.00132	0	200.5
2400	0.93	1200	800	25M	20M	No	0.00406	0.00132	100	209.7
2400	0.93	1200	800	25M	20M	No	0.00406	0.00132	250	222.6
2400	0.93	1200	800	25M	20M	No	0.00406	0.00132	500	237.4
2400	0.93	1200	800	25M	20M	No	0.00406	0.00132	1000	265.9
2400	0.93	1200	800	25M	20M	No	0.00406	0.00132	1500	290.7
2400	0.93	1200	800	25M	20M	Yes	0.00406	0.00189	0	204.1
2400	0.93	1200	800	25M	20M	Yes	0.00406	0.00189	100	213.0
2400	0.93	1200	800	25M	20M	Yes	0.00406	0.00189	250	224.5
2400	0.93	1200	800	25M	20M	Yes	0.00406	0.00189	500	240.1
2400	0.93	1200	800	25M	20M	Yes	0.00406	0.00189	1000	267.4
2400	0.93	1200	800	25M	20M	Yes	0.00406	0.00189	1500	292.4
2400	0.93	1200	800	30M	10M	No	0.00569	0.00044	0	205.2
2400	0.93	1200	800	30M	10M	No	0.00569	0.00044	100	214.1
2400	0.93	1200	800	30M	10M	No	0.00569	0.00044	250	223.5
2400	0.93	1200	800	30M	10M	No	0.00569	0.00044	500	237.6
2400	0.93	1200	800	30M	10M	No	0.00569	0.00044	1000	267.1

Wall Height (mm)	Aspect Ratio	Reinforcement Spacing (mm)		Reinforcement Size		Bed-Joint Reinforcement	Reinforcement Ratio		Axial Stress (kPa)	Load Capacity (kN)
		Horizontal	Vertical	Horizontal	Vertical		Horizontal	Vertical		
2400	0.93	1200	800	30M	10M	No	0.00569	0.00044	1500	290.2
2400	0.93	1200	800	30M	10M	Yes	0.00569	0.00101	0	0.0
2400	0.93	1200	800	30M	10M	Yes	0.00569	0.00101	100	216.7
2400	0.93	1200	800	30M	10M	Yes	0.00569	0.00101	250	227.1
2400	0.93	1200	800	30M	10M	Yes	0.00569	0.00101	500	242.6
2400	0.93	1200	800	30M	10M	Yes	0.00569	0.00101	1000	268.4
2400	0.93	1200	800	30M	10M	Yes	0.00569	0.00101	1500	292.4
2400	0.93	1200	800	30M	15M	No	0.00569	0.00088	0	206.6
2400	0.93	1200	800	30M	15M	No	0.00569	0.00088	100	216.0
2400	0.93	1200	800	30M	15M	No	0.00569	0.00088	250	226.3
2400	0.93	1200	800	30M	15M	No	0.00569	0.00088	500	239.4
2400	0.93	1200	800	30M	15M	No	0.00569	0.00088	1000	268.5
2400	0.93	1200	800	30M	15M	No	0.00569	0.00088	1500	291.2
2400	0.93	1200	800	30M	15M	Yes	0.00569	0.00145	0	209.7
2400	0.93	1200	800	30M	15M	Yes	0.00569	0.00145	100	218.0
2400	0.93	1200	800	30M	15M	Yes	0.00569	0.00145	250	229.2
2400	0.93	1200	800	30M	15M	Yes	0.00569	0.00145	500	243.7
2400	0.93	1200	800	30M	15M	Yes	0.00569	0.00145	1000	270.3
2400	0.93	1200	800	30M	15M	Yes	0.00569	0.00145	1500	293.5
2400	0.93	1200	800	30M	20M	No	0.00569	0.00132	100	216.2
2400	0.93	1200	800	30M	20M	No	0.00569	0.00132	250	227.6
2400	0.93	1200	800	30M	20M	No	0.00569	0.00132	500	241.0
2400	0.93	1200	800	30M	20M	No	0.00569	0.00132	1000	269.5
2400	0.93	1200	800	30M	20M	No	0.00569	0.00132	1500	292.5
2400	0.93	1200	800	30M	20M	Yes	0.00569	0.00189	0	210.0
2400	0.93	1200	800	30M	20M	Yes	0.00569	0.00189	100	218.0
2400	0.93	1200	800	30M	20M	Yes	0.00569	0.00189	250	230.7
2400	0.93	1200	800	30M	20M	Yes	0.00569	0.00189	500	244.6
2400	0.93	1200	800	30M	20M	Yes	0.00569	0.00189	1000	271.4
2400	0.93	1200	800	30M	20M	Yes	0.00569	0.00189	1500	295.2

Wall Height (mm)	Aspect Ratio	Reinforcement Spacing (mm)		Reinforcement Size		Bed-Joint Reinforcement	Reinforcement Ratio		Axial Stress (kPa)	Load Capacity (kN)
		Horizontal	Vertical	Horizontal	Vertical		Horizontal	Vertical		
2400	0.93	1200	600	20M	10M	No	0.00305	0.00044	0	234.9
2400	0.93	1200	600	20M	10M	No	0.00305	0.00044	100	244.1
2400	0.93	1200	600	20M	10M	No	0.00305	0.00044	250	247.6
2400	0.93	1200	600	20M	10M	No	0.00305	0.00044	500	274.2
2400	0.93	1200	600	20M	10M	No	0.00305	0.00044	1000	304.1
2400	0.93	1200	600	20M	10M	No	0.00305	0.00044	1500	322.5
2400	0.93	1200	600	20M	10M	Yes	0.00305	0.00101	0	237.0
2400	0.93	1200	600	20M	10M	Yes	0.00305	0.00101	100	243.7
2400	0.93	1200	600	20M	10M	Yes	0.00305	0.00101	250	258.5
2400	0.93	1200	600	20M	10M	Yes	0.00305	0.00101	500	275.9
2400	0.93	1200	600	20M	10M	Yes	0.00305	0.00101	1000	308.0
2400	0.93	1200	600	20M	10M	Yes	0.00305	0.00101	1500	324.4
2400	0.93	1200	600	20M	15M	No	0.00305	0.00088	0	236.8
2400	0.93	1200	600	20M	15M	No	0.00305	0.00088	100	246.1
2400	0.93	1200	600	20M	15M	No	0.00305	0.00088	250	258.7
2400	0.93	1200	600	20M	15M	No	0.00305	0.00088	500	276.1
2400	0.93	1200	600	20M	15M	No	0.00305	0.00088	1000	308.0
2400	0.93	1200	600	20M	15M	No	0.00305	0.00088	1500	326.1
2400	0.93	1200	600	20M	15M	Yes	0.00305	0.00145	0	238.4
2400	0.93	1200	600	20M	15M	Yes	0.00305	0.00145	100	255.9
2400	0.93	1200	600	20M	15M	Yes	0.00305	0.00145	250	262.3
2400	0.93	1200	600	20M	15M	Yes	0.00305	0.00145	500	278.9
2400	0.93	1200	600	20M	15M	Yes	0.00305	0.00145	1000	311.7
2400	0.93	1200	600	20M	15M	Yes	0.00305	0.00145	1500	329.5
2400	0.93	1200	600	20M	20M	No	0.00305	0.00132	0	237.7
2400	0.93	1200	600	20M	20M	No	0.00305	0.00132	100	247.5
2400	0.93	1200	600	20M	20M	No	0.00305	0.00132	250	261.7
2400	0.93	1200	600	20M	20M	No	0.00305	0.00132	500	277.3
2400	0.93	1200	600	20M	20M	No	0.00305	0.00132	1000	312.8
2400	0.93	1200	600	20M	20M	No	0.00305	0.00132	1500	327.0

Wall Height (mm)	Aspect Ratio	Reinforcement Spacing (mm)		Reinforcement Size		Bed-Joint Reinforcement	Reinforcement Ratio		Axial Stress (kPa)	Load Capacity (kN)
		Horizontal	Vertical	Horizontal	Vertical		Horizontal	Vertical		
2400	0.93	1200	600	20M	20M	Yes	0.00305	0.00189	0	239.5
2400	0.93	1200	600	20M	20M	Yes	0.00305	0.00189	100	249.7
2400	0.93	1200	600	20M	20M	Yes	0.00305	0.00189	250	264.0
2400	0.93	1200	600	20M	20M	Yes	0.00305	0.00189	500	283.0
2400	0.93	1200	600	20M	20M	Yes	0.00305	0.00189	1000	314.9
2400	0.93	1200	600	20M	20M	Yes	0.00305	0.00189	1500	331.2
2400	0.93	1200	600	25M	10M	No	0.00508	0.00044	0	269.5
2400	0.93	1200	600	25M	10M	No	0.00508	0.00044	100	273.5
2400	0.93	1200	600	25M	10M	No	0.00508	0.00044	250	280.1
2400	0.93	1200	600	25M	10M	No	0.00508	0.00044	500	289.0
2400	0.93	1200	600	25M	10M	No	0.00508	0.00044	1000	308.9
2400	0.93	1200	600	25M	10M	No	0.00508	0.00044	1500	327.7
2400	0.93	1200	600	25M	10M	Yes	0.00508	0.00101	0	274.6
2400	0.93	1200	600	25M	10M	Yes	0.00508	0.00101	100	277.9
2400	0.93	1200	600	25M	10M	Yes	0.00508	0.00101	250	285.0
2400	0.93	1200	600	25M	10M	Yes	0.00508	0.00101	500	294.4
2400	0.93	1200	600	25M	10M	Yes	0.00508	0.00101	1000	314.3
2400	0.93	1200	600	25M	10M	Yes	0.00508	0.00101	1500	330.8
2400	0.93	1200	600	25M	15M	No	0.00508	0.00088	0	275.5
2400	0.93	1200	600	25M	15M	No	0.00508	0.00088	100	279.2
2400	0.93	1200	600	25M	15M	No	0.00508	0.00088	250	285.8
2400	0.93	1200	600	25M	15M	No	0.00508	0.00088	500	295.1
2400	0.93	1200	600	25M	15M	No	0.00508	0.00088	1000	314.5
2400	0.93	1200	600	25M	15M	No	0.00508	0.00088	1500	332.0
2400	0.93	1200	600	25M	15M	Yes	0.00508	0.00145	0	279.2
2400	0.93	1200	600	25M	15M	Yes	0.00508	0.00145	100	284.3
2400	0.93	1200	600	25M	15M	Yes	0.00508	0.00145	250	290.3
2400	0.93	1200	600	25M	15M	Yes	0.00508	0.00145	500	299.4
2400	0.93	1200	600	25M	15M	Yes	0.00508	0.00145	1000	320.7
2400	0.93	1200	600	25M	15M	Yes	0.00508	0.00145	1500	336.1

Wall Height (mm)	Aspect Ratio	Reinforcement Spacing (mm)		Reinforcement Size		Bed-Joint Reinforcement	Reinforcement Ratio		Axial Stress (kPa)	Load Capacity (kN)
		Horizontal	Vertical	Horizontal	Vertical		Horizontal	Vertical		
2400	0.93	1200	600	25M	20M	No	0.00508	0.00132	0	279.4
2400	0.93	1200	600	25M	20M	No	0.00508	0.00132	100	283.6
2400	0.93	1200	600	25M	20M	No	0.00508	0.00132	250	289.7
2400	0.93	1200	600	25M	20M	No	0.00508	0.00132	500	299.2
2400	0.93	1200	600	25M	20M	No	0.00508	0.00132	1000	319.8
2400	0.93	1200	600	25M	20M	No	0.00508	0.00132	1500	335.9
2400	0.93	1200	600	25M	20M	Yes	0.00508	0.00189	0	282.7
2400	0.93	1200	600	25M	20M	Yes	0.00508	0.00189	100	288.0
2400	0.93	1200	600	25M	20M	Yes	0.00508	0.00189	250	292.5
2400	0.93	1200	600	25M	20M	Yes	0.00508	0.00189	500	303.2
2400	0.93	1200	600	25M	20M	Yes	0.00508	0.00189	1000	323.6
2400	0.93	1200	600	25M	20M	Yes	0.00508	0.00189	1500	338.8
2400	0.93	1200	600	30M	10M	No	0.00711	0.00044	0	277.5
2400	0.93	1200	600	30M	10M	No	0.00711	0.00044	100	278.9
2400	0.93	1200	600	30M	10M	No	0.00711	0.00044	250	286.3
2400	0.93	1200	600	30M	10M	No	0.00711	0.00044	500	294.4
2400	0.93	1200	600	30M	10M	No	0.00711	0.00044	1000	312.2
2400	0.93	1200	600	30M	10M	No	0.00711	0.00044	1500	330.8
2400	0.93	1200	600	30M	10M	Yes	0.00711	0.00101	0	283.6
2400	0.93	1200	600	30M	10M	Yes	0.00711	0.00101	100	285.8
2400	0.93	1200	600	30M	10M	Yes	0.00711	0.00101	250	291.0
2400	0.93	1200	600	30M	10M	Yes	0.00711	0.00101	500	299.8
2400	0.93	1200	600	30M	10M	Yes	0.00711	0.00101	1000	317.8
2400	0.93	1200	600	30M	10M	Yes	0.00711	0.00101	1500	335.1
2400	0.93	1200	600	30M	15M	No	0.00711	0.00088	0	284.4
2400	0.93	1200	600	30M	15M	No	0.00711	0.00088	100	287.6
2400	0.93	1200	600	30M	15M	No	0.00711	0.00088	250	292.4
2400	0.93	1200	600	30M	15M	No	0.00711	0.00088	500	300.5
2400	0.93	1200	600	30M	15M	No	0.00711	0.00088	1000	319.7
2400	0.93	1200	600	30M	15M	No	0.00711	0.00088	1500	336.5

Wall Height (mm)	Aspect Ratio	Reinforcement Spacing (mm)		Reinforcement Size		Bed-Joint Reinforcement	Reinforcement Ratio		Axial Stress (kPa)	Load Capacity (kN)
		Horizontal	Vertical	Horizontal	Vertical		Horizontal	Vertical		
2400	0.93	1200	600	30M	15M	Yes	0.00711	0.00145	0	289.3
2400	0.93	1200	600	30M	15M	Yes	0.00711	0.00145	100	292.8
2400	0.93	1200	600	30M	15M	Yes	0.00711	0.00145	250	297.0
2400	0.93	1200	600	30M	15M	Yes	0.00711	0.00145	500	305.3
2400	0.93	1200	600	30M	15M	Yes	0.00711	0.00145	1000	324.9
2400	0.93	1200	600	30M	15M	Yes	0.00711	0.00145	1500	340.0
2400	0.93	1200	600	30M	20M	No	0.00711	0.00132	0	288.9
2400	0.93	1200	600	30M	20M	No	0.00711	0.00132	100	292.0
2400	0.93	1200	600	30M	20M	No	0.00711	0.00132	250	296.7
2400	0.93	1200	600	30M	20M	No	0.00711	0.00132	500	305.0
2400	0.93	1200	600	30M	20M	No	0.00711	0.00132	1000	324.4
2400	0.93	1200	600	30M	20M	No	0.00711	0.00132	1500	340.2
2400	0.93	1200	600	30M	20M	Yes	0.00711	0.00189	0	293.2
2400	0.93	1200	600	30M	20M	Yes	0.00711	0.00189	100	296.9
2400	0.93	1200	600	30M	20M	Yes	0.00711	0.00189	250	301.1
2400	0.93	1200	600	30M	20M	Yes	0.00711	0.00189	500	309.4
2400	0.93	1200	600	30M	20M	Yes	0.00711	0.00189	1000	329.0
2400	0.93	1200	600	30M	20M	Yes	0.00711	0.00189	1500	343.5
2400	0.93	800	1200	20M	10M	No	0.00183	0.00066	0	155.1
2400	0.93	800	1200	20M	10M	No	0.00183	0.00066	250	181.0
2400	0.93	800	1200	20M	10M	No	0.00183	0.00066	500	217.0
2400	0.93	800	1200	20M	10M	No	0.00183	0.00066	1000	260.3
2400	0.93	800	1200	20M	10M	No	0.00183	0.00066	1500	290.1
2400	0.93	800	1200	20M	10M	Yes	0.00183	0.00123	0	157.3
2400	0.93	800	1200	20M	10M	Yes	0.00183	0.00123	100	96.0
2400	0.93	800	1200	20M	10M	Yes	0.00183	0.00123	250	183.5
2400	0.93	800	1200	20M	10M	Yes	0.00183	0.00123	500	217.4
2400	0.93	800	1200	20M	10M	Yes	0.00183	0.00123	1000	263.3
2400	0.93	800	1200	20M	10M	Yes	0.00183	0.00123	1500	293.5
2400	0.93	800	1200	20M	15M	No	0.00183	0.00132	0	155.6

Wall Height (mm)	Aspect Ratio	Reinforcement Spacing (mm)		Reinforcement Size		Bed-Joint Reinforcement	Reinforcement Ratio		Axial Stress (kPa)	Load Capacity (kN)
		Horizontal	Vertical	Horizontal	Vertical		Horizontal	Vertical		
2400	0.93	800	1200	20M	15M	No	0.00183	0.00132	250	180.9
2400	0.93	800	1200	20M	15M	No	0.00183	0.00132	500	217.7
2400	0.93	800	1200	20M	15M	No	0.00183	0.00132	1000	263.5
2400	0.93	800	1200	20M	15M	No	0.00183	0.00132	1500	293.7
2400	0.93	800	1200	20M	15M	Yes	0.00183	0.00189	0	157.8
2400	0.93	800	1200	20M	15M	Yes	0.00183	0.00189	100	117.9
2400	0.93	800	1200	20M	15M	Yes	0.00183	0.00189	250	184.8
2400	0.93	800	1200	20M	15M	Yes	0.00183	0.00189	500	218.8
2400	0.93	800	1200	20M	15M	Yes	0.00183	0.00189	1000	262.2
2400	0.93	800	1200	20M	15M	Yes	0.00183	0.00189	1500	295.2
2400	0.93	800	1200	20M	20M	No	0.00183	0.00198	0	156.2
2400	0.93	800	1200	20M	20M	No	0.00183	0.00198	100	166.3
2400	0.93	800	1200	20M	20M	No	0.00183	0.00198	250	183.2
2400	0.93	800	1200	20M	20M	No	0.00183	0.00198	500	216.3
2400	0.93	800	1200	20M	20M	No	0.00183	0.00198	1000	264.7
2400	0.93	800	1200	20M	20M	No	0.00183	0.00198	1500	294.5
2400	0.93	800	1200	20M	20M	Yes	0.00183	0.00255	0	158.6
2400	0.93	800	1200	20M	20M	Yes	0.00183	0.00255	100	106.6
2400	0.93	800	1200	20M	20M	Yes	0.00183	0.00255	250	183.9
2400	0.93	800	1200	20M	20M	Yes	0.00183	0.00255	500	218.7
2400	0.93	800	1200	20M	20M	Yes	0.00183	0.00255	1000	263.3
2400	0.93	800	1200	20M	20M	Yes	0.00183	0.00255	1500	296.4
2400	0.93	800	1200	25M	10M	No	0.00305	0.00066	0	171.8
2400	0.93	800	1200	25M	10M	No	0.00305	0.00066	100	176.2
2400	0.93	800	1200	25M	10M	No	0.00305	0.00066	250	191.8
2400	0.93	800	1200	25M	10M	No	0.00305	0.00066	500	221.7
2400	0.93	800	1200	25M	10M	No	0.00305	0.00066	1000	260.0
2400	0.93	800	1200	25M	10M	No	0.00305	0.00066	1500	294.3
2400	0.93	800	1200	25M	10M	Yes	0.00305	0.00123	0	169.6
2400	0.93	800	1200	25M	10M	Yes	0.00305	0.00123	100	177.5

Wall Height (mm)	Aspect Ratio	Reinforcement Spacing (mm)		Reinforcement Size		Bed-Joint Reinforcement	Reinforcement Ratio		Axial Stress (kPa)	Load Capacity (kN)
		Horizontal	Vertical	Horizontal	Vertical		Horizontal	Vertical		
2400	0.93	800	1200	25M	10M	Yes	0.00305	0.00123	250	194.6
2400	0.93	800	1200	25M	10M	Yes	0.00305	0.00123	500	225.7
2400	0.93	800	1200	25M	10M	Yes	0.00305	0.00123	1000	264.2
2400	0.93	800	1200	25M	10M	Yes	0.00305	0.00123	1500	294.7
2400	0.93	800	1200	25M	15M	No	0.00305	0.00132	0	168.8
2400	0.93	800	1200	25M	15M	No	0.00305	0.00132	100	177.0
2400	0.93	800	1200	25M	15M	No	0.00305	0.00132	250	194.3
2400	0.93	800	1200	25M	15M	No	0.00305	0.00132	500	224.1
2400	0.93	800	1200	25M	15M	No	0.00305	0.00132	1000	264.0
2400	0.93	800	1200	25M	15M	No	0.00305	0.00132	1500	295.5
2400	0.93	800	1200	25M	15M	Yes	0.00305	0.00189	0	170.7
2400	0.93	800	1200	25M	15M	Yes	0.00305	0.00189	100	185.1
2400	0.93	800	1200	25M	15M	Yes	0.00305	0.00189	250	196.3
2400	0.93	800	1200	25M	15M	Yes	0.00305	0.00189	500	226.9
2400	0.93	800	1200	25M	15M	Yes	0.00305	0.00189	1000	266.0
2400	0.93	800	1200	25M	15M	Yes	0.00305	0.00189	1500	294.7
2400	0.93	800	1200	25M	20M	No	0.00305	0.00198	0	177.6
2400	0.93	800	1200	25M	20M	No	0.00305	0.00198	250	195.5
2400	0.93	800	1200	25M	20M	No	0.00305	0.00198	500	225.5
2400	0.93	800	1200	25M	20M	No	0.00305	0.00198	1000	265.0
2400	0.93	800	1200	25M	20M	No	0.00305	0.00198	1500	295.7
2400	0.93	800	1200	25M	20M	Yes	0.00305	0.00255	0	172.1
2400	0.93	800	1200	25M	20M	Yes	0.00305	0.00255	100	185.5
2400	0.93	800	1200	25M	20M	Yes	0.00305	0.00255	250	197.4
2400	0.93	800	1200	25M	20M	Yes	0.00305	0.00255	500	227.8
2400	0.93	800	1200	25M	20M	Yes	0.00305	0.00255	1000	266.5
2400	0.93	800	1200	25M	20M	Yes	0.00305	0.00255	1500	296.5
2400	0.93	800	1200	30M	10M	No	0.00427	0.00066	0	179.2
2400	0.93	800	1200	30M	10M	No	0.00427	0.00066	100	184.0
2400	0.93	800	1200	30M	10M	No	0.00427	0.00066	250	198.6

Wall Height (mm)	Aspect Ratio	Reinforcement Spacing (mm)		Reinforcement Size		Bed-Joint Reinforcement	Reinforcement Ratio		Axial Stress (kPa)	Load Capacity (kN)
		Horizontal	Vertical	Horizontal	Vertical		Horizontal	Vertical		
2400	0.93	800	1200	30M	10M	No	0.00427	0.00066	500	225.7
2400	0.93	800	1200	30M	10M	No	0.00427	0.00066	1000	265.3
2400	0.93	800	1200	30M	10M	No	0.00427	0.00066	1500	293.9
2400	0.93	800	1200	30M	10M	Yes	0.00427	0.00123	0	180.3
2400	0.93	800	1200	30M	10M	Yes	0.00427	0.00123	100	194.1
2400	0.93	800	1200	30M	10M	Yes	0.00427	0.00123	250	201.9
2400	0.93	800	1200	30M	10M	Yes	0.00427	0.00123	500	229.1
2400	0.93	800	1200	30M	10M	Yes	0.00427	0.00123	1000	266.7
2400	0.93	800	1200	30M	10M	Yes	0.00427	0.00123	1500	295.1
2400	0.93	800	1200	30M	15M	No	0.00427	0.00132	0	181.7
2400	0.93	800	1200	30M	15M	No	0.00427	0.00132	100	191.9
2400	0.93	800	1200	30M	15M	No	0.00427	0.00132	250	202.0
2400	0.93	800	1200	30M	15M	No	0.00427	0.00132	500	228.2
2400	0.93	800	1200	30M	15M	No	0.00427	0.00132	1000	268.7
2400	0.93	800	1200	30M	15M	No	0.00427	0.00132	1500	296.1
2400	0.93	800	1200	30M	15M	Yes	0.00427	0.00189	0	183.9
2400	0.93	800	1200	30M	15M	Yes	0.00427	0.00189	100	196.0
2400	0.93	800	1200	30M	15M	Yes	0.00427	0.00189	250	205.4
2400	0.93	800	1200	30M	15M	Yes	0.00427	0.00189	500	231.7
2400	0.93	800	1200	30M	15M	Yes	0.00427	0.00189	1000	270.1
2400	0.93	800	1200	30M	15M	Yes	0.00427	0.00189	1500	296.7
2400	0.93	800	1200	30M	20M	No	0.00427	0.00198	0	191.2
2400	0.93	800	1200	30M	20M	No	0.00427	0.00198	100	187.8
2400	0.93	800	1200	30M	20M	No	0.00427	0.00198	250	203.5
2400	0.93	800	1200	30M	20M	No	0.00427	0.00198	500	231.3
2400	0.93	800	1200	30M	20M	No	0.00427	0.00198	1000	269.8
2400	0.93	800	1200	30M	20M	No	0.00427	0.00198	1500	297.0
2400	0.93	800	1200	30M	20M	Yes	0.00427	0.00255	0	184.5
2400	0.93	800	1200	30M	20M	Yes	0.00427	0.00255	100	193.5
2400	0.93	800	1200	30M	20M	Yes	0.00427	0.00255	250	204.0

Wall Height (mm)	Aspect Ratio	Reinforcement Spacing (mm)		Reinforcement Size		Bed-Joint Reinforcement	Reinforcement Ratio		Axial Stress (kPa)	Load Capacity (kN)
		Horizontal	Vertical	Horizontal	Vertical		Horizontal	Vertical		
2400	0.93	800	1200	30M	20M	Yes	0.00427	0.00255	500	233.2
2400	0.93	800	1200	30M	20M	Yes	0.00427	0.00255	1000	271.4
2400	0.93	800	1200	30M	20M	Yes	0.00427	0.00255	1500	298.1
2400	0.93	800	800	20M	10M	No	0.00244	0.00066	0	196.8
2400	0.93	800	800	20M	10M	No	0.00244	0.00066	100	206.2
2400	0.93	800	800	20M	10M	No	0.00244	0.00066	250	225.2
2400	0.93	800	800	20M	10M	No	0.00244	0.00066	500	248.3
2400	0.93	800	800	20M	10M	No	0.00244	0.00066	1000	277.9
2400	0.93	800	800	20M	10M	No	0.00244	0.00066	1500	307.6
2400	0.93	800	800	20M	10M	Yes	0.00244	0.00123	0	198.1
2400	0.93	800	800	20M	10M	Yes	0.00244	0.00123	100	209.2
2400	0.93	800	800	20M	10M	Yes	0.00244	0.00123	250	226.1
2400	0.93	800	800	20M	10M	Yes	0.00244	0.00123	500	252.4
2400	0.93	800	800	20M	10M	Yes	0.00244	0.00123	1000	278.5
2400	0.93	800	800	20M	10M	Yes	0.00244	0.00123	1500	309.4
2400	0.93	800	800	20M	15M	No	0.00244	0.00132	0	198.3
2400	0.93	800	800	20M	15M	No	0.00244	0.00132	100	210.7
2400	0.93	800	800	20M	15M	No	0.00244	0.00132	250	227.5
2400	0.93	800	800	20M	15M	No	0.00244	0.00132	500	252.5
2400	0.93	800	800	20M	15M	No	0.00244	0.00132	1000	280.7
2400	0.93	800	800	20M	15M	No	0.00244	0.00132	1500	310.7
2400	0.93	800	800	20M	15M	Yes	0.00244	0.00189	0	200.3
2400	0.93	800	800	20M	15M	Yes	0.00244	0.00189	100	211.8
2400	0.93	800	800	20M	15M	Yes	0.00244	0.00189	250	229.2
2400	0.93	800	800	20M	15M	Yes	0.00244	0.00189	500	253.5
2400	0.93	800	800	20M	15M	Yes	0.00244	0.00189	1000	281.4
2400	0.93	800	800	20M	15M	Yes	0.00244	0.00189	1500	311.3
2400	0.93	800	800	20M	20M	No	0.00244	0.00198	0	200.0
2400	0.93	800	800	20M	20M	No	0.00244	0.00198	100	211.9
2400	0.93	800	800	20M	20M	No	0.00244	0.00198	250	229.9

Wall Height (mm)	Aspect Ratio	Reinforcement Spacing (mm)		Reinforcement Size		Bed-Joint Reinforcement	Reinforcement Ratio		Axial Stress (kPa)	Load Capacity (kN)
		Horizontal	Vertical	Horizontal	Vertical		Horizontal	Vertical		
2400	0.93	800	800	20M	20M	No	0.00244	0.00198	500	255.5
2400	0.93	800	800	20M	20M	No	0.00244	0.00198	1000	282.1
2400	0.93	800	800	20M	20M	No	0.00244	0.00198	1500	311.1
2400	0.93	800	800	20M	20M	Yes	0.00244	0.00255	0	201.5
2400	0.93	800	800	20M	20M	Yes	0.00244	0.00255	100	213.2
2400	0.93	800	800	20M	20M	Yes	0.00244	0.00255	250	230.4
2400	0.93	800	800	20M	20M	Yes	0.00244	0.00255	500	255.6
2400	0.93	800	800	20M	20M	Yes	0.00244	0.00255	1000	284.3
2400	0.93	800	800	20M	20M	Yes	0.00244	0.00255	1500	313.1
2400	0.93	800	800	25M	10M	No	0.00406	0.00066	0	217.5
2400	0.93	800	800	25M	10M	No	0.00406	0.00066	100	226.7
2400	0.93	800	800	25M	10M	No	0.00406	0.00066	250	240.0
2400	0.93	800	800	25M	10M	No	0.00406	0.00066	500	255.3
2400	0.93	800	800	25M	10M	No	0.00406	0.00066	1000	281.9
2400	0.93	800	800	25M	10M	No	0.00406	0.00066	1500	309.2
2400	0.93	800	800	25M	10M	Yes	0.00406	0.00123	0	220.0
2400	0.93	800	800	25M	10M	Yes	0.00406	0.00123	100	229.2
2400	0.93	800	800	25M	10M	Yes	0.00406	0.00123	250	242.3
2400	0.93	800	800	25M	10M	Yes	0.00406	0.00123	500	257.8
2400	0.93	800	800	25M	10M	Yes	0.00406	0.00123	1000	283.2
2400	0.93	800	800	25M	10M	Yes	0.00406	0.00123	1500	311.1
2400	0.93	800	800	25M	15M	No	0.00406	0.00132	0	221.8
2400	0.93	800	800	25M	15M	No	0.00406	0.00132	100	231.5
2400	0.93	800	800	25M	15M	No	0.00406	0.00132	250	244.8
2400	0.93	800	800	25M	15M	No	0.00406	0.00132	500	260.1
2400	0.93	800	800	25M	15M	No	0.00406	0.00132	1000	288.1
2400	0.93	800	800	25M	15M	No	0.00406	0.00132	1500	311.9
2400	0.93	800	800	25M	15M	Yes	0.00406	0.00189	0	224.9
2400	0.93	800	800	25M	15M	Yes	0.00406	0.00189	100	233.3
2400	0.93	800	800	25M	15M	Yes	0.00406	0.00189	250	246.5

Wall Height (mm)	Aspect Ratio	Reinforcement Spacing (mm)		Reinforcement Size		Bed-Joint Reinforcement	Reinforcement Ratio		Axial Stress (kPa)	Load Capacity (kN)
		Horizontal	Vertical	Horizontal	Vertical		Horizontal	Vertical		
2400	0.93	800	800	25M	15M	Yes	0.00406	0.00189	500	262.9
2400	0.93	800	800	25M	15M	Yes	0.00406	0.00189	1000	288.9
2400	0.93	800	800	25M	15M	Yes	0.00406	0.00189	1500	314.2
2400	0.93	800	800	25M	20M	No	0.00406	0.00198	0	225.0
2400	0.93	800	800	25M	20M	No	0.00406	0.00198	100	234.4
2400	0.93	800	800	25M	20M	No	0.00406	0.00198	250	247.8
2400	0.93	800	800	25M	20M	No	0.00406	0.00198	500	263.8
2400	0.93	800	800	25M	20M	No	0.00406	0.00198	1000	290.0
2400	0.93	800	800	25M	20M	No	0.00406	0.00198	1500	314.9
2400	0.93	800	800	25M	20M	Yes	0.00406	0.00255	0	228.4
2400	0.93	800	800	25M	20M	Yes	0.00406	0.00255	100	236.5
2400	0.93	800	800	25M	20M	Yes	0.00406	0.00255	250	249.7
2400	0.93	800	800	25M	20M	Yes	0.00406	0.00255	500	266.2
2400	0.93	800	800	25M	20M	Yes	0.00406	0.00255	1000	291.3
2400	0.93	800	800	25M	20M	Yes	0.00406	0.00255	1500	317.3
2400	0.93	800	800	30M	10M	No	0.00569	0.00066	0	225.8
2400	0.93	800	800	30M	10M	No	0.00569	0.00066	100	234.1
2400	0.93	800	800	30M	10M	No	0.00569	0.00066	250	244.8
2400	0.93	800	800	30M	10M	No	0.00569	0.00066	500	261.4
2400	0.93	800	800	30M	10M	No	0.00569	0.00066	1000	286.4
2400	0.93	800	800	30M	10M	No	0.00569	0.00066	1500	311.3
2400	0.93	800	800	30M	10M	Yes	0.00569	0.00123	100	236.4
2400	0.93	800	800	30M	10M	Yes	0.00569	0.00123	250	248.1
2400	0.93	800	800	30M	10M	Yes	0.00569	0.00123	500	264.0
2400	0.93	800	800	30M	10M	Yes	0.00569	0.00123	1000	288.6
2400	0.93	800	800	30M	10M	Yes	0.00569	0.00123	1500	313.0
2400	0.93	800	800	30M	15M	No	0.00569	0.00132	100	239.9
2400	0.93	800	800	30M	15M	No	0.00569	0.00132	250	251.2
2400	0.93	800	800	30M	15M	No	0.00569	0.00132	500	266.7
2400	0.93	800	800	30M	15M	No	0.00569	0.00132	1000	291.4

Wall Height (mm)	Aspect Ratio	Reinforcement Spacing (mm)		Reinforcement Size		Bed-Joint Reinforcement	Reinforcement Ratio		Axial Stress (kPa)	Load Capacity (kN)
		Horizontal	Vertical	Horizontal	Vertical		Horizontal	Vertical		
2400	0.93	800	800	30M	15M	No	0.00569	0.00132	1500	315.4
2400	0.93	800	800	30M	15M	Yes	0.00569	0.00189	100	242.0
2400	0.93	800	800	30M	15M	Yes	0.00569	0.00189	250	253.5
2400	0.93	800	800	30M	15M	Yes	0.00569	0.00189	500	269.1
2400	0.93	800	800	30M	15M	Yes	0.00569	0.00189	1000	293.0
2400	0.93	800	800	30M	15M	Yes	0.00569	0.00189	1500	316.7
2400	0.93	800	800	30M	20M	No	0.00569	0.00198	100	243.0
2400	0.93	800	800	30M	20M	No	0.00569	0.00198	250	255.0
2400	0.93	800	800	30M	20M	No	0.00569	0.00198	500	269.6
2400	0.93	800	800	30M	20M	No	0.00569	0.00198	1000	294.4
2400	0.93	800	800	30M	20M	No	0.00569	0.00198	1500	317.8
2400	0.93	800	800	30M	20M	Yes	0.00569	0.00255	100	246.6
2400	0.93	800	800	30M	20M	Yes	0.00569	0.00255	250	257.6
2400	0.93	800	800	30M	20M	Yes	0.00569	0.00255	500	271.8
2400	0.93	800	800	30M	20M	Yes	0.00569	0.00255	1000	295.9
2400	0.93	800	800	30M	20M	Yes	0.00569	0.00255	1500	319.5
2400	0.93	800	600	20M	10M	No	0.00305	0.00066	0	234.7
2400	0.93	800	600	20M	10M	No	0.00305	0.00066	100	247.0
2400	0.93	800	600	20M	10M	No	0.00305	0.00066	250	247.7
2400	0.93	800	600	20M	10M	No	0.00305	0.00066	500	274.2
2400	0.93	800	600	20M	10M	No	0.00305	0.00066	1000	304.2
2400	0.93	800	600	20M	10M	No	0.00305	0.00066	1500	322.5
2400	0.93	800	600	20M	10M	Yes	0.00305	0.00123	0	236.9
2400	0.93	800	600	20M	10M	Yes	0.00305	0.00123	100	243.8
2400	0.93	800	600	20M	10M	Yes	0.00305	0.00123	250	258.5
2400	0.93	800	600	20M	10M	Yes	0.00305	0.00123	500	275.9
2400	0.93	800	600	20M	10M	Yes	0.00305	0.00123	1000	307.9
2400	0.93	800	600	20M	10M	Yes	0.00305	0.00123	1500	324.7
2400	0.93	800	600	20M	15M	No	0.00305	0.00132	0	237.0
2400	0.93	800	600	20M	15M	No	0.00305	0.00132	100	246.6

Wall Height (mm)	Aspect Ratio	Reinforcement Spacing (mm)		Reinforcement Size		Bed-Joint Reinforcement	Reinforcement Ratio		Axial Stress (kPa)	Load Capacity (kN)
		Horizontal	Vertical	Horizontal	Vertical		Horizontal	Vertical		
2400	0.93	800	600	20M	15M	No	0.00305	0.00132	250	258.5
2400	0.93	800	600	20M	15M	No	0.00305	0.00132	500	276.1
2400	0.93	800	600	20M	15M	No	0.00305	0.00132	1000	308.2
2400	0.93	800	600	20M	15M	No	0.00305	0.00132	1500	326.1
2400	0.93	800	600	20M	15M	Yes	0.00305	0.00189	0	238.4
2400	0.93	800	600	20M	15M	Yes	0.00305	0.00189	100	253.0
2400	0.93	800	600	20M	15M	Yes	0.00305	0.00189	250	262.3
2400	0.93	800	600	20M	15M	Yes	0.00305	0.00189	500	278.8
2400	0.93	800	600	20M	15M	Yes	0.00305	0.00189	1000	311.9
2400	0.93	800	600	20M	15M	Yes	0.00305	0.00189	1500	329.3
2400	0.93	800	600	20M	20M	No	0.00305	0.00198	0	237.7
2400	0.93	800	600	20M	20M	No	0.00305	0.00198	100	252.6
2400	0.93	800	600	20M	20M	No	0.00305	0.00198	250	261.7
2400	0.93	800	600	20M	20M	No	0.00305	0.00198	500	277.3
2400	0.93	800	600	20M	20M	No	0.00305	0.00198	1000	312.8
2400	0.93	800	600	20M	20M	No	0.00305	0.00198	1500	328.2
2400	0.93	800	600	20M	20M	Yes	0.00305	0.00255	0	239.5
2400	0.93	800	600	20M	20M	Yes	0.00305	0.00255	100	249.8
2400	0.93	800	600	20M	20M	Yes	0.00305	0.00255	250	264.0
2400	0.93	800	600	20M	20M	Yes	0.00305	0.00255	500	283.2
2400	0.93	800	600	20M	20M	Yes	0.00305	0.00255	1000	315.0
2400	0.93	800	600	20M	20M	Yes	0.00305	0.00255	1500	331.2
2400	0.93	800	600	25M	10M	No	0.00508	0.00066	0	269.5
2400	0.93	800	600	25M	10M	No	0.00508	0.00066	100	273.8
2400	0.93	800	600	25M	10M	No	0.00508	0.00066	250	280.0
2400	0.93	800	600	25M	10M	No	0.00508	0.00066	500	289.0
2400	0.93	800	600	25M	10M	No	0.00508	0.00066	1000	309.0
2400	0.93	800	600	25M	10M	No	0.00508	0.00066	1500	327.7
2400	0.93	800	600	25M	10M	Yes	0.00508	0.00123	0	274.9
2400	0.93	800	600	25M	10M	Yes	0.00508	0.00123	100	277.9

Wall Height (mm)	Aspect Ratio	Reinforcement Spacing (mm)		Reinforcement Size		Bed-Joint Reinforcement	Reinforcement Ratio		Axial Stress (kPa)	Load Capacity (kN)
		Horizontal	Vertical	Horizontal	Vertical		Horizontal	Vertical		
2400	0.93	800	600	25M	10M	Yes	0.00508	0.00123	250	285.0
2400	0.93	800	600	25M	10M	Yes	0.00508	0.00123	500	294.4
2400	0.93	800	600	25M	10M	Yes	0.00508	0.00123	1000	314.5
2400	0.93	800	600	25M	10M	Yes	0.00508	0.00123	1500	330.8
2400	0.93	800	600	25M	15M	No	0.00508	0.00132	0	275.5
2400	0.93	800	600	25M	15M	No	0.00508	0.00132	100	279.3
2400	0.93	800	600	25M	15M	No	0.00508	0.00132	250	285.8
2400	0.93	800	600	25M	15M	No	0.00508	0.00132	500	294.9
2400	0.93	800	600	25M	15M	No	0.00508	0.00132	1000	314.4
2400	0.93	800	600	25M	15M	No	0.00508	0.00132	1500	332.0
2400	0.93	800	600	25M	15M	Yes	0.00508	0.00189	0	279.4
2400	0.93	800	600	25M	15M	Yes	0.00508	0.00189	100	284.3
2400	0.93	800	600	25M	15M	Yes	0.00508	0.00189	250	290.2
2400	0.93	800	600	25M	15M	Yes	0.00508	0.00189	500	299.4
2400	0.93	800	600	25M	15M	Yes	0.00508	0.00189	1000	320.7
2400	0.93	800	600	25M	15M	Yes	0.00508	0.00189	1500	336.1
2400	0.93	800	600	25M	20M	No	0.00508	0.00198	0	279.5
2400	0.93	800	600	25M	20M	No	0.00508	0.00198	100	283.3
2400	0.93	800	600	25M	20M	No	0.00508	0.00198	250	289.9
2400	0.93	800	600	25M	20M	No	0.00508	0.00198	500	299.0
2400	0.93	800	600	25M	20M	No	0.00508	0.00198	1000	319.9
2400	0.93	800	600	25M	20M	No	0.00508	0.00198	1500	336.1
2400	0.93	800	600	25M	20M	Yes	0.00508	0.00255	0	283.0
2400	0.93	800	600	25M	20M	Yes	0.00508	0.00255	100	287.9
2400	0.93	800	600	25M	20M	Yes	0.00508	0.00255	250	292.4
2400	0.93	800	600	25M	20M	Yes	0.00508	0.00255	500	303.1
2400	0.93	800	600	25M	20M	Yes	0.00508	0.00255	1000	323.6
2400	0.93	800	600	25M	20M	Yes	0.00508	0.00255	1500	338.8
2400	0.93	800	600	30M	10M	No	0.00711	0.00066	0	277.5
2400	0.93	800	600	30M	10M	No	0.00711	0.00066	100	281.0

Wall Height (mm)	Aspect Ratio	Reinforcement Spacing (mm)		Reinforcement Size		Bed-Joint Reinforcement	Reinforcement Ratio		Axial Stress (kPa)	Load Capacity (kN)
		Horizontal	Vertical	Horizontal	Vertical		Horizontal	Vertical		
2400	0.93	800	600	30M	10M	No	0.00711	0.00066	250	286.1
2400	0.93	800	600	30M	10M	No	0.00711	0.00066	500	294.2
2400	0.93	800	600	30M	10M	No	0.00711	0.00066	1000	312.4
2400	0.93	800	600	30M	10M	No	0.00711	0.00066	1500	330.8
2400	0.93	800	600	30M	10M	Yes	0.00711	0.00123	0	283.4
2400	0.93	800	600	30M	10M	Yes	0.00711	0.00123	100	285.8
2400	0.93	800	600	30M	10M	Yes	0.00711	0.00123	250	291.8
2400	0.93	800	600	30M	10M	Yes	0.00711	0.00123	500	300.0
2400	0.93	800	600	30M	10M	Yes	0.00711	0.00123	1000	317.8
2400	0.93	800	600	30M	10M	Yes	0.00711	0.00123	1500	335.0
2400	0.93	800	600	30M	15M	No	0.00711	0.00132	0	284.4
2400	0.93	800	600	30M	15M	No	0.00711	0.00132	100	287.1
2400	0.93	800	600	30M	15M	No	0.00711	0.00132	250	292.3
2400	0.93	800	600	30M	15M	No	0.00711	0.00132	500	300.4
2400	0.93	800	600	30M	15M	No	0.00711	0.00132	1000	319.7
2400	0.93	800	600	30M	15M	No	0.00711	0.00132	1500	336.5
2400	0.93	800	600	30M	15M	Yes	0.00711	0.00189	0	289.5
2400	0.93	800	600	30M	15M	Yes	0.00711	0.00189	100	292.7
2400	0.93	800	600	30M	15M	Yes	0.00711	0.00189	250	297.3
2400	0.93	800	600	30M	15M	Yes	0.00711	0.00189	500	305.3
2400	0.93	800	600	30M	15M	Yes	0.00711	0.00189	1000	325.1
2400	0.93	800	600	30M	15M	Yes	0.00711	0.00189	1500	340.0
2400	0.93	800	600	30M	20M	No	0.00711	0.00198	0	289.4
2400	0.93	800	600	30M	20M	No	0.00711	0.00198	100	291.9
2400	0.93	800	600	30M	20M	No	0.00711	0.00198	250	296.9
2400	0.93	800	600	30M	20M	No	0.00711	0.00198	500	304.8
2400	0.93	800	600	30M	20M	No	0.00711	0.00198	1000	324.6
2400	0.93	800	600	30M	20M	No	0.00711	0.00198	1500	340.0
2400	0.93	800	600	30M	20M	Yes	0.00711	0.00255	0	293.4
2400	0.93	800	600	30M	20M	Yes	0.00711	0.00255	100	296.8

Wall Height (mm)	Aspect Ratio	Reinforcement Spacing (mm)		Reinforcement Size		Bed-Joint Reinforcement	Reinforcement Ratio		Axial Stress (kPa)	Load Capacity (kN)
		Horizontal	Vertical	Horizontal	Vertical		Horizontal	Vertical		
2400	0.93	800	600	30M	20M	Yes	0.00711	0.00255	250	300.9
2400	0.93	800	600	30M	20M	Yes	0.00711	0.00255	500	309.5
2400	0.93	800	600	30M	20M	Yes	0.00711	0.00255	1000	328.9
2400	0.93	800	600	30M	20M	Yes	0.00711	0.00255	1500	343.5
2400	0.93	400	1200	20M	10M	No	0.00183	0.00132	0	161.8
2400	0.93	400	1200	20M	10M	No	0.00183	0.00132	100	172.4
2400	0.93	400	1200	20M	10M	No	0.00183	0.00132	250	192.4
2400	0.93	400	1200	20M	10M	No	0.00183	0.00132	500	230.3
2400	0.93	400	1200	20M	10M	No	0.00183	0.00132	1000	276.3
2400	0.93	400	1200	20M	10M	No	0.00183	0.00132	1500	306.2
2400	0.93	400	1200	20M	10M	Yes	0.00183	0.00189	0	162.4
2400	0.93	400	1200	20M	10M	Yes	0.00183	0.00189	100	173.1
2400	0.93	400	1200	20M	10M	Yes	0.00183	0.00189	250	193.5
2400	0.93	400	1200	20M	10M	Yes	0.00183	0.00189	500	228.7
2400	0.93	400	1200	20M	10M	Yes	0.00183	0.00189	1000	276.8
2400	0.93	400	1200	20M	10M	Yes	0.00183	0.00189	1500	306.9
2400	0.93	400	1200	20M	15M	No	0.00183	0.00264	0	162.0
2400	0.93	400	1200	20M	15M	No	0.00183	0.00264	100	173.4
2400	0.93	400	1200	20M	15M	No	0.00183	0.00264	250	194.5
2400	0.93	400	1200	20M	15M	No	0.00183	0.00264	500	230.3
2400	0.93	400	1200	20M	15M	No	0.00183	0.00264	1000	281.0
2400	0.93	400	1200	20M	15M	No	0.00183	0.00264	1500	307.6
2400	0.93	400	1200	20M	15M	Yes	0.00183	0.00321	0	162.9
2400	0.93	400	1200	20M	15M	Yes	0.00183	0.00321	100	174.0
2400	0.93	400	1200	20M	15M	Yes	0.00183	0.00321	250	195.3
2400	0.93	400	1200	20M	15M	Yes	0.00183	0.00321	500	230.1
2400	0.93	400	1200	20M	15M	Yes	0.00183	0.00321	1000	277.8
2400	0.93	400	1200	20M	15M	Yes	0.00183	0.00321	1500	310.4
2400	0.93	400	1200	20M	20M	No	0.00183	0.00396	0	162.7
2400	0.93	400	1200	20M	20M	No	0.00183	0.00396	250	195.5

Wall Height (mm)	Aspect Ratio	Reinforcement Spacing (mm)		Reinforcement Size		Bed-Joint Reinforcement	Reinforcement Ratio		Axial Stress (kPa)	Load Capacity (kN)
		Horizontal	Vertical	Horizontal	Vertical		Horizontal	Vertical		
2400	0.93	400	1200	20M	20M	No	0.00183	0.00396	500	230.9
2400	0.93	400	1200	20M	20M	No	0.00183	0.00396	1000	282.7
2400	0.93	400	1200	20M	20M	No	0.00183	0.00396	1500	311.4
2400	0.93	400	1200	20M	20M	Yes	0.00183	0.00453	0	163.3
2400	0.93	400	1200	20M	20M	Yes	0.00183	0.00453	100	175.0
2400	0.93	400	1200	20M	20M	Yes	0.00183	0.00453	250	196.6
2400	0.93	400	1200	20M	20M	Yes	0.00183	0.00453	500	231.1
2400	0.93	400	1200	20M	20M	Yes	0.00183	0.00453	1000	280.1
2400	0.93	400	1200	20M	20M	Yes	0.00183	0.00453	1500	310.5
2400	0.93	400	1200	25M	10M	No	0.00305	0.00132	0	174.5
2400	0.93	400	1200	25M	10M	No	0.00305	0.00132	100	183.2
2400	0.93	400	1200	25M	10M	No	0.00305	0.00132	250	201.3
2400	0.93	400	1200	25M	10M	No	0.00305	0.00132	500	236.3
2400	0.93	400	1200	25M	10M	No	0.00305	0.00132	1000	279.4
2400	0.93	400	1200	25M	10M	No	0.00305	0.00132	1500	309.6
2400	0.93	400	1200	25M	10M	Yes	0.00305	0.00189	0	177.7
2400	0.93	400	1200	25M	10M	Yes	0.00305	0.00189	100	184.8
2400	0.93	400	1200	25M	10M	Yes	0.00305	0.00189	250	203.1
2400	0.93	400	1200	25M	10M	Yes	0.00305	0.00189	500	236.7
2400	0.93	400	1200	25M	10M	Yes	0.00305	0.00189	1000	279.1
2400	0.93	400	1200	25M	10M	Yes	0.00305	0.00189	1500	311.9
2400	0.93	400	1200	25M	15M	No	0.00305	0.00264	0	178.2
2400	0.93	400	1200	25M	15M	No	0.00305	0.00264	100	186.6
2400	0.93	400	1200	25M	15M	No	0.00305	0.00264	250	204.0
2400	0.93	400	1200	25M	15M	No	0.00305	0.00264	500	239.2
2400	0.93	400	1200	25M	15M	No	0.00305	0.00264	1000	282.7
2400	0.93	400	1200	25M	15M	No	0.00305	0.00264	1500	313.0
2400	0.93	400	1200	25M	15M	Yes	0.00305	0.00321	0	181.2
2400	0.93	400	1200	25M	15M	Yes	0.00305	0.00321	100	188.4
2400	0.93	400	1200	25M	15M	Yes	0.00305	0.00321	250	205.4

Wall Height (mm)	Aspect Ratio	Reinforcement Spacing (mm)		Reinforcement Size		Bed-Joint Reinforcement	Reinforcement Ratio		Axial Stress (kPa)	Load Capacity (kN)
		Horizontal	Vertical	Horizontal	Vertical		Horizontal	Vertical		
2400	0.93	400	1200	25M	15M	Yes	0.00305	0.00321	500	241.4
2400	0.93	400	1200	25M	15M	Yes	0.00305	0.00321	1000	283.4
2400	0.93	400	1200	25M	15M	Yes	0.00305	0.00321	1500	313.6
2400	0.93	400	1200	25M	20M	No	0.00305	0.00396	0	179.3
2400	0.93	400	1200	25M	20M	No	0.00305	0.00396	100	188.4
2400	0.93	400	1200	25M	20M	No	0.00305	0.00396	250	206.3
2400	0.93	400	1200	25M	20M	No	0.00305	0.00396	500	241.3
2400	0.93	400	1200	25M	20M	No	0.00305	0.00396	1000	284.8
2400	0.93	400	1200	25M	20M	No	0.00305	0.00396	1500	314.7
2400	0.93	400	1200	25M	20M	Yes	0.00305	0.00453	0	182.3
2400	0.93	400	1200	25M	20M	Yes	0.00305	0.00453	100	189.1
2400	0.93	400	1200	25M	20M	Yes	0.00305	0.00453	250	206.8
2400	0.93	400	1200	25M	20M	Yes	0.00305	0.00453	500	240.6
2400	0.93	400	1200	25M	20M	Yes	0.00305	0.00453	1000	285.5
2400	0.93	400	1200	25M	20M	Yes	0.00305	0.00453	1500	314.1
2400	0.93	400	1200	30M	10M	No	0.00427	0.00132	0	186.0
2400	0.93	400	1200	30M	10M	No	0.00427	0.00132	100	190.1
2400	0.93	400	1200	30M	10M	No	0.00427	0.00132	250	206.7
2400	0.93	400	1200	30M	10M	No	0.00427	0.00132	500	240.7
2400	0.93	400	1200	30M	10M	No	0.00427	0.00132	1000	282.3
2400	0.93	400	1200	30M	10M	No	0.00427	0.00132	1500	311.3
2400	0.93	400	1200	30M	10M	Yes	0.00427	0.00189	0	187.6
2400	0.93	400	1200	30M	10M	Yes	0.00427	0.00189	100	192.5
2400	0.93	400	1200	30M	10M	Yes	0.00427	0.00189	250	209.0
2400	0.93	400	1200	30M	10M	Yes	0.00427	0.00189	500	240.6
2400	0.93	400	1200	30M	10M	Yes	0.00427	0.00189	1000	280.5
2400	0.93	400	1200	30M	10M	Yes	0.00427	0.00189	1500	312.2
2400	0.93	400	1200	30M	15M	No	0.00427	0.00264	0	187.2
2400	0.93	400	1200	30M	15M	No	0.00427	0.00264	100	194.5
2400	0.93	400	1200	30M	15M	No	0.00427	0.00264	250	210.8

Wall Height (mm)	Aspect Ratio	Reinforcement Spacing (mm)		Reinforcement Size		Bed-Joint Reinforcement	Reinforcement Ratio		Axial Stress (kPa)	Load Capacity (kN)
		Horizontal	Vertical	Horizontal	Vertical		Horizontal	Vertical		
2400	0.93	400	1200	30M	15M	No	0.00427	0.00264	500	243.4
2400	0.93	400	1200	30M	15M	No	0.00427	0.00264	1000	283.0
2400	0.93	400	1200	30M	15M	No	0.00427	0.00264	1500	313.7
2400	0.93	400	1200	30M	15M	Yes	0.00427	0.00321	0	191.4
2400	0.93	400	1200	30M	15M	Yes	0.00427	0.00321	100	195.3
2400	0.93	400	1200	30M	15M	Yes	0.00427	0.00321	250	211.5
2400	0.93	400	1200	30M	15M	Yes	0.00427	0.00321	500	244.2
2400	0.93	400	1200	30M	15M	Yes	0.00427	0.00321	1000	286.2
2400	0.93	400	1200	30M	15M	Yes	0.00427	0.00321	1500	314.4
2400	0.93	400	1200	30M	20M	No	0.00427	0.00396	0	193.7
2400	0.93	400	1200	30M	20M	No	0.00427	0.00396	100	196.3
2400	0.93	400	1200	30M	20M	No	0.00427	0.00396	250	212.4
2400	0.93	400	1200	30M	20M	No	0.00427	0.00396	500	245.9
2400	0.93	400	1200	30M	20M	No	0.00427	0.00396	1000	287.5
2400	0.93	400	1200	30M	20M	No	0.00427	0.00396	1500	315.6
2400	0.93	400	1200	30M	20M	Yes	0.00427	0.00453	0	199.0
2400	0.93	400	1200	30M	20M	Yes	0.00427	0.00453	100	207.6
2400	0.93	400	1200	30M	20M	Yes	0.00427	0.00453	250	213.4
2400	0.93	400	1200	30M	20M	Yes	0.00427	0.00453	500	246.5
2400	0.93	400	1200	30M	20M	Yes	0.00427	0.00453	1000	288.3
2400	0.93	400	1200	30M	20M	Yes	0.00427	0.00453	1500	316.2
2400	0.93	400	800	20M	10M	No	0.00244	0.00132	0	205.0
2400	0.93	400	800	20M	10M	No	0.00244	0.00132	250	234.5
2400	0.93	400	800	20M	10M	No	0.00244	0.00132	500	261.9
2400	0.93	400	800	20M	10M	No	0.00244	0.00132	1000	299.3
2400	0.93	400	800	20M	10M	No	0.00244	0.00132	1500	333.0
2400	0.93	400	800	20M	10M	Yes	0.00244	0.00189	0	206.4
2400	0.93	400	800	20M	10M	Yes	0.00244	0.00189	100	219.1
2400	0.93	400	800	20M	10M	Yes	0.00244	0.00189	250	235.4
2400	0.93	400	800	20M	10M	Yes	0.00244	0.00189	500	262.4

Wall Height (mm)	Aspect Ratio	Reinforcement Spacing (mm)		Reinforcement Size		Bed-Joint Reinforcement	Reinforcement Ratio		Axial Stress (kPa)	Load Capacity (kN)
		Horizontal	Vertical	Horizontal	Vertical		Horizontal	Vertical		
2400	0.93	400	800	20M	10M	Yes	0.00244	0.00189	1000	299.0
2400	0.93	400	800	20M	10M	Yes	0.00244	0.00189	1500	332.7
2400	0.93	400	800	20M	15M	No	0.00244	0.00264	0	207.6
2400	0.93	400	800	20M	15M	No	0.00244	0.00264	100	220.9
2400	0.93	400	800	20M	15M	No	0.00244	0.00264	250	237.7
2400	0.93	400	800	20M	15M	No	0.00244	0.00264	500	264.3
2400	0.93	400	800	20M	15M	No	0.00244	0.00264	1000	301.4
2400	0.93	400	800	20M	15M	No	0.00244	0.00264	1500	335.2
2400	0.93	400	800	20M	15M	Yes	0.00244	0.00321	0	208.1
2400	0.93	400	800	20M	15M	Yes	0.00244	0.00321	100	218.3
2400	0.93	400	800	20M	15M	Yes	0.00244	0.00321	250	238.0
2400	0.93	400	800	20M	15M	Yes	0.00244	0.00321	500	264.9
2400	0.93	400	800	20M	15M	Yes	0.00244	0.00321	1000	304.9
2400	0.93	400	800	20M	15M	Yes	0.00244	0.00321	1500	336.3
2400	0.93	400	800	20M	20M	No	0.00244	0.00396	0	209.2
2400	0.93	400	800	20M	20M	No	0.00244	0.00396	100	218.8
2400	0.93	400	800	20M	20M	No	0.00244	0.00396	250	239.1
2400	0.93	400	800	20M	20M	No	0.00244	0.00396	500	266.2
2400	0.93	400	800	20M	20M	No	0.00244	0.00396	1000	306.3
2400	0.93	400	800	20M	20M	No	0.00244	0.00396	1500	338.8
2400	0.93	400	800	20M	20M	Yes	0.00244	0.00453	0	210.4
2400	0.93	400	800	20M	20M	Yes	0.00244	0.00453	100	221.1
2400	0.93	400	800	20M	20M	Yes	0.00244	0.00453	250	239.5
2400	0.93	400	800	20M	20M	Yes	0.00244	0.00453	500	266.6
2400	0.93	400	800	20M	20M	Yes	0.00244	0.00453	1000	305.7
2400	0.93	400	800	20M	20M	Yes	0.00244	0.00453	1500	339.4
2400	0.93	400	800	25M	10M	No	0.00406	0.00132	0	235.8
2400	0.93	400	800	25M	10M	No	0.00406	0.00132	100	243.4
2400	0.93	400	800	25M	10M	No	0.00406	0.00132	250	255.6
2400	0.93	400	800	25M	10M	No	0.00406	0.00132	500	271.4

Wall Height (mm)	Aspect Ratio	Reinforcement Spacing (mm)		Reinforcement Size		Bed-Joint Reinforcement	Reinforcement Ratio		Axial Stress (kPa)	Load Capacity (kN)
		Horizontal	Vertical	Horizontal	Vertical		Horizontal	Vertical		
2400	0.93	400	800	25M	10M	No	0.00406	0.00132	1000	307.4
2400	0.93	400	800	25M	10M	No	0.00406	0.00132	1500	335.4
2400	0.93	400	800	25M	10M	Yes	0.00406	0.00189	0	238.0
2400	0.93	400	800	25M	10M	Yes	0.00406	0.00189	100	244.2
2400	0.93	400	800	25M	10M	Yes	0.00406	0.00189	250	257.3
2400	0.93	400	800	25M	10M	Yes	0.00406	0.00189	500	272.9
2400	0.93	400	800	25M	10M	Yes	0.00406	0.00189	1000	305.6
2400	0.93	400	800	25M	10M	Yes	0.00406	0.00189	1500	336.6
2400	0.93	400	800	25M	15M	No	0.00406	0.00264	0	240.5
2400	0.93	400	800	25M	15M	No	0.00406	0.00264	100	248.4
2400	0.93	400	800	25M	15M	No	0.00406	0.00264	250	261.2
2400	0.93	400	800	25M	15M	No	0.00406	0.00264	500	277.1
2400	0.93	400	800	25M	15M	No	0.00406	0.00264	1000	309.5
2400	0.93	400	800	25M	15M	No	0.00406	0.00264	1500	339.9
2400	0.93	400	800	25M	15M	Yes	0.00406	0.00321	0	243.4
2400	0.93	400	800	25M	15M	Yes	0.00406	0.00321	100	249.6
2400	0.93	400	800	25M	15M	Yes	0.00406	0.00321	250	261.9
2400	0.93	400	800	25M	15M	Yes	0.00406	0.00321	500	279.4
2400	0.93	400	800	25M	15M	Yes	0.00406	0.00321	1000	309.9
2400	0.93	400	800	25M	15M	Yes	0.00406	0.00321	1500	340.7
2400	0.93	400	800	25M	20M	No	0.00406	0.00396	0	245.0
2400	0.93	400	800	25M	20M	No	0.00406	0.00396	100	251.5
2400	0.93	400	800	25M	20M	No	0.00406	0.00396	250	264.7
2400	0.93	400	800	25M	20M	No	0.00406	0.00396	500	282.0
2400	0.93	400	800	25M	20M	No	0.00406	0.00396	1000	313.3
2400	0.93	400	800	25M	20M	No	0.00406	0.00396	1500	343.1
2400	0.93	400	800	25M	20M	Yes	0.00406	0.00453	0	247.4
2400	0.93	400	800	25M	20M	Yes	0.00406	0.00453	100	250.6
2400	0.93	400	800	25M	20M	Yes	0.00406	0.00453	250	265.9
2400	0.93	400	800	25M	20M	Yes	0.00406	0.00453	500	283.3

Wall Height (mm)	Aspect Ratio	Reinforcement Spacing (mm)		Reinforcement Size		Bed-Joint Reinforcement	Reinforcement Ratio		Axial Stress (kPa)	Load Capacity (kN)
		Horizontal	Vertical	Horizontal	Vertical		Horizontal	Vertical		
2400	0.93	400	800	25M	20M	Yes	0.00406	0.00453	1000	314.1
2400	0.93	400	800	25M	20M	Yes	0.00406	0.00453	1500	343.8
2400	0.93	400	800	30M	10M	No	0.00569	0.00132	0	245.0
2400	0.93	400	800	30M	10M	No	0.00569	0.00132	100	251.5
2400	0.93	400	800	30M	10M	No	0.00569	0.00132	250	262.0
2400	0.93	400	800	30M	10M	No	0.00569	0.00132	500	276.7
2400	0.93	400	800	30M	10M	No	0.00569	0.00132	1000	309.8
2400	0.93	400	800	30M	10M	No	0.00569	0.00132	1500	337.3
2400	0.93	400	800	30M	10M	Yes	0.00569	0.00189	0	245.6
2400	0.93	400	800	30M	10M	Yes	0.00569	0.00189	100	253.6
2400	0.93	400	800	30M	10M	Yes	0.00569	0.00189	250	263.7
2400	0.93	400	800	30M	10M	Yes	0.00569	0.00189	500	279.2
2400	0.93	400	800	30M	10M	Yes	0.00569	0.00189	1000	311.1
2400	0.93	400	800	30M	10M	Yes	0.00569	0.00189	1500	339.3
2400	0.93	400	800	30M	15M	No	0.00569	0.00264	0	251.4
2400	0.93	400	800	30M	15M	No	0.00569	0.00264	100	254.9
2400	0.93	400	800	30M	15M	No	0.00569	0.00264	250	269.0
2400	0.93	400	800	30M	15M	No	0.00569	0.00264	500	284.0
2400	0.93	400	800	30M	15M	No	0.00569	0.00264	1000	314.7
2400	0.93	400	800	30M	15M	No	0.00569	0.00264	1500	341.9
2400	0.93	400	800	30M	15M	Yes	0.00569	0.00321	0	252.6
2400	0.93	400	800	30M	15M	Yes	0.00569	0.00321	100	259.8
2400	0.93	400	800	30M	15M	Yes	0.00569	0.00321	250	270.5
2400	0.93	400	800	30M	15M	Yes	0.00569	0.00321	500	285.8
2400	0.93	400	800	30M	15M	Yes	0.00569	0.00321	1000	315.4
2400	0.93	400	800	30M	15M	Yes	0.00569	0.00321	1500	343.1
2400	0.93	400	800	30M	20M	No	0.00569	0.00396	0	254.2
2400	0.93	400	800	30M	20M	No	0.00569	0.00396	100	262.2
2400	0.93	400	800	30M	20M	No	0.00569	0.00396	250	273.0
2400	0.93	400	800	30M	20M	No	0.00569	0.00396	500	289.4

Wall Height (mm)	Aspect Ratio	Reinforcement Spacing (mm)		Reinforcement Size		Bed-Joint Reinforcement	Reinforcement Ratio		Axial Stress (kPa)	Load Capacity (kN)
		Horizontal	Vertical	Horizontal	Vertical		Horizontal	Vertical		
2400	0.93	400	800	30M	20M	No	0.00569	0.00396	1000	319.3
2400	0.93	400	800	30M	20M	No	0.00569	0.00396	1500	345.4
2400	0.93	400	800	30M	20M	Yes	0.00569	0.00453	0	255.7
2400	0.93	400	800	30M	20M	Yes	0.00569	0.00453	100	261.4
2400	0.93	400	800	30M	20M	Yes	0.00569	0.00453	250	275.0
2400	0.93	400	800	30M	20M	Yes	0.00569	0.00453	500	289.7
2400	0.93	400	800	30M	20M	Yes	0.00569	0.00453	1000	319.7
2400	0.93	400	800	30M	20M	Yes	0.00569	0.00453	1500	346.8
2400	0.93	400	600	20M	10M	No	0.00305	0.00132	0	244.5
2400	0.93	400	600	20M	10M	No	0.00305	0.00132	100	256.4
2400	0.93	400	600	20M	10M	No	0.00305	0.00132	250	270.4
2400	0.93	400	600	20M	10M	No	0.00305	0.00132	500	291.5
2400	0.93	400	600	20M	10M	No	0.00305	0.00132	1000	323.9
2400	0.93	400	600	20M	10M	No	0.00305	0.00132	1500	346.0
2400	0.93	400	600	20M	10M	Yes	0.00305	0.00189	0	245.5
2400	0.93	400	600	20M	10M	Yes	0.00305	0.00189	100	258.0
2400	0.93	400	600	20M	10M	Yes	0.00305	0.00189	250	272.1
2400	0.93	400	600	20M	10M	Yes	0.00305	0.00189	500	293.3
2400	0.93	400	600	20M	10M	Yes	0.00305	0.00189	1000	326.8
2400	0.93	400	600	20M	10M	Yes	0.00305	0.00189	1500	348.9
2400	0.93	400	600	20M	15M	No	0.00305	0.00264	0	245.9
2400	0.93	400	600	20M	15M	No	0.00305	0.00264	100	258.7
2400	0.93	400	600	20M	15M	No	0.00305	0.00264	250	274.5
2400	0.93	400	600	20M	15M	No	0.00305	0.00264	500	295.8
2400	0.93	400	600	20M	15M	No	0.00305	0.00264	1000	329.9
2400	0.93	400	600	20M	15M	No	0.00305	0.00264	1500	352.3
2400	0.93	400	600	20M	15M	Yes	0.00305	0.00321	0	246.8
2400	0.93	400	600	20M	15M	Yes	0.00305	0.00321	100	268.5
2400	0.93	400	600	20M	15M	Yes	0.00305	0.00321	250	275.9
2400	0.93	400	600	20M	15M	Yes	0.00305	0.00321	500	297.5

Wall Height (mm)	Aspect Ratio	Reinforcement Spacing (mm)		Reinforcement Size		Bed-Joint Reinforcement	Reinforcement Ratio		Axial Stress (kPa)	Load Capacity (kN)
		Horizontal	Vertical	Horizontal	Vertical		Horizontal	Vertical		
2400	0.93	400	600	20M	15M	Yes	0.00305	0.00321	1000	333.6
2400	0.93	400	600	20M	15M	Yes	0.00305	0.00321	1500	354.9
2400	0.93	400	600	20M	20M	No	0.00305	0.00396	0	247.0
2400	0.93	400	600	20M	20M	No	0.00305	0.00396	100	255.1
2400	0.93	400	600	20M	20M	No	0.00305	0.00396	250	277.7
2400	0.93	400	600	20M	20M	No	0.00305	0.00396	500	299.2
2400	0.93	400	600	20M	20M	No	0.00305	0.00396	1000	335.8
2400	0.93	400	600	20M	20M	No	0.00305	0.00396	1500	355.7
2400	0.93	400	600	20M	20M	Yes	0.00305	0.00453	0	248.0
2400	0.93	400	600	20M	20M	Yes	0.00305	0.00453	100	261.6
2400	0.93	400	600	20M	20M	Yes	0.00305	0.00453	250	278.8
2400	0.93	400	600	20M	20M	Yes	0.00305	0.00453	500	299.8
2400	0.93	400	600	20M	20M	Yes	0.00305	0.00453	1000	336.6
2400	0.93	400	600	20M	20M	Yes	0.00305	0.00453	1500	357.6
2400	0.93	400	600	25M	10M	No	0.00508	0.00132	0	288.6
2400	0.93	400	600	25M	10M	No	0.00508	0.00132	100	277.6
2400	0.93	400	600	25M	10M	No	0.00508	0.00132	250	302.5
2400	0.93	400	600	25M	10M	No	0.00508	0.00132	500	314.0
2400	0.93	400	600	25M	10M	No	0.00508	0.00132	1000	337.8
2400	0.93	400	600	25M	10M	No	0.00508	0.00132	1500	353.4
2400	0.93	400	600	25M	10M	Yes	0.00508	0.00189	0	291.7
2400	0.93	400	600	25M	10M	Yes	0.00508	0.00189	100	296.3
2400	0.93	400	600	25M	10M	Yes	0.00508	0.00189	250	306.1
2400	0.93	400	600	25M	10M	Yes	0.00508	0.00189	500	315.7
2400	0.93	400	600	25M	10M	Yes	0.00508	0.00189	1000	339.3
2400	0.93	400	600	25M	10M	Yes	0.00508	0.00189	1500	356.9
2400	0.93	400	600	25M	15M	No	0.00508	0.00264	0	294.4
2400	0.93	400	600	25M	15M	No	0.00508	0.00264	100	297.5
2400	0.93	400	600	25M	15M	No	0.00508	0.00264	250	309.4
2400	0.93	400	600	25M	15M	No	0.00508	0.00264	500	319.4

Wall Height (mm)	Aspect Ratio	Reinforcement Spacing (mm)		Reinforcement Size		Bed-Joint Reinforcement	Reinforcement Ratio		Axial Stress (kPa)	Load Capacity (kN)
		Horizontal	Vertical	Horizontal	Vertical		Horizontal	Vertical		
2400	0.93	400	600	25M	15M	No	0.00508	0.00264	1000	342.6
2400	0.93	400	600	25M	15M	No	0.00508	0.00264	1500	360.7
2400	0.93	400	600	25M	15M	Yes	0.00508	0.00321	0	297.0
2400	0.93	400	600	25M	15M	Yes	0.00508	0.00321	100	303.3
2400	0.93	400	600	25M	15M	Yes	0.00508	0.00321	250	313.4
2400	0.93	400	600	25M	15M	Yes	0.00508	0.00321	500	323.1
2400	0.93	400	600	25M	15M	Yes	0.00508	0.00321	1000	346.1
2400	0.93	400	600	25M	15M	Yes	0.00508	0.00321	1500	362.9
2400	0.93	400	600	25M	20M	No	0.00508	0.00396	0	297.9
2400	0.93	400	600	25M	20M	No	0.00508	0.00396	100	304.4
2400	0.93	400	600	25M	20M	No	0.00508	0.00396	250	314.1
2400	0.93	400	600	25M	20M	No	0.00508	0.00396	500	324.7
2400	0.93	400	600	25M	20M	No	0.00508	0.00396	1000	348.1
2400	0.93	400	600	25M	20M	No	0.00508	0.00396	1500	364.7
2400	0.93	400	600	25M	20M	Yes	0.00508	0.00453	0	300.7
2400	0.93	400	600	25M	20M	Yes	0.00508	0.00453	100	296.5
2400	0.93	400	600	25M	20M	Yes	0.00508	0.00453	250	316.9
2400	0.93	400	600	25M	20M	Yes	0.00508	0.00453	500	326.5
2400	0.93	400	600	25M	20M	Yes	0.00508	0.00453	1000	349.8
2400	0.93	400	600	25M	20M	Yes	0.00508	0.00453	1500	367.1
2400	0.93	400	600	30M	10M	No	0.00711	0.00132	0	302.2
2400	0.93	400	600	30M	10M	No	0.00711	0.00132	100	305.0
2400	0.93	400	600	30M	10M	No	0.00711	0.00132	250	311.7
2400	0.93	400	600	30M	10M	No	0.00711	0.00132	500	319.9
2400	0.93	400	600	30M	10M	No	0.00711	0.00132	1000	340.4
2400	0.93	400	600	30M	10M	No	0.00711	0.00132	1500	356.2
2400	0.93	400	600	30M	10M	Yes	0.00711	0.00189	0	307.0
2400	0.93	400	600	30M	10M	Yes	0.00711	0.00189	100	307.3
2400	0.93	400	600	30M	10M	Yes	0.00711	0.00189	250	315.9
2400	0.93	400	600	30M	10M	Yes	0.00711	0.00189	500	324.5

Wall Height (mm)	Aspect Ratio	Reinforcement Spacing (mm)		Reinforcement Size		Bed-Joint Reinforcement	Reinforcement Ratio		Axial Stress (kPa)	Load Capacity (kN)
		Horizontal	Vertical	Horizontal	Vertical		Horizontal	Vertical		
2400	0.93	400	600	30M	10M	Yes	0.00711	0.00189	1000	345.3
2400	0.93	400	600	30M	10M	Yes	0.00711	0.00189	1500	360.6
2400	0.93	400	600	30M	15M	No	0.00711	0.00264	0	311.9
2400	0.93	400	600	30M	15M	No	0.00711	0.00264	100	312.4
2400	0.93	400	600	30M	15M	No	0.00711	0.00264	250	320.8
2400	0.93	400	600	30M	15M	No	0.00711	0.00264	500	327.2
2400	0.93	400	600	30M	15M	No	0.00711	0.00264	1000	349.3
2400	0.93	400	600	30M	15M	No	0.00711	0.00264	1500	362.8
2400	0.93	400	600	30M	15M	Yes	0.00711	0.00321	0	317.7
2400	0.93	400	600	30M	15M	Yes	0.00711	0.00321	100	317.1
2400	0.93	400	600	30M	15M	Yes	0.00711	0.00321	250	324.2
2400	0.93	400	600	30M	15M	Yes	0.00711	0.00321	500	331.9
2400	0.93	400	600	30M	15M	Yes	0.00711	0.00321	1000	352.7
2400	0.93	400	600	30M	15M	Yes	0.00711	0.00321	1500	365.4
2400	0.93	400	600	30M	20M	No	0.00711	0.00396	0	320.1
2400	0.93	400	600	30M	20M	No	0.00711	0.00396	100	300.5
2400	0.93	400	600	30M	20M	No	0.00711	0.00396	250	325.9
2400	0.93	400	600	30M	20M	No	0.00711	0.00396	500	332.3
2400	0.93	400	600	30M	20M	No	0.00711	0.00396	1000	354.6
2400	0.93	400	600	30M	20M	No	0.00711	0.00396	1500	368.2
2400	0.93	400	600	30M	20M	Yes	0.00711	0.00453	0	323.0
2400	0.93	400	600	30M	20M	Yes	0.00711	0.00453	100	270.9
2400	0.93	400	600	30M	20M	Yes	0.00711	0.00453	250	326.2
2400	0.93	400	600	30M	20M	Yes	0.00711	0.00453	500	336.0
2400	0.93	400	600	30M	20M	Yes	0.00711	0.00453	1000	358.0
2400	0.93	400	600	30M	20M	Yes	0.00711	0.00453	1500	370.7
3200	1.24	800	1200	20M	10M	No	0.00183	0.00066	0	130.9
3200	1.24	800	1200	20M	10M	No	0.00183	0.00066	100	145.6
3200	1.24	800	1200	20M	10M	No	0.00183	0.00066	250	163.7
3200	1.24	800	1200	20M	10M	No	0.00183	0.00066	500	192.9

Wall Height (mm)	Aspect Ratio	Reinforcement Spacing (mm)		Reinforcement Size		Bed-Joint Reinforcement	Reinforcement Ratio		Axial Stress (kPa)	Load Capacity (kN)
		Horizontal	Vertical	Horizontal	Vertical		Horizontal	Vertical		
3200	1.24	800	1200	20M	10M	No	0.00183	0.00066	1000	229.1
3200	1.24	800	1200	20M	10M	No	0.00183	0.00066	1500	255.8
3200	1.24	800	1200	20M	10M	Yes	0.00183	0.00123	0	130.9
3200	1.24	800	1200	20M	10M	Yes	0.00183	0.00123	100	146.2
3200	1.24	800	1200	20M	10M	Yes	0.00183	0.00123	250	164.6
3200	1.24	800	1200	20M	10M	Yes	0.00183	0.00123	500	193.5
3200	1.24	800	1200	20M	10M	Yes	0.00183	0.00123	1000	231.1
3200	1.24	800	1200	20M	10M	Yes	0.00183	0.00123	1500	256.7
3200	1.24	800	1200	20M	15M	No	0.00183	0.00132	0	131.0
3200	1.24	800	1200	20M	15M	No	0.00183	0.00132	100	145.8
3200	1.24	800	1200	20M	15M	No	0.00183	0.00132	250	164.2
3200	1.24	800	1200	20M	15M	No	0.00183	0.00132	500	192.2
3200	1.24	800	1200	20M	15M	No	0.00183	0.00132	1000	230.6
3200	1.24	800	1200	20M	15M	No	0.00183	0.00132	1500	257.0
3200	1.24	800	1200	20M	15M	Yes	0.00183	0.00189	0	131.0
3200	1.24	800	1200	20M	15M	Yes	0.00183	0.00189	100	145.2
3200	1.24	800	1200	20M	15M	Yes	0.00183	0.00189	250	164.7
3200	1.24	800	1200	20M	15M	Yes	0.00183	0.00189	500	194.2
3200	1.24	800	1200	20M	15M	Yes	0.00183	0.00189	1000	233.8
3200	1.24	800	1200	20M	15M	Yes	0.00183	0.00189	1500	258.1
3200	1.24	800	1200	20M	20M	No	0.00183	0.00198	0	131.2
3200	1.24	800	1200	20M	20M	No	0.00183	0.00198	100	145.0
3200	1.24	800	1200	20M	20M	No	0.00183	0.00198	250	164.5
3200	1.24	800	1200	20M	20M	No	0.00183	0.00198	500	191.9
3200	1.24	800	1200	20M	20M	No	0.00183	0.00198	1000	232.6
3200	1.24	800	1200	20M	20M	No	0.00183	0.00198	1500	255.8
3200	1.24	800	1200	20M	20M	Yes	0.00183	0.00255	0	131.1
3200	1.24	800	1200	20M	20M	Yes	0.00183	0.00255	100	144.6
3200	1.24	800	1200	20M	20M	Yes	0.00183	0.00255	250	164.9
3200	1.24	800	1200	20M	20M	Yes	0.00183	0.00255	500	194.6

Wall Height (mm)	Aspect Ratio	Reinforcement Spacing (mm)		Reinforcement Size		Bed-Joint Reinforcement	Reinforcement Ratio		Axial Stress (kPa)	Load Capacity (kN)
		Horizontal	Vertical	Horizontal	Vertical		Horizontal	Vertical		
3200	1.24	800	1200	20M	20M	Yes	0.00183	0.00255	1000	234.1
3200	1.24	800	1200	20M	20M	Yes	0.00183	0.00255	1500	260.1
3200	1.24	800	1200	25M	10M	No	0.00305	0.00066	0	162.7
3200	1.24	800	1200	25M	10M	No	0.00305	0.00066	100	157.8
3200	1.24	800	1200	25M	10M	No	0.00305	0.00066	250	178.2
3200	1.24	800	1200	25M	10M	No	0.00305	0.00066	500	202.7
3200	1.24	800	1200	25M	10M	No	0.00305	0.00066	1000	236.1
3200	1.24	800	1200	25M	10M	No	0.00305	0.00066	1500	261.8
3200	1.24	800	1200	25M	10M	Yes	0.00305	0.00123	0	162.6
3200	1.24	800	1200	25M	10M	Yes	0.00305	0.00123	100	167.6
3200	1.24	800	1200	25M	10M	Yes	0.00305	0.00123	250	183.9
3200	1.24	800	1200	25M	10M	Yes	0.00305	0.00123	500	206.2
3200	1.24	800	1200	25M	10M	Yes	0.00305	0.00123	1000	238.2
3200	1.24	800	1200	25M	10M	Yes	0.00305	0.00123	1500	262.8
3200	1.24	800	1200	25M	15M	No	0.00305	0.00132	0	161.4
3200	1.24	800	1200	25M	15M	No	0.00305	0.00132	100	166.9
3200	1.24	800	1200	25M	15M	No	0.00305	0.00132	250	179.3
3200	1.24	800	1200	25M	15M	No	0.00305	0.00132	500	203.9
3200	1.24	800	1200	25M	15M	No	0.00305	0.00132	1000	238.0
3200	1.24	800	1200	25M	15M	No	0.00305	0.00132	1500	263.0
3200	1.24	800	1200	25M	15M	Yes	0.00305	0.00189	0	162.7
3200	1.24	800	1200	25M	15M	Yes	0.00305	0.00189	100	168.9
3200	1.24	800	1200	25M	15M	Yes	0.00305	0.00189	250	188.5
3200	1.24	800	1200	25M	15M	Yes	0.00305	0.00189	500	207.1
3200	1.24	800	1200	25M	15M	Yes	0.00305	0.00189	1000	239.4
3200	1.24	800	1200	25M	15M	Yes	0.00305	0.00189	1500	263.9
3200	1.24	800	1200	25M	20M	No	0.00305	0.00198	0	161.7
3200	1.24	800	1200	25M	20M	No	0.00305	0.00198	100	168.0
3200	1.24	800	1200	25M	20M	No	0.00305	0.00198	250	179.8
3200	1.24	800	1200	25M	20M	No	0.00305	0.00198	500	205.3

Wall Height (mm)	Aspect Ratio	Reinforcement Spacing (mm)		Reinforcement Size		Bed-Joint Reinforcement	Reinforcement Ratio		Axial Stress (kPa)	Load Capacity (kN)
		Horizontal	Vertical	Horizontal	Vertical		Horizontal	Vertical		
3200	1.24	800	1200	25M	20M	No	0.00305	0.00198	1000	238.5
3200	1.24	800	1200	25M	20M	No	0.00305	0.00198	1500	263.9
3200	1.24	800	1200	25M	20M	Yes	0.00305	0.00255	0	163.1
3200	1.24	800	1200	25M	20M	Yes	0.00305	0.00255	100	172.1
3200	1.24	800	1200	25M	20M	Yes	0.00305	0.00255	250	182.6
3200	1.24	800	1200	25M	20M	Yes	0.00305	0.00255	500	207.6
3200	1.24	800	1200	25M	20M	Yes	0.00305	0.00255	1000	240.0
3200	1.24	800	1200	25M	20M	Yes	0.00305	0.00255	1500	265.1
3200	1.24	800	1200	30M	10M	No	0.00427	0.00066	0	171.3
3200	1.24	800	1200	30M	10M	No	0.00427	0.00066	100	176.1
3200	1.24	800	1200	30M	10M	No	0.00427	0.00066	250	187.2
3200	1.24	800	1200	30M	10M	No	0.00427	0.00066	500	210.3
3200	1.24	800	1200	30M	10M	No	0.00427	0.00066	1000	240.6
3200	1.24	800	1200	30M	10M	No	0.00427	0.00066	1500	265.9
3200	1.24	800	1200	30M	10M	Yes	0.00427	0.00123	0	173.7
3200	1.24	800	1200	30M	10M	Yes	0.00427	0.00123	100	180.4
3200	1.24	800	1200	30M	10M	Yes	0.00427	0.00123	250	193.8
3200	1.24	800	1200	30M	10M	Yes	0.00427	0.00123	500	213.0
3200	1.24	800	1200	30M	10M	Yes	0.00427	0.00123	1000	238.6
3200	1.24	800	1200	30M	10M	Yes	0.00427	0.00123	1500	267.0
3200	1.24	800	1200	30M	15M	No	0.00427	0.00132	0	176.9
3200	1.24	800	1200	30M	15M	No	0.00427	0.00132	100	181.6
3200	1.24	800	1200	30M	15M	No	0.00427	0.00132	250	194.4
3200	1.24	800	1200	30M	15M	No	0.00427	0.00132	500	212.4
3200	1.24	800	1200	30M	15M	No	0.00427	0.00132	1000	238.2
3200	1.24	800	1200	30M	15M	No	0.00427	0.00132	1500	266.1
3200	1.24	800	1200	30M	15M	Yes	0.00427	0.00189	0	179.5
3200	1.24	800	1200	30M	15M	Yes	0.00427	0.00189	100	180.7
3200	1.24	800	1200	30M	15M	Yes	0.00427	0.00189	250	196.9
3200	1.24	800	1200	30M	15M	Yes	0.00427	0.00189	500	214.9

Wall Height (mm)	Aspect Ratio	Reinforcement Spacing (mm)		Reinforcement Size		Bed-Joint Reinforcement	Reinforcement Ratio		Axial Stress (kPa)	Load Capacity (kN)
		Horizontal	Vertical	Horizontal	Vertical		Horizontal	Vertical		
3200	1.24	800	1200	30M	15M	Yes	0.00427	0.00189	1000	243.2
3200	1.24	800	1200	30M	15M	Yes	0.00427	0.00189	1500	267.4
3200	1.24	800	1200	30M	20M	No	0.00427	0.00198	0	171.1
3200	1.24	800	1200	30M	20M	No	0.00427	0.00198	100	181.5
3200	1.24	800	1200	30M	20M	No	0.00427	0.00198	250	190.5
3200	1.24	800	1200	30M	20M	No	0.00427	0.00198	500	213.6
3200	1.24	800	1200	30M	20M	No	0.00427	0.00198	1000	239.2
3200	1.24	800	1200	30M	20M	No	0.00427	0.00198	1500	268.2
3200	1.24	800	1200	30M	20M	Yes	0.00427	0.00255	0	170.9
3200	1.24	800	1200	30M	20M	Yes	0.00427	0.00255	100	185.2
3200	1.24	800	1200	30M	20M	Yes	0.00427	0.00255	250	198.5
3200	1.24	800	1200	30M	20M	Yes	0.00427	0.00255	500	218.2
3200	1.24	800	1200	30M	20M	Yes	0.00427	0.00255	1000	244.1
3200	1.24	800	1200	30M	20M	Yes	0.00427	0.00255	1500	269.2
3200	1.24	800	800	20M	10M	No	0.00244	0.00066	0	168.8
3200	1.24	800	800	20M	10M	No	0.00244	0.00066	100	179.7
3200	1.24	800	800	20M	10M	No	0.00244	0.00066	250	195.1
3200	1.24	800	800	20M	10M	No	0.00244	0.00066	500	215.6
3200	1.24	800	800	20M	10M	No	0.00244	0.00066	1000	246.5
3200	1.24	800	800	20M	10M	No	0.00244	0.00066	1500	274.7
3200	1.24	800	800	20M	10M	Yes	0.00244	0.00123	0	169.1
3200	1.24	800	800	20M	10M	Yes	0.00244	0.00123	100	180.6
3200	1.24	800	800	20M	10M	Yes	0.00244	0.00123	250	195.8
3200	1.24	800	800	20M	10M	Yes	0.00244	0.00123	500	216.3
3200	1.24	800	800	20M	10M	Yes	0.00244	0.00123	1000	250.8
3200	1.24	800	800	20M	10M	Yes	0.00244	0.00123	1500	276.9
3200	1.24	800	800	20M	15M	No	0.00244	0.00132	0	169.4
3200	1.24	800	800	20M	15M	No	0.00244	0.00132	100	180.9
3200	1.24	800	800	20M	15M	No	0.00244	0.00132	250	196.1
3200	1.24	800	800	20M	15M	No	0.00244	0.00132	500	216.4

Wall Height (mm)	Aspect Ratio	Reinforcement Spacing (mm)		Reinforcement Size		Bed-Joint Reinforcement	Reinforcement Ratio		Axial Stress (kPa)	Load Capacity (kN)
		Horizontal	Vertical	Horizontal	Vertical		Horizontal	Vertical		
3200	1.24	800	800	20M	15M	No	0.00244	0.00132	1000	248.7
3200	1.24	800	800	20M	15M	No	0.00244	0.00132	1500	277.6
3200	1.24	800	800	20M	15M	Yes	0.00244	0.00189	0	169.6
3200	1.24	800	800	20M	15M	Yes	0.00244	0.00189	100	180.2
3200	1.24	800	800	20M	15M	Yes	0.00244	0.00189	250	197.1
3200	1.24	800	800	20M	15M	Yes	0.00244	0.00189	500	217.5
3200	1.24	800	800	20M	15M	Yes	0.00244	0.00189	1000	249.1
3200	1.24	800	800	20M	15M	Yes	0.00244	0.00189	1500	277.6
3200	1.24	800	800	20M	20M	No	0.00244	0.00198	0	169.6
3200	1.24	800	800	20M	20M	No	0.00244	0.00198	100	181.4
3200	1.24	800	800	20M	20M	No	0.00244	0.00198	250	197.0
3200	1.24	800	800	20M	20M	No	0.00244	0.00198	500	217.4
3200	1.24	800	800	20M	20M	No	0.00244	0.00198	1000	250.3
3200	1.24	800	800	20M	20M	No	0.00244	0.00198	1500	277.4
3200	1.24	800	800	20M	20M	Yes	0.00244	0.00255	0	169.8
3200	1.24	800	800	20M	20M	Yes	0.00244	0.00255	100	181.3
3200	1.24	800	800	20M	20M	Yes	0.00244	0.00255	250	197.8
3200	1.24	800	800	20M	20M	Yes	0.00244	0.00255	500	219.6
3200	1.24	800	800	20M	20M	Yes	0.00244	0.00255	1000	250.0
3200	1.24	800	800	20M	20M	Yes	0.00244	0.00255	1500	281.8
3200	1.24	800	800	25M	10M	No	0.00406	0.00066	0	207.9
3200	1.24	800	800	25M	10M	No	0.00406	0.00066	100	212.7
3200	1.24	800	800	25M	10M	No	0.00406	0.00066	250	225.0
3200	1.24	800	800	25M	10M	No	0.00406	0.00066	500	236.7
3200	1.24	800	800	25M	10M	No	0.00406	0.00066	1000	257.4
3200	1.24	800	800	25M	10M	No	0.00406	0.00066	1500	281.9
3200	1.24	800	800	25M	10M	Yes	0.00406	0.00123	0	210.3
3200	1.24	800	800	25M	10M	Yes	0.00406	0.00123	100	215.5
3200	1.24	800	800	25M	10M	Yes	0.00406	0.00123	250	224.6
3200	1.24	800	800	25M	10M	Yes	0.00406	0.00123	500	239.3

Wall Height (mm)	Aspect Ratio	Reinforcement Spacing (mm)		Reinforcement Size		Bed-Joint Reinforcement	Reinforcement Ratio		Axial Stress (kPa)	Load Capacity (kN)
		Horizontal	Vertical	Horizontal	Vertical		Horizontal	Vertical		
3200	1.24	800	800	25M	10M	Yes	0.00406	0.00123	1000	259.7
3200	1.24	800	800	25M	10M	Yes	0.00406	0.00123	1500	283.4
3200	1.24	800	800	25M	15M	No	0.00406	0.00132	0	211.8
3200	1.24	800	800	25M	15M	No	0.00406	0.00132	100	217.8
3200	1.24	800	800	25M	15M	No	0.00406	0.00132	250	228.3
3200	1.24	800	800	25M	15M	No	0.00406	0.00132	500	240.8
3200	1.24	800	800	25M	15M	No	0.00406	0.00132	1000	260.2
3200	1.24	800	800	25M	15M	No	0.00406	0.00132	1500	283.8
3200	1.24	800	800	25M	15M	Yes	0.00406	0.00189	0	213.8
3200	1.24	800	800	25M	15M	Yes	0.00406	0.00189	100	219.7
3200	1.24	800	800	25M	15M	Yes	0.00406	0.00189	250	230.2
3200	1.24	800	800	25M	15M	Yes	0.00406	0.00189	500	242.7
3200	1.24	800	800	25M	15M	Yes	0.00406	0.00189	1000	261.7
3200	1.24	800	800	25M	15M	Yes	0.00406	0.00189	1500	285.5
3200	1.24	800	800	25M	20M	No	0.00406	0.00198	0	214.3
3200	1.24	800	800	25M	20M	No	0.00406	0.00198	100	211.6
3200	1.24	800	800	25M	20M	No	0.00406	0.00198	250	228.9
3200	1.24	800	800	25M	20M	No	0.00406	0.00198	500	243.1
3200	1.24	800	800	25M	20M	No	0.00406	0.00198	1000	262.3
3200	1.24	800	800	25M	20M	No	0.00406	0.00198	1500	283.8
3200	1.24	800	800	25M	20M	Yes	0.00406	0.00255	0	215.8
3200	1.24	800	800	25M	20M	Yes	0.00406	0.00255	100	221.9
3200	1.24	800	800	25M	20M	Yes	0.00406	0.00255	250	230.4
3200	1.24	800	800	25M	20M	Yes	0.00406	0.00255	500	244.7
3200	1.24	800	800	25M	20M	Yes	0.00406	0.00255	1000	264.0
3200	1.24	800	800	25M	20M	Yes	0.00406	0.00255	1500	286.0
3200	1.24	800	800	30M	10M	No	0.00569	0.00066	0	216.5
3200	1.24	800	800	30M	10M	No	0.00569	0.00066	100	222.7
3200	1.24	800	800	30M	10M	No	0.00569	0.00066	250	231.9
3200	1.24	800	800	30M	10M	No	0.00569	0.00066	500	243.4

Wall Height (mm)	Aspect Ratio	Reinforcement Spacing (mm)		Reinforcement Size		Bed-Joint Reinforcement	Reinforcement Ratio		Axial Stress (kPa)	Load Capacity (kN)
		Horizontal	Vertical	Horizontal	Vertical		Horizontal	Vertical		
3200	1.24	800	800	30M	10M	No	0.00569	0.00066	1000	262.0
3200	1.24	800	800	30M	10M	No	0.00569	0.00066	1500	285.3
3200	1.24	800	800	30M	10M	Yes	0.00569	0.00123	0	220.4
3200	1.24	800	800	30M	10M	Yes	0.00569	0.00123	100	224.9
3200	1.24	800	800	30M	10M	Yes	0.00569	0.00123	250	234.1
3200	1.24	800	800	30M	10M	Yes	0.00569	0.00123	500	245.6
3200	1.24	800	800	30M	10M	Yes	0.00569	0.00123	1000	263.7
3200	1.24	800	800	30M	10M	Yes	0.00569	0.00123	1500	286.1
3200	1.24	800	800	30M	15M	No	0.00569	0.00132	0	221.4
3200	1.24	800	800	30M	15M	No	0.00569	0.00132	100	227.7
3200	1.24	800	800	30M	15M	No	0.00569	0.00132	250	233.6
3200	1.24	800	800	30M	15M	No	0.00569	0.00132	500	247.6
3200	1.24	800	800	30M	15M	No	0.00569	0.00132	1000	265.5
3200	1.24	800	800	30M	15M	No	0.00569	0.00132	1500	287.9
3200	1.24	800	800	30M	15M	Yes	0.00569	0.00189	0	224.0
3200	1.24	800	800	30M	15M	Yes	0.00569	0.00189	100	230.8
3200	1.24	800	800	30M	15M	Yes	0.00569	0.00189	250	238.4
3200	1.24	800	800	30M	15M	Yes	0.00569	0.00189	500	249.9
3200	1.24	800	800	30M	15M	Yes	0.00569	0.00189	1000	267.2
3200	1.24	800	800	30M	15M	Yes	0.00569	0.00189	1500	291.0
3200	1.24	800	800	30M	20M	No	0.00569	0.00198	0	224.8
3200	1.24	800	800	30M	20M	No	0.00569	0.00198	100	229.4
3200	1.24	800	800	30M	20M	No	0.00569	0.00198	250	234.3
3200	1.24	800	800	30M	20M	No	0.00569	0.00198	500	250.7
3200	1.24	800	800	30M	20M	No	0.00569	0.00198	1000	267.9
3200	1.24	800	800	30M	20M	No	0.00569	0.00198	1500	291.6
3200	1.24	800	800	30M	20M	Yes	0.00569	0.00255	0	230.6
3200	1.24	800	800	30M	20M	Yes	0.00569	0.00255	100	230.9
3200	1.24	800	800	30M	20M	Yes	0.00569	0.00255	250	238.3
3200	1.24	800	800	30M	20M	Yes	0.00569	0.00255	500	252.9

Wall Height (mm)	Aspect Ratio	Reinforcement Spacing (mm)		Reinforcement Size		Bed-Joint Reinforcement	Reinforcement Ratio		Axial Stress (kPa)	Load Capacity (kN)
		Horizontal	Vertical	Horizontal	Vertical		Horizontal	Vertical		
3200	1.24	800	800	30M	20M	Yes	0.00569	0.00255	1000	269.7
3200	1.24	800	800	30M	20M	Yes	0.00569	0.00255	1500	293.1
3200	1.24	800	600	20M	10M	No	0.00305	0.00066	0	197.2
3200	1.24	800	600	20M	10M	No	0.00305	0.00066	100	207.6
3200	1.24	800	600	20M	10M	No	0.00305	0.00066	250	221.6
3200	1.24	800	600	20M	10M	No	0.00305	0.00066	500	239.7
3200	1.24	800	600	20M	10M	No	0.00305	0.00066	1000	267.6
3200	1.24	800	600	20M	10M	No	0.00305	0.00066	1500	287.5
3200	1.24	800	600	20M	10M	Yes	0.00305	0.00123	0	197.9
3200	1.24	800	600	20M	10M	Yes	0.00305	0.00123	100	210.8
3200	1.24	800	600	20M	10M	Yes	0.00305	0.00123	250	221.8
3200	1.24	800	600	20M	10M	Yes	0.00305	0.00123	500	241.4
3200	1.24	800	600	20M	10M	Yes	0.00305	0.00123	1000	270.0
3200	1.24	800	600	20M	10M	Yes	0.00305	0.00123	1500	290.8
3200	1.24	800	600	20M	15M	No	0.00305	0.00132	0	197.9
3200	1.24	800	600	20M	15M	No	0.00305	0.00132	100	208.0
3200	1.24	800	600	20M	15M	No	0.00305	0.00132	250	220.9
3200	1.24	800	600	20M	15M	No	0.00305	0.00132	500	239.7
3200	1.24	800	600	20M	15M	No	0.00305	0.00132	1000	270.0
3200	1.24	800	600	20M	15M	No	0.00305	0.00132	1500	290.4
3200	1.24	800	600	20M	15M	Yes	0.00305	0.00189	0	198.4
3200	1.24	800	600	20M	15M	Yes	0.00305	0.00189	100	209.1
3200	1.24	800	600	20M	15M	Yes	0.00305	0.00189	250	221.7
3200	1.24	800	600	20M	15M	Yes	0.00305	0.00189	500	241.7
3200	1.24	800	600	20M	15M	Yes	0.00305	0.00189	1000	271.8
3200	1.24	800	600	20M	15M	Yes	0.00305	0.00189	1500	291.7
3200	1.24	800	600	20M	20M	No	0.00305	0.00198	0	198.5
3200	1.24	800	600	20M	20M	No	0.00305	0.00198	100	208.7
3200	1.24	800	600	20M	20M	No	0.00305	0.00198	250	221.5
3200	1.24	800	600	20M	20M	No	0.00305	0.00198	500	241.1

Wall Height (mm)	Aspect Ratio	Reinforcement Spacing (mm)		Reinforcement Size		Bed-Joint Reinforcement	Reinforcement Ratio		Axial Stress (kPa)	Load Capacity (kN)
		Horizontal	Vertical	Horizontal	Vertical		Horizontal	Vertical		
3200	1.24	800	600	20M	20M	No	0.00305	0.00198	1000	271.9
3200	1.24	800	600	20M	20M	No	0.00305	0.00198	1500	293.2
3200	1.24	800	600	20M	20M	Yes	0.00305	0.00255	0	199.0
3200	1.24	800	600	20M	20M	Yes	0.00305	0.00255	100	209.5
3200	1.24	800	600	20M	20M	Yes	0.00305	0.00255	250	222.2
3200	1.24	800	600	20M	20M	Yes	0.00305	0.00255	500	244.0
3200	1.24	800	600	20M	20M	Yes	0.00305	0.00255	1000	273.5
3200	1.24	800	600	20M	20M	Yes	0.00305	0.00255	1500	296.0
3200	1.24	800	600	25M	10M	No	0.00508	0.00066	0	246.2
3200	1.24	800	600	25M	10M	No	0.00508	0.00066	100	251.0
3200	1.24	800	600	25M	10M	No	0.00508	0.00066	250	253.9
3200	1.24	800	600	25M	10M	No	0.00508	0.00066	500	268.6
3200	1.24	800	600	25M	10M	No	0.00508	0.00066	1000	287.9
3200	1.24	800	600	25M	10M	No	0.00508	0.00066	1500	298.6
3200	1.24	800	600	25M	10M	Yes	0.00508	0.00123	0	249.5
3200	1.24	800	600	25M	10M	Yes	0.00508	0.00123	100	254.5
3200	1.24	800	600	25M	10M	Yes	0.00508	0.00123	250	260.5
3200	1.24	800	600	25M	10M	Yes	0.00508	0.00123	500	272.7
3200	1.24	800	600	25M	10M	Yes	0.00508	0.00123	1000	292.0
3200	1.24	800	600	25M	10M	Yes	0.00508	0.00123	1500	302.2
3200	1.24	800	600	25M	15M	No	0.00508	0.00132	0	249.7
3200	1.24	800	600	25M	15M	No	0.00508	0.00132	100	255.0
3200	1.24	800	600	25M	15M	No	0.00508	0.00132	250	256.8
3200	1.24	800	600	25M	15M	No	0.00508	0.00132	500	273.0
3200	1.24	800	600	25M	15M	No	0.00508	0.00132	1000	289.2
3200	1.24	800	600	25M	15M	No	0.00508	0.00132	1500	303.2
3200	1.24	800	600	25M	15M	Yes	0.00508	0.00189	0	252.6
3200	1.24	800	600	25M	15M	Yes	0.00508	0.00189	100	256.9
3200	1.24	800	600	25M	15M	Yes	0.00508	0.00189	250	263.9
3200	1.24	800	600	25M	15M	Yes	0.00508	0.00189	500	276.5

Wall Height (mm)	Aspect Ratio	Reinforcement Spacing (mm)		Reinforcement Size		Bed-Joint Reinforcement	Reinforcement Ratio		Axial Stress (kPa)	Load Capacity (kN)
		Horizontal	Vertical	Horizontal	Vertical		Horizontal	Vertical		
3200	1.24	800	600	25M	15M	Yes	0.00508	0.00189	1000	298.0
3200	1.24	800	600	25M	15M	Yes	0.00508	0.00189	1500	305.4
3200	1.24	800	600	25M	20M	No	0.00508	0.00198	0	252.1
3200	1.24	800	600	25M	20M	No	0.00508	0.00198	100	256.8
3200	1.24	800	600	25M	20M	No	0.00508	0.00198	250	263.5
3200	1.24	800	600	25M	20M	No	0.00508	0.00198	500	275.8
3200	1.24	800	600	25M	20M	No	0.00508	0.00198	1000	295.7
3200	1.24	800	600	25M	20M	No	0.00508	0.00198	1500	306.4
3200	1.24	800	600	25M	20M	Yes	0.00508	0.00255	0	255.3
3200	1.24	800	600	25M	20M	Yes	0.00508	0.00255	100	258.9
3200	1.24	800	600	25M	20M	Yes	0.00508	0.00255	250	261.8
3200	1.24	800	600	25M	20M	Yes	0.00508	0.00255	500	279.1
3200	1.24	800	600	25M	20M	Yes	0.00508	0.00255	1000	300.8
3200	1.24	800	600	25M	20M	Yes	0.00508	0.00255	1500	308.3
3200	1.24	800	600	30M	10M	No	0.00711	0.00066	0	267.1
3200	1.24	800	600	30M	10M	No	0.00711	0.00066	100	269.0
3200	1.24	800	600	30M	10M	No	0.00711	0.00066	250	266.5
3200	1.24	800	600	30M	10M	No	0.00711	0.00066	500	278.3
3200	1.24	800	600	30M	10M	No	0.00711	0.00066	1000	292.6
3200	1.24	800	600	30M	10M	No	0.00711	0.00066	1500	303.2
3200	1.24	800	600	30M	10M	Yes	0.00711	0.00123	0	272.6
3200	1.24	800	600	30M	10M	Yes	0.00711	0.00123	100	229.4
3200	1.24	800	600	30M	10M	Yes	0.00711	0.00123	250	272.4
3200	1.24	800	600	30M	10M	Yes	0.00711	0.00123	500	285.2
3200	1.24	800	600	30M	10M	Yes	0.00711	0.00123	1000	299.0
3200	1.24	800	600	30M	10M	Yes	0.00711	0.00123	1500	307.3
3200	1.24	800	600	30M	15M	No	0.00711	0.00132	0	273.0
3200	1.24	800	600	30M	15M	No	0.00711	0.00132	100	267.2
3200	1.24	800	600	30M	15M	No	0.00711	0.00132	250	273.1
3200	1.24	800	600	30M	15M	No	0.00711	0.00132	500	284.3

Wall Height (mm)	Aspect Ratio	Reinforcement Spacing (mm)		Reinforcement Size		Bed-Joint Reinforcement	Reinforcement Ratio		Axial Stress (kPa)	Load Capacity (kN)
		Horizontal	Vertical	Horizontal	Vertical		Horizontal	Vertical		
3200	1.24	800	600	30M	15M	No	0.00711	0.00132	1000	299.8
3200	1.24	800	600	30M	15M	No	0.00711	0.00132	1500	308.6
3200	1.24	800	600	30M	15M	Yes	0.00711	0.00189	0	278.4
3200	1.24	800	600	30M	15M	Yes	0.00711	0.00189	100	276.5
3200	1.24	800	600	30M	15M	Yes	0.00711	0.00189	250	263.7
3200	1.24	800	600	30M	15M	Yes	0.00711	0.00189	500	290.7
3200	1.24	800	600	30M	15M	Yes	0.00711	0.00189	1000	303.7
3200	1.24	800	600	30M	15M	Yes	0.00711	0.00189	1500	312.0
3200	1.24	800	600	30M	20M	No	0.00711	0.00198	0	277.3
3200	1.24	800	600	30M	20M	No	0.00711	0.00198	100	278.3
3200	1.24	800	600	30M	20M	No	0.00711	0.00198	250	277.0
3200	1.24	800	600	30M	20M	No	0.00711	0.00198	500	289.1
3200	1.24	800	600	30M	20M	No	0.00711	0.00198	1000	303.1
3200	1.24	800	600	30M	20M	No	0.00711	0.00198	1500	311.4
3200	1.24	800	600	30M	20M	Yes	0.00711	0.00255	0	282.3
3200	1.24	800	600	30M	20M	Yes	0.00711	0.00255	100	235.4
3200	1.24	800	600	30M	20M	Yes	0.00711	0.00255	250	276.8
3200	1.24	800	600	30M	20M	Yes	0.00711	0.00255	500	294.1
3200	1.24	800	600	30M	20M	Yes	0.00711	0.00255	1000	306.8
3200	1.24	800	600	30M	20M	Yes	0.00711	0.00255	1500	315.3

APPENDIX B: PARAMETRIC ANALYSIS RESULTS (PLOTS)

Figures B.1 through B.90 presents the predicted load capacity – applied axial stress plots for the complete parametric study dataset. Each plot contains the results for different vertical reinforcement spacings (s_v). Specimen identification labels are as follows:

WHaaaa-BBbbbb-ccM-ddM-BJe

Where:

aaaa = Wall Height in mm (1600 mm, 2400 mm, or 3200 mm)

bbbb = Bond Beam Spacing in mm (400 mm, 800 mm, or 1200 mm)

cc = Size of the Vertical Reinforcement (20M, 25M, or 30M)

dd = Size of the Horizontal Reinforcement (10M, 15M, or 20M)

e = The Presence of Bed-Joint Reinforcement (Y = Yes, N = No)

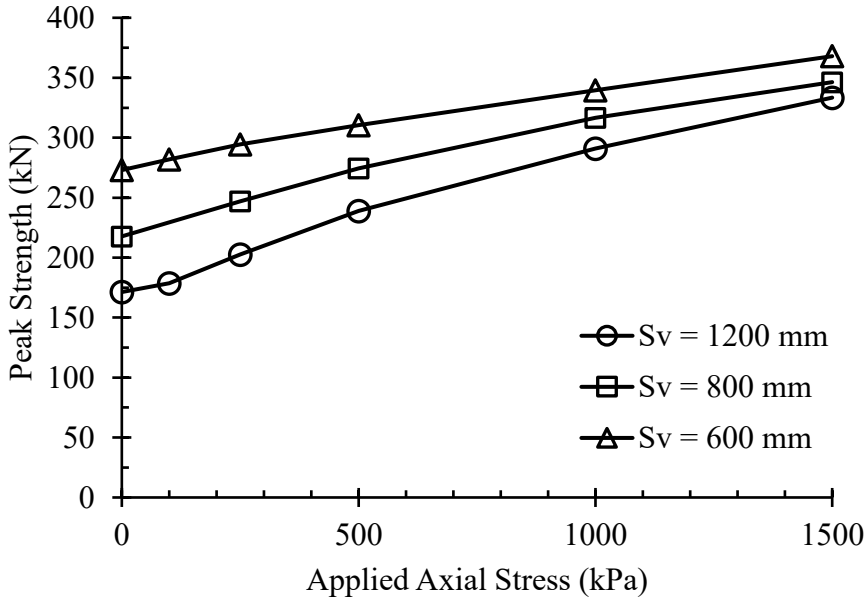

Figure B.1 – Parametric Results (WH1600-BB800-20M-10M-BJN)

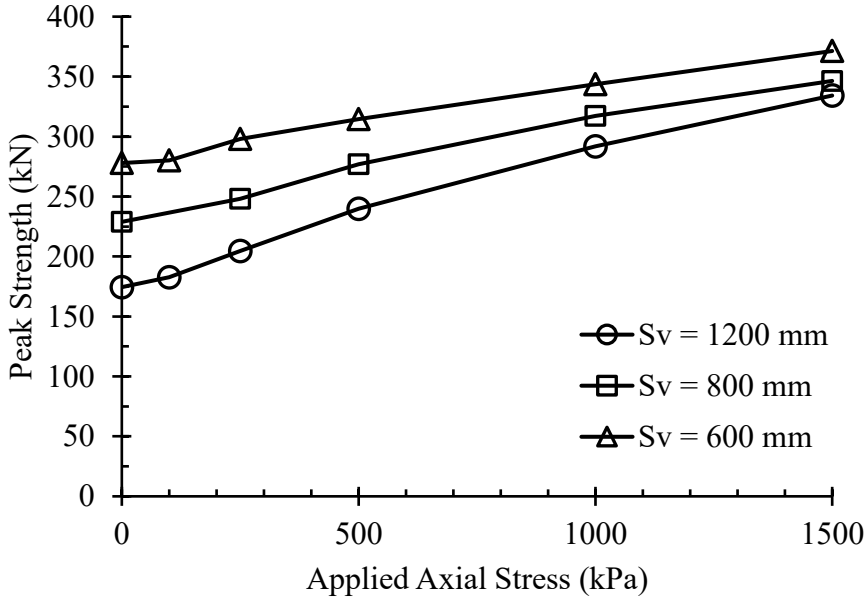

Figure B.2 – Parametric Results (WH1600-BB800-20M-10M-BJY)

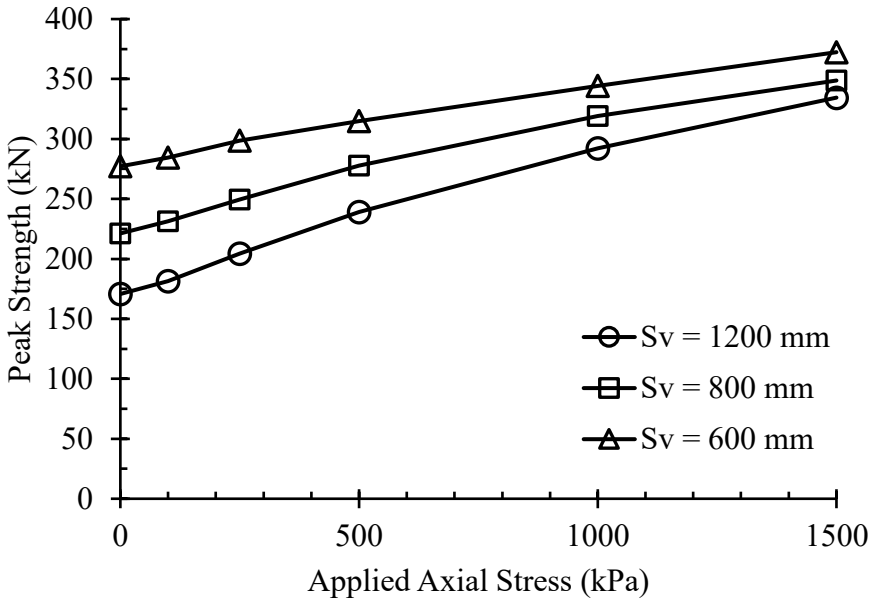

Figure B.3 – Parametric Results (WH1600-BB800-20M-15M-BJN)

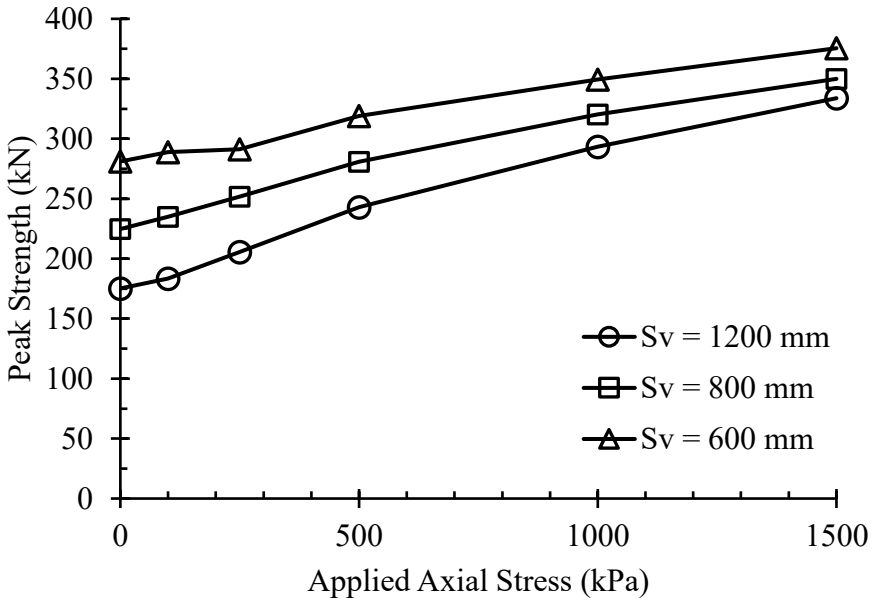

Figure B.4 – Parametric Results (WH1600-BB800-20M-15M-BJY)

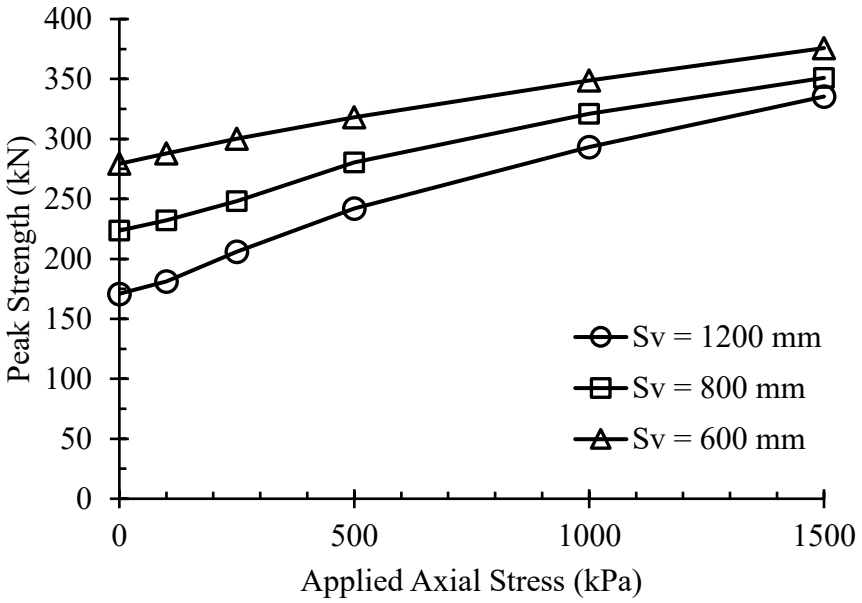

Figure B.5 – Parametric Results (WH1600-BB800-20M-20M-BJN)

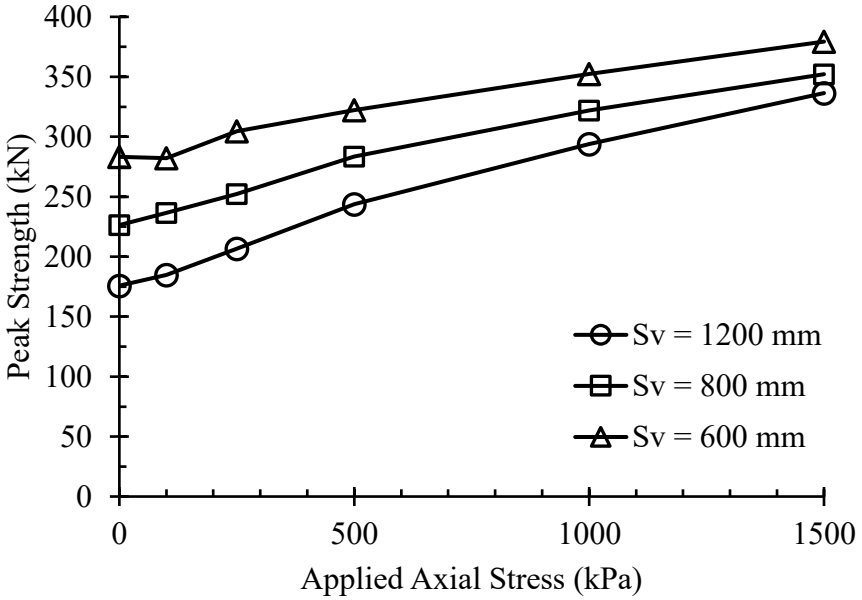

Figure B.6 – Parametric Results (WH1600-BB800-20M-20M-BJY)

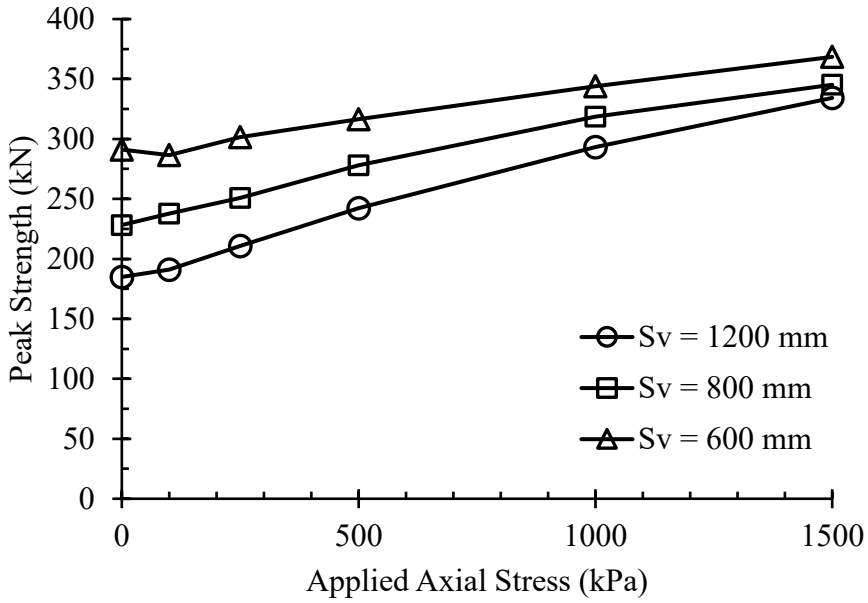

Figure B.7 – Parametric Results (WH1600-BB800-25M-10M-BJN)

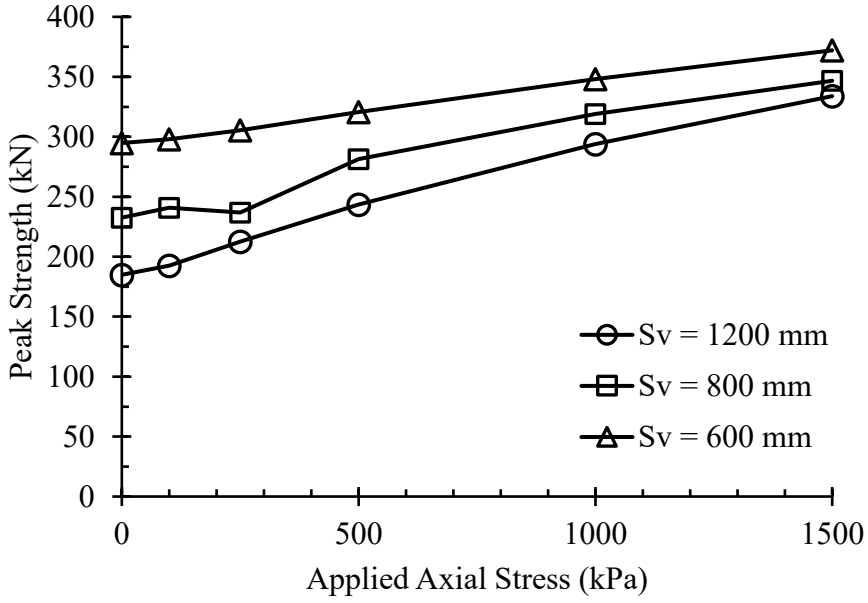

Figure B.8 – Parametric Results (WH1600-BB800-25M-10M-BJY)

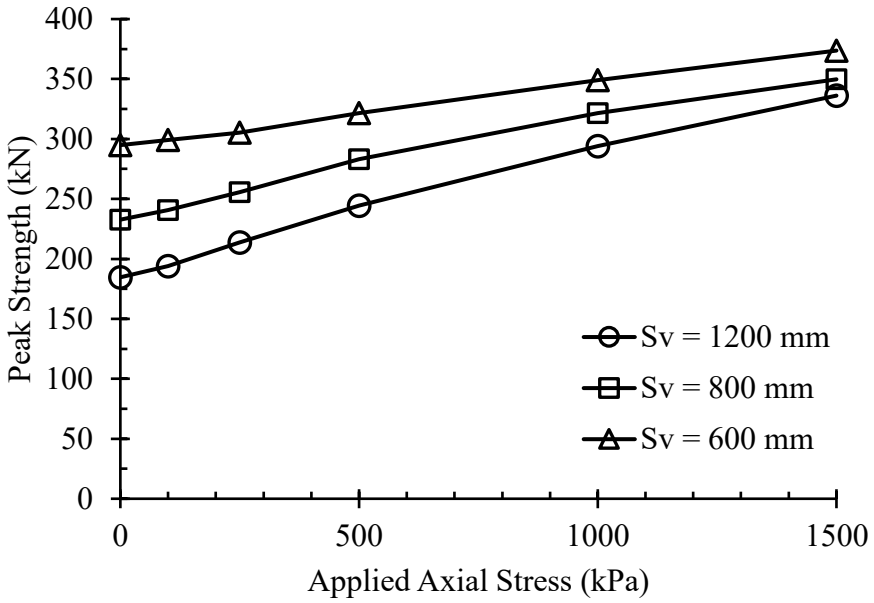

Figure B.9 – Parametric Results (WH1600-BB800-25M-15M-BJN)

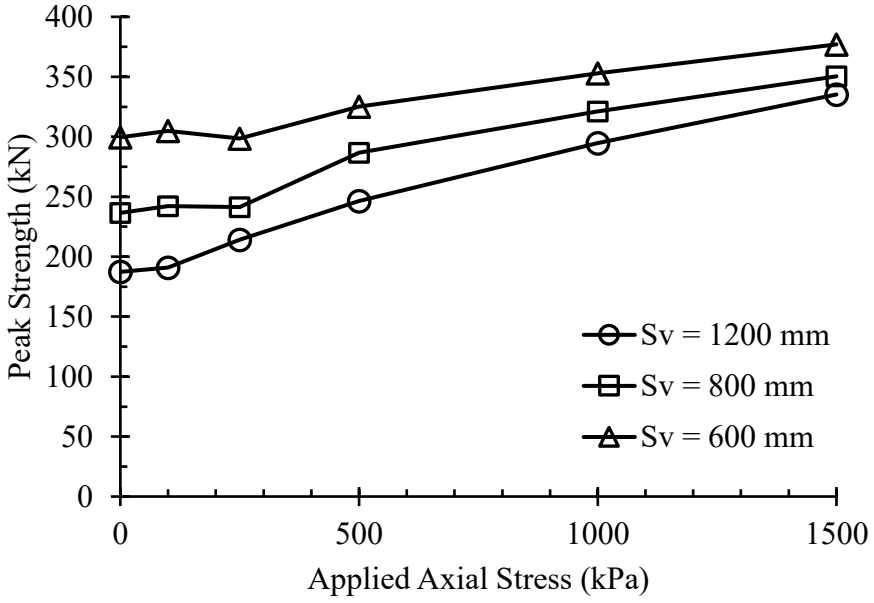

Figure B.10 – Parametric Results (WH1600-BB800-25M-15M-BJY)

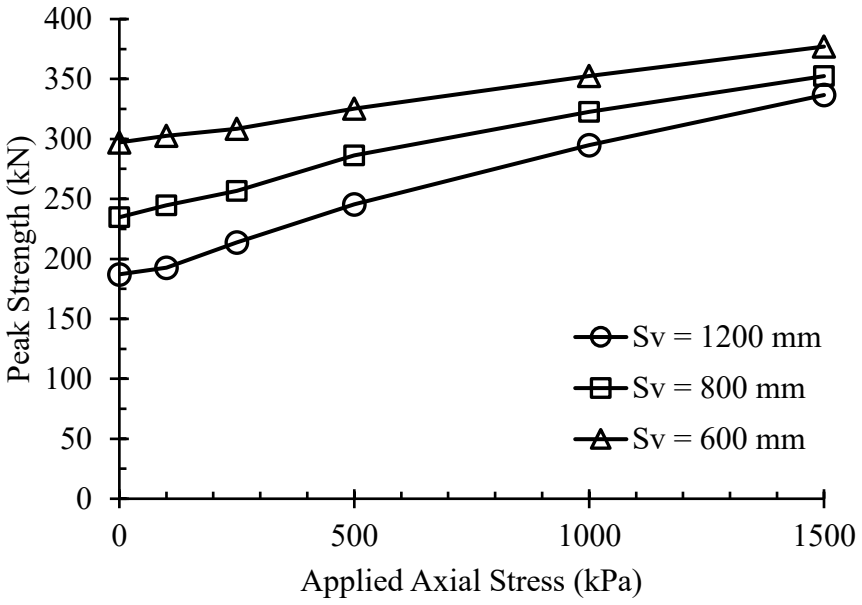

Figure B.11 – Parametric Results (WH1600-BB800-25M-20M-BJN)

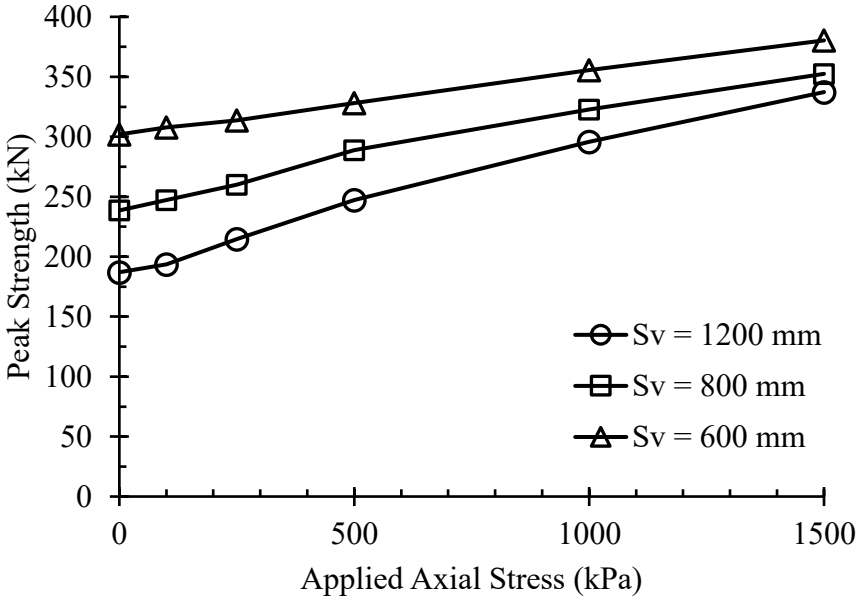

Figure B.12 – Parametric Results (WH1600-BB800-25M-20M-BJY)

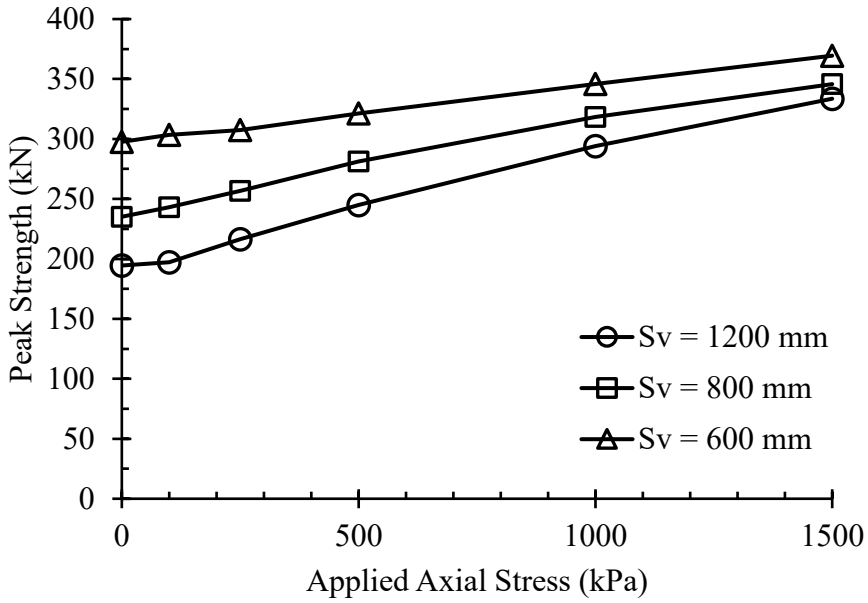

Figure B.13 – Parametric Results (WH1600-BB800-30M-10M-BJN)

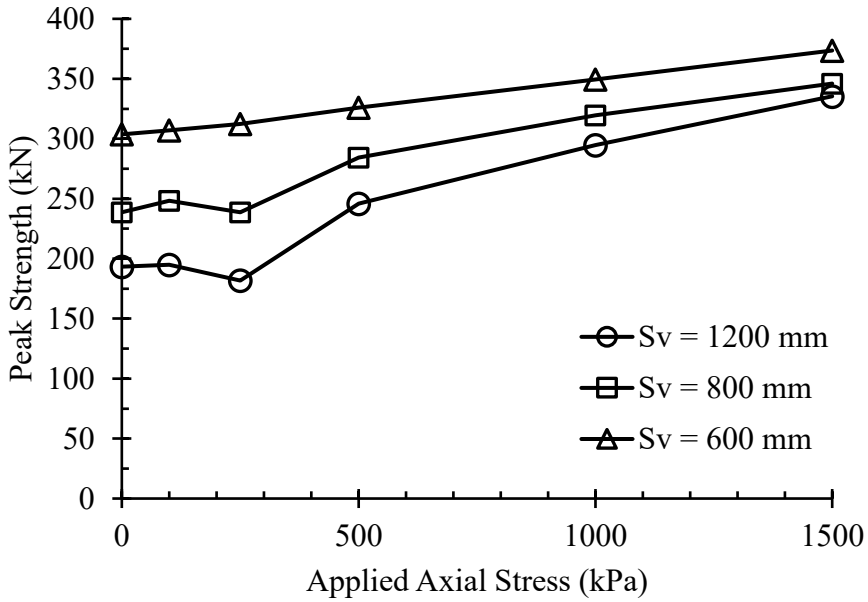

Figure B.14 – Parametric Results (WH1600-BB800-30M-10M-BJY)

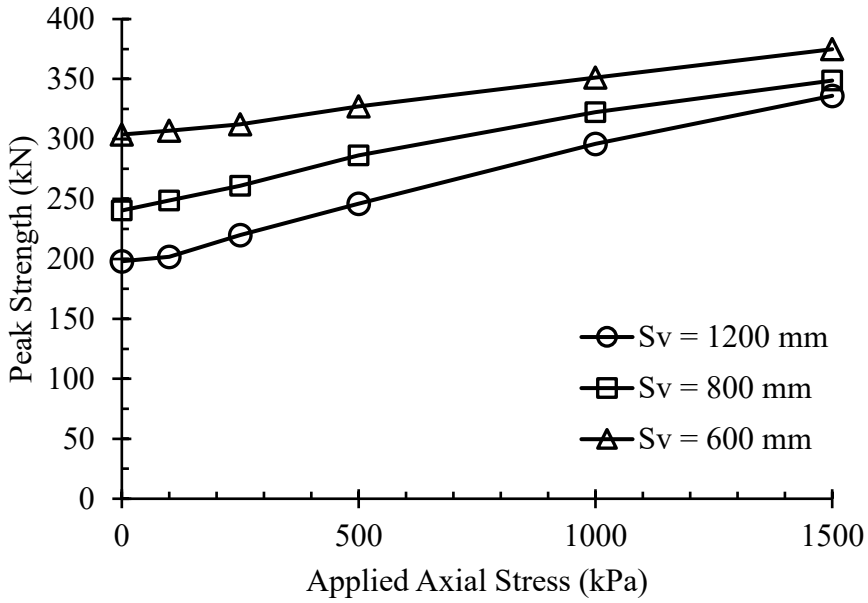

Figure B.15 – Parametric Results (WH1600-BB800-30M-15M-BJN)

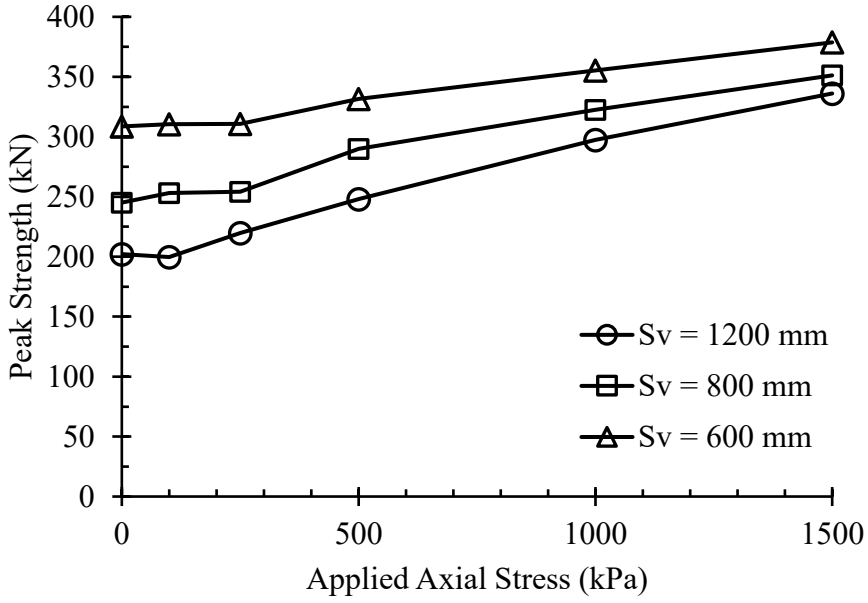

Figure B.16 – Parametric Results (WH1600-BB800-30M-15M-BJY)

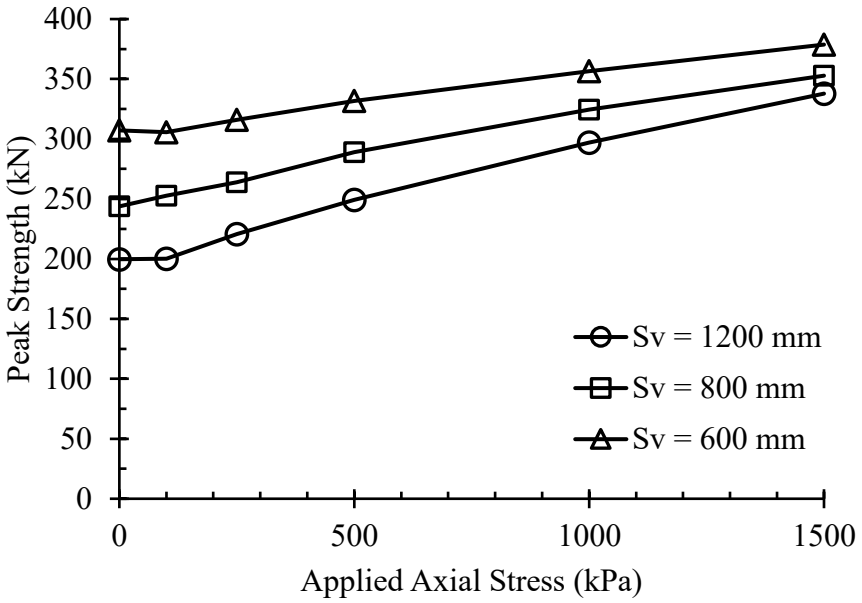

Figure B.17 – Parametric Results (WH1600-BB800-30M-20M-BJN)

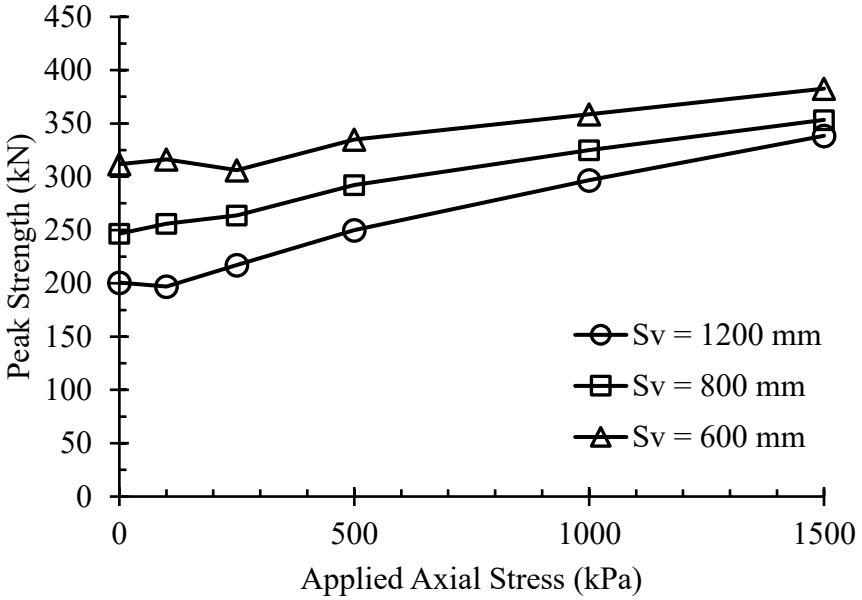

Figure B.18 – Parametric Results (WH1600-BB800-30M-20M-BJY)

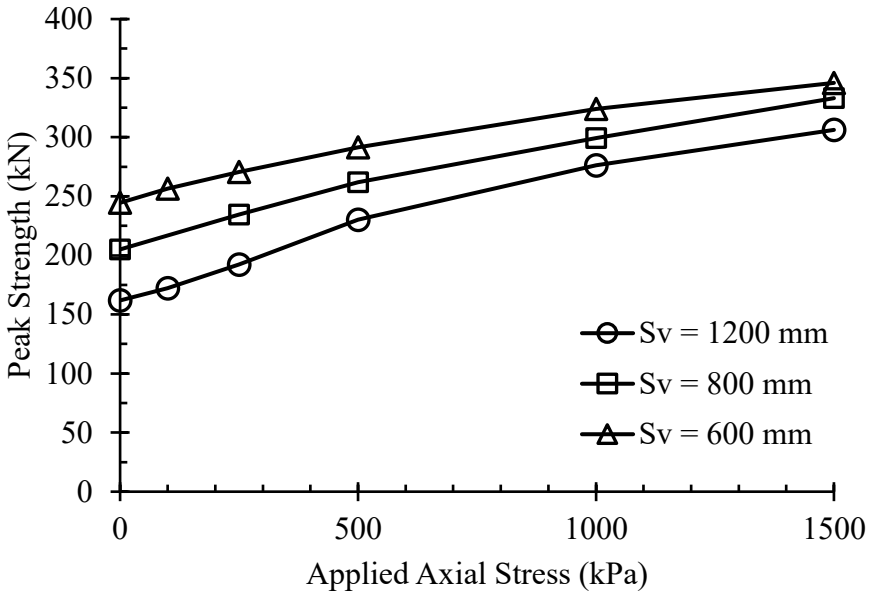

Figure B.19 – Parametric Results (WH2400-BB400-20M-10M-BJN)

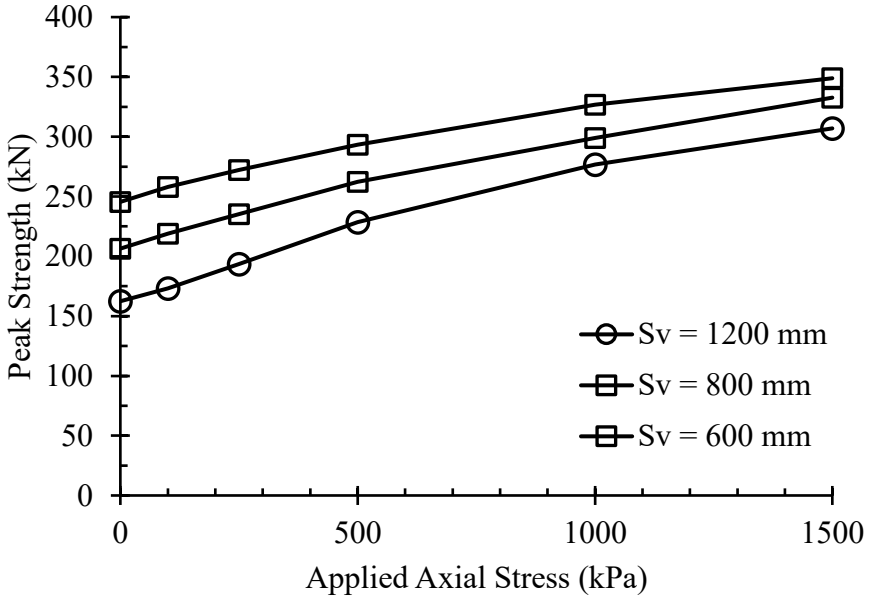

Figure B.20 – Parametric Results (WH2400-BB400-20M-10M-BJY)

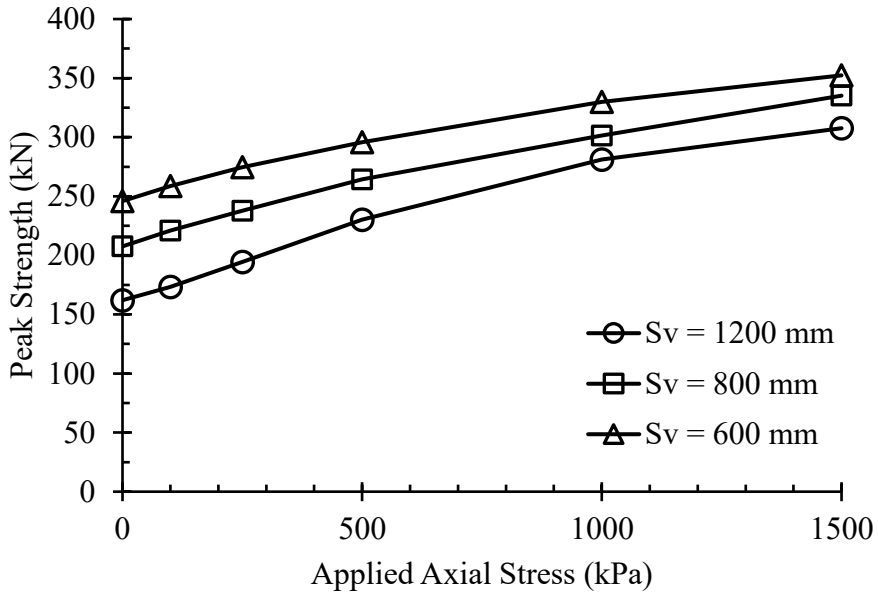

Figure B.21 – Parametric Results (WH2400-BB400-20M-15M-BJN)

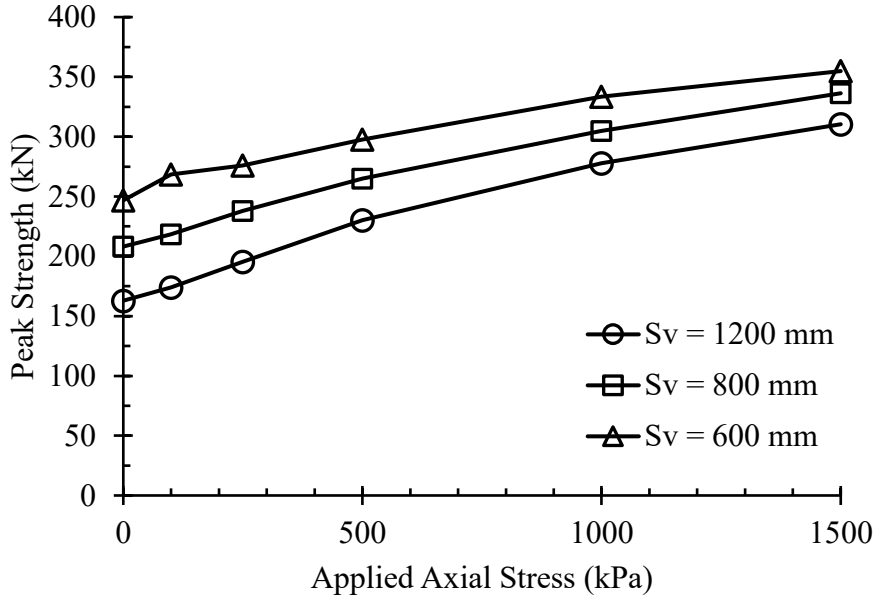

Figure B.22 – Parametric Results (WH2400-BB400-20M-15M-BJY)

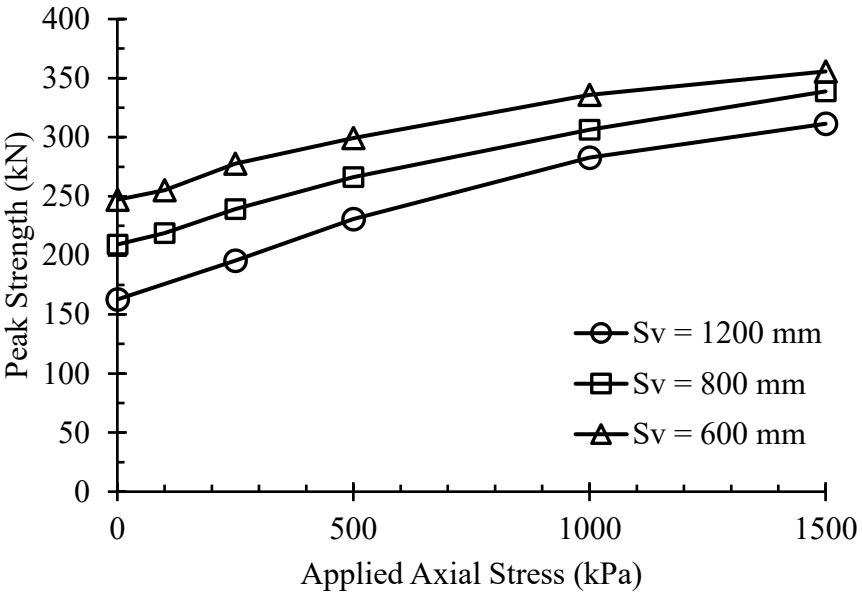

Figure B.23 – Parametric Results (WH2400-BB400-20M-20M-BJN)

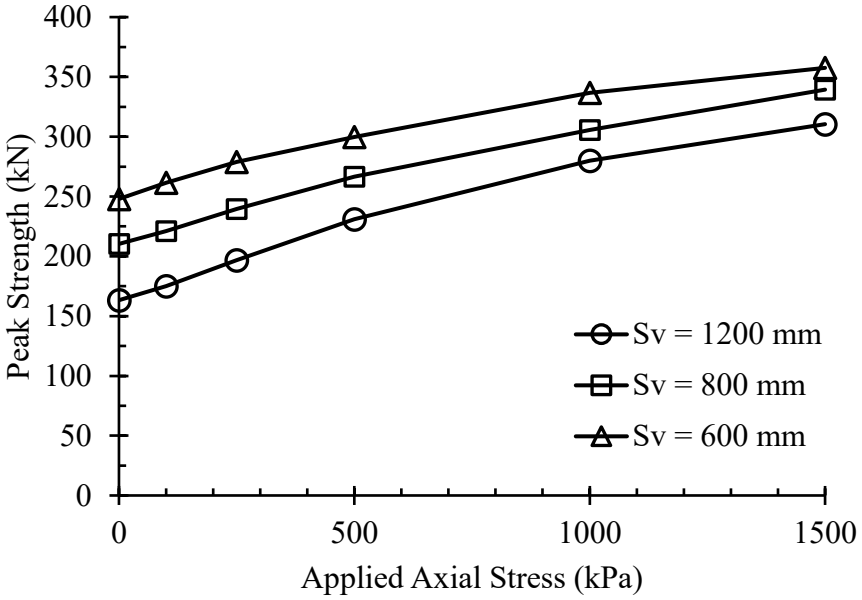

Figure B.24 – Parametric Results (WH2400-BB400-20M-20M-BJY)

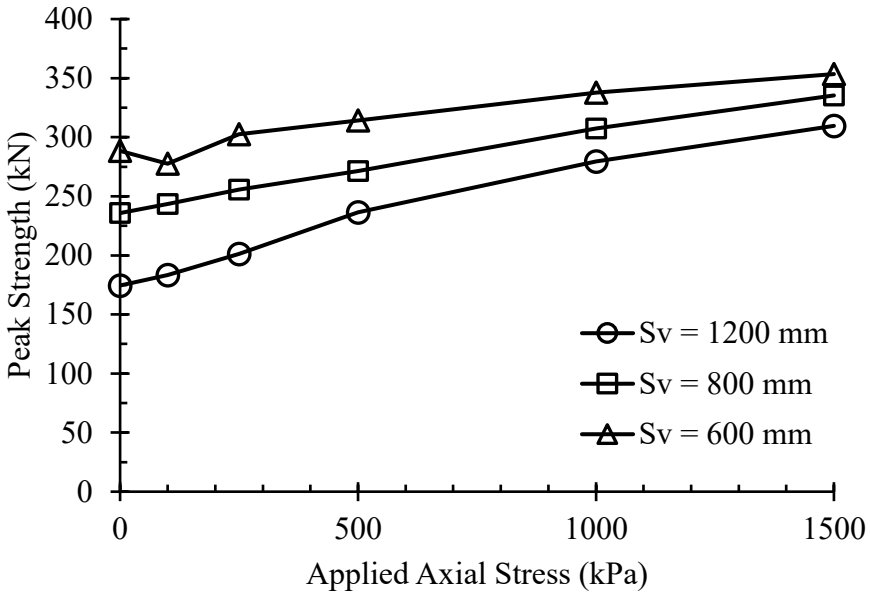

Figure B.25 – Parametric Results (WH2400-BB400-25M-10M-BJN)

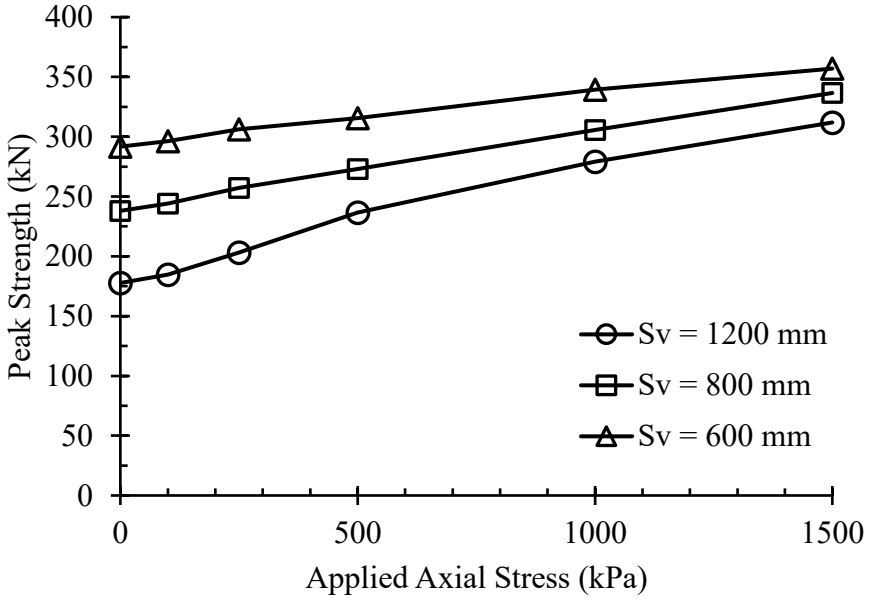

Figure B.26 – Parametric Results (WH2400-BB400-25M-10M-BJY)

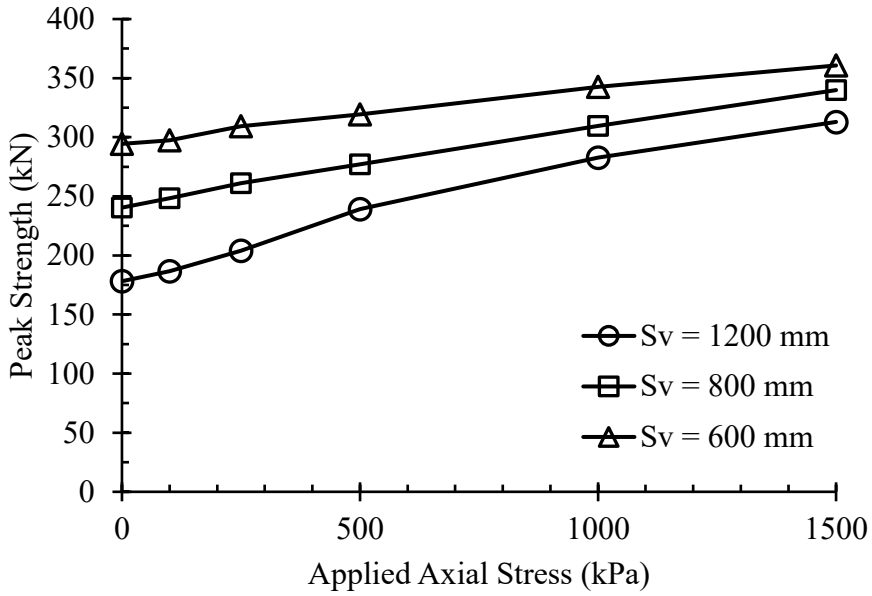

Figure B.27 – Parametric Results (WH2400-BB400-25M-15M-BJN)

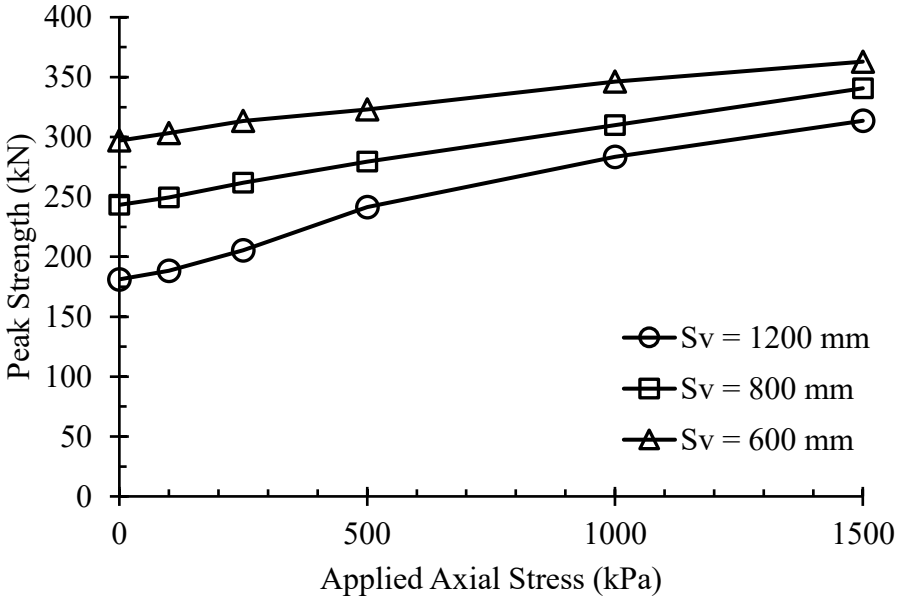

Figure B.28 – Parametric Results (WH2400-BB400-25M-15M-BJY)

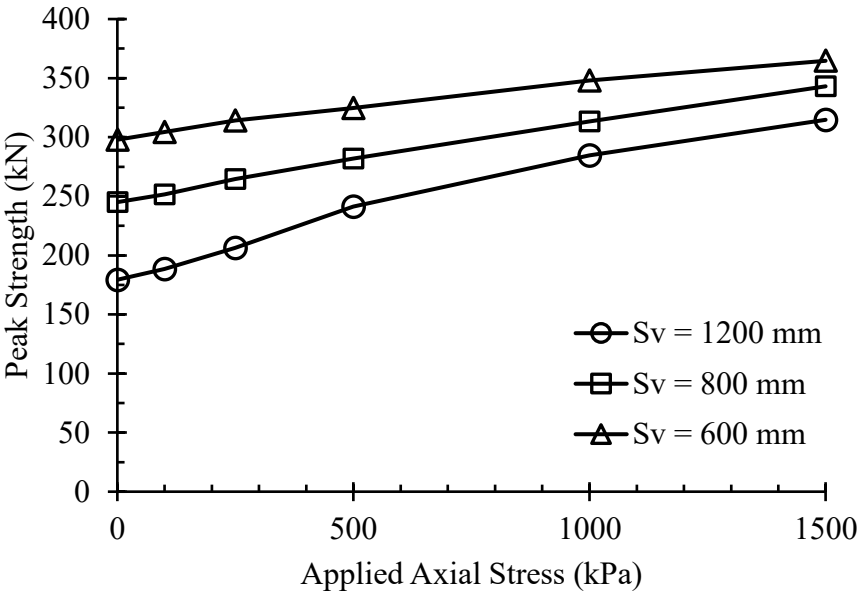

Figure B.29 – Parametric Results (WH2400-BB400-25M-20M-BJN)

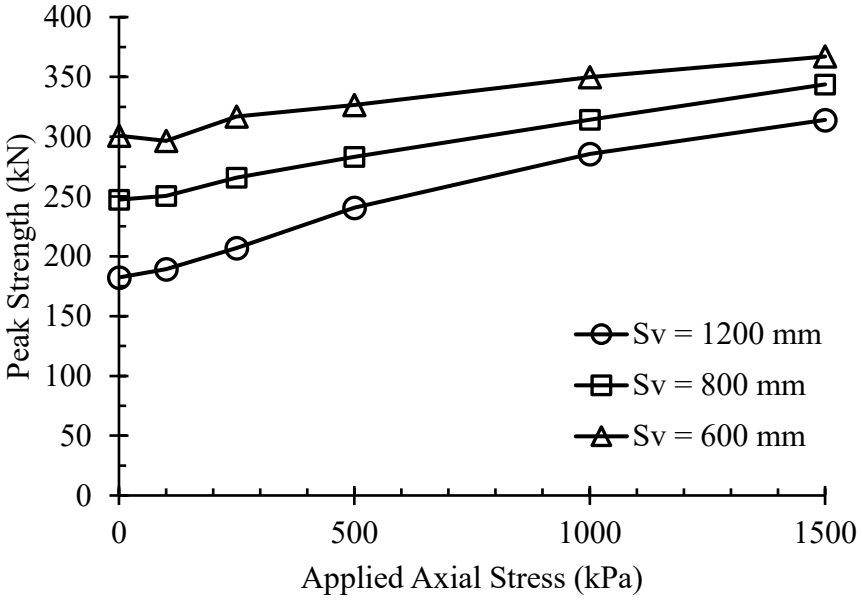

Figure B.30 – Parametric Results (WH2400-BB400-25M-20M-BJY)

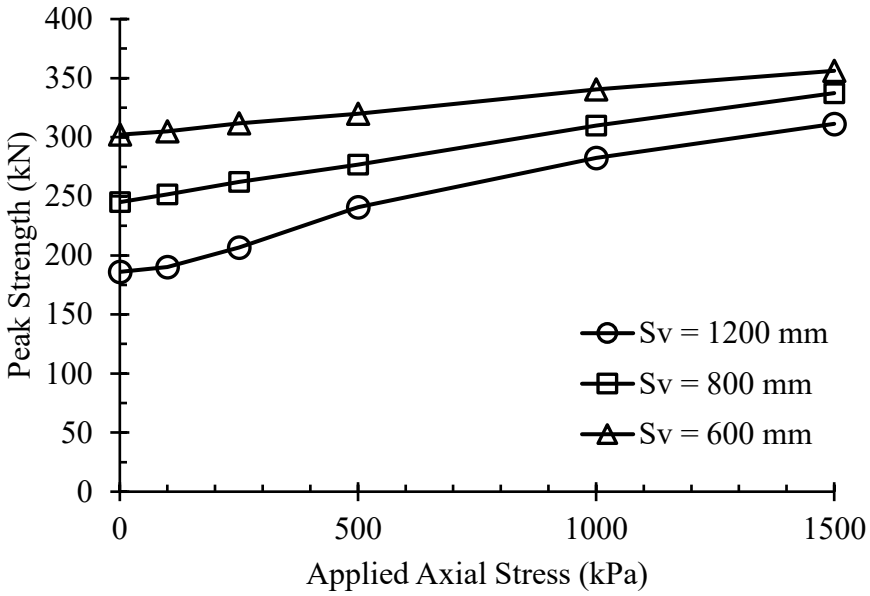

Figure B.31 – Parametric Results (WH2400-BB400-30M-10M-BJN)

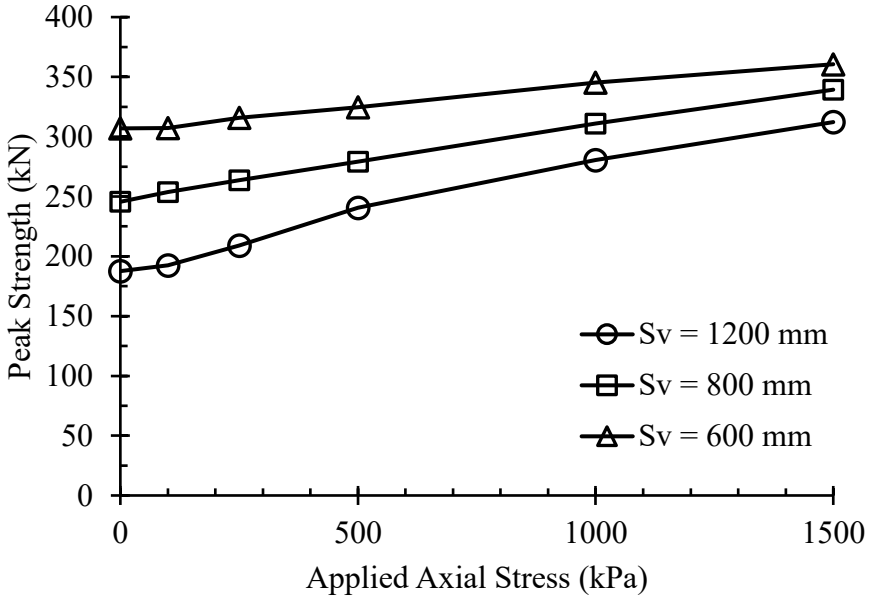

Figure B.32 – Parametric Results (WH2400-BB400-30M-10M-BJY)

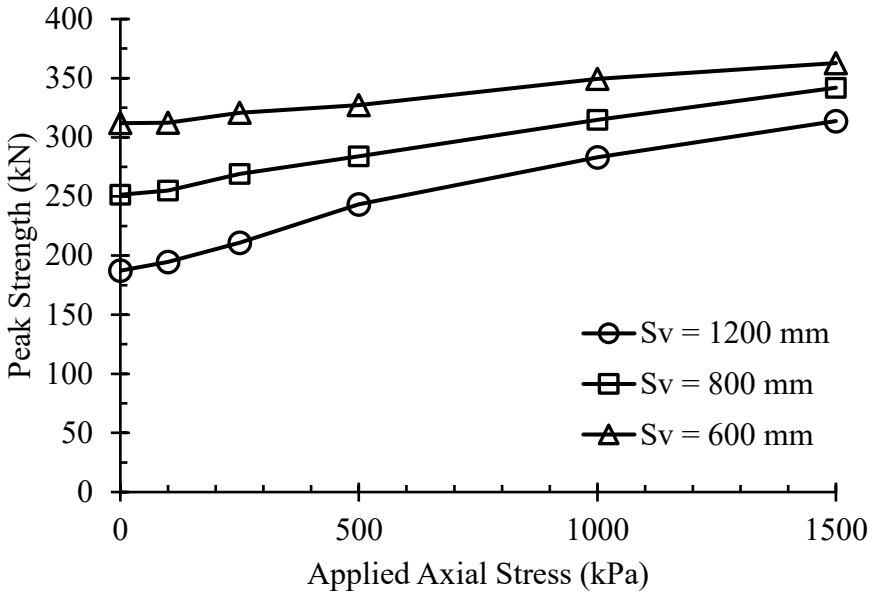

Figure B.33 – Parametric Results (WH2400-BB400-30M-15M-BJN)

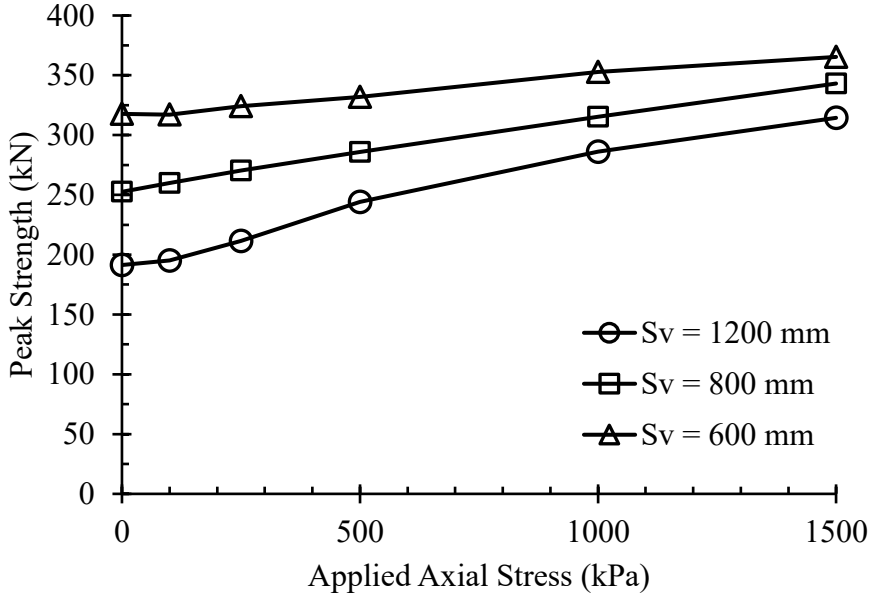

Figure B.34 – Parametric Results (WH2400-BB400-30M-15M-BJY)

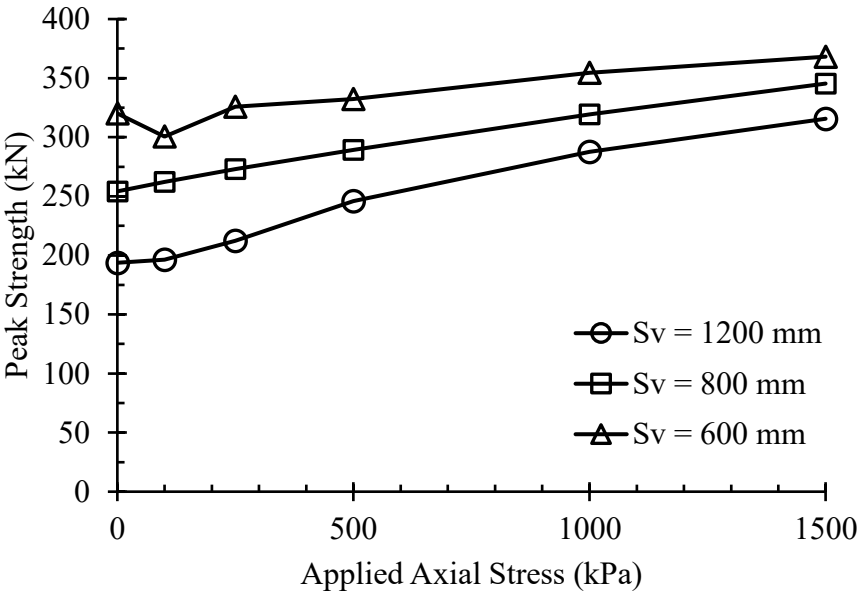

Figure B.35 – Parametric Results (WH2400-BB400-30M-20M-BJN)

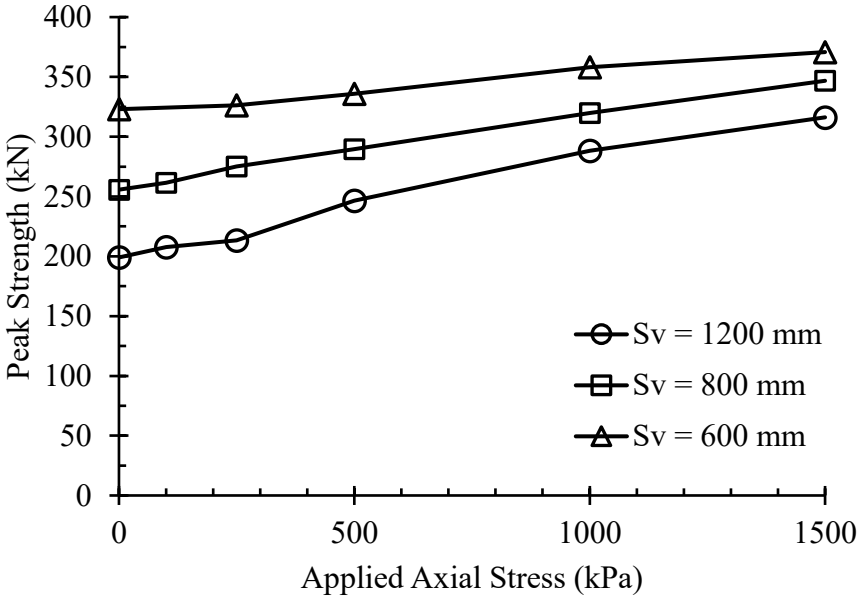

Figure B.36 – Parametric Results (WH2400-BB400-30M-20M-BJY)

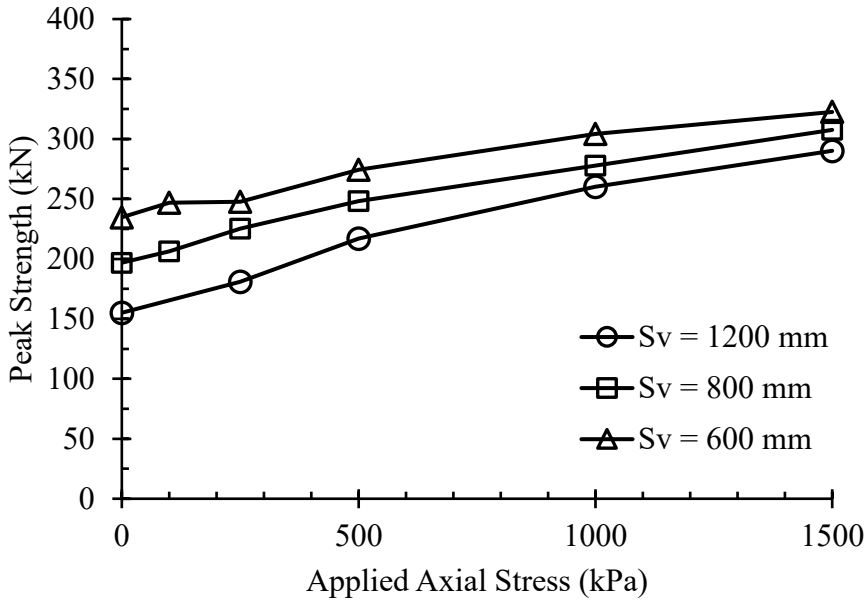

Figure B.37 – Parametric Results (WH2400-BB800-20M-10M-BJN)

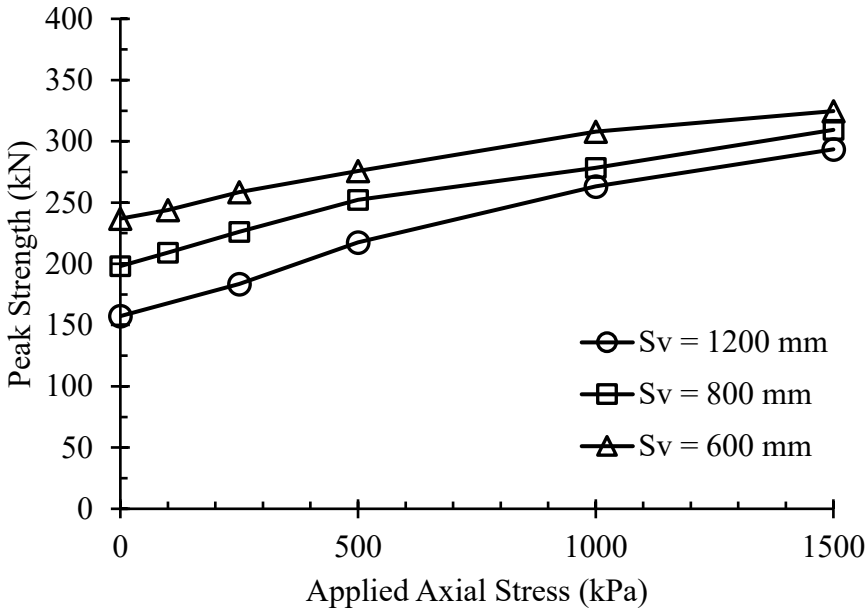

Figure B.38 – Parametric Results (WH2400-BB800-20M-10M-BJY)

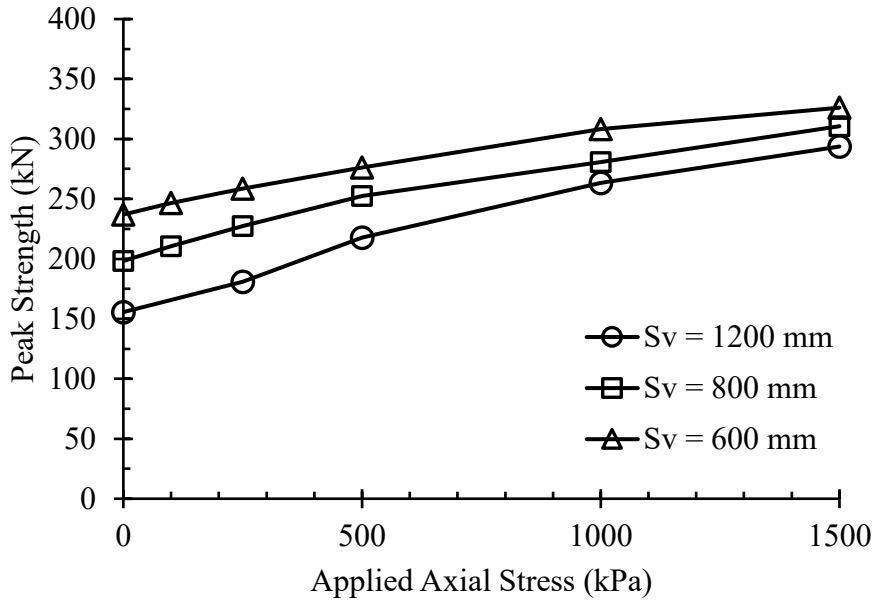

Figure B.39 – Parametric Results (WH2400-BB800-20M-15M-BJN)

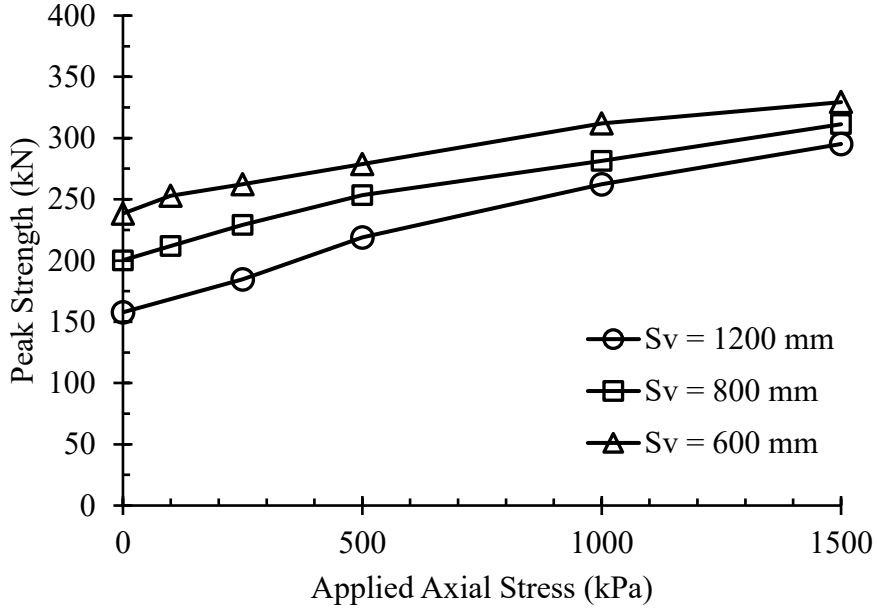

Figure B.40 – Parametric Results (WH2400-BB800-20M-15M-BJY)

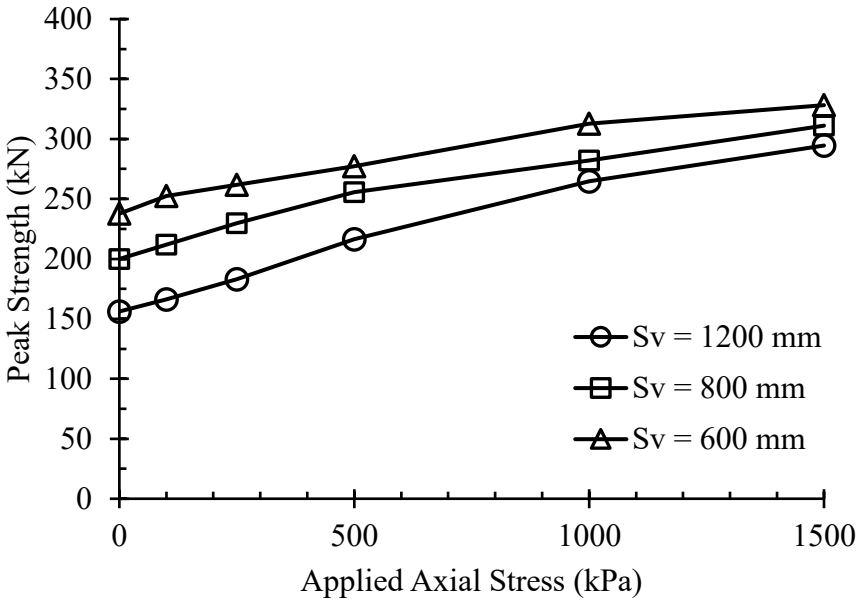

Figure B.41 – Parametric Results (WH2400-BB800-20M-20M-BJN)

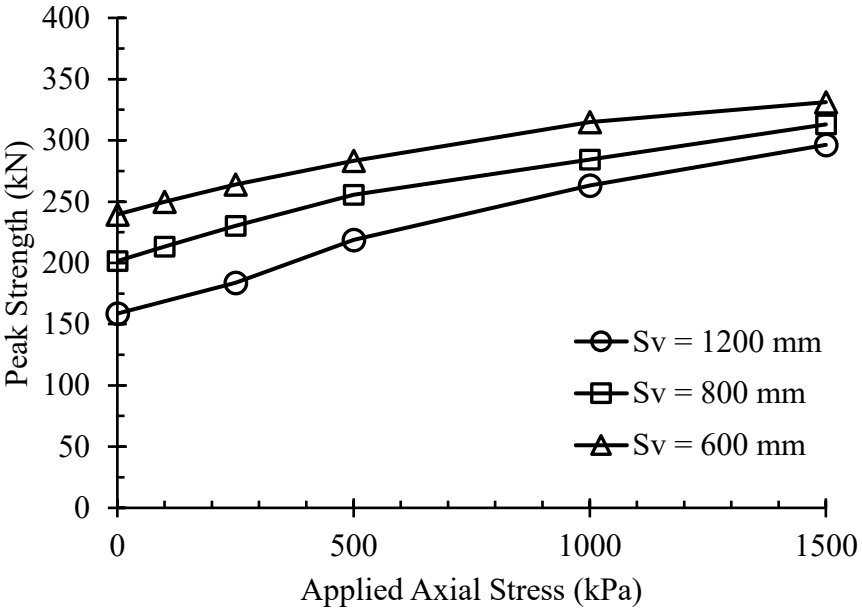

Figure B.42 – Parametric Results (WH2400-BB800-20M-20M-BJY)

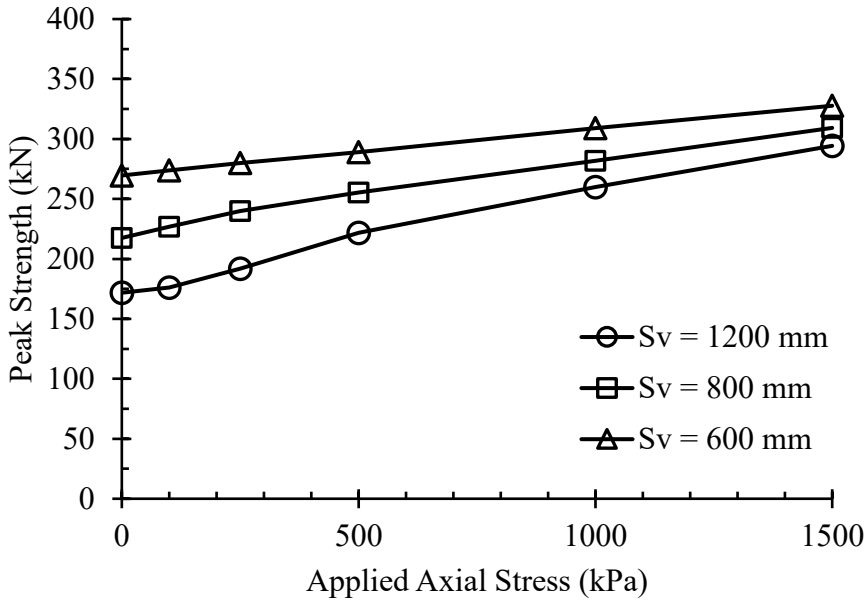

Figure B.43 – Parametric Results (WH2400-BB800-25M-10M-BJN)

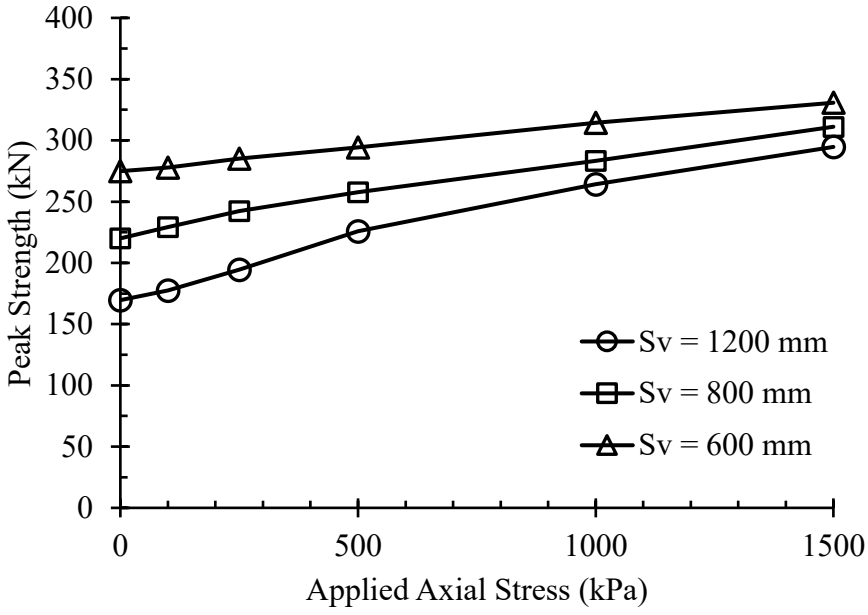

Figure B.44 – Parametric Results (WH2400-BB800-25M-10M-BJY)

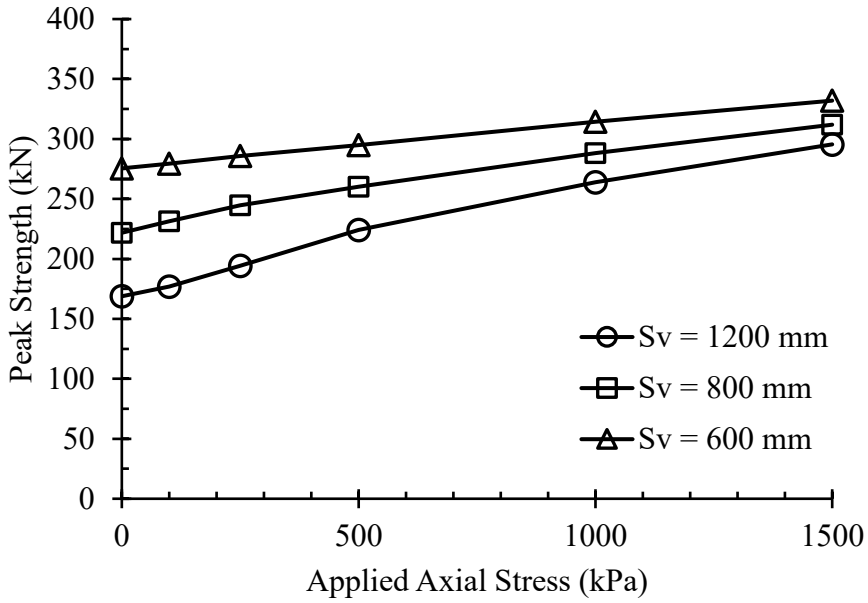

Figure B.45 – Parametric Results (WH2400-BB800-25M-15M-BJN)

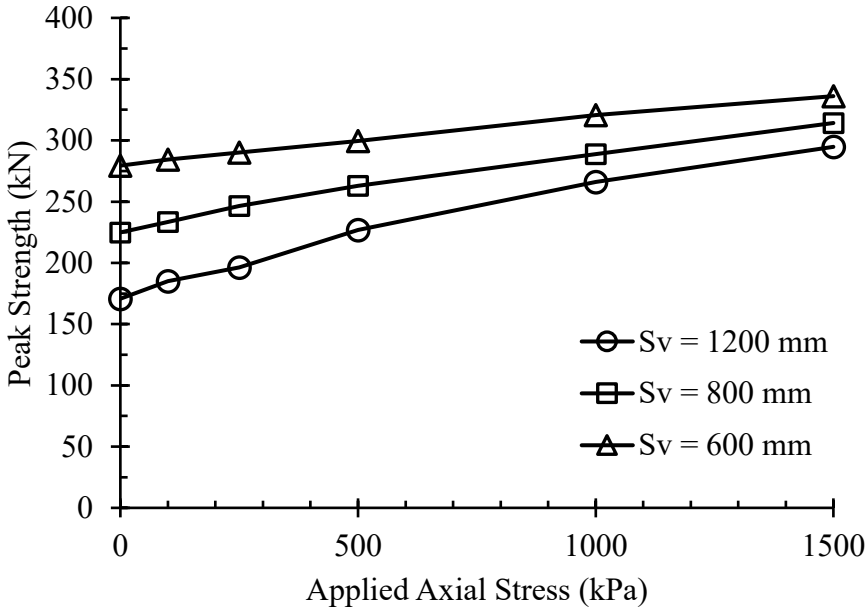

Figure B.46 – Parametric Results (WH2400-BB800-25M-15M-BJY)

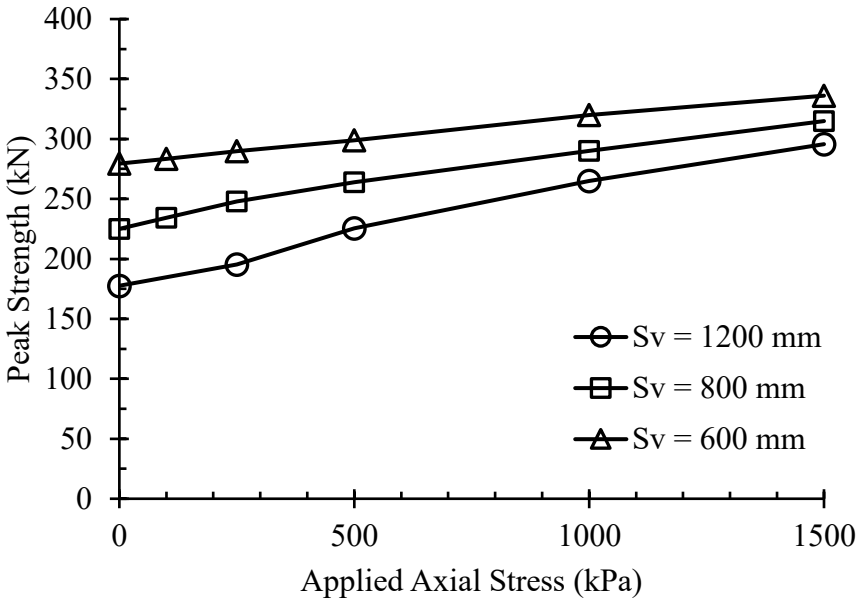

Figure B.47 – Parametric Results (WH2400-BB800-25M-20M-BJN)

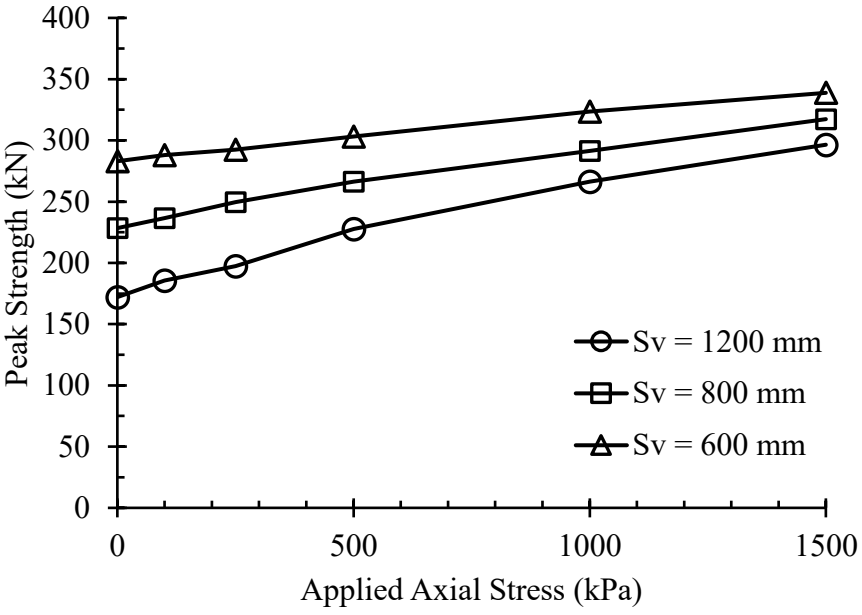

Figure B.48 – Parametric Results (WH2400-BB800-25M-20M-BJY)

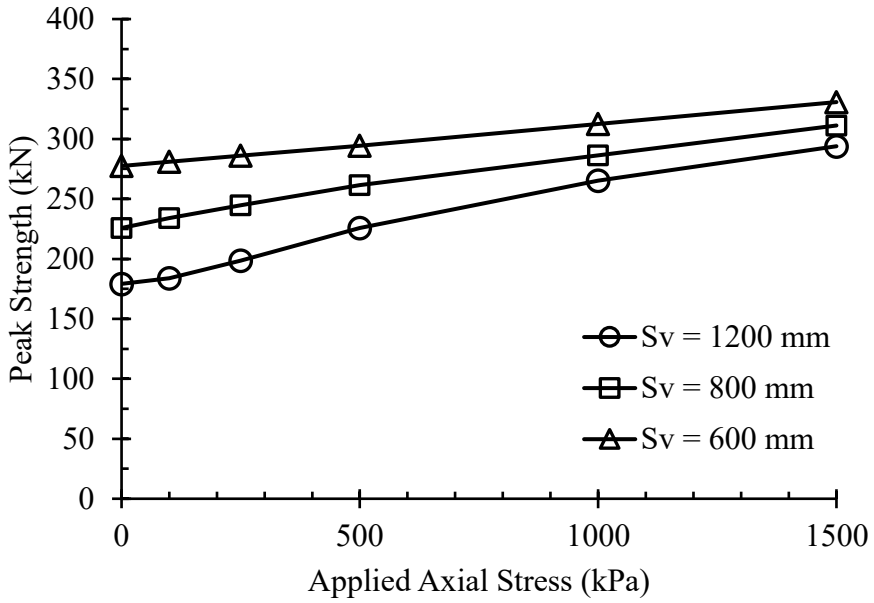

Figure B.49 – Parametric Results (WH2400-BB800-30M-10M-BJN)

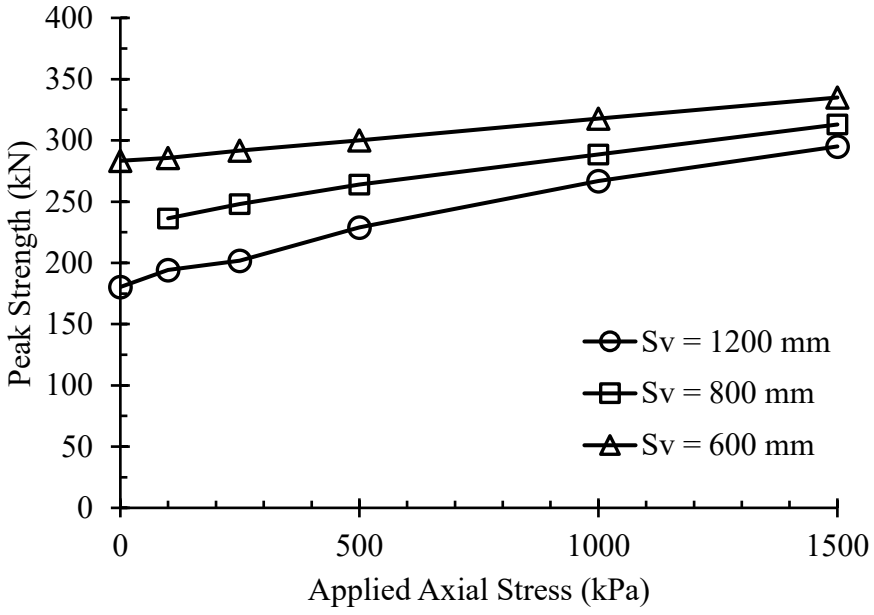

Figure B.50 – Parametric Results (WH2400-BB800-30M-10M-BJY)

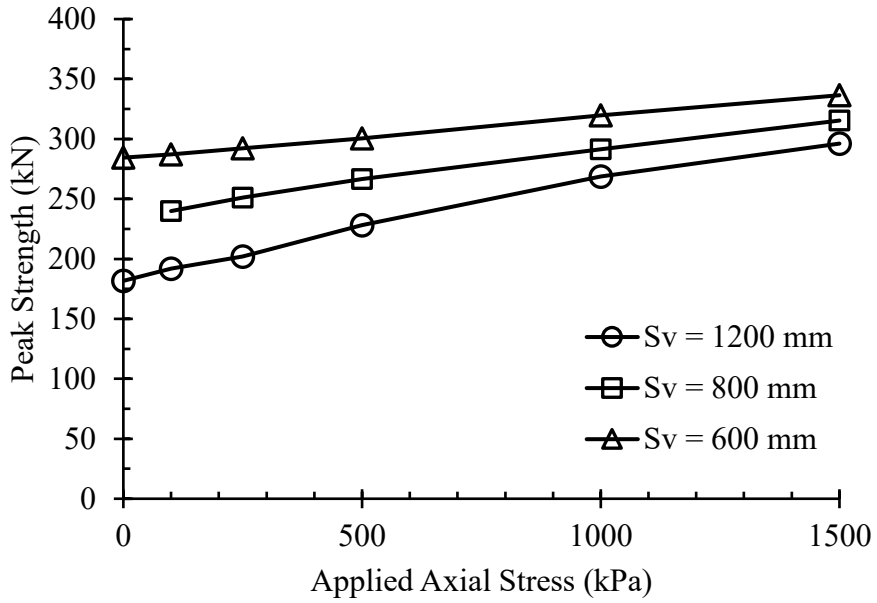

Figure B.51 – Parametric Results (WH2400-BB800-30M-15M-BJN)

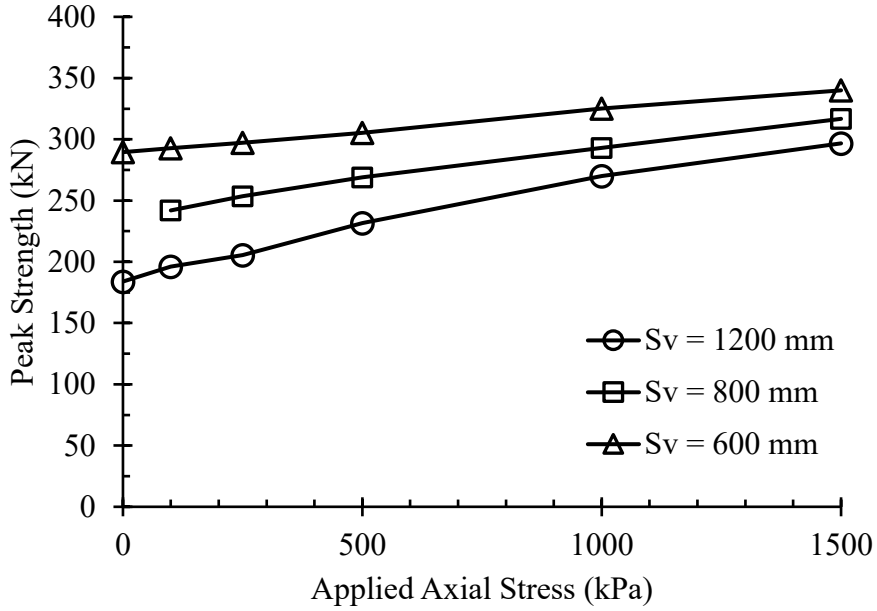

Figure B.52 – Parametric Results (WH2400-BB800-30M-15M-BJY)

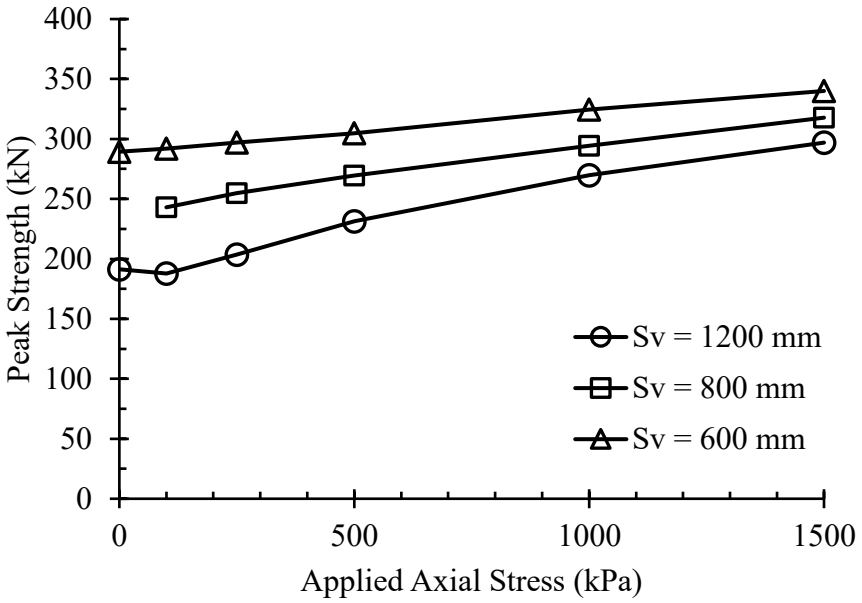

Figure B.53 – Parametric Results (WH2400-BB800-30M-20M-BJN)

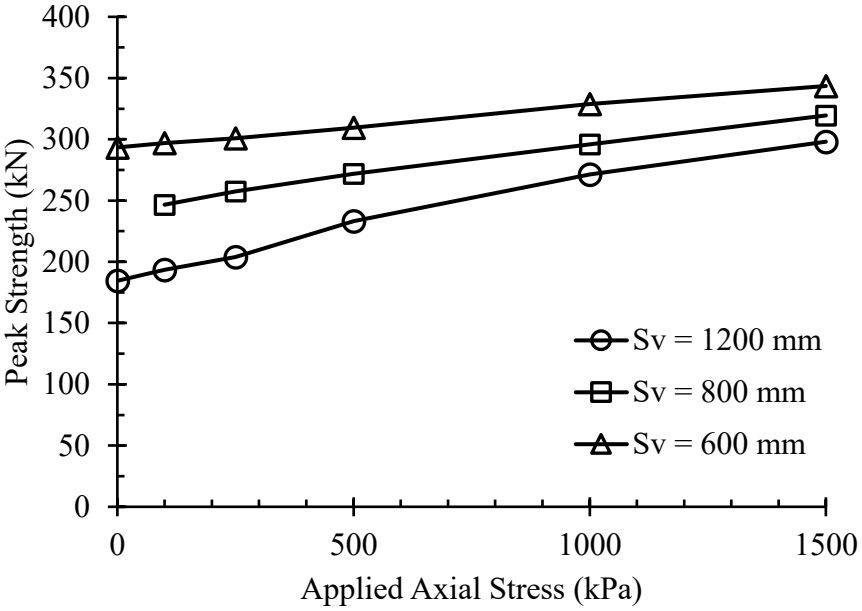

Figure B.54 – Parametric Results (WH2400-BB800-30M-20M-BJY)

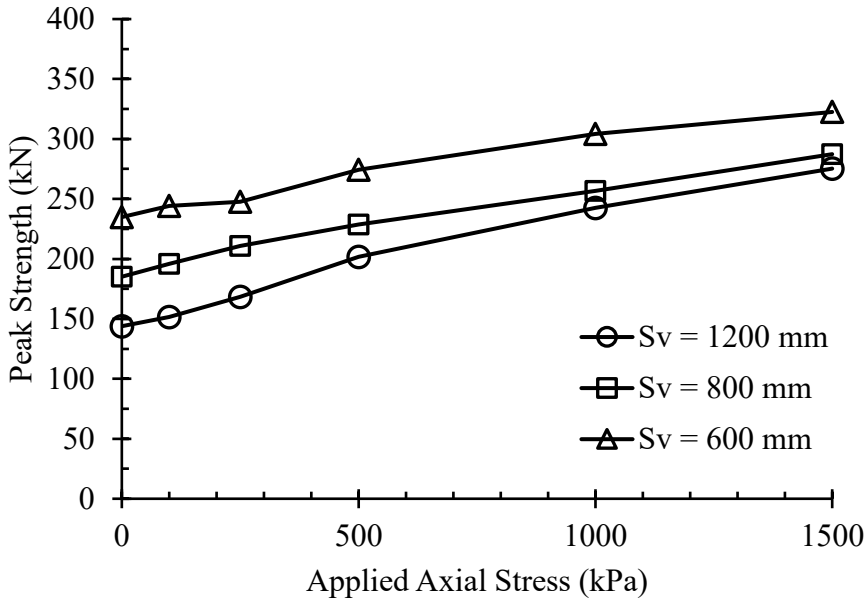

Figure B.55 – Parametric Results (WH2400-BB1200-20M-10M-BJN)

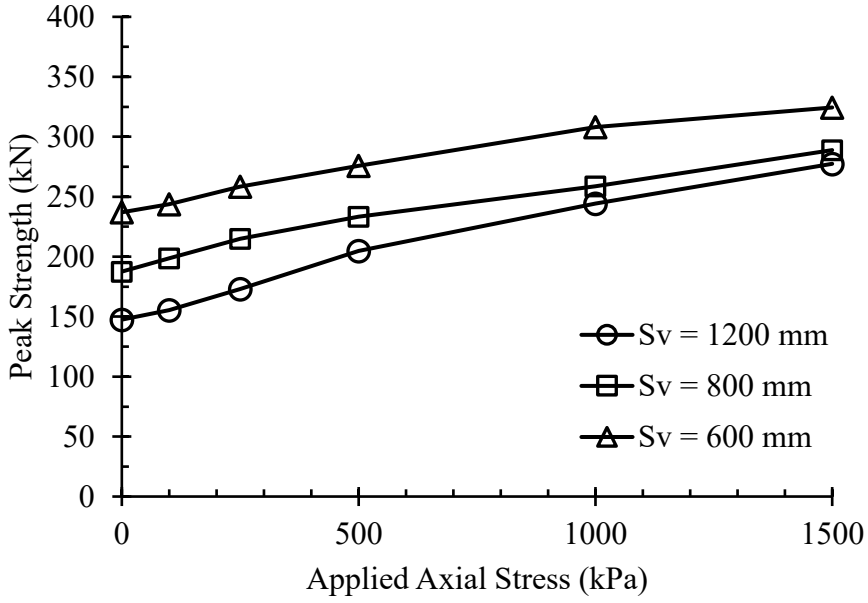

Figure B.56 – Parametric Results (WH2400-BB1200-20M-10M-BJY)

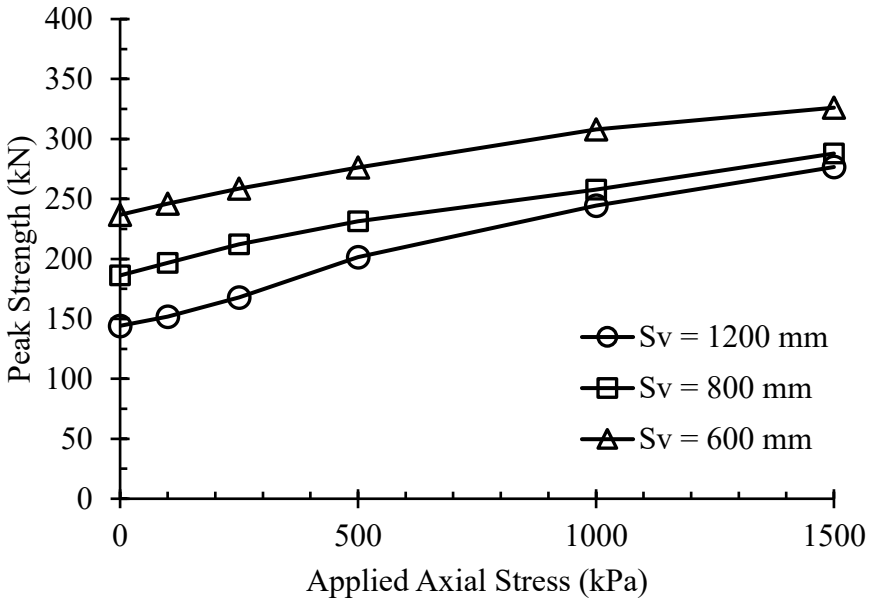

Figure B.57 – Parametric Results (WH2400-BB1200-20M-15M-BJN)

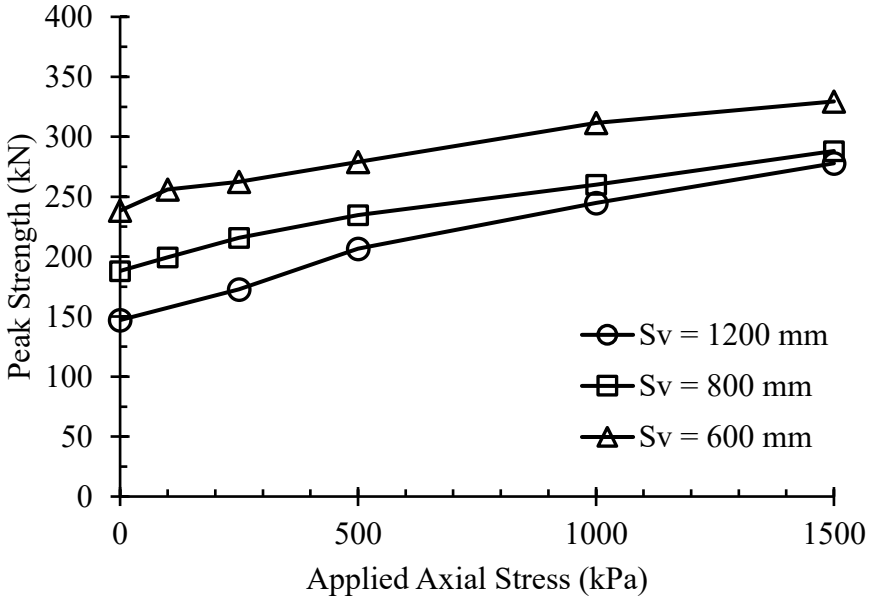

Figure B.58 – Parametric Results (WH2400-BB1200-20M-15M-BJY)

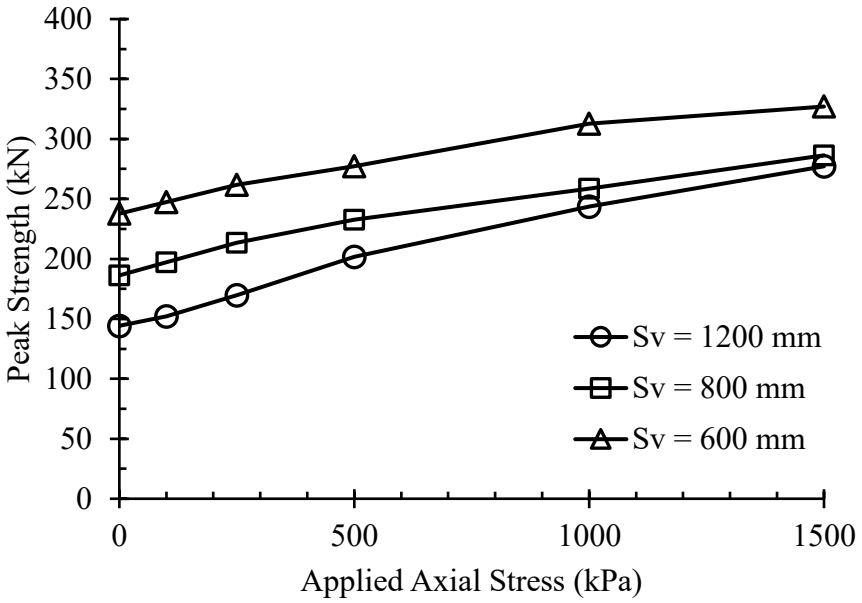

Figure B.59 – Parametric Results (WH2400-BB1200-20M-20M-BJN)

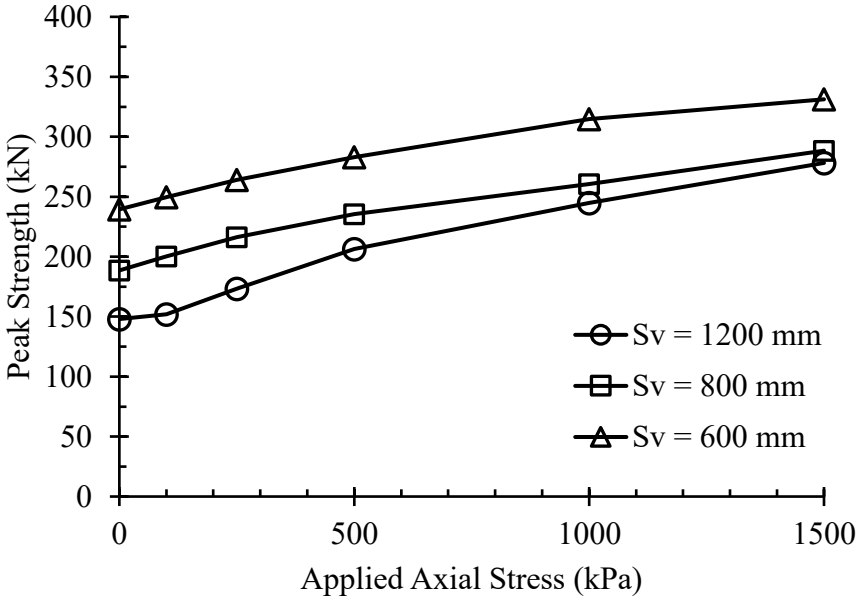

Figure B.60 – Parametric Results (WH2400-BB1200-20M-20M-BJY)

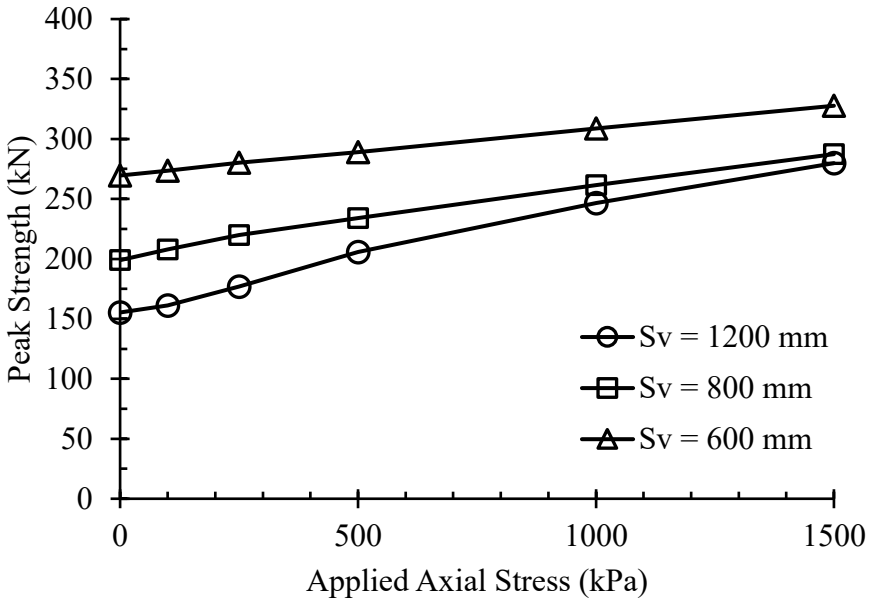

Figure B.61 – Parametric Results (WH2400-BB1200-25M-10M-BJN)

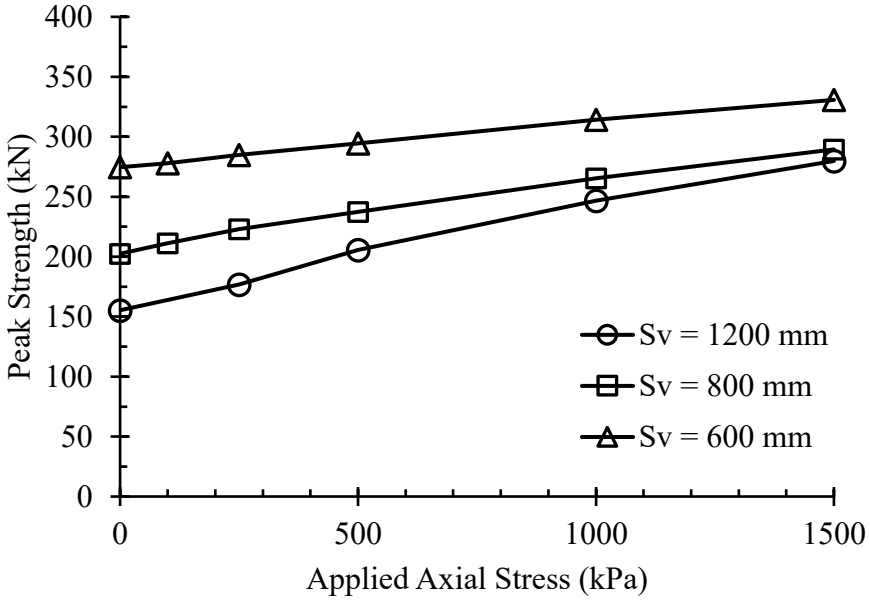

Figure B.62 – Parametric Results (WH2400-BB1200-25M-10M-BJY)

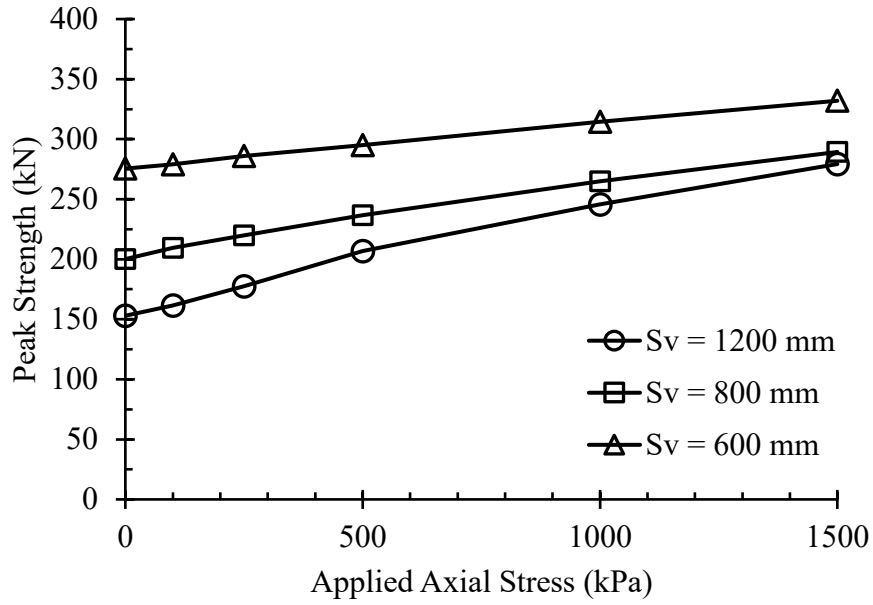

Figure B.63 – Parametric Results (WH2400-BB1200-25M-15M-BJN)

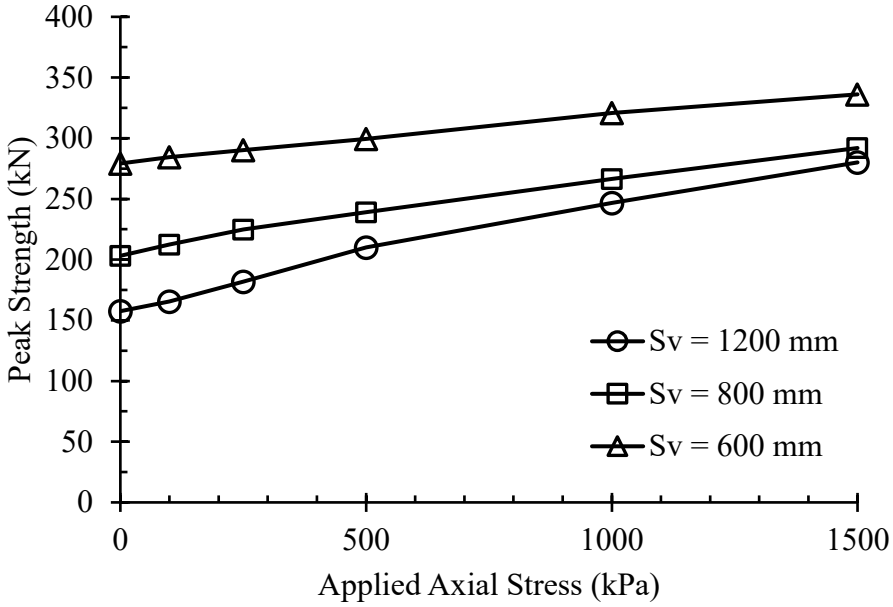

Figure B.64 – Parametric Results (WH2400-BB1200-25M-15M-BJY)

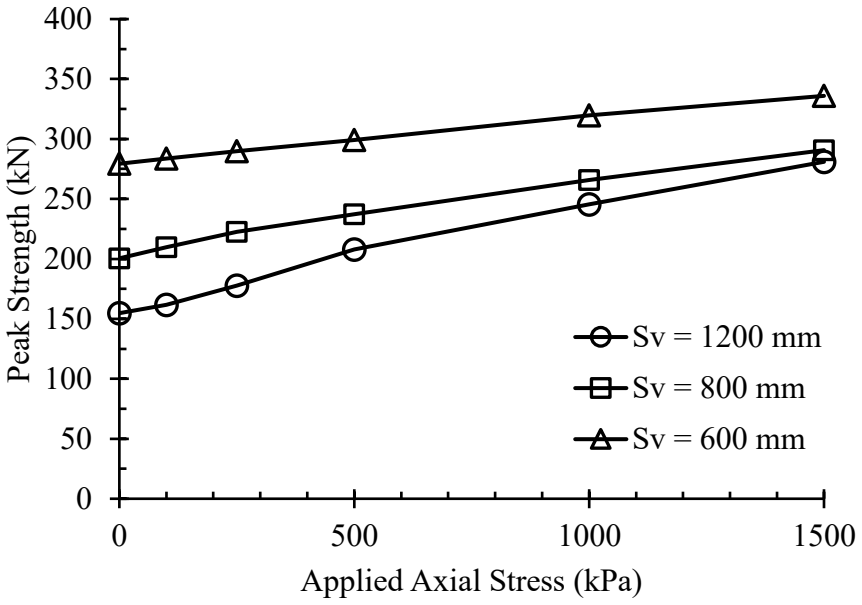

Figure B.65 – Parametric Results (WH2400-BB1200-25M-20M-BJN)

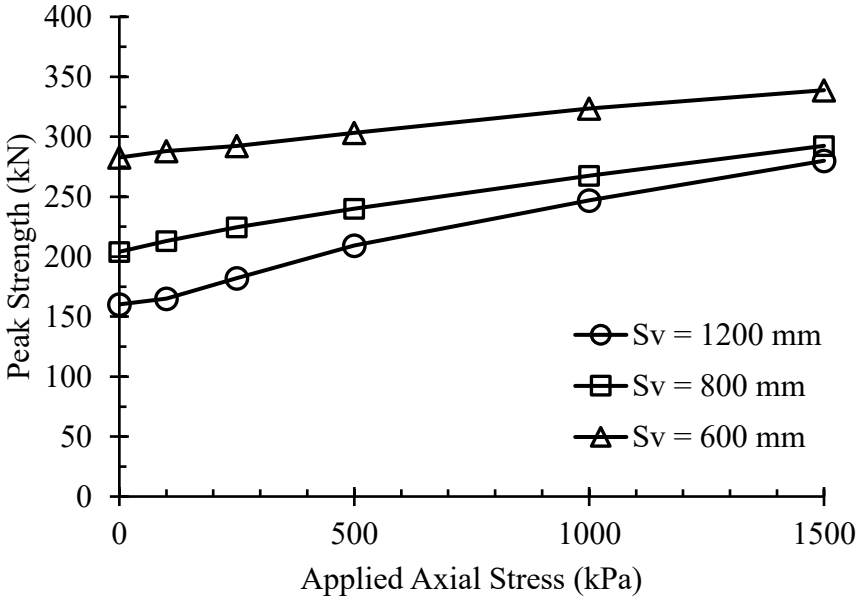

Figure B.66 – Parametric Results (WH2400-BB1200-25M-20M-BJY)

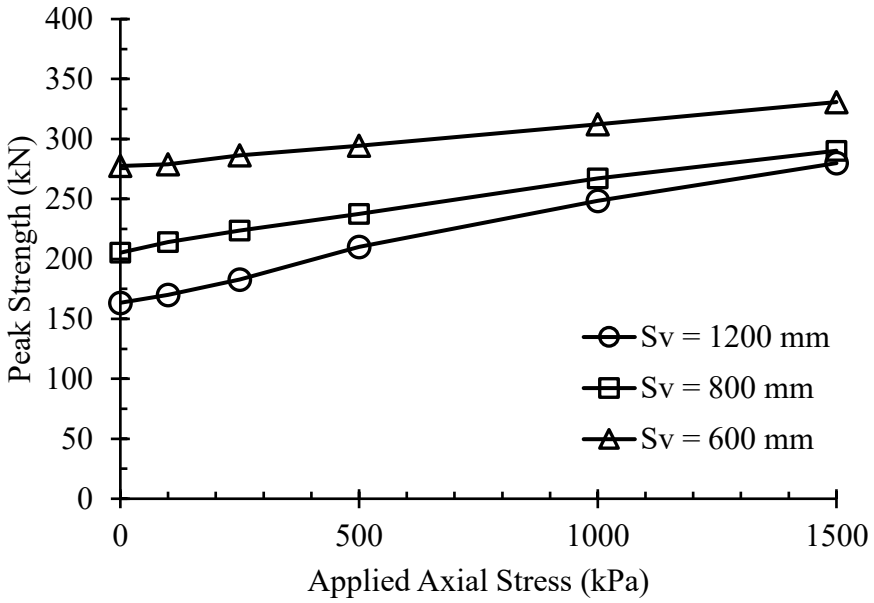

Figure B.67 – Parametric Results (WH2400-BB1200-30M-10M-BJN)

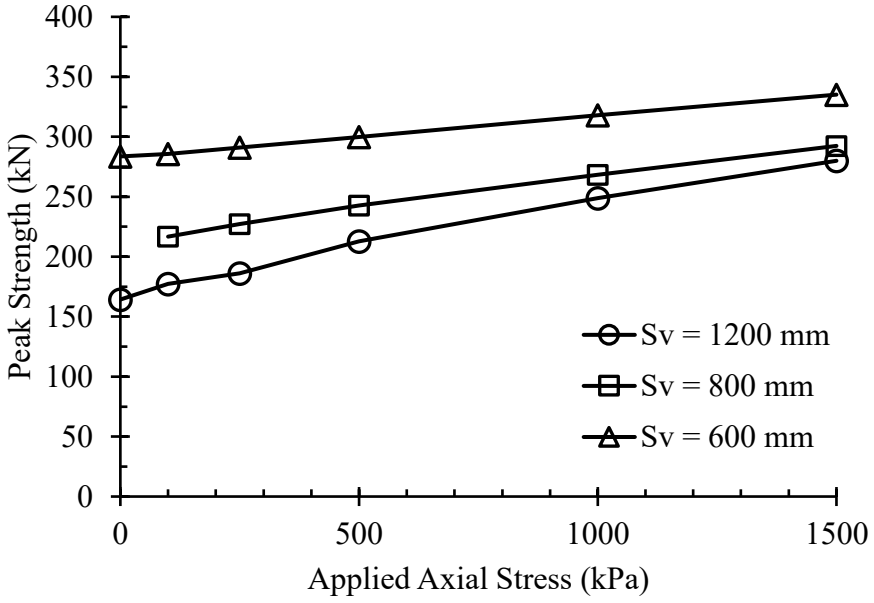

Figure B.68 – Parametric Results (WH2400-BB1200-30M-10M-BJY)

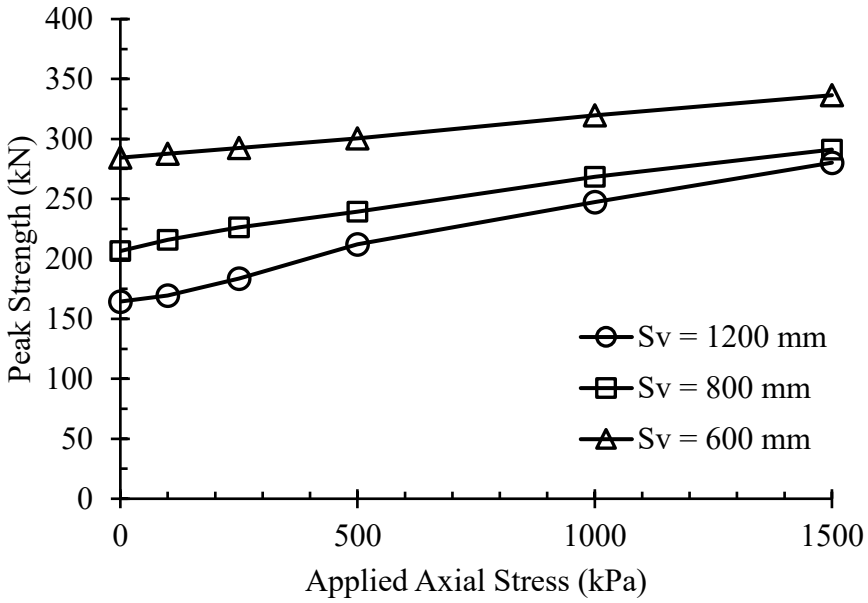

Figure B.69 – Parametric Results (WH2400-BB1200-30M-15M-BJN)

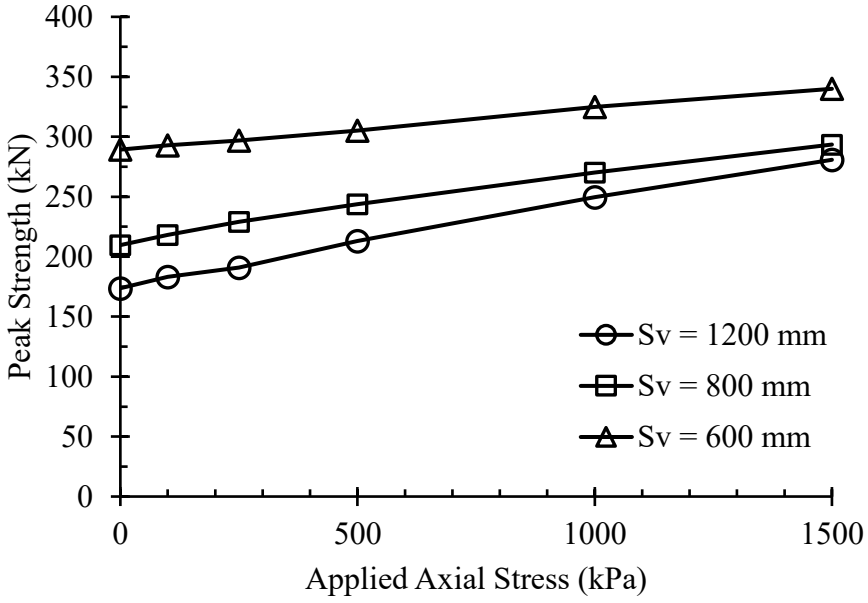

Figure B.70 – Parametric Results (WH2400-BB1200-30M-15M-BJY)

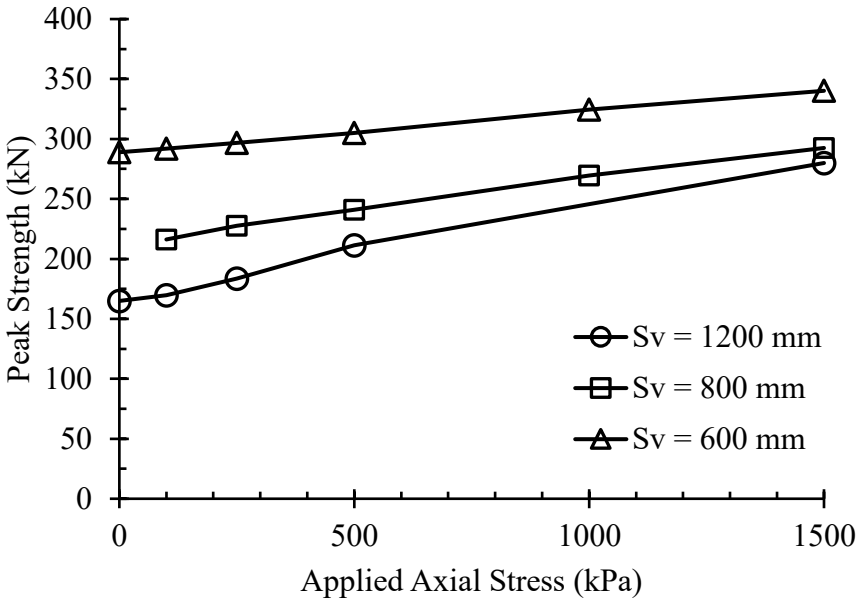

Figure B.71 – Parametric Results (WH2400-BB1200-30M-20M-BJN)

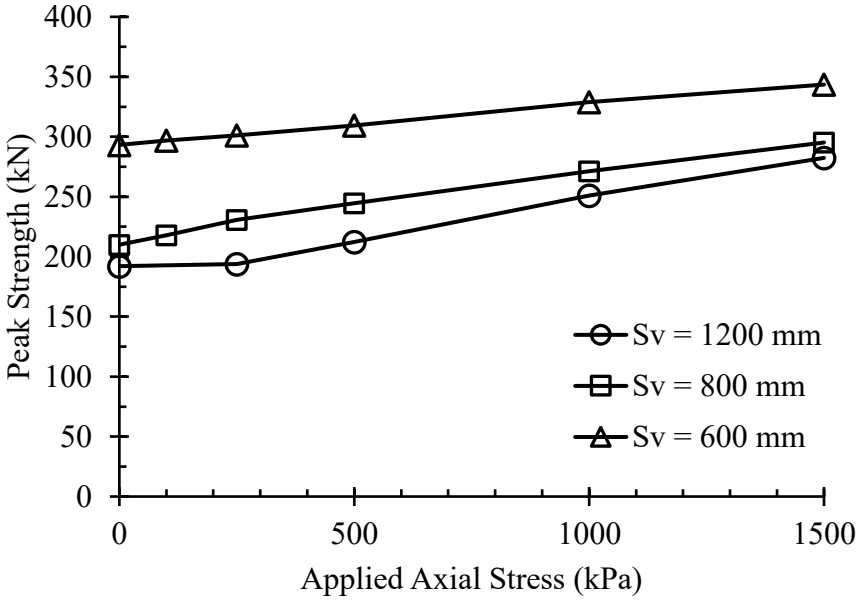

Figure B.72 – Parametric Results (WH2400-BB1200-30M-20M-BJY)

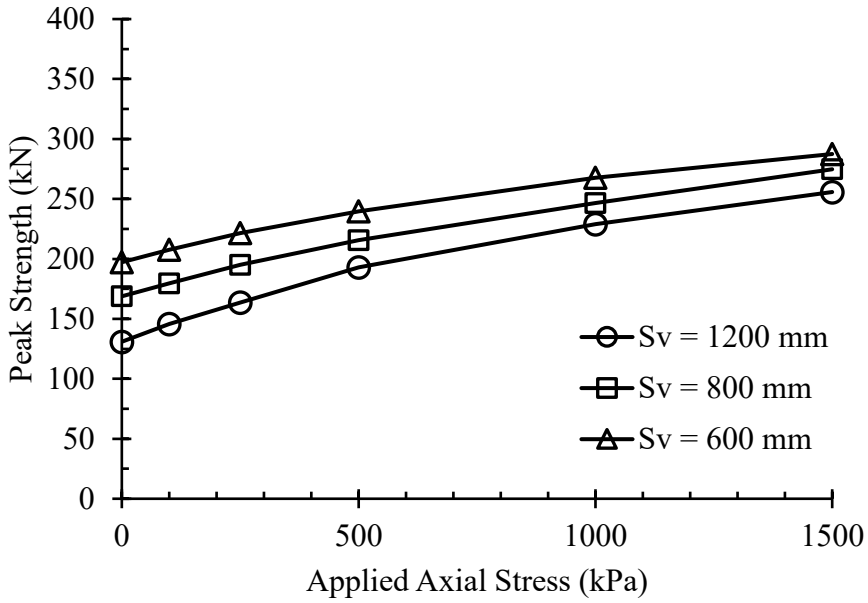

Figure B.73 – Parametric Results (WH3200-BB800-20M-10M-BJN)

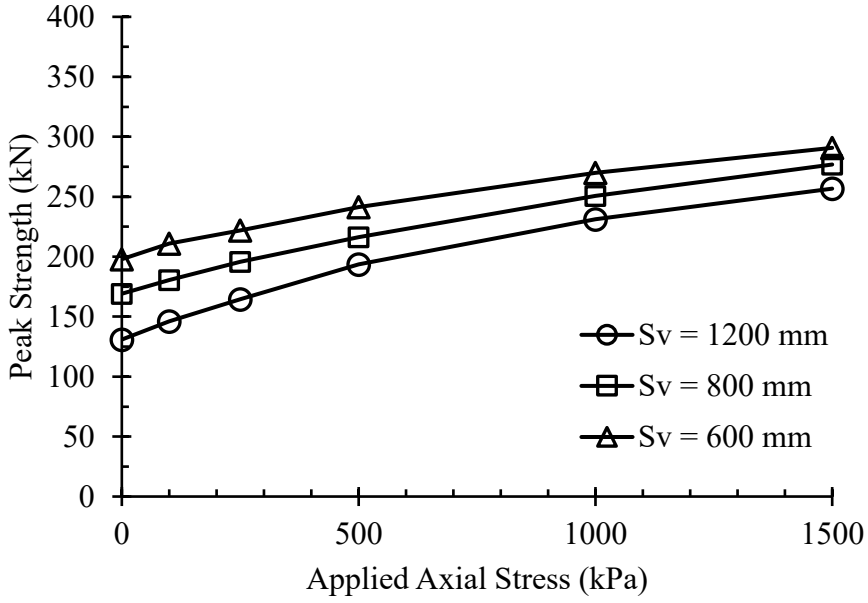

Figure B.74 – Parametric Results (WH3200-BB800-20M-10M-BJY)

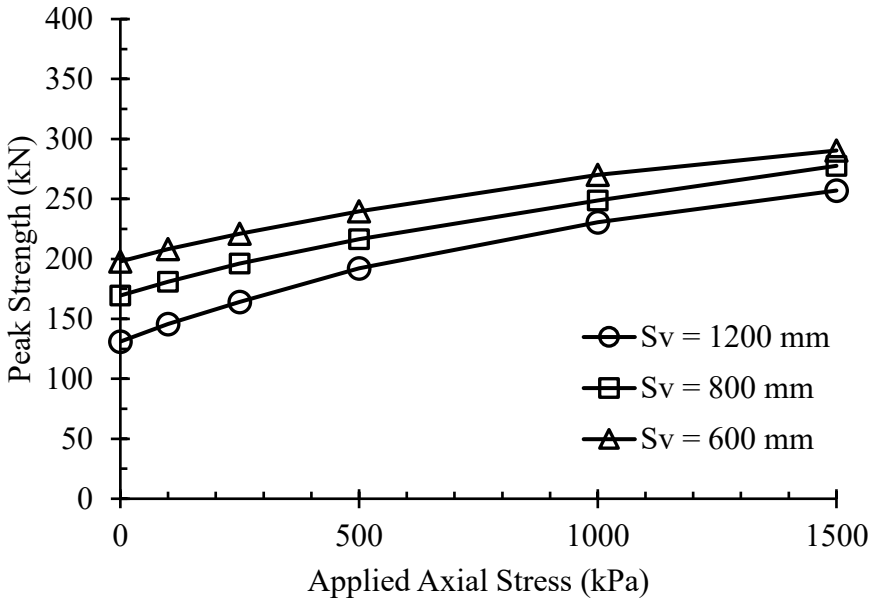

Figure B.75 – Parametric Results (WH3200-BB800-20M-15M-BJN)

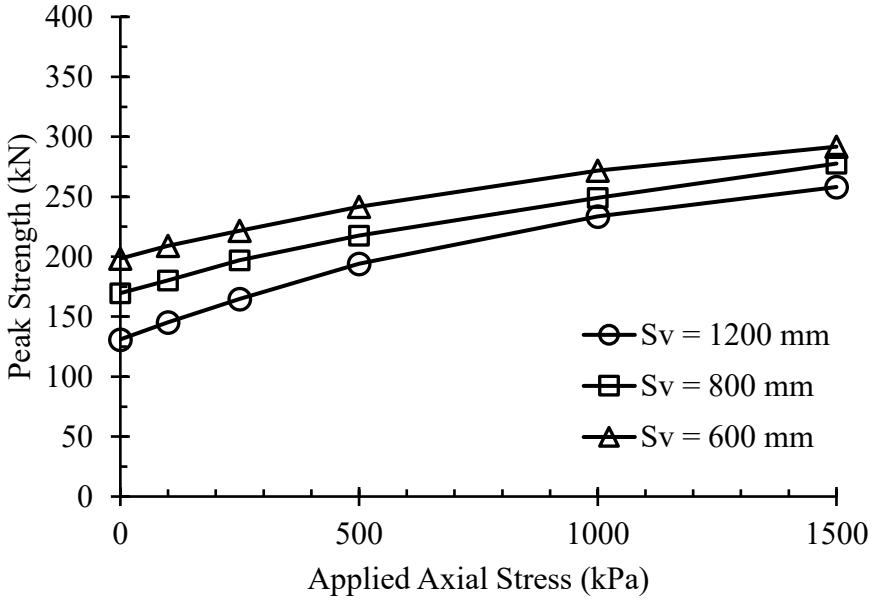

Figure B.76 – Parametric Results (WH3200-BB800-20M-15M-BJY)

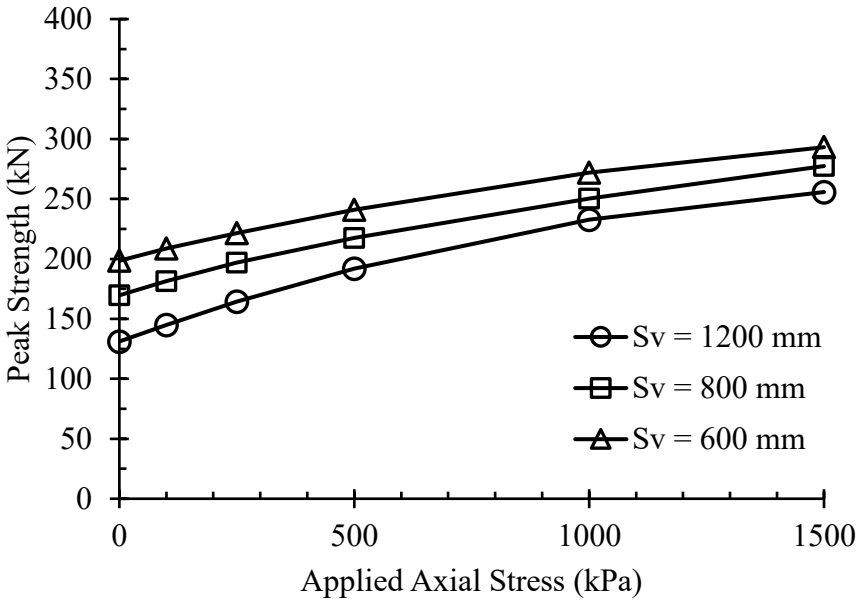

Figure B.77 – Parametric Results (WH3200-BB800-20M-20M-BJN)

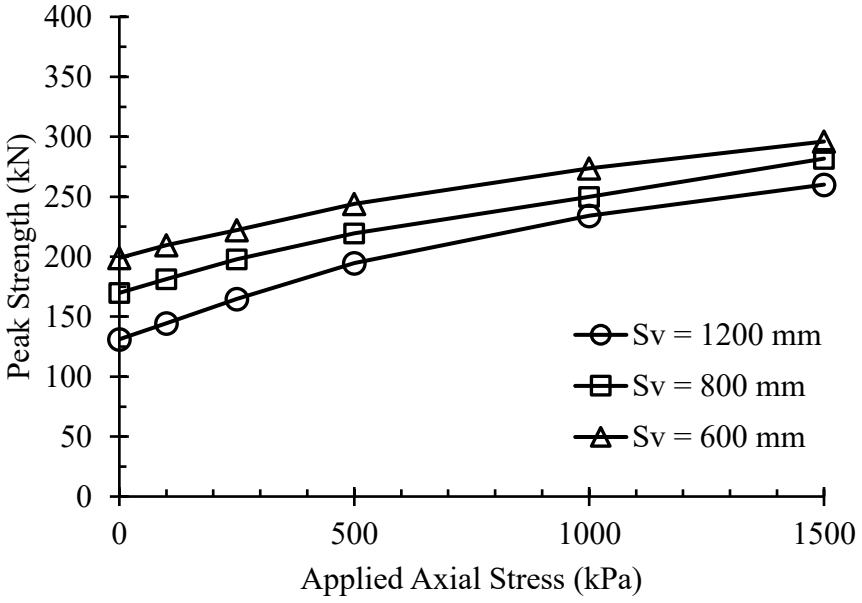

Figure B.78 – Parametric Results (WH3200-BB800-20M-20M-BJY)

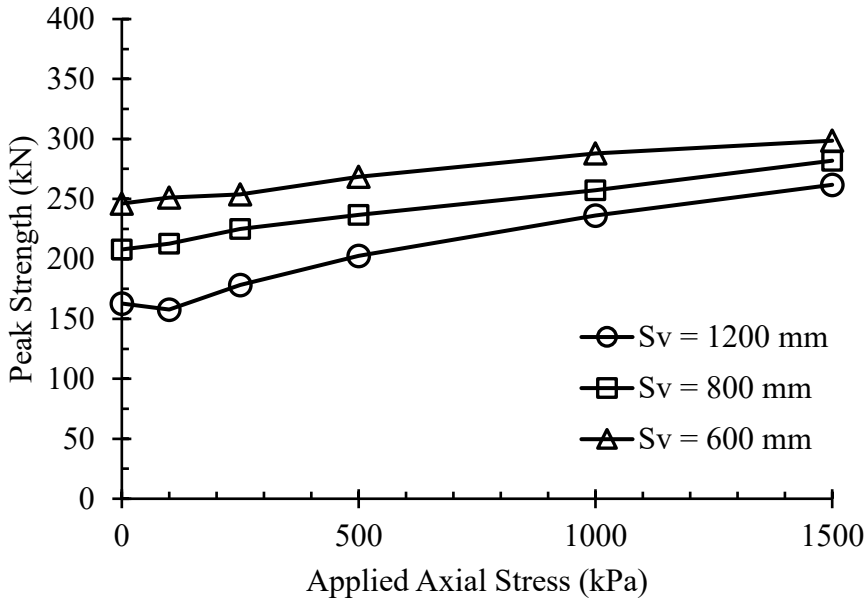

Figure B.79 – Parametric Results (WH3200-BB800-25M-10M-BJN)

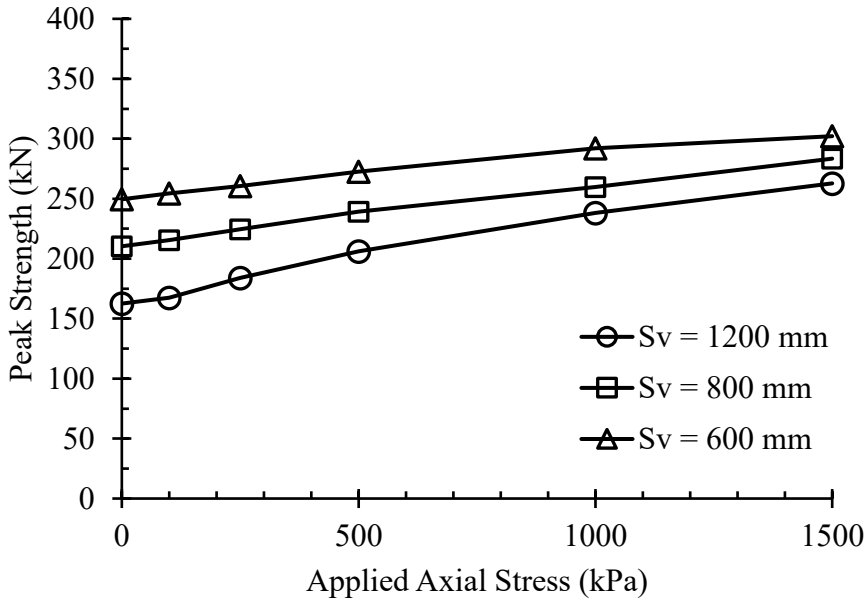

Figure B.80 – Parametric Results (WH3200-BB800-25M-10M-BJY)

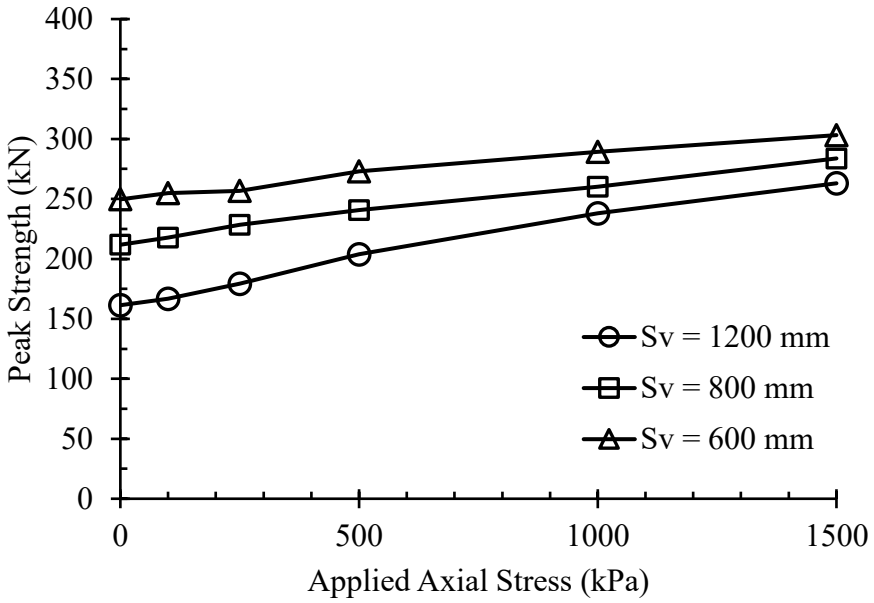

Figure B.81 – Parametric Results (WH3200-BB800-25M-15M-BJN)

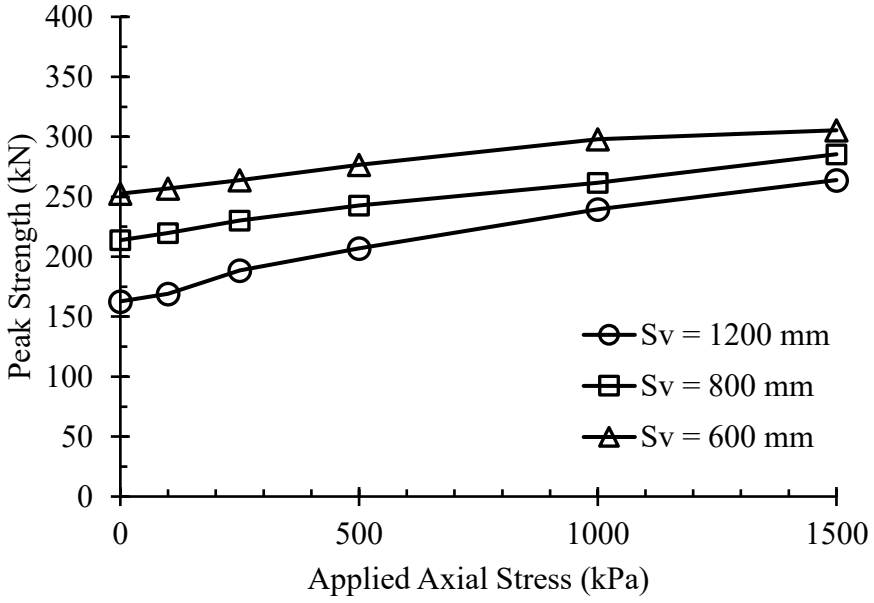

Figure B.82 – Parametric Results (WH3200-BB800-25M-15M-BJY)

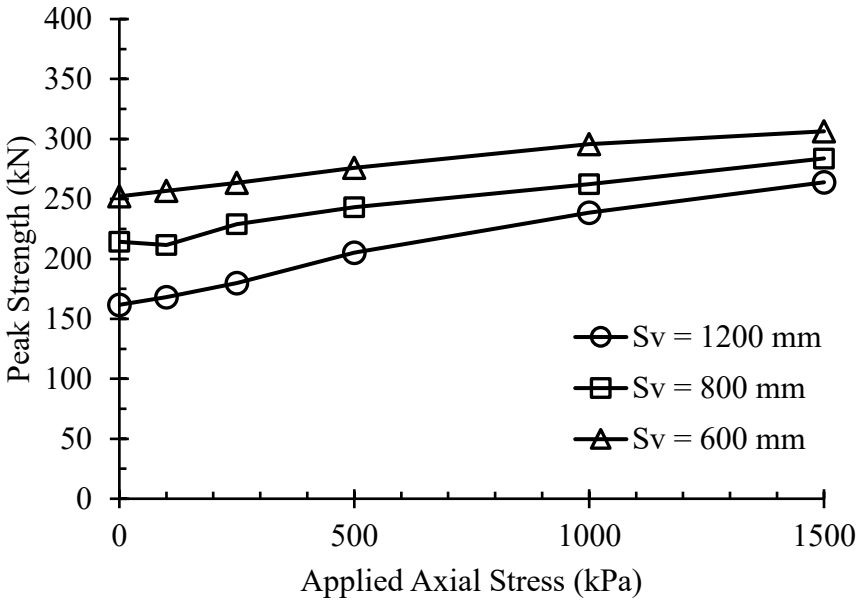

Figure B.83 – Parametric Results (WH3200-BB800-25M-20M-BJN)

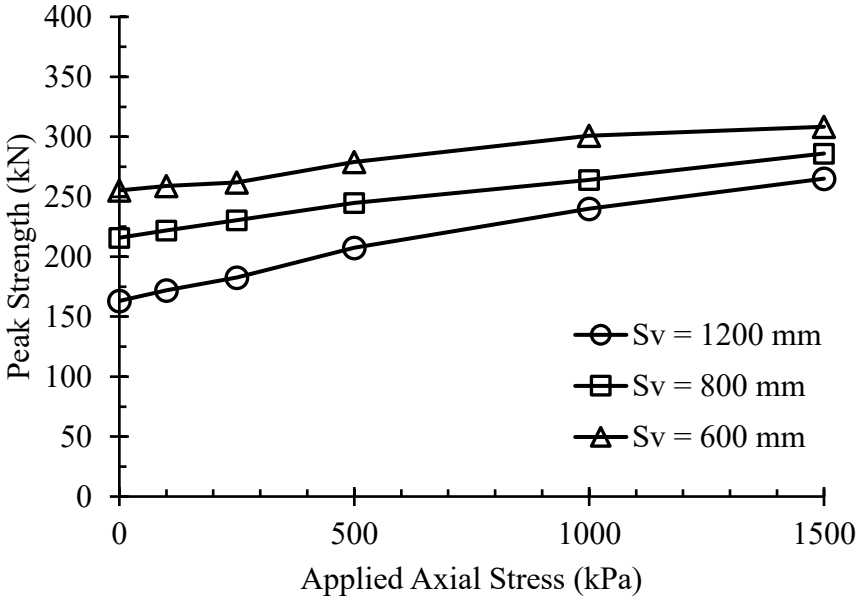

Figure B.84 – Parametric Results (WH3200-BB800-25M-20M-BJY)

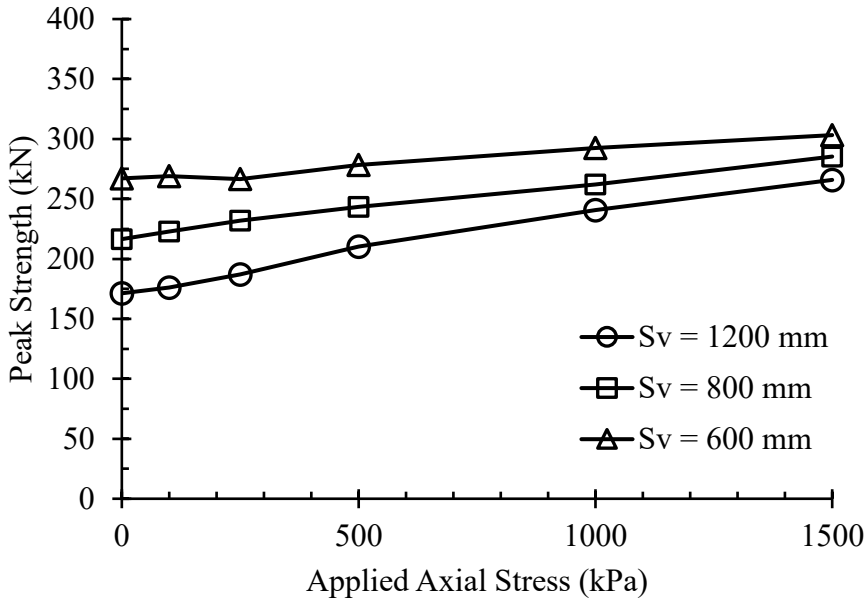

Figure B.85 – Parametric Results (WH3200-BB800-30M-10M-BJN)

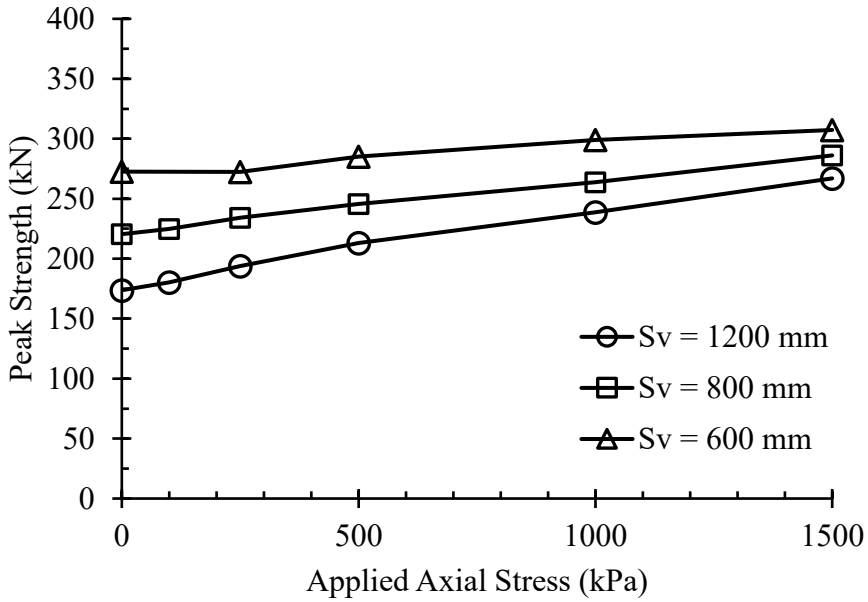

Figure B.86 – Parametric Results (WH3200-BB800-30M-10M-BJY)

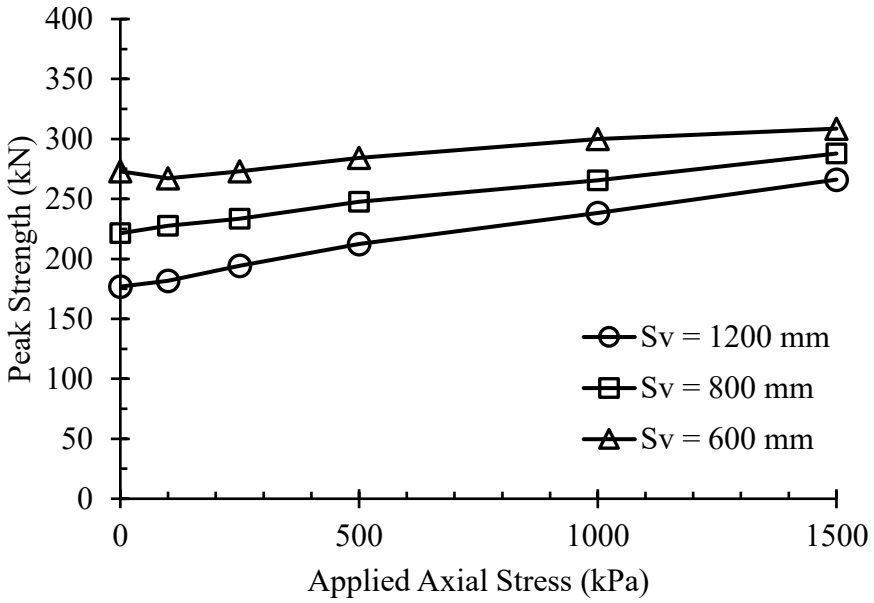

Figure B.87 – Parametric Results (WH3200-BB800-30M-15M-BJN)

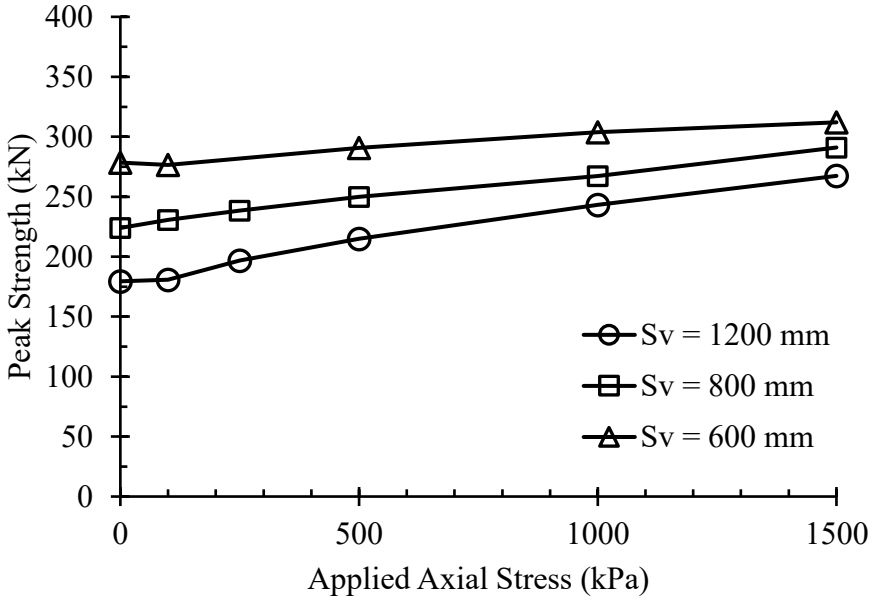

Figure B.88 – Parametric Results (WH3200-BB800-30M-15M-BJY)

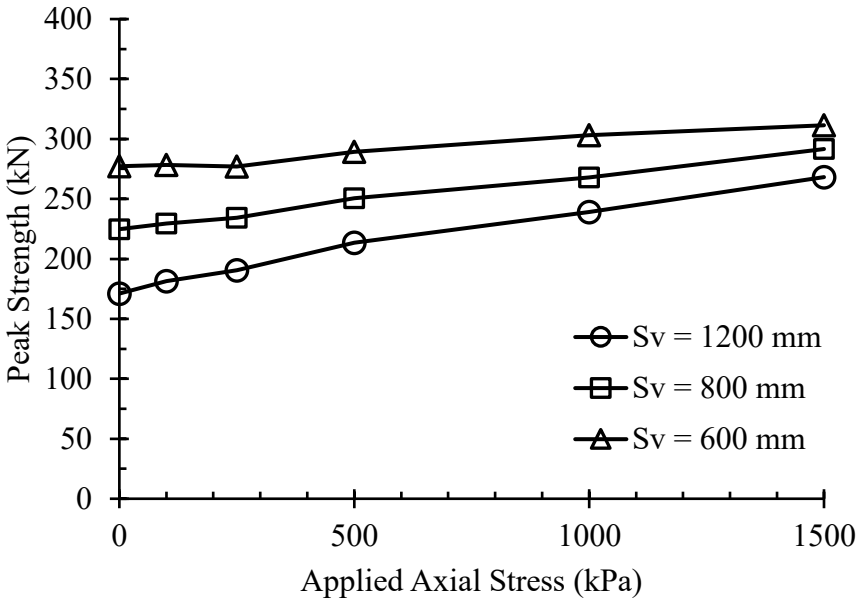

Figure B.89 – Parametric Results (WH3200-BB800-30M-20M-BJN)

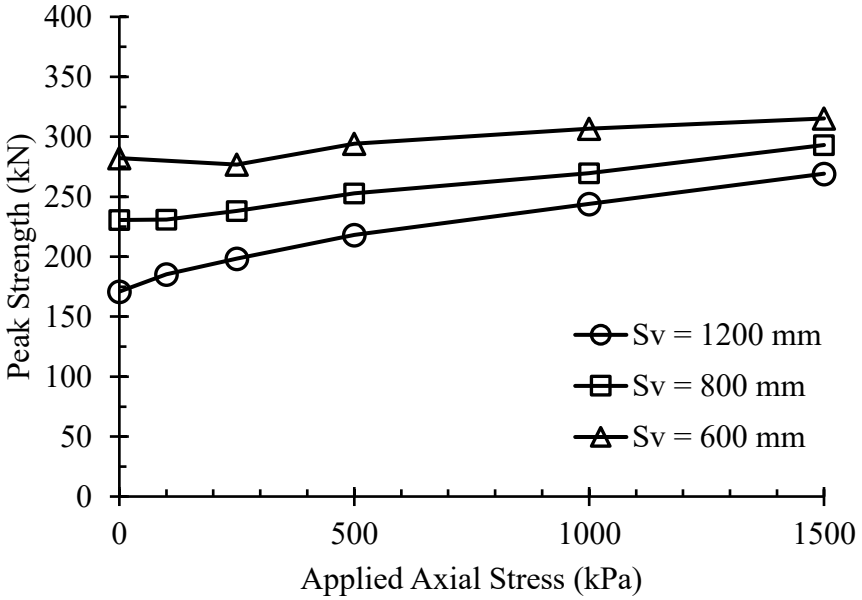

Figure B.90 – Parametric Results (WH3200-BB800-30M-20M-BJY)

APPENDIX C: MASONRY STM CALCULATOR (MATLAB CODE)

```
function [paraOutputs] = node_calculator(paraInputs)

    %% Set Values
    node_calc = paraInputs(1);
    nodeHeight = paraInputs(2);
    axialForce = paraInputs(3);
    wallHeight = paraInputs(4);
    groutedThickness = paraInputs(5);
    ungroutedThickness = paraInputs(6);
    feg = paraInputs(7);
    feug = paraInputs(8);
    Fyh = paraInputs(9);
    Fyv = paraInputs(10);
    Asv = paraInputs(11);
    Ash = paraInputs(12);
    prevTransfer = paraInputs(13);
    prevRebar = paraInputs(14);
    prevBond = paraInputs(15);
    prevBase = paraInputs(16);
    maxStrutWidth = paraInputs(17);
    assumedStrutWidth = paraInputs(18);
    prevRebar2 = paraInputs(19);

    %% Initial Values
    transferForce = 0;
    appliedForce = 0;
    rebarForce = 0;
    rebarForce1 = 0;
    rebarForce2 = 0;
    bondForce = 0;
    totalStrutBase = 0;

    %% Strut Calculations
    % Leading Strut
    if node_calc == 1

        % Leading Strut Approximation
        strutAngle = atand(wallHeight/100) + 0.25;

        % Iterations
        conv = 0;
        while conv == 0

            % Strut Width and Base
            strutBase = (2*(100-(wallHeight/tand(strutAngle))));
            strutWidth = strutBase*sind(strutAngle);
```

```
            % Strut Force
            strutForce = feg*strutWidth*groutedThickness;

            % Transfer Force
            transferForce = strutForce*cosd(strutAngle);

            % Reinforcement Force
            rebarForce = strutForce*sind(strutAngle) -
axialForce;

            % Reinforcement Stress
            rebarStress = rebarForce/Asv;

            % Check Geometric Constraints
            geomError = 100-(wallHeight/tand(strutAngle))-
(1/2)*strutBase;
            if geomError > 0.1
                strutAngle = strutAngle - 0.0001;
            elseif geomError < 0
                strutAngle = strutAngle + 0.0001;
            else
                conv = 1;
            end

        end

        % Base Force
        baseForce = strutForce*cosd(strutAngle);
        totalStrutBase = strutBase;

        % Print the Results
        fprintf('Strut Analysis: \n')
        fprintf('   Strut Force = %3.2f kN \n',strutForce/1000)
        fprintf('   Transfer Force = %3.2f kN
\n',transferForce/1000)
        fprintf('   Reinforcement Force = %3.2f kN
\n',rebarForce/1000)
        fprintf('   Reinforcement Stress = %3.2f MPa
\n',rebarStress)
        fprintf('   Base Force = %3.2f kN \n',baseForce/1000)
        fprintf('   Strut Base = %3.2f mm \n\n',strutBase)

    % Bent Strut (Without a Bond Beam or Grout Core)
    elseif node_calc == 2

        % Top Strut
        % Strut Force
        strutForce1 = axialForce/sind(45);

        % Check Strut Stresses
```

```
        if strutForce1 > feug*maxStrutWidth*ungroutedThickness
            fprintf('Strut Capacity Exceeded!')
            return
        end

        % Transfer Force
        transferForce = prevTransfer + strutForce1*cosd(45);

        % Bent Strut
        % Leading Strut Approximation
        strutAngle = atand(nodeHeight/200) + 0.25;

        % Iterations
        conv = 0;
        while conv == 0

            % Strut Force
            strutForce2 =
strutForce1*(cosd(45)/cosd(strutAngle));

            % Strut Width and Base
            strutWidth = strutForce2/(feg*groutedThickness);
            strutBase = strutWidth/sind(strutAngle);

            % Reinforcement Force
            rebarForce = prevRebar + strutForce1*sind(45) -
strutForce2*sind(strutAngle);

            % Reinforcement Stress
            rebarStress = rebarForce/Asv;

            % Check Geometric Constraints
            geomError = 200-(nodeHeight/tand(strutAngle))-
(1/2)*strutBase-prevBase;
            if geomError > 0.1
                strutAngle = strutAngle - 0.0001;
            elseif geomError < 0
                strutAngle = strutAngle + 0.0001;
            else
                conv = 1;
            end

        end

        % Base Force
        baseForce = strutForce2*cosd(strutAngle);
        totalStrutBase = prevBase + strutBase;

        % Print the Results
        fprintf('Strut Analysis: \n')
```

```
        fprintf('   Top Strut Force = %3.2f kN
\n',strutForce1/1000)
        fprintf('   Bottom Strut Force = %3.2f kN
\n',strutForce2/1000)
        fprintf('   Transfer Force = %3.2f kN
\n',transferForce/1000)
        fprintf('   Reinforcement Force = %3.2f kN
\n',rebarForce/1000)
        fprintf('   Reinforcement Stress = %3.2f MPa
\n',rebarStress)
        fprintf('   Base Force = %3.2f kN \n',baseForce/1000)
        fprintf('   Total Strut Base = %3.2f mm
\n\n',totalStrutBase)

    % Bent Strut (With a Bond Beam but Without a Grout Core)
    elseif node_calc == 3

        % Top Strut
        % Strut Force
        strutForce1 = axialForce/sind(45);

        % Check Strut Stresses
        if strutForce1 > feug*maxStrutWidth*ungroutedThickness
            print('Strut Capacity Exceeded!')
            return
        end

        % Transfer Force
        transferForce = prevTransfer + strutForce1*cosd(45);

        % Bent Strut
        % Leading Strut Approximation
        strutAngle = atand(nodeHeight/200) + 0.25;

        % Strut Width Approximation
        strutWidth = assumedStrutWidth;

        % Iterations
        conv = 0;
        while conv == 0

            % Check Geometry
            geomCheck = 1;

            % Strut Force
            strutForce2 = feg*groutedThickness*strutWidth;

            % Strut Base
            strutBase = strutWidth/sind(strutAngle);
            totalStrutBase = prevBase + strutBase;
```

```
            % Bond Beam Force
            bondForce = strutForce1*cosd(45) -
strutForce2*cosd(strutAngle);

            % Bond Beam Stress
            bondStress = bondForce/Ash;

            % Check Bond Beam Yielding
            if abs(bondStress) > Fyh
                strutWidth = strutWidth + 0.1;
                geomCheck = 0;
            end

            % Reinforcement Force
            rebarForce = prevRebar + strutForce1*sind(45) -
strutForce2*sind(strutAngle);

            % Reinforcement Stress
            rebarStress = rebarForce/Asv;

            % Check Geometric Constraints
            if geomCheck == 1
                geomError = 200-(nodeHeight/tand(strutAngle))-
(1/2)*strutBase-prevBase;
                if geomError > 0.1
                    strutAngle = strutAngle - 0.0001;
                elseif geomError < 0
                    strutAngle = strutAngle + 0.0001;
                else
                    conv = 1;
                end
            end

        end

        % Base Force
        baseForce = strutForce2*cosd(strutAngle);

        % Print the Results
        fprintf('Strut Analysis: \n')
        fprintf('   Top Strut Force = %3.2f kN
\n',strutForce1/1000)
        fprintf('   Bottom Strut Force = %3.2f kN
\n',strutForce2/1000)
        fprintf('   Transfer Force = %3.2f kN
\n',transferForce/1000)
        fprintf('   Bond Beam Force = %3.2f kN
\n',bondForce/1000)
        fprintf('   Bond Beam Stress = %3.2f MPa \n',bondStress)
```

```
        fprintf('   Reinforcement Force = %3.2f kN
\n',rebarForce/1000)
        fprintf('   Reinforcement Stress = %3.2f MPa
\n',rebarStress)
        fprintf('   Base Force = %3.2f kN \n',baseForce/1000)
        fprintf('   Strut Base = %3.2f mm \n\n',totalStrutBase)

    % Bent Strut (Without a Bond Beam but With a Grout Core)
    elseif node_calc == 4

        % Top Strut
        % Strut Force
        strutForce1 = feug*maxStrutWidth*ungroutedThickness;

        % Bent Strut
        % Leading Strut Approximation
        strutAngle = atand(nodeHeight/200) + 0.25;

        % Iterations
        conv = 0;
        while conv == 0

            % Check Geometry
            geomCheck = 1;

            % Transfer Force
            transferForce = prevTransfer + strutForce1*cosd(45);

            % Reinforcement Force
            rebarForce1 = strutForce1*sind(45) - axialForce;

            % Reinforcement Stress
            rebarStress1 = rebarForce1/Asv;

            % Strut Force
            strutForce2 =
strutForce1*(cosd(45)/cosd(strutAngle));

            % Strut Width and Base
            strutWidth = strutForce2/(feg*groutedThickness);
            strutBase = strutWidth/sind(strutAngle);

            % Reinforcement Force
            rebarForce2 = prevRebar + strutForce1*sind(45) -
strutForce2*sind(strutAngle);

            % Reinforcement Stress
            rebarStress2 = rebarForce2/Asv;

            % Check Reinforcement Stress
```

```
            if abs(rebarStress2) > Fyv
                strutForce1 = strutForce1 - 10;
                strutAngle = atand(nodeHeight/200) + 0.25;
                geomCheck = 0;
            end

            if strutBase > assumedStrutWidth
                strutForce1 = strutForce1 - 10;
                strutAngle = atand(nodeHeight/200) + 0.25;
                geomCheck = 0;
            end

            % Check Geometric Constraints
            if geomCheck == 1
                geomError = 200-(nodeHeight/tand(strutAngle))-
(1/2)*strutBase-prevBase;
                if geomError > 0.1
                    strutAngle = strutAngle - 0.0001;
                elseif geomError < 0
                    strutAngle = strutAngle + 0.0001;
                else
                    conv = 1;
                end
            end

            % Decrease the Strut Force (If Required)
            if strutAngle >= 90
                strutForce1 = strutForce1 - 10;
                strutAngle = atand(nodeHeight/200) + 0.25;
            end

        end

        % New Base
        totalStrutBase = prevBase + strutBase;

        % Base Force
        baseForce = strutForce2*cosd(strutAngle);

        % Print the Results
        fprintf('Strut Analysis: \n')
        fprintf('   Top Strut Force = %3.2f kN
\n',strutForce1/1000)
        fprintf('   Bottom Strut Force = %3.2f kN
\n',strutForce2/1000)
        fprintf('   Transfer Force = %3.2f kN
\n',transferForce/1000)
        fprintf('   Left Reinforcement Force = %3.2f kN
\n',rebarForce1/1000)
```

```
        fprintf('   Left Reinforcement Stress = %3.2f MPa
\n',rebarStress1)
        fprintf('   Right Reinforcement Force = %3.2f kN
\n',rebarForce2/1000)
        fprintf('   Right Reinforcement Stress = %3.2f MPa
\n',rebarStress2)
        fprintf('   Base Force = %3.2f kN \n',baseForce/1000)
        fprintf('   Total Strut Base = %3.2f mm
\n\n',totalStrutBase)

    % Bent Strut (With a Bond Beam and a Grout Core)
    elseif node_calc == 5

        % Top Strut
        % Strut Force
        strutForce1 = feug*maxStrutWidth*ungroutedThickness;

        % Bent Strut
        % Leading Strut Approximation
        strutAngle = atand(nodeHeight/200) + 0.25;
        strutWidth = assumedStrutWidth;

        % Iterations
        conv = 0;
        while conv == 0

            % Check Geometry
            geomCheck = 1;

            % Top Strut
            % Transfer Force
            transferForce = prevTransfer + strutForce1*cosd(45);

            % Reinforcement Force
            rebarForce1 = strutForce1*sind(45) - axialForce;

            % Reinforcement Stress
            rebarStress1 = rebarForce1/Asv;

            % Bottom Strut
            % Strut Force
            strutForce2 = feg*groutedThickness*strutWidth;

            % Strut Width and Base
            strutBase = strutWidth/sind(strutAngle);

            % Reinforcement Force
            rebarForce2 = prevRebar + strutForce1*sind(45) -
strutForce2*sind(strutAngle);
```

```
            % Reinforcement Stress
            rebarStress2 = rebarForce2/Asv;

            % Bond Force
            bondForce = strutForce1*cosd(45) -
strutForce2*cosd(strutAngle);

            % Bond Stress
            bondStress = bondForce/Ash;

            % Check Reinforcement Stress
            if abs(rebarStress2) > Fyv || abs(bondStress > Fyh)
                strutForce1 = strutForce1 - 10;
                strutAngle = atand(nodeHeight/200) + 0.25;
                geomCheck = 0;
            end

            % Check Geometric Constraints
            if geomCheck == 1
                geomError = 200-(nodeHeight/tand(strutAngle))-
(1/2)*strutBase-prevBase;
                if geomError > 0.1
                    strutAngle = strutAngle - 0.0001;
                elseif geomError < 0
                    strutAngle = strutAngle + 0.0001;
                else
                    conv = 1;
                end
            end

            % Increase the Strut Width or Decrease the Strut
Force (If Required)
            if strutAngle >= 90
                strutForce1 = strutForce1 - 10;
                strutAngle = atand(nodeHeight/200) + 0.25;
            end

        end

        % Base Force
        baseForce = strutForce2*cosd(strutAngle);
        totalStrutBase = prevBase + strutBase;

        % Print the Results
        fprintf('Strut Analysis: \n')
        fprintf('   Top Strut Force = %3.2f kN
\n',strutForce1/1000)
        fprintf('   Bottom Strut Force = %3.2f kN
\n',strutForce2/1000)
```

```
        fprintf('   Transfer Force = %3.2f kN
\n',transferForce/1000)
        fprintf('   Left Reinforcement Force = %3.2f kN
\n',rebarForce1/1000)
        fprintf('   Left Reinforcement Stress = %3.2f MPa
\n',rebarStress1)
        fprintf('   Right Reinforcement Force = %3.2f kN
\n',rebarForce2/1000)
        fprintf('   Right Reinforcement Stress = %3.2f MPa
\n',rebarStress2)
        fprintf('   Bond Beam Force = %3.2f kN
\n',bondForce/1000)
        fprintf('   Bond Beam Stress = %3.2f MPa \n',bondStress)
        fprintf('   Base Force = %3.2f kN \n',baseForce/1000)
        fprintf('   Total Strut Base = %3.2f mm
\n\n',totalStrutBase)

    % Straight Strut (Without a Bond Beam or Grout Core)
    elseif node_calc == 6

        % Strut Force
        strutForce = axialForce/sind(45);

        % Check Strut Stresses
        if strutForce > feug*maxStrutWidth*ungroutedThickness
            fprintf('Strut Capacity Exceeded!')
            return
        end

        % Transfer Force
        transferForce = prevTransfer + strutForce*cosd(45);

        % Base Force
        baseForce = strutForce*cosd(45);

        % Print the Results
        fprintf('Strut Analysis:')
        fprintf('   Strut Force = %3.2f kN \n',strutForce/1000)
        fprintf('   Transfer/Base Force = %3.2f kN
\n',transferForce/1000)
        fprintf('   Base Force = %3.2f kN \n\n',baseForce/1000)

    % Straight Strut (Without a Bond Beam but With a Grout Core)
    elseif node_calc == 7

        % Strut Force
        strutForce = feug*maxStrutWidth*ungroutedThickness;

        % Transfer Force
        transferForce = prevTransfer + strutForce*cosd(45);
```

```
        % Reinforcement Force
        rebarForce = strutForce*sind(45) - axialForce;

        % Reinforcement Stress
        rebarStress = rebarForce/Asv;

        % Base Force
        baseForce = strutForce*cosd(45);

        % Print the Results
        fprintf('Strut Analysis: \n')
        fprintf('   Strut Force = %3.2f kN \n',strutForce/1000)
        fprintf('   Transfer Force = %3.2f kN
\n',transferForce/1000)
        fprintf('   Reinforcement Force = %3.2f kN
\n',rebarForce/1000)
        fprintf('   Reinforcement Stress = %3.2f MPa
\n',rebarStress)
        fprintf('   Base Force = %3.2f kN \n\n',baseForce/1000)

    % Straight Strut (With a Bond Beam but Without Grout Core)
    elseif node_calc == 8

        % Top Strut
        % Strut Force
        strutForce1 = axialForce/sind(45);

        % Begin Iterations
        conv = 0;
        while conv == 0

            % Tranfser Force
            transferForce = prevTransfer + strutForce1*cosd(45);

            % Bottom Strut
            % Strut Force
            strutForce2 = feug*ungroutedThickness*maxStrutWidth;

            % Reinforcement Force
            rebarForce = prevRebar + strutForce2*sind(45) -
strutForce1*sind(45);

            % Reinforcement Stress
            rebarStress = rebarForce/Asv;

            % Bond Beam Force
            bondForce = prevBond + strutForce1*cosd(45) -
strutForce2*cosd(45);
```

```
            % Bond Beam Stress
            bondStress = bondForce/Ash;

            % Check Yielding
            if abs(rebarStress) > Fyv || abs(bondStress) > Fyh
                strutForce1 = strutForce1 - 10;
            else
                conv = 1;
            end

        end

        % Base Force
        baseForce = strutForce2*cosd(45);

        % Print the Results
        fprintf('Strut Analysis: \n')
        fprintf('   Top Strut Force = %3.2f kN
\n',strutForce1/1000)
        fprintf('   Bottom Strut Force = %3.2f kN
\n',strutForce2/1000)
        fprintf('   Transfer Force = %3.2f kN
\n',transferForce/1000)
        fprintf('   Reinforcement Force = %3.2f kN
\n',rebarForce/1000)
        fprintf('   Reinforcement Stress = %3.2f MPa
\n',rebarStress)
        fprintf('   Bond Beam Force = %3.2f kN
\n',bondForce/1000)
        fprintf('   Bond Beam Stress = %3.2f MPa \n',bondStress)
        fprintf('   Base Force = %3.2f kN \n\n',baseForce/1000)

    % Straight Strut (With a Bond Beam and a Grout Core)
    elseif node_calc == 9

        % Top Strut
        % Strut Force
        strutForce1 = feug*ungroutedThickness*maxStrutWidth;

        % Begin Iterations
        conv = 0;
        while conv == 0

            % Tranfser Force
            transferForce = prevTransfer + strutForce1*cosd(45);

            % Top Reinforcement Force
            rebarForce1 = strutForce1*sind(45) - axialForce;

            % Top Reinforcement Stress
```

```
            rebarStress1 = rebarForce1/Asv;

            % Bottom Strut
            % Strut Force
            strutForce2 = feug*ungroutedThickness*maxStrutWidth;

            % Bottom Reinforcement Force
            rebarForce2 = prevRebar + strutForce2*sind(45) -
strutForce1*sind(45);

            % Reinforcement Stress
            rebarStress2 = rebarForce2/Asv;

            % Bond Beam Force
            bondForce = prevBond + strutForce1*cosd(45) -
strutForce2*cosd(45);

            % Bond Beam Stress
            bondStress = bondForce/Ash;

            % Check Yielding
            if abs(rebarStress1) > Fyv || abs(rebarStress2) >
Fyv || abs(bondStress) > Fyh
                strutForce1 = strutForce1 - 10;
            else
                conv = 1;
            end

        end

        % Base Force
        baseForce = strutForce2*cosd(45);

        % Print the Results
        fprintf('Strut Analysis: \n')
        fprintf('   Top Strut Force = %3.2f kN
\n',strutForce1/1000)
        fprintf('   Bottom Strut Force = %3.2f kN
\n',strutForce2/1000)
        fprintf('   Transfer Force = %3.2f kN
\n',transferForce/1000)
        fprintf('   Top Reinforcement Force = %3.2f kN
\n',rebarForce1/1000)
        fprintf('   Top Reinforcement Stress = %3.2f MPa
\n',rebarStress1)
        fprintf('   Bottom Reinforcement Force = %3.2f kN
\n',rebarForce2/1000)
        fprintf('   Bottom Reinforcement Stress = %3.2f MPa
\n',rebarStress2)
```

```
        fprintf('   Bond Beam Force = %3.2f kN
\n',bondForce/1000)
        fprintf('   Bond Beam Stress = %3.2f MPa \n',bondStress)
        fprintf('   Base Force = %3.2f kN \n\n',baseForce/1000)

    % Side Strut (With an End Bond Beam)
    elseif node_calc == 10

        % Strut Force
        strutForce = feug*ungroutedThickness*maxStrutWidth;

        % Applied Force
        appliedForce = strutForce*cosd(45) - prevBond;

        % Reinforcement Force
        rebarForce = prevRebar + strutForce*sind(45);

        % Reinforcement Stress
        rebarStress = rebarForce/Asv;

        % Check Yielding
        if rebarStress > Fyv
            fprintf('Yielding')
            rebarForce = Asv*Fyv;
            strutForce = (rebarForce-prevRebar)/sind(45);
            appliedForce = strutForce*cosd(45) - prevBond;
        end

        % Base Force
        baseForce = strutForce*cosd(45);

        % Print the Results
        fprintf('Strut Analysis: \n')
        fprintf('   Strut Force = %3.2f kN \n',strutForce/1000)
        fprintf('   Applied Force = %3.2f kN
\n',appliedForce/1000)
        fprintf('   Reinforcement Force = %3.2f kN
\n',rebarForce/1000)
        fprintf('   Reinforcement Stress = %3.2f MPa
\n',rebarStress)
        fprintf('   Base Force = %3.2f kN \n\n',baseForce/1000)

    % Side Struts (Without a Bond Beam)
    elseif node_calc == 11

        % Strut Force
        strutForce = feug*ungroutedThickness*maxStrutWidth;

        % Applied Force
        appliedForce = strutForce*cosd(45);
```

```
        % Reinforcement Force
        rebarForce = prevRebar + strutForce*sind(45);

        % Reinforcement Stress
        rebarStress = rebarForce/Asv;

        % Check Yielding
        if rebarStress > Fyv
            fprintf('Yielding')
            rebarForce = Asv*Fyv;
            strutForce = (rebarForce-prevRebar)/sind(45);
            appliedForce = strutForce*cosd(45);
        end

        % Base Force
        baseForce = strutForce*cosd(45);

        % Print the Results
        fprintf('Strut Analysis: \n')
        fprintf('   Strut Force = %3.2f kN \n',strutForce/1000)
        fprintf('   Applied Force = %3.2f kN
\n',appliedForce/1000)
        fprintf('   Reinforcement Force = %3.2f kN
\n',rebarForce/1000)
        fprintf('   Reinforcement Stress = %3.2f MPa
\n',rebarStress)
        fprintf('   Base Force = %3.2f kN \n\n',baseForce/1000)

    % Side Struts (With an Intermediate Bond Beam)
    elseif node_calc == 12


        % Top Strut
        % Strut Force
        strutForce1 = feug*ungroutedThickness*maxStrutWidth;

        % Applied Force
        appliedForce = strutForce1*cosd(45);

        % Reinforcement Force
        rebarForce1 = prevRebar + strutForce1*sind(45);

        % Reinforcement Stress
        rebarStress1 = rebarForce1/Asv;

        % Check Yielding
        if rebarStress1 > Fyv
            rebarForce1 = Asv*Fyv;
            strutForce1 = (rebarForce1-prevRebar)/sind(45);
```

```
            appliedForce = strutForce1*cosd(45);
        end

        % Bottom Strut
        if strutForce1 == feug*ungroutedThickness*maxStrutWidth
            strutForce2 = strutForce1;
            rebarForce2 = prevRebar2;
            rebarStress2 = rebarStress1;
            bondForce = prevBond;
        else
            % Strut Force
            strutForce2 = feug*ungroutedThickness*maxStrutWidth;

            % Bond Beam Force
            bondForce = prevBond + strutForce1*cosd(45) -
strutForce2*cosd(45);

            % Reinforcement Force
            rebarForce2 = prevRebar2 + strutForce2*sind(45) -
strutForce1*sind(45);

            % Reinforcement Stress
            rebarStress2 = rebarForce2/Asv;

            % Check Yielding
            if rebarStress2 > Fyv
                rebarForce2 = Asv*Fyv;
                strutForce2 = (rebarForce2 +
strutForce1*sind(45) - prevRebar2)/sind(45);
                bondForce = prevBond + strutForce1*cosd(45) -
strutForce2*cosd(45);
            end
        end

        % Base Force
        baseForce = strutForce2*cosd(45);

        % Bond Stress
        bondStress = bondForce/Ash;

        % Print the Results
        fprintf('Strut Analysis: \n')
        fprintf('   Strut Force 1 = %3.2f kN
\n',strutForce1/1000)
        fprintf('   Strut Force 2 = %3.2f kN
\n',strutForce2/1000)
        fprintf('   Applied Force = %3.2f kN
\n',appliedForce/1000)
        fprintf('   Left Reinforcement Force = %3.2f kN
\n',rebarForce1/1000)
```

```
        fprintf('   Left Reinforcement Stress = %3.2f MPa
\n',rebarStress1)
        fprintf('   Right Reinforcement Force = %3.2f kN
\n',rebarForce2/1000)
        fprintf('   Right Reinforcement Stress = %3.2f MPa
\n',rebarStress2)
        fprintf('   Base Force = %3.2f kN \n',baseForce/1000)
        fprintf('   Bond Beam Force = %3.2f kN
\n',bondForce/1000)
        fprintf('   Bond Beam Stress = %3.2f MPa
\n\n',bondStress)

    end

    %% Outputs
    paraOutputs =
[transferForce,appliedForce,rebarForce,rebarForce1,rebarForce2,b
ondForce,baseForce,totalStrutBase];
```